Freie Universität Berlin

Fachbereich Geowissenschaften

Assessment of the dynamics of terrestrial vegetation using satellite observations of greenness and sun-induced chlorophyll fluorescence

Dissertation

zur Erlangung des akademischen Grades
eines Doktors der Naturwissenschaften
doctor rerum naturalium

vorgelegt von:
Sophia Bettina Walther

Berlin, 2018

Erstgutachter: Prof. Dr. Luis Guanter
Zweitgutachter: Prof. Dr. Jürgen Fischer
Tag der Disputation: 06. Juli 2018

Eidesstattliche Erklärung

Hiermit versichere ich, dass ich die vorliegende Arbeit selbstständig verfasst und keine anderen als die angegebenen Quellen und Hilfsmittel benutzt habe. Die Arbeit wurde in keinem früheren Promotionsverfahren eingereicht.

Sophia Walther

Abstract Photosynthesis is one of the most fundamental processes on Earth fuelling life by providing food and energy. Moreover, terrestrial vegetation is a key element in the climate system as it importantly affects exchange processes of carbon, water and energy between the land surface and the atmosphere. In times of a changing climate there is urgent need for detailed knowledge on the factors driving plant activity and for reliable observational systems of the terrestrial vegetation. Satellite remote sensing is the only means to obtain measurements with global coverage, including remote and inaccessible regions, in a spatially and temporally continuous manner. This thesis presents an assessment of our current observational capabilities of vegetation dynamics from space. Three complementary approaches of spaceborne ecosystem monitoring are inter-compared: 1) Spectral measurements of the land surface reflectance in the optical range give an indication of the amount of green biomass (as an integrative signal of leaf quantity and quality) and hence of the potential to perform photosynthesis. 2) In the red and far-red spectral regions, satellite instruments register a very small additive signal to the reflected radiance which originates from photosynthetically active chlorophyll pigments, termed sun-induced chlorophyll fluorescence (SIF). 3) Carbon fluxes measured *in-situ* are upscaled to a global data set of model gross photosynthetic carbon uptake (known as GPP - gross primary production) using empirical relationships with remotely sensed land surface and environmental variables. Three case studies focus i) on the spring phenology in boreal forests, ii) on the peak growing season in circumpolar treeless regions, and iii) on phenological changes in ecosystems with varying abundances of trees globally in times of fluctuations in soil moisture availability. The results of all three case studies highlight the intrinsic differences between greenness on the one hand and photosynthetic activity on the other hand. Specifically – for the first time on synoptic scales – a decoupling of photosynthesis (as indicated by SIF and model GPP) and greenness (approximated by various indices derived from spectral reflectance measurements) could be observed in evergreen needleleaf forests during spring recovery. Similarly, a temporal mismatch occurs in northern hemisphere forests during the growing season. There, changes in incoming light co-vary with soil moisture and immediately affect photosynthetic performance but barely greenness. Moreover, it has emerged that the timing of peak photosynthesis and peak greenness are asynchronous in tundra areas, which is indicative of differing dynamics. Conversely, there is high consistency between the three approaches regarding the length of growing season in deciduous forests and moisture-related phenological shifts in non-forested ecosystems. The work in this thesis demonstrates that SIF represents an asset for the monitoring of the dynamics of photosynthesis and carbon uptake compared to greenness-based approaches. There are further indications of SIF to track changes in photosynthetic yields. However, despite these promising results for the accurate tracking of photosynthesis from space, further research is required to provide higher resolution data sets with clearer signals. Further, ground-based validation efforts are necessary to improve our mechanistic understanding of physiological and radiative transfer processes controlling the SIF signal.

Kurzzusammenfassung Photosynthese ist ein essenzieller Prozess, da er durch die Bereitstellung von Nahrung und Energie die Grundlage für Leben auf der Erde ist. Zusätzlich beeinflussen die Aktivität und das Wachstum von Pflanzen den Austausch von Kohlenstoff, Wasser und Energie zwischen der Landoberfläche und der Atmosphäre. Aus der wichtigen Rolle, die die terrestrische Vegetation dadurch im Klimasystem einnimmt, folgt die Notwendigkeit eines detaillierten Verständnisses der Einflussfaktoren sowie zuverlässiger Beobachtungsverfahren globaler Ökosysteme. Im Gegensatz zu anderen Methoden ermöglicht Satellitenfernerkundung räumlich und zeitlich hoch aufgelöste Beobachtungen mit globaler Abdeckung, abgelegene und unzugängliche Regionen eingeschlossen. In dieser Dissertation werden drei verschiedene Ansätze der weltraumbasierten Beobachtung der terrestrischen Vegetation hinsichtlich ihrer zeitlichen Muster miteinander verglichen: 1) Aus Messungen der spektralen Reflektivität im optischen Bereich kann die Grünheit der Erdoberfläche (als kombiniertes Signal von Blattmaterial und Chlorophyllpigmenten) und damit potentielle Photosynthese abgeschätzt werden. 2) Im roten und nahen infraroten Wellenlängenbereich emittiert photosynthetisch aktives Chlorophyll ein Stahlungssignal (solarinduzierte Chlorophyllfluoreszenz, sun-induced chlorophyll fluorescence, SIF), das die Satelliteninstrumente zusätzlich zur reflektierten Solarstrahlung detektieren können. 3) Aus *in-situ* Messungen von Kohlenstoffflüssen und deren empirischer Beziehung zu fernerkundlich bestimmbaren Eigenschaften der Landoberfläche und der Umwelt kann die globale Bruttoprimärproduktion (gross primary productivity, GPP) statistisch modelliert werden. In drei Fallstudien werden phänologische Muster analysiert: i) das Ende der Winterdormanz und den Übergang zum Frühling in borealen Wäldern, ii) das Maximum der Vegetationsperiode in Tundragebieten, und iii) phänologische Effekte bei veränderlicher Bodenfeuchte in globalen Ökosystemen mit unterschiedlich stark ausgeprägtem Baumbestand. Die Ergebnisse aller drei Fallstudien stellen insbesondere den intrinsischen Unterschied zwischen Grünheit einerseits und Photosyntheseaktivität andererseits heraus. Im Einzelnen konnte gezeigt werden - zum ersten Mal auf der synoptischen Skala, dass das photosynthetische Frühjahrserwachen (abgeschätzt durch SIF und Modell-GPP) in borealen Nadelwäldern unabhängig von Veränderungen in diversen spektralen Indizes der Grünheit erfolgt. In ähnlicher Weise wurde beobachtet, dass Grünheit und Photosynthese inkongruente zeitliche Muster in Wäldern während des nordhemisphärischen Sommers zeigen. Einfallende solare Strahlung, die mit der Bodenfeuchte kovariiert, kontrolliert die Photosyntheseleistung unmittelbar, beeinflusst die Grünheit jedoch kaum. Ein weiteres wichtiges Ergebnis dieser Arbeit ist das asynchrone Verhalten der Jahresmaxima von Photosynthese und Grünheit in baumlosen Gebieten der hohen Breiten - ein weiteres Indiz der Entkopplung. Andererseits gibt es hohe Übereinstimmung hinsichtlich der zeitlichen Begrenzung der Vegetationsperiode zwischen den drei Beobachtungsansätzen in laubabwerfenden Wäldern als auch bezüglich der Bodenfeuchteeinflüsse auf die Vegetation in Ökosystemen mit geringem Baumbestand. Die Ergebnisse der vorliegenden Dissertation verdeutlichen, dass SIF vorteilhafte Eigenschaften zur fernerkundlichen Abschätzung von Photosyntheseaktivität gegenüber Grünheitsmessungen aufweist. Desweiteren gibt es Hinweise, dass SIF zusätzlich Veränderungen der Effizienz der Photosynthese anzeigen kann. Trotz dieser aussichtsreichen Ergebnisse für eine direktere weltraumgestützte Beobachtung von Photosynthese, ist weitere Forschung notwendig um die Auflösung und Qualität der Datensätze zu verbessern. Ferner werden bodengestützte Validierungsverfahren benötigt um ein besseres Verständnis physiologischer Mechanismen und von Strahlungstransportprozessen zu erlangen.

CONTENTS

CHAPTER I

INTRODUCTION

I.1 Preface

Photosynthesis is the starting point of the terrestrial carbon cycle and the fundamental process through which food, energy and an oxygenic atmosphere are provided to sustain humankind. Together with soil and plant respiration, the carbon uptake by vegetation drives the terrestrial carbon exchange on time scales from days to decades. However, the mechanisms of interaction between the land surface and the atmosphere are not fully understood and constrained which is largely a consequence of limited observational capabilities of the same. Knowledge about the exchange processes of carbon and its drivers is key for accurate projections of atmospheric CO_2 concentrations and climate in times of high anthropogenic carbon emissions and a changing climate.
Currently, there is no method or instrument to directly measure gross photosynthetic carbon uptake by the terrestrial biosphere (Baldocchi *et al.*, 2016). For decades, researchers have used satellite measurements of spectral reflectance to estimate the amount of green biomass and hence photosynthetic potential to monitor the health and status of the vegetation globally. In vitro, chlorophyll fluorescence - a small radiation signal in the red and far-red that is emitted by photosynthesising chlorophyll pigments - has helped to infer photosynthetic efficiency in laboratory measurements. In 2007, it has been demonstrated for the first time that the fluorescence flux is observable from space (Guanter *et al.*, 2007) and four years later the first global retrievals have been achieved (Frankenberg *et al.*, 2011a; Joiner *et al.*, 2011). Therefore, vegetation can be now globally monitored by observing the signal emitted directly by photosynthesising plants.
This thesis contributes to an enhanced understanding of the benefits and limitations of both approaches with respect to the global space-based assessment of the dynamics of vegetation activity. Next to reflectance-based greenness estimates and measurements of sun-induced chlorophyll fluorescence, data-driven model results of gross photosynthetic carbon uptake are used as a third data source throughout the thesis. Variability in time of photosynthesis and green biomass is explored jointly and presented in three case studies: The phenology of greenness indices, chlorophyll fluorescence and model photosynthetic carbon uptake is explored in boreal forests (first study) and in tundra ecosystems (second study). Both biomes pose major challenges for reflectance-based monitoring of vegetation

dynamics due to their small annual greenness changes and background influences on the signal. The third study has a global context. The aim is to understand the phenological behaviour of the three vegetation proxies with changing water availability while taking into account the amount of tree cover that is present in an ecosystem.
The thesis is presented as an accumulation of three research papers that have been published or submitted to peer-reviewed journals or that are currently under peer-review. My work has been funded by the GlobFluo-Project of the Emmy-Noether-Programme of the Deutsche Forschungsgemeinschaft (GU 1276/1-1). The subject of the thesis supports the aims of the project which is the 'global assessment of vegetation photosynthesis through the monitoring of chlorophyll fluorescence from space'.
I will first summarize the relevant research background and context to understand the work of this thesis by explaining the functioning of the terrestrial carbon cycle and its significance in the global climate system. The role of photosynthesis as an important driver of atmospheric CO_2 concentrations is presented and related to environmental conditions. I will then switch from the global to the molecular scale to describe the relevant processes and mechanisms of photosynthesis and its relation to chlorophyll fluorescence, before elaborating on the principles of observing and assessing vegetation dynamics from space. In chapters II, III, IV the three study cases are presented. Chapter V gives a synthesis and conclusions of this thesis.

I.2 Research background and context

I.2.1 The relevance of vegetation in the carbon cycle and for climate

Vegetation abundance and activity is a key part of the global climate system because it critically affects exchange processes of carbon, water and energy between the land surface and the atmosphere. In the context of rising atmospheric CO_2 concentrations with the inherent reinforcement of the greenhouse effect, of climate change and human impacts on the climate, it is important to understand and quantify those exchange processes. The knowledge can subsequently be used for model projections of the future evolvement of the Earth system. However, current model results diverge strongly in magnitude, variability and partly phase of the carbon fluxes and have high uncertainties (Huntzinger *et al.*, 2012; Schaefer *et al.*, 2012; Anav *et al.*, 2015). The simulations even disagree on whether the land surface will be a carbon sink or source (Piao *et al.*, 2013). This indicates that important driving variables and mechanistic understanding are still missing in the models (Beer *et al.*, 2010; Jung *et al.*, 2011). Reliable climate scenarios cannot be accomplished without a detailed knowledge and modelling of the functioning of ecosystems. The work done in the context of this thesis contributes to advance knowledge on gross carbon uptake by vegetation through photosynthesis which is the starting point of the terrestrial carbon cycle.

I.2.1.1 The carbon cycle

I.2.1.1.1 The global carbon cycle Carbon cycles globally between the solid Earth, the land surface, the oceans and the atmosphere (Fig. I.1 left). Solid Earth processes are negligible on time scales of up to centuries. Ocean uptake as well as terrestrial photosynthesis are the only pathways through which carbon can be removed from the atmosphere. The gross amount of carbon taken up through photosynthesis is commonly referred to as

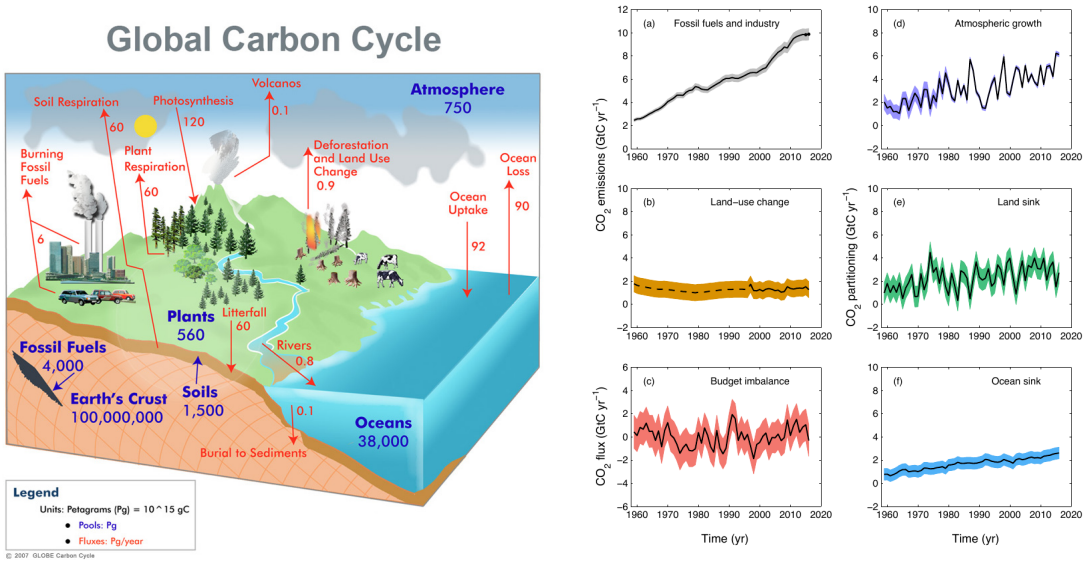

Figure I.1: Left: Carbon fluxes between different pools/components of the climate system. From http://kfrserver.natur.cuni.cz/globe/materialy/03Others/CCdiagram-english.jpg, accessed February, 9th 2018. Right: Evolvement of components of the global carbon budget as of 2017 with uncertainties as one σ. From Le Quéré *et al.* (2017).

gross primary productivity (GPP, carbon per unit of time and area) and globally amounts to approximately 120 PgC/year (Le Quéré *et al.*, 2017). However, there is a large spread between different model estimates ranging from 112 to 169 PgC/year (Anav *et al.*, 2015) or between 105 and 150 PgC/year (Beer *et al.*, 2010). About half of the GPP is released back to the atmosphere through plant respirational processes for cell maintenance and growth (autotrophic respiration). Also heterotrophic respiration by microbes and the fauna in the soil causes a flux of carbon to the atmosphere. The net gain of photosynthesis in the form of accumulated plant biomass is called net ecosystem productivity, or from an atmospheric perspective, net ecosystem exchange (NEE). Other processes that influence carbon concentrations in the atmosphere are changes in land cover and land use (de-/afforestation, forest degradation, expansion and abandonment of agricultural areas, shrub expansion in the Arctic), burning of fossil fuels and oceanic carbon release (Fig. I.1 left).

I.2.1.1.2 Partitioning of the carbon budget The time series in the right part of Fig. I.1 show the temporal evolution of estimates of the different components of the global carbon budget over the recent decades. Emissions by fossil fuels have been steadily increasing and by 2017 have reached a level of about 500 % of the value of 1960. Changes in land use have created relatively stable emissions over the last decades, but are not well constrained. The sum of these (mostly anthropogenically caused) emissions is partitioned between the ocean, the land and the atmosphere. The ocean is taking up about a quarter of the carbon emissions, even with an apparently increasing trend in the total uptake since 1960. The land surface (the land sink) is largely responsible for taking up another quarter of the total emissions through net photosynthesis (gross photosynthesis

minus respiration)[1]. Further, there is considerable change in the estimated strength of the land sink between years (Fig. I.1e). This interannual variability represents the imprint of environmental conditions on the functioning of the terrestrial vegetation and on the release processes associated with respiration (e.g. Keeling *et al.*, 1995; Houghton, 2000). Figure I.1d further illustrates that the variability in the land sink is directly translated into variability in the rate of increase in atmospheric CO_2 concentrations between years (CO_2 atmospheric growth rate). Roughly half of the emissions remains in the atmosphere (Le Quéré *et al.*, 2009). Next to the year-to-year variability there is also a trend towards increased amounts of the emissions to accumulate in the atmosphere, despite a strengthening ocean sink (Fig. I.1d,f). This might indicate that the removal of carbon from the atmosphere by the land surface is not necessarily increasing at the same rate.
Generally, the magnitude of the sources and sinks is not sufficiently constrained in different regions of the Earth. There remains a certain imbalance (Fig. I.1c) in the budget from the various approximations and this illustrates the large uncertainties and possibly biases in the component estimates (Le Quéré *et al.*, 2017). Similarly, when focussing on the carbon fluxes between the land surface and the atmosphere, different approaches to constrain them give very different results (Reuter *et al.*, 2017). The average magnitude of the land-atmosphere fluxes for different regions of the Earth as inferred from an ensemble of global dynamic vegetation models for the 1990s and the 2000s is depicted in green-coloured bars in Fig. I.2. This is usually referred to as the 'bottom-up' approach. The 'top-down' approach consists in measuring atmospheric CO_2 concentrations and applying atmospheric transport models as well as ancillary information to infer the location and the magnitude of the land carbon fluxes. Such estimates are depicted in the red and orange bars in Fig. I.2. There is a considerable gap in the estimated magnitudes of the fluxes between top-down and bottom-up approaches, with the inversions showing generally higher fluxes. A second major conclusion is that the different approaches in some regions do not even agree on the sign of fluxes, i.e. whether the region is actually a sink or a source of carbon (e.g. the tropical regions of America and Asia). This illustrates that there is urgent need to constrain the global carbon budget in a better way, both through improvements in observational capabilities as well as through advancements in land surface and global Earth system models.

I.2.1.1.3 The roles of gross primary productivity and respiration in the global carbon budget One major source of uncertainty in the carbon fluxes is the lack of understanding of how different processes drive the sink strength of the land surface and of the regional contributions to the global total (Schimel *et al.*, 2001). Anderegg *et al.* (2015) report on strong correlations between tropical nighttime temperature and interannual changes in the strength of the global land sink mediated though changes in respiration. Ballantyne *et al.* (2017) explain an observed increase of the land uptake in the recent decade by the effect of the warming hiatus on respiration. In line with that, Schneising *et al.* (2014) find a decreased strength of land carbon uptake in warm years due to enhanced respiration in the recent decade. Conversely, several other publications stress the importance of GPP with respect to respiration in driving interannual changes in the strength of

[1] A record of daily measurements of atmospheric CO_2 concentrations on Mauna Loa, Hawaii, that extends back to the 1950s (the well-known Keeling curve, not shown) exhibits annual oscillations overlaid on an increasing trend. This illustrates the dominant effect of vegetation activity on atmospheric CO_2 concentrations very well.

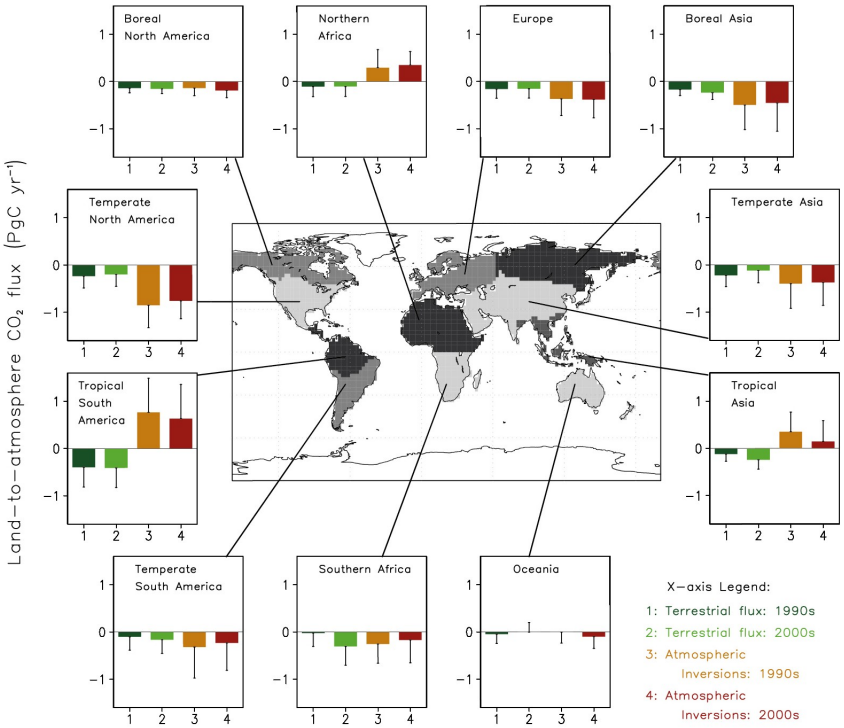

Figure I.2: Average of the carbon fluxes between the land and the atmosphere for the two decades from 1990-2000 and 2000-2010 for different regions of the Earth as inferred from 10 different atmospheric CO_2 inversions (yellow and orange, denoted as 'top-down') and simulated by 10 dynamic vegetation models (DGVMs, green and light green, denoted as 'bottom-up'). From Ciais *et al.* (2013, Fig.6.15).

the global carbon sink (Wang *et al.*, 2016; Marcolla *et al.*, 2017) as well as the dominant role of low and mid-latitude water-limited ecosystems (Liu *et al.*, 2013; Zscheischler *et al.*, 2014; Huang *et al.*, 2016; Jung *et al.*, 2017). For example, Ahlström *et al.* (2015) argue that the variability in global net biome productivity is dominated by semi-arid regions where GPP is most strongly driven by temperature and precipitation anomalies. Similar results were obtained from the evaluation of empirical model studies by Jung *et al.* (2017). They find that hotspots of interannual variability of carbon fluxes are concentrated in semi-arid/ semi-humid areas and that overall GPP more strongly affects net ecosystem carbon exchange variability than respiration (except in the south-American and east-Asian tropics). Poulter *et al.* (2014) correlate the 2011 record land sink with strong vegetation growth in semi-arid regions of the southern hemisphere, particularly Australia, as a result of enhanced precipitation under La Niña conditions. High sensitivity of the GPP to water limitation and short carbon turnover times cause the strong contribution of semi-arid regions to interannual variability of the terrestrial carbon sink (Poulter *et al.*, 2014; Ma *et al.*, 2015, 2016). In contrast to that, during the strong El Niño of 2015/16, major reductions in the pantropical land uptake due to the effects of heat and drought on respiration, GPP, and fire activity led to a record high in atmospheric CO_2 concentrations (Liu *et al.*, 2017b). Next to the ENSO conditions, also the North Atlantic Oscillation in an interplay with the East Atlantic pattern affect the land sink through meteorological influences on photosynthesis and also respiration in middle and higher latitudes (Bastos *et al.*, 2016).
In essence, changes in environmental conditions as controlling variables of the terrestrial land uptake are unquestionable, but the exact feedback mechanisms and their quantification for gross photosynthesis and respiration remain uncertain, both globally and regionally.

I.2.1.2 Vegetation and climate

I.2.1.2.1 Vegetation and climate change Enhanced understanding of the functioning of the terrestrial biosphere is vital considering that a changing climate will critically affect global and regional GPP and respiration. However, the feedback mechanisms between the atmosphere and the vegetation are not fully understood. Consequently, model projections on the future land sink, its sensitivity to environmental conditions as well as its variability diverge widely (e.g., Friedlingstein *et al.*, 2006).
Rising atmospheric CO_2 concentration may have a fertilizing effect on plant activity and carbon uptake (Zhu *et al.*, 2016). Even climate change induced forest mortality (Allen *et al.*, 2010) might be alleviated by higher CO_2 (Liu *et al.*, 2017c). However, Friedlingstein *et al.* (2006) report from an evaluation of coupled climate-carbon cycle simulations that there is "unanimous agreement among the models that future climate change will reduce the efficiency of the earth system to absorb the anthropogenic carbon perturbation." (Friedlingstein *et al.*, 2006, abstract). Indeed, there are indications that the sink efficiency of the land surface has already been decreasing in the last five decades[2] which represents a shift from a CO_2 fertilization-dominated sink towards increasing constraints by climate effects, but uncertainties are high (Le Quéré *et al.*, 2009; Peñuelas *et al.*, 2017). Conversely, Ballantyne *et al.* (2012) conclude the opposite by inferring an enhanced carbon sink in both land and ocean in the last five decades with no decrease in its efficiency.

[2]despite an increase in the absolute sink strength

Keenan *et al.* (2016) explain an observed pause in the atmospheric CO_2 growth rate with enhanced land uptake as a consequence of fertilization. At the same time, the observed hiatus in global warming reduces warming-related increases in respiration and in that way has enhanced land uptake in the last decade (Keenan *et al.*, 2016; Ballantyne *et al.*, 2017).

One example for changes in the biosphere is the widespread greening of the land surface, particularly in boreal and polar areas, that is observed as a consequence of warming, longer growing seasons and northward shifts of higher vegetation (Sturm *et al.*, 2001; Nemani *et al.*, 2003; Elmendorf *et al.*, 2012). Increased GPP due to warming and plant growth is believed to dominate the observed increase in the seasonal amplitude of atmospheric CO_2 in northern latitudes with respect to respiration (Graven *et al.*, 2013; Forkel *et al.*, 2016). However, warming might enhance autumn respiration in northern ecosystems (Piao *et al.*, 2008) and attenuate night minimum temperatures which enhances respiration as well. At the same time, in several regions of the Earth aridity increases and drylands expand with strong alterations in ecosystem composition and functioning (Feng and Fu, 2013; Huang *et al.*, 2015; Schlaepfer *et al.*, 2017). Next to a shift in the mean state, climate change is also expected to enhance climate variability with more frequent and stronger extremes, e.g. droughts and floods or heat waves (Seneviratne *et al.*, 2012). It will put constraints on the carbon uptake by plants and enlarge its variability. As stated above, especially water availability has been a major recent focus of research with respect to global GPP (Poulter *et al.*, 2014; Ahlström *et al.*, 2015; Papagiannopoulou *et al.*, 2017). This is particularly critical for agriculture and food production for a growing world population and might severely impact food security (Wheeler and von Braun, 2013).

I.2.1.2.2 Vegetation and the terrestrial energy and water cycles Vegetation is not only a fundamental component of the climate system because of the role that photosynthesis plays in the carbon cycle, but also because of its biophysical impacts on climate. Regionally strong biosphere-atmosphere feedbacks exist (Green *et al.*, 2017) through the coupling of vegetation abundance and activity to the energy and hydrological cycle. Through physiological regulation of transpiration by opening and closing the leaf pores (stomata) and root water uptake, vegetation importantly affects the water transport between the land surface and the atmosphere (Seneviratne *et al.*, 2010; Teuling *et al.*, 2010). A plant transpires up to 500 g water for each gram carbon fixed through photosynthesis (Blankenship, 2014). Moreover, the abundance of different types of vegetation controls the energy budget of the land surface (e.g. Duveiller *et al.*, 2018). Land cover change, and in particular modifications in forest cover, have been shown to lead to strong alterations in the albedo and absorption of solar radiation as well as in evapotranspiration (Alkama and Cescatti, 2016; Forzieri *et al.*, 2017; Duveiller *et al.*, 2018). Through the significant role that vegetation plays in the partitioning of energy between latent and sensible heat to the atmosphere (Bowen ratio, e.g. Forzieri *et al.*, 2017) plants may even partly adjust their growing conditions by modifying rain fall patterns (Miralles *et al.*, 2016; Teuling *et al.*, 2017). As another example, agricultural intensification in the middle US, and its effects on evapotranspiration, are considered the driving mechanism of an observed attenuation of summer high temperatures, despite effects of land cover conversion and of enhanced atmospheric CO_2 concentrations on temperature in the opposite direction (Mueller *et al.*, 2016).

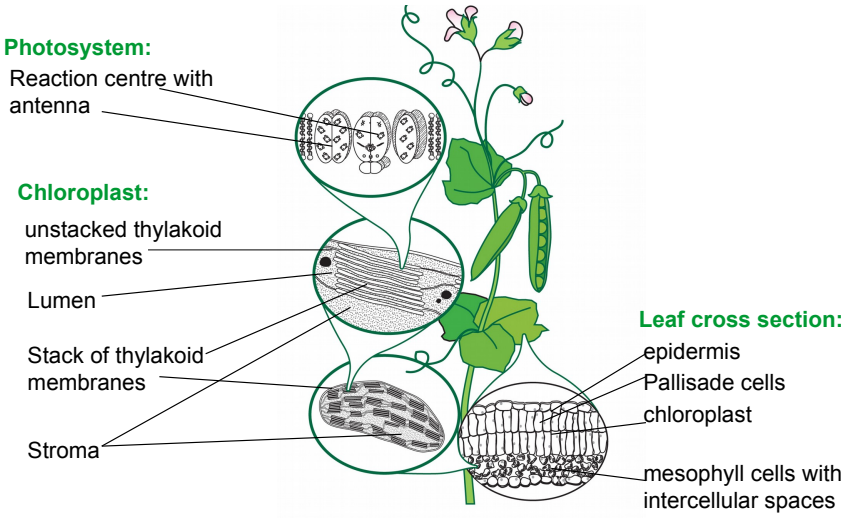

Figure I.3: Anatomy of a leaf. Adapted from Blankenship (2014).

Gross photosynthetic carbon uptake is the starting point of the terrestrial carbon cycle. Because of its direct impact on atmospheric CO_2 concentrations it is of key importance to understand the drivers of photosynthesis globally, regionally, and in time, and to have an observation system in place that has the capacity to reliably monitor vegetation abundance, health and activity. Constraining photosynthetic carbon fluxes is a field of active research with key relevance for climate modelling studies. The work in this thesis relates to the carbon effects of vegetation and is a contribution to understand our current satellite-based capacities to monitor environmental effects on ecosystem photosynthetic activity. The focus is exclusively on the inference of changes in GPP as no satellite-based proxies of respiration exist. The temporal patterns in reflectance-based greenness indices as well as measurements of sun-induced chlorophyll fluorescence will be compared. In order to understand how these proxies are related to actual GPP, the next section will change the focus from the regional and global scale of carbon budgets to the leaf, molecular and quantum scale to explain the processes involved in photosynthesis, their interdependence and control by environmental conditions, as well as its relation to fluorescence.

I.2.2 Photosynthesis and sun-induced chlorophyll fluorescence

"Life on Earth ultimately depends on energy derived from the sun. Photosynthesis is the only process of biological importance that can harvest this energy."(Taiz and Zeiger, 1991, p.179)

I.2.2.1 The phases of photosynthesis and its regulation by plants

I.2.2.1.1 The anatomy of a leaf and the organisation of pigments Photosynthesis describes a complex system of chemical reactions and physical processes that plants continuously adjust. Pigments use solar energy, water and CO_2 to produce sugars and starch for the maintenance of existing and synthesis of new plant material whilst releasing oxygen. In a first phase of photosynthesis, light energy is absorbed and converted into

chemical energy (light reactions). In a second step, this chemical energy is used to fix carbon and synthesize sugars and starch (Calvin cycle, dark reactions, Taiz and Zeiger, 1991). In order to maximize the energy supply to photosynthesis, the structure of leaves is tailored to an efficient absorption of sunlight: Under a 'cover layer' (epidermis, the outermost layer of a leaf), a zone of pillars of cells containing large amounts of chlorophyll (palisade cells, cf. Fig.I.3) take up a high fraction of the incident solar energy. Only a fraction of the incident light energy can pass through the spaces between them to deeper layers in the leaf. In the interior of the leaf, cells are shaped irregularly creating many air spaces between them (spongy mesophyll, see Fig.I.3). At their cell walls, transmitted light is scattered which enlarges the probability of the light energy of being ultimately absorbed. This results in an efficient and homogeneous absorption in the leaf. 85 % to 90 % of the incident photosynthetically active radiation (PAR, light in the 400 to 700 nm wavelength range) are absorbed. The remaining incident PAR is either reflected or transmitted to lower canopy layers (Taiz and Zeiger, 1991).
Photosynthesis takes place in chloroplasts, disk shaped structures in mesophyll cells containing chlorophyll (see the bottom left zoom in in Fig. I.3). Inside a chloroplast, there is the stroma, a gel-like liquid where the carbon fixation reactions take place. In the stroma lie structures called thylakoids, membrane systems with an inner space, the lumen. The thylakoid membrane is the site where the light harvesting (light reactions) takes place. In the thylakoid membrane, pigments are organized in photosystems (Bonan, 2008). A photosystem (PS) describes the compound of an antenna/light harvesting complex and the reaction centre (RC). The antenna is a combination of pigments and proteins arranged in a specific and unique way that helps to efficiently 'harvest' the solar energy. The energy is then transferred to the RC, another complex of proteins and pigments with a specialized pair of chlorophyll (Raven *et al.*, 1999).
There are several groups of pigments involved in the absorption of solar energy. Chlorophylls absorb in two bands in the UV/blue and in the red/far-red (Fig. I.4). Higher plants contain chlorophyll-a and chlorophyll-b, which differ only in one functional group. Chlorophyll-b is found only in the antenna and helps absorb and transfer solar energy to the RC, while chlorophyll-a is part of both the antenna and the RC. In the RC, chlorophyll-a plays an important role in the chemistry of light reactions (cf. section I.2.2.1.2). Another important group of pigments are the carotenoids that populate the antenna. They help absorb energy in the range between 400–500 nm and transfer this energy in the antenna. They play an important role in quenching excess absorbed energy as well (Blankenship, 2014). Pigments and proteins are composed and arranged together in a PS in a specific way which affects the absorption spectrum of the pigments. Two types of PS are differentiated, PSI and PSII. PSII maximally absorbs at 680 nm and PSI at 700 nm. The two types of PS operate together but are spatially mostly separated between the unstacked and stacked parts of the thylakoids, respectively (cf. Fig. I.3, Blankenship, 2014).

I.2.2.1.2 The light reactions

Light absorption and funnelling of energy in the photosystems Upon absorption of a photon sunlight, an electron of a pigment is excited. This quantum ('exciton') is subsequently transported through the antenna to the RC of the PS. The structure of the antenna with pigments in close vicinity to the RC having a lower energy required for excitation allows the energy to be transferred ('funnelled') efficiently towards a RC with

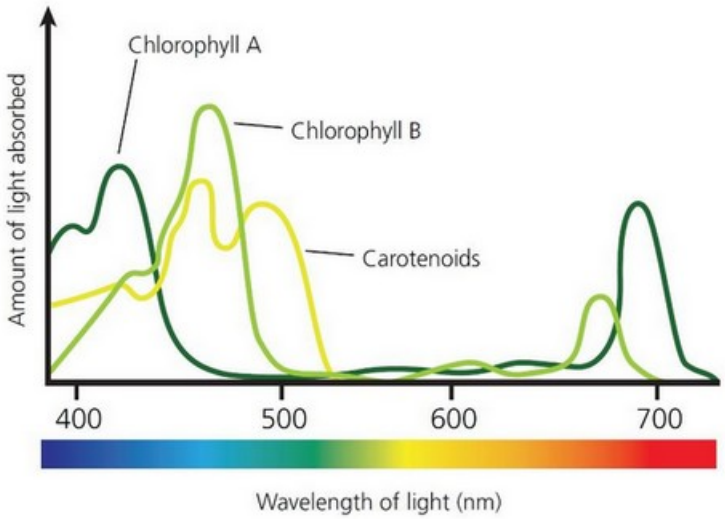

Figure I.4: Absorption spectra of chlorophyll-a, b and carotenoids. From horti daily (n.d.).

only small losses of heat (Blankenship, 2014; Porcar-Castell *et al.*, 2014). Once the exciton has arrived in the RC (or has possibly directly been absorbed by the chlorophyll-a in the RC), a special pair of chlorophyll-a molecules is excited and the excited electron is given to the primary electron acceptor pheophytin. In contrast to the physical energy transfer in the antenna, the reduction of the primary electron acceptor represents a chemical reaction (Taiz and Zeiger, 1991; Blankenship, 2014).

Electron transport between photosystems and energy storage Excited electrons from the RC chlorophyll-a of PSII move via the primary electron acceptor pheophytin into a series of redox systems in the thylakoid membrane. The redox systems are a pool of complexes that channel the electron from PSII to the RC of PSI (Fig. I.5). The RC chlorophyll of PSI has to be in an oxidized state to accept the arriving electron. From there, the electron moves further downstream through additional redox systems and its energy is finally stored by the reduction of $NADP^+$ to NADPH. NADPH is an energetic compound consumed later on in the dark reactions (cf. I.2.2.1.3). Attached to PSII is the oxygen-evolving complex which splits water using light energy (photolysis) into oxygen, protons and electrons (Fig. I.5). The resulting electrons will replenish the electron deficit in the RC of PSII. The oxygen is released as a by-product of photosynthesis into the intercellular space and finally leaves the leaf through stomata (pore openings in the epidermis) while the protons are given into the lumen (Porcar-Castell *et al.*, 2014). The passage of the electron from the oxygen-evolving complex, through the RC chlorophyll-a of PSII, the redox systems, to the RC chlorophyll of PSI and further to $NADP^+$ is called the linear electron transfer (LET, see Fig. I.5).

Another key carrier of energy that will be consumed in carbon fixation is adenosintriphosphate (ATP). ATP is built through secondary reactions that are associated with the electron movement through the redox systems between PSII and PSI. In that, protons are pumped from the stroma into the lumen. Together with the protons from the photolysis

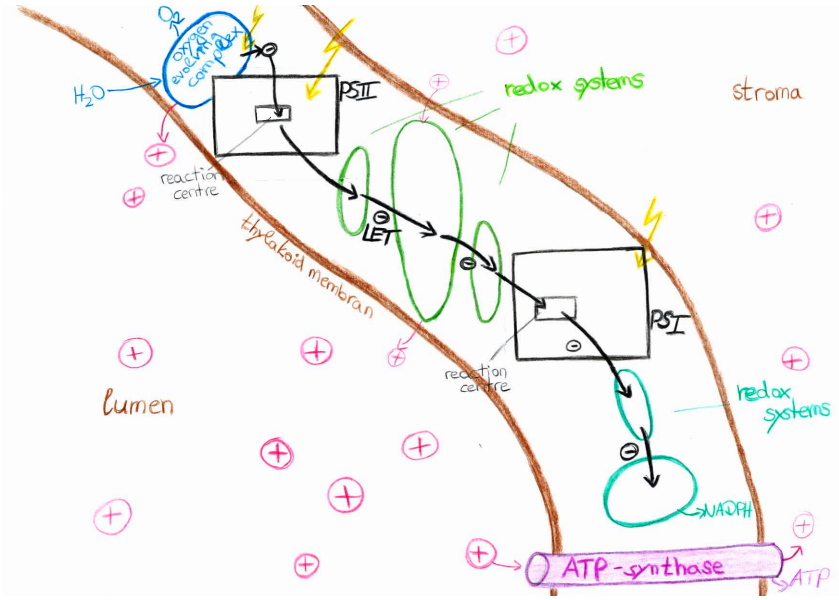

Figure I.5: Sketch of the thylakoid membrane and the linear electron flow from the oxgen evolving complex through the reaction centre of photosystem II, via several redox systems to the reaction centre of photosystem I and finally to $NADP^+$. The figure does not show the cyclic electron transport around photosystem I. Adapted from Porcar-Castell *et al.* (2014); Blankenship (2014).

of water, a proton gradient with an associated electric potential is created across the thylakoid membrane between the stroma and the lumen. This potential energy is converted into chemical energy in the form of ATP when the protons move from the lumen to the stroma against the proton gradient through enzymes in the thylakoid membrane that are called ATP-synthase (non-cyclic phosphorylation, cf. Fig. I.5, Bonan, 2008; Blankenship, 2014).
Additional ATP is built when PSI works independently of PSII in a process called cyclic photo-phosphorylation. In that, the electron given from the PSI RC chlorophyll-a to the primary electron acceptor is not directly transported downstream to be used for the generation of NADPH, but can instead move to an electron acceptor in the chain of redoxsystems between PSII and PSI. From there, the electron moves back to the RC of PSI (cyclic electron transfer, CET) whilst pumping protons from the stroma into the lumen (Raven *et al.*, 1999).

I.2.2.1.3 The dark reactions

The Calvin cycle Once absorbed solar energy is chemically stored in the form of NADPH and ATP, it can be used in the carbon fixation and transformation. This happens in the Calvin cycle, a sequence of reactions that does not directly depend on light and are therefore also termed the dark reactions. The first step is the carboxylation of CO_2: In the stroma, CO_2 is bound to ribulose 1,5-bisphosphat (RuBP), a molecule containing five carbon atoms, with the help of water and the most abundant enzyme that

exists on Earth, ribulose 1,5 bishosphat-carboxylase/oxygenase (rubisco). The resulting molecule is not stable and immediately separates to two molecules containing three carbon molecules each (Raven *et al.*, 1999; Bonan, 2008). The activity of rubisco depends on the intensity of the incoming light, temperature and on the electron transport activity (Blankenship, 2014). In a second step, the reduction phase, the two three-carbon molecules are reduced with electrons from NADPH and energy from ATP to a stable form of sugar, glycerinaldehyd-3-phosphate. On average, one out of six of these molecules is used for the generation of carbohydrates such as glucose and starch. In the third and last phase, the regeneration phase, the remaining five out of six molecules (on average) of the glycerinaldehyd-3-phosphates as well as ATP are consumed in the regeneration of the primary reaction partner of CO_2, RuBP (Raven *et al.*, 1999; Bonan, 2008). As a third pathway, glycerinaldehyd-3-phosphate might also serve the generation of additional RuBP (Blankenship, 2014). Thus, the Calvin cycle starts and ends with RuBP.

Photorespiration The enzyme rubisco that catalizes the carboxylation phase is not only compatible with CO_2, but also with molecular oxygen. Therefore, it can also catalize the oxygenation of RuBP. The recovery of the oxygenized molecule consumes additional ATP and NADPH and releases CO_2. This is the process of photorespiration. It effectively and variably lowers the net CO_2 uptake. Thus, the actual photosynthetic rate is actually 120-130% of the rate of net photosynthesis. Although rubisco is much more affine to CO_2 than to O_2, the concentration of the latter one is much higher in the cells. Thus, the rate of photorespiration depends on the fraction of CO_2 to O_2 in the stroma[3], but also on the supply of RuBP, as well as on temperature as it affects the solubility of CO_2 and the kinetics of rubisco (Taiz and Zeiger, 1991; Bonan, 2008)[4].

I.2.2.1.4 The balance between light and dark reactions Photosynthetic rates increase with light intensity as more electrons are being excited and eventually transferred through the LET chain (producing ATP) and stored downstream of PSI in NADPH. At the same time, light activates enzymes that promote the dark reactions and signals the opening of stomata to take up CO_2 (Maxwell and Johnson, 2000). As long as increasing light intensity enhances photosynthesis, one refers to a light limitation of photosynthesis. At a certain point, however, photosynthesis does not increase any more with incoming light, it saturates, as then the light energy cannot be consumed in the Calvin cycle at the same rate as it is produced in the light reactions. The concentration of CO_2 or the activity of rubisco might be the limiting factors then. Other restrictions might be the regeneration rate of RuBP, the velocity with which carbohydrates are transported out of the cell or photorespiration (Baker, 2008). This state of photosynthesis is termed enzyme-limited.
Plants are steadily adjusting light absorption and energy consumption in order to reach a balance between both (photostasis). This is important for a high efficiency of the photosynthetic process while avoiding cell damage due to excessive energy (see paragraph

[3]Enhanced CO_2 lowers photorespirational effects and is one aspect of the discussed CO_2 fertilization.

[4]The biological role of this process is much discussed. It might assume a protective role in high light and low CO_2 concentration to deplete excessive NADPH and ATP (Taiz and Zeiger, 1991). In very recent research it has been suggested that although photorespiration reduces carboxylation, it might help enhance carbon uptake by assimilating nitrogen via the photorespirative pathway (Busch *et al.*, 2018).

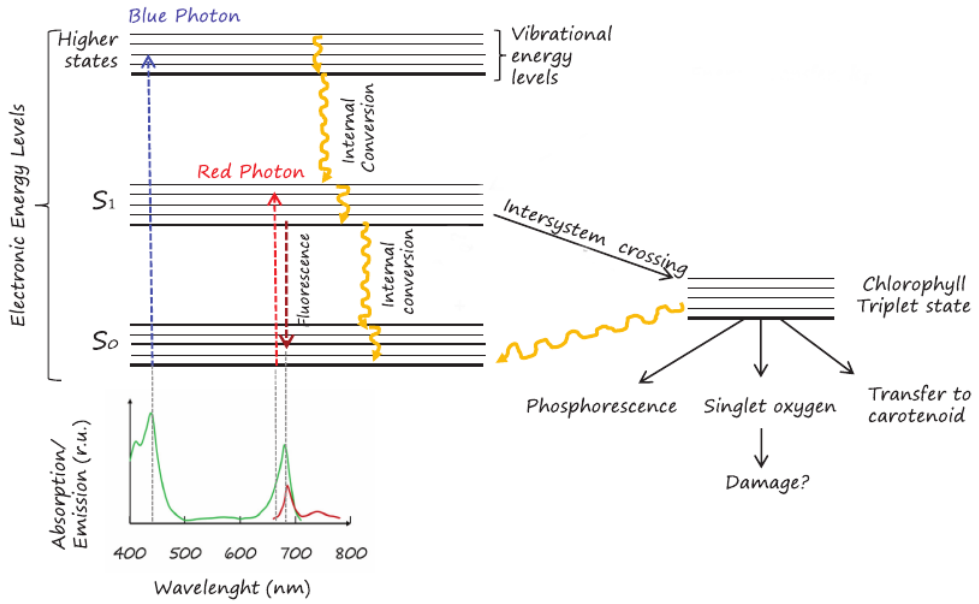

Figure I.6: Excitation by light absorption and decay pathways of a molecule. Adapted from Porcar-Castell *et al.* (2014).

on non-photochemical quenching and photo-inhibition in section I.2.2.2.1). For example, plants can adapt to light according to the environmental conditions by adjusting leaf surface properties and leaf angles towards or away from the sun, and by moving chloroplasts within plant cells (Taiz and Zeiger, 1991). They are further able to dynamically adjust the size of the cross sections of the PS, the concentration of pigments as well as their allocation ratio between PSI and PSII(Blankenship, 2014; Porcar-Castell *et al.*, 2014). Next to adaptations in the amount of absorbed energy, plants dynamically quench excess absorbed energy in several pathways that exist as alternatives to carbon fixation/ photochemical quenching in order to avoid damage to the cells. The mechanisms involved in these alternative energy quenching pathways and its relation to photochemical quenching are the topic of the next section.

I.2.2.2 The origin of sun-induced chlorophyll fluorescence and its relation to carbon fixation across scales

I.2.2.2.1 The origin of chlorophyll fluorescence and heat dissipation

Excited states of pigments The process of light absorption in chlorophyll and carotenoid pigments obeys quantum mechanics. Only photons can be absorbed that equal the energy difference between specific allowed energy states of the corresponding pigment. Of interest in the context of light absorption are the electronic and vibrational energy transitions of a pigment. Electronic transitions are associated with the orbital energy of an electron in a molecule. The spatial organization of the nucleus and the electrons will be the result of a compromise between attractive and repellent forces of charges in a molecule. Vibrational energy transitions correspond to vibrational movements of a molecule around its equilibrium state of nuclear separation. When a quantum of the incident light is

absorbed, a pigment molecule is shifted from the ground electrical and vibrational state to a higher electrical state, so the excited electron moves to a higher orbital away from the nucleus. The spatial re-organization of the electrons in the molecule entails a new vibrational equilibrium state of the excited molecule. In contrast to the electrons, the nuclei of the molecule, however, do present some inertia in their rearrangement due to their higher masses. The result is vibrations of the molecule around its new equilibrium state. Upon re-organisation of the nuclei, the vibrational movements will cease and the excited vibrational state will decay non-radiatively to the ground vibrational state (Fig. I.6, Blankenship, 2014).
Three excited electrical states exist: S2 is the highest excitation that can be created by blue light absorption. It rapidly decays to the longer-lived first excited electrical state S1 by internal conversion (Fig. I.6): The energies of higher vibrational states of S1 and the ground vibrational state of S2 overlap and the molecule can thus shift from S2 to S1 by means of non-radiative heat emission. S1 with its vibrational states can be also attained by absorption of red light. As a consequence of the immediate non-radiative decay of the higher excited states to the ground vibrational state of S1, only the number of photons (light intensity), not their energy (wavelength) is decisive for the population of S1.
As soon as S1 attains the ground vibrational state via non-radiative emission, the relatively long-lived S1 can decay to the ground electrical state S0 in several ways: i) It might dissipate non-radiatively as heat, either by internal conversion or in a physiologically controlled manner (non-photochemical quenching, see last paragraph if this section). ii) Alternatively, a small amount of heat and light of a slightly longer wavelength, fluorescence, are emitted. iii) A third pathway is the transfer of the energy to an electron of another pigment or - in case an electron of a chlorophyll molecule in a RC is excited - by giving the electron to an electron acceptor and sending it down the LET to ultimately serve carbon fixation (photochemical quenching, section I.2.2.1). By heat emission by inter-system crossing, S1 might further change to an intermediate state between S1 and S0, $S_{triplett}$, which is a very reactive and long-lived state. $S_{triplett}$ can decay to the ground state S0 via phosphorescence, heat emission or energy transfer to carotenoid pigments or to oxygen. In the latter case, reactive singulett oxygen is built which can damage PS and needs to be avoided (Blankenship, 2014; Porcar-Castell *et al.*, 2014). The probabilities of the three pathways of quenching of S1 (photochemical quenching, non-photochemical quenching, fluorescence emission) depend on environmental conditions and are under physiological control (as outlined below).

Fluorescence as a quenching pathway of excess absorbed light Plant physiological processes work towards efficient photochemical quenching of S1. The charge separation from the excited PSII RC chlorophyll to the primary electron acceptor, however, is a process that is much slower than the exciton transfer in the antenna towards the RC (Krause and Weis, 1991). Further, the electron of the excited RC chlorophyll-a cannot be passed to the electron acceptor if the latter is still in a reduced state (Baker, 2008) due to electrostatic repulsion (Blankenship, 2014). This means that for a short period of time the RC of a PS is effectively inactivated or closed for the excitons still arriving from the antenna and the energy cannot be used in photochemistry (Maxwell and Johnson, 2000; Baker, 2008). Instead, the energy is re-emitted from the pigments as a small amount of heat and light, chlorophyll fluorescence (Maxwell and Johnson, 2000; Porcar-Castell *et al.*, 2014): The decay of the vibrational ground state of S1 involves the change of the electron to a

lower orbit (and hence to S0) and the emission of a photon (fluorescence). The molecule in S0 has another optimal organization of particles than S1 regarding the distance between nuclei that minimises vibrational energy. As, again, the re-arrangement of the electrons happens much faster than the ones of the nuclei, vibrational states of S0 are excited. Therefore, the ground vibrational state of S1 decays to the excited vibrational states of S0 (Fig. I.6). Hence, the fluorescence light is of slightly longer wavelengths than the energy of the exciton difference between the ground vibrational states of S1 and S0 (Stokes-shift). The remaining energy that drives the molecular vibrations decays non-radiatively (Fig. I.6, Blankenship, 2014).
When light intensity increases, more photons are absorbed and transported to the RC of the PS. LET for the storage of the energy in the chemical compounds ATP and NADPH is enhanced. At the same time, higher LET also means that a higher fraction of RC temporarily cannot accept an exciton and are effectively closed which results in higher emission of the excess energy as fluorescence and heat (Maxwell and Johnson, 2000).

Contribution of PSI and PSII to the fluorescence spectrum The emission of chlorophyll fluorescence takes place in the wavelength region between 650 and 800 nm. The fluorescence spectrum exhibits two peaks at 685 and around 740 nm according to the wavelengths of maximal absorption by chlorophyll-a in the two types of PS (Fig. I.7). The relative contribution of fluorescence from PSI and PSII to the total fluorescence depends on the relative abundances of PSI and PSII and on the wavelength at which fluorescence is evaluated (Porcar-Castell *et al.*, 2014). In general, the life time of PSI in the oxidized state is much longer than of PSII (Krause and Weis, 1991) and the former efficiently dissipates excess energy primarily as heat (Blankenship, 2014). In addition, the RC of PSII represents a less deep trap for excitons than the RC of PSI. Thus, the quenching of PSI is independent of the redox-states of the electron acceptor or the donor chlorophyll-a (Blankenship, 2014) and is not controlled by physiological heat dissipation or photochemical quenching (Porcar-Castell *et al.*, 2014). This causes a relatively low and stable contribution of PSI fluorescence to the total fluorescence with light (Baker, 2008; Porcar-Castell *et al.*, 2014). Therefore, it can be summarized that dynamic changes in fluorescence emission track changes in the fraction of 'open' RC in PS II and consequently in the rate of LET through PSII (Maxwell and Johnson, 2000; Baker, 2008).

Non-photochemical quenching – NPQ Next to the basal heat dissipation of vibrational states and internal conversion, there is the physiologically controlled component of heat dissipation, NPQ. With this mechanism plants seek to keep the time of the PSII RC in 'closed conditions' as short as possible and in that way prevent photo-oxidative damage to the leaf by reactive oxygen. NPQ relates to several processes that promote the immediate release of absorbed energy by the antenna pigments themselves. Excitons are not transferred to the RC, even if it was open. NPQ is physiologically regulated by several mechanisms (Porcar-Castell *et al.*, 2014): In case of light saturation, protons from the LET and CET around PSI accumulate in the lumen. It has recently been shown that under conditions of excess light, specific changes in the spatial arrangement of the thylakoids favour CET over LET and consequently a proton accumulation in the lumen (Wood *et al.*, 2018). The resulting change of the pH value of the lumen controls

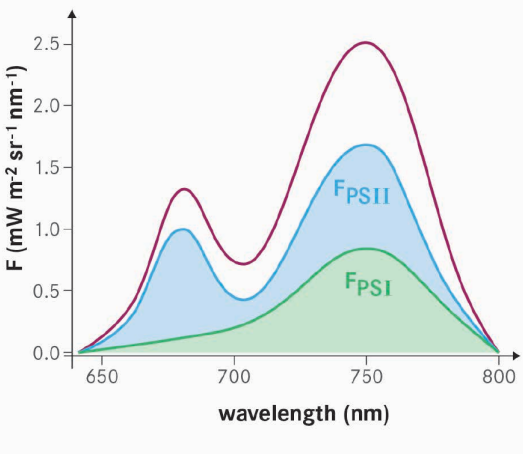

Figure I.7: Idealized example of an emission spectrum of chlorophyll fluorescence (here named F) and the contributions of photosystems I and II to the total (red line). From ESA (2015).

an enzyme that drives the xanthophyll cycle. The xanthophyll cycle describes a cyclic conversion of peripheral antenna carotenoid pigments between states of higher and lower capacity of heat dissipation. In addition, proteins in the antennae can take up protons, which also activates NPQ. This pathway of quenching of absorbed energy is dynamically up-regulated or reduced depending on the environmental conditions in order to prevent impairment of the photosynthetic machinery. If PS are damaged at a higher rate by light than they are repaired by temperature-dependent reactions, the amount of intact PS in a leaf and consequently its photosynthetic capacity will effectively be lowered (photoinhibition, Porcar-Castell *et al.*, 2014).

I.2.2.2.2 The relation of chlorophyll fluorescence to carbon fixation at the molecular and leaf scale The partitioning of absorbed energy between the three pathways of photochemical quenching, chlorophyll fluorescence and heat dissipation is under physiological control. According to the environmental conditions and the activity of NPQ, the relationship between the amounts of absorbed energy being quenched photochemically or through fluorescence is variable. About one to two percent of the total absorbed PAR is re-emitted as fluorescence (Maxwell and Johnson, 2000). As stated above, the fluorescent radiance flux is proportional to the rate of electron flow through PSII. Because plants always seek an equilibrium between the amount of energy produced in the light reactions and the one consumed in the Calvin-cycle, chlorophyll fluorescence might be used as a proxy for the efficiency of PSII photochemistry and subsequently for the one of carbon assimilation. That is, from observations of fluorescence (giving information on the LET in the light reactions) knowledge on the carbon fixation can be inferred. However, fluorescence is - in the vast majority of cases - not linearly related to the synthesis of NADPH and ATP and their consumption in carbon fixation (Baker, 2008). There are several confounding factors in that relationship, and the processes happen with different velocities and dependencies on environmental conditions. Several, temporally variable, mechanisms

confound a possible direct relationship between the fluorescence flux and CO_2 assimilation even at the molecular level: i) CET around PSI produces additional ATP that is not related to the energy compounds created through the LET. ii) Photorespiration consumes both ATP, NADPH and O_2. This leads to a decoupling of the energy provided by the LET from the one consumed in carbon fixation and further creates a discrepancy between net and actual amounts of carbon fixed. iii) Alternative electron sinks next to carbon fixation exist as well as alternative energy sinks. These are examples of processes that variably affect and confound the proportionality between chlorophyll fluorescence and the LET on the one hand and the synthesis and consumption of ATP and NADPH and carbon fixation on the other hand (Maxwell and Johnson, 2000; Baker, 2008; Porcar-Castell *et al.*, 2014).

At the leaf level, a hyperbolic relationship between instantaneous fluorescence and carbon assimilation has been found (e.g. van der Tol *et al.*, 2009; Zhang *et al.*, 2016a). The saturation point depends on the magnitude of photorespiration. This is the result of a linear increase of fluorescence with illumination while carbon assimilation increases with light only until a point of light saturation is reached and upon higher illumination it remains stable as processes and substrates in the Calvin cycle become limiting for carbon assimilation (van der Tol *et al.*, 2009).

I.2.3 Observing vegetation from space: methods and purposes

In the following I will move the focus from the mechanistic understanding of photosynthesis on molecular scales to the much larger synoptic scales of observation as employed in this thesis. The terminology will be slightly changed, as at the canopy scale, carbon assimilation is commonly referred to as gross primary productivity (GPP) and because chlorophyll fluorescence will always be excited by sunlight, from now on it will be termed sun-induced chlorophyll fluorescence (SIF)[5].

There is no single way or method to measure GPP directly, neither *in-situ* nor using spaceborne approaches (Baldocchi *et al.*, 2016). The same is true for respiration from plants and the soil. However, large-scale approximations of the vegetation health and activity are needed and spaceborne remote sensing has been proven useful in the last decades to continuously monitor land ecosystems through time. In the following, I will introduce the three different concepts of global assessment of terrestrial photosynthesis that are compared in this thesis. Optical remote sensing is based on differential leaf absorption/ reflectance and can provide an estimate of the amount of green biomass on the land surface. Hence, it can be used as a proxy of photosynthetic potential. SIF as a by-product of the conversion

[5]In the laboratory and in the field, another approach exists of actively illuminating plant tissue with artificial (in contrast to solar) actinic light sources of known wavelength. Measurements of fluorescence emission under known and variable illumination conditions after dark adaptation have been used for decades to study photosynthetic processes. A major part of the knowledge on the photosynthetic mechanisms summarized above have emerged from this technique. The retrieved parameters are strictly different from passive measurements of chlorophyll fluorescence. The former observe fluorescence quenching of a dark adapted leaf exposed to high light. There is a characteristic decreasing pattern of fluorescence in time (Kautsky-curve) which results from the physiological activation of the Calvin-Cycle upon light absorption until a balance between absorbed energy and consumption and therefore steady fluorescence emission is reached (Maxwell and Johnson, 2000; Baker, 2008). Passive measurements of chlorophyll fluorescence represent the conditions of the plants in steady state.

of the light energy into chemical energy during the light reactions might represent a useful proxy of variability in photosynthetic activity. Lastly, eddy-covariance measurements (EC) deliver *in-situ* net fluxes of carbon and other gasses between the land surface and the atmosphere. Those fluxes can empirically be separated into GPP and respiration and further be up-scaled to the globe using machine learning algorithms.

I.2.3.1 The Monteith-model of productivity

In order to understand how the satellite observations might give information on terrestrial photosynthesis, the model on plant productivity based on light-use efficiency (LUE) introduced by Monteith (1972) is helpful.

$$GPP = fPAR * PAR * LUE_p = APAR * LUE_p \tag{I.1}$$

In that, GPP results from the interaction of incoming PAR, the fraction of PAR that is absorbed by photosynthesising pigments (fPAR) in the canopy and the efficiency with which the absorbed energy is used for carbon fixation $\mathrm{LUE_p}$. $\mathrm{LUE_p}$ depends on environmental conditions and the activity of alternative sinks for energy than photochemical quenching (see section I.2.2.1). The approaches of estimating greenness and observing SIF serve the inference of different parts of this equation.

I.2.3.2 Moderate resolution remote sensing in the optical range

I.2.3.2.1 Spectral reflectance of green vegetation As outlined in section I.2.2.1, photosynthetic pigments absorb solar radiation in the visible range. The absorption of purple and blue light by carotenoids as well as the affinity of chlorophyll for blue and orange/red light (cf. Fig. I.4) create the spectral reflectance curve of green vegetation (top panel of Fig. I.8). Characteristic is the very low reflectivity in the blue and red and intermittent higher reflection of the green wavelengths. At longer wavelengths than the PAR-range, light does not interact significantly with the pigments anymore but is rather affected by the cell structures. Near infra-red radiation (NIR) passes through the uppermost leaf layers of the palisade cells into the leaf interior where it is scattered at the interfaces of the spongy mesophyll cells (Taiz and Zeiger, 1991). Therefore, much of the NIR light is reflected upwards (or transmitted through the leaf downwards), causing a sharp transition from the low reflection in the red to high in the NIR. This 'red-edge' between 700 and 800 nm is characteristic of green vegetation. The contrast is larger the greener the surface as higher pigment amounts mean higher absorption in the red and more leaves with spongy mesophyll mean enhanced scattering in the NIR. In the middle infra-red (and also in the NIR), vegetation exhibits characteristic water absorption bands (Fig. I.8, upper panel). Their depth indicates both leaf water content and leaf thickness. Plant photosynthetic tissues are the outcome of photosynthesis and on the long run the plants adapt their photosynthetic capacity to environmental conditions. Therefore, the reflected radiation by a canopy contains convoluted information on the density of vegetation cover, on the number of leaves and pigments, their spatial and angular distribution, on chemical composition, age, thickness, surface properties, structure and water content of leaves. As such, it represents an integrated species-specific measure of plant phenology,

health and activity (Glenn *et al.*, 2008).

I.2.3.2.2 Vegetation indices

Definition and information content with respect to GPP The combined evaluation of the surface reflectance in different wavelengths in the form of vegetation indices enhances the information retrieved with respect to vegetation greenness while effects of other landscape elements like the soil background or illumination effects, topography, cloud shadows are minimized (Huete *et al.*, 2002). Among a multitude of several formulations the most widely used vegetation indices are the normalized difference vegetation index, NDVI ($\frac{\rho_{NIR}-\rho_{red}}{\rho_{NIR}+\rho_{red}}$, Tucker, 1979) and the enhanced vegetation index, EVI ($G \cdot \frac{\rho_{NIR}-\rho_{red}}{\rho_{NIR}+C_1 \cdot \rho_{red}-C_2 \cdot \rho_{blue}+L}$, with gain factor G=2.5, canopy background adjustment L=1, aerosol correction coefficients C_1=6.5, C_2=7.5 for the MODIS instrument, Huete *et al.*, 2002). NDVI is rather chlorophyll sensitive, EVI is more related to structure. Therefore, the EVI exhibits different values for needleleaf and broadleaf canopies. NDVI values are generally higher than EVI (Huete *et al.*, 2002).
Several biophysical parameters can be derived from reflectance-based observations by evaluating the red-edge. Examples are fPAR, chlorophyll content, leaf area index or aboveground biomass, albedo, amongst others (Glenn *et al.*, 2008). Following the Monteith-logic, with an estimate of fPAR inferred from vegetation indices, GPP can be approximated already very well, as the amount of absorbed photosynthetically active radiation (APAR) is a key driver of GPP. In other words, vegetation indices, are designed to give an indication of the absorption capacity and consequently of the photosynthetic potential of the land surface. There is a close temporal relationship between greenness and GPP if GPP is driven by photosynthetic potential (potentially jointly with synchronously changing meteorology, and not interchangeably by only one of them) and if there is a seasonality in photosynthetic potential (Restrepo-Coupe *et al.*, 2016). Reflectance measurements have been used as reliable indicators of photosynthesis in phenological studies (Sims *et al.*, 2006; Zhang *et al.*, 2006; Hadley *et al.*, 2009; Harris and Dash, 2010; Richardson *et al.*, 2010; Gonsamo *et al.*, 2012; Ma *et al.*, 2013; Shen *et al.*, 2014; D'Odorico *et al.*, 2015). There has been extensive controversy on the drivers of the seasonality of greenness and photosynthesis seasonality in the tropics (e.g. Huete *et al.*, 2006; Myneni *et al.*, 2007; Saleska *et al.*, 2007; Morton *et al.*, 2014; Wu *et al.*, 2018). Other studies focused on the monitoring of long-term trends (Myneni *et al.*, 1997; Zhang *et al.*, 2017) and internannual variability (Allen *et al.*, 2010), the classification of land-use and the monitoring of land-cover changes (Bartholomé and Belward, 2005). Another application of vegetation indices is to use them as key inputs for the estimation of evapotranspiration (Seevers and Ottmann, 1994; Glenn *et al.*, 2011).

Confounding factors and limitations to track GPP However, there are several factors that confound and limit the applicability of vegetation indices to infer GPP. First of all and most important to keep in mind is that vegetation indices of greenness give an estimate of the maximum potential photosynthesis that could happen if all the energy absorbed was finally used in carbon fixation. This is usually not the case (see also section I.2.2.2.1) as temperature, light, or water and nutrient availability might limit photosynthetic efficiency (the LUE_p-term in the Monteith equation I.1) and the photosynthetic potential cannot

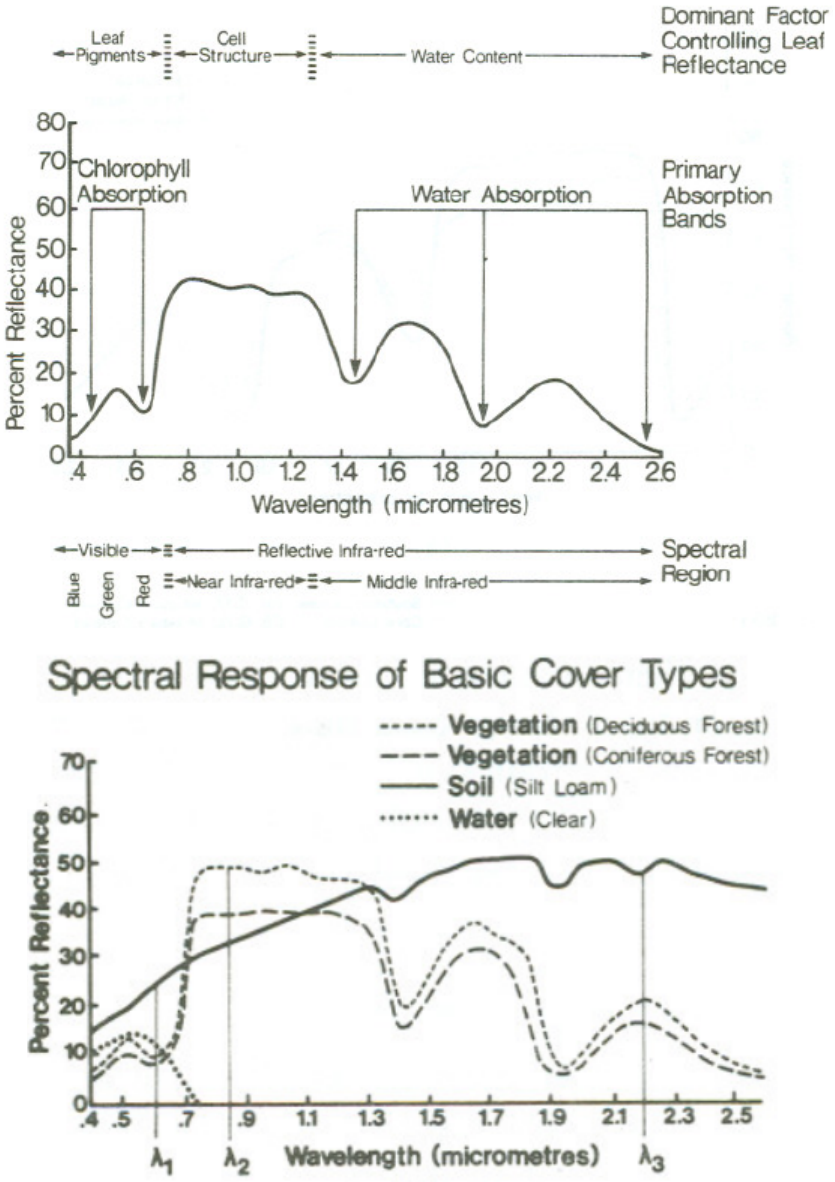

Figure I.8: Top: Typical spectral reflectance of green vegetation in the visible and infra-red and the associated characteristics of plants that cause the absorption features. Bottom: Typical spectral reflectance of different components in a satellite footprint and three wavelengths, $\lambda_1, \lambda_2, \lambda_3$, that help to distinguish them. From Hoffer (1984).

be fully tapped. Canopy greenness is mostly insensitive to changes in LUE_p that initially affect gross photosynthesis on short time scales (Zarco-Tejada *et al.*, 2013; Frank *et al.*, 2015; Zhang *et al.*, 2016c). Therefore, there will be a mismatch between greenness and photosynthesis. Additional information on environmental conditions needs to be involved to estimate a down-regulated value of LUE_p. This adds uncertainty to the final estimates of actual photosynthesis. In case of nutrient scarcity as a limiting factor, this additional information even is often not available and productivity cannot adequately be approximated (Perez-Priego *et al.*, 2015). Only severe and irreversible changes in photosynthetic potential due to changes in chlorophyll concentration and leaf area (such as during senescence, wilting, pigment degradation, morphological phenology) can be tracked by reflectance-based observations. This poses important challenges on the reflectance-based tracking of photosynthetic changes in evergreens (Shen *et al.*, 2014).
Next, as indicated by the different spectral reflectance between deciduous and coniferous canopies in the lower panel of Fig. I.8, the relationship between vegetation indices and vegetation parameters are vegetation type-specific. Different canopy structures can result in very different vegetation indices at comparable canopy density (Jackson and Huete, 1991; Huete *et al.*, 2002). Similarly, through physiological processes (and hence LUE_p) being regulated in a different way between vegetation types, the relationships between vegetation indices (or fPAR) and gross photosynthesis are vegetation-type specific (e.g. Heinsch *et al.*, 2006; Wu *et al.*, 2011).
A third aspect that needs to be considered is that - despite strong linearity - the relationship between vegetation indices and GPP is of saturating nature for high biomass/ leaf area regions (Frankenberg *et al.*, 2011b; Daumard *et al.*, 2012; Guanter *et al.*, 2014; Restrepo-Coupe *et al.*, 2016). Especially indices that strongly rely on the absorption in the red (like the NDVI, Huete *et al.*, 2002) are prone to saturation as red light is strongly absorbed by the upper canopy leaf layers and little information from lower canopy layers arrives at the satellite sensors. Conversely, the NIR penetrates deeper into the canopy through scattering and transmission giving also information on lower canopy layers. Therefore, vegetation indices that give stronger weight to the NIR (like the EVI) are less prone to saturation with respect to GPP (where GPP is a measure of the whole canopy) in high biomass regions (Huete *et al.*, 2002; Glenn *et al.*, 2008). The fast saturation of NDVI in dense canopies at the same time represents an advantage due to its enhanced sensitivity to changes in low density canopies (Jackson and Huete, 1991).

From a remote-sensing perspective, background effects, sun-sensor-geometry as well as light conditions are important determinants of the reflectance results (Jackson and Huete, 1991; Huete *et al.*, 2002). Next to the canopy there are always other landscape and ecosystem components in the field of view of the satellite and contribute to the reflectance signal - but not to photosynthetic light absorption. In the bottom panel of Fig. I.8, the spectral behaviour of common landscape components in a field of view are shown, namely those of soil and water. Soil generally shows smaller differences between red and NIR reflectance than vegetation resulting in generally low vegetation indices. This is subject to variability depending on the type and wetness of the soil (Jackson and Huete, 1991). Because of the high absorption in the NIR, water can usually be distinguished well from vegetation. Other structures that contribute to the spectral signal but not to photosynthesis are branches and stems, litter, shadows, snow or artificial surfaces (Jackson and Huete, 1991; Hadley *et al.*, 2009). Depending on the fractional canopy cover and the index used, observations

are affected by this mixed pixel problem to a varying extent. It leads us to often using and interpreting fPAR of a given field of view with respect to GPP, although what is actually needed is only the fPAR of green vegetation in the field of view (Restrepo-Coupe *et al.*, 2016). Recently, a new vegetation index has been proposed, the near infra-red reflectance of vegetation, NIRv. It is defined as the product of total NIR in a scene and the NDVI of the same field of view to measure the contribution of vegetation to the NIR signal (Badgley *et al.*, 2017). NIRv is claimed to remove much of the mixed pixel problem while at the same time being sensitive to canopy structure as an important determinant of GPP.
Changes in the observation and illumination geometry may confound reflectance measurements (Morton *et al.*, 2014) as the amount of sunlit and shaded leaves as well the visible soil background vary depending on the relative positions of sun and satellite. In addition to that, the structure of the canopy and leaf angle distributions play a significant role. Changes of up to 30% in the vegetation indices between erectophile and planophile canopies can be observed at comparable vegetation densities. To minimize the effects of varying sun-sensor geometry, a normalization is recommended by modelling the bidirectional reflectance distribution function of a scene. This function describes the reflectance behaviour for different viewing and illumination geometries and therefore contains information on the canopy structure. Finally, atmospheric properties like cloud cover or aerosol content change the quality (direct and diffuse) of the light and affect the retrieval of surface reflectance (Jackson and Huete, 1991; Huete *et al.*, 2002).

I.2.3.3 Sun-induced chlorophyll fluorescence

The second type of spaceborne observation evaluated in this thesis is SIF. The physiological and biogeochemical mechanisms causing the emission of radiation by chlorophyll have been explained in section I.2.2.2. I will now briefly outline how this tiny signal can be tracked from space and afterwards discuss the relationship between SIF and GPP at the ecosystem scale.

I.2.3.3.1 Spaceborne measurement

The retrieval approach In the near infra-red, fluorescence constitutes only about one to five percent of the total top-of-atmosphere radiance. Disentangling the contribution of such a weak signal from the one of solar radiation reflected at the Earth's surface to the at-sensor-radiance is therefore challenging. Retrievals exploit the fact that the magnitude of SIF relative to the solar reflected radiation is higher in solar (Fraunhofer lines) or telluric absorption lines compared to spectral ranges outside the absorption features in the continuum (Meroni *et al.*, 2009). Different retrieval approaches have been developed and applied to sensors that were originally designed for atmospheric measurements. In fact, SIF may interfere with the retrievals of atmospheric chemical components from these instruments.
In this thesis, I mainly analysed one SIF data set (Köhler *et al.*, 2015a), which was derived by using a statistical approach to model top-of-atmosphere radiance spectra (Guanter *et al.*, 2012; Joiner *et al.*, 2013). Measurements to which the retrieval was applied were taken by the GOME-2 instrument onboard the satellite MetOp-A. It has an equator crossing of 9.30 a.m. local time and a footprint size of 80 km x 40 km (since July 2013 40 km x 40 km with halved swath width). Theoretical global coverage is achieved in

1.5 days (three days). The spectral range to estimate the amount of SIF (retrieval window) used by Köhler *et al.* (2015a) covers wavelengths between 720–758 nm. The retrieval window hence encompasses the far-red peak of the SIF spectrum at 740 nm (Fig. I.7). The basic idea to disentangle the contribution of SIF is that any top-of-atmosphere radiance spectrum can be modelled by a set of spectral functions (principal components) plus a spectrally resolved reference SIF emission shape. The principal components are derived from spectra recorded over reference targets, such as deserts, ice, and oceans.
Several aspects need to be considered when evaluating this and other SIF data sets. Here, I want to mention three of them in particular: the effects of cloud cover, the South Atlantic Anomaly (SAA) and of the satellite overpass time. It has been shown that cloud cover leads to decreasing absolute SIF values due to a shielding effect. However, empirical and simulation based analysis suggest that the impact on temporal patterns is limited when screening just for thick clouds and high cloud frations in the field of view (Frankenberg *et al.*, 2012; Guanter *et al.*, 2015; Köhler *et al.*, 2015a). A second aspect to be aware of is the SAA, a region in the southern Atlantic off the Brazilian coast where the magnetic field of the Earth presents a weak anomaly. This allows cosmic particles to penetrate to the altitude of the satellite orbit. The comparatively higher flux of cosmic particles in this region causes higher photon fluxes at the sensor and higher retrieval noise. High caution is therefore necessary when interpreting GOME2 SIF data over the south-eastern coast of South America. A third aspect to be aware of is a drift in the orbit of MetOp-A that causes slightly earlier local overpass times over the years and a negative trend in the retrieved SIF.

I.2.3.3.2 What SIF can tell us about GPP - The Monteith model for SIF SIF is approximated in a similar way like GPP (equation I.1) with a model following the idea of Monteith (1972) with only the LUE-term being different.

$$SIF^{\lambda} = fPAR * PAR * LUE_f^{\lambda} * \epsilon_{escape}^{\lambda} = APAR * LUE_f^{\lambda} * \epsilon_{escape}^{\lambda} \quad \text{(I.2)}$$

$$GPP = SIF^{\lambda} * LUE_p/(LUE_f^{\lambda} * \epsilon_{escape}^{\lambda}) \quad \text{(I.3)}$$

The term $LUE_f{}^{\lambda}$ incorporates the fraction of absorbed energy that is quenched as chlorophyll fluorescence. $\epsilon_{escape}^{\lambda}$ describes the escape probability of the fluorescence photons of a given wavelength from the canopy for a fixed structure and chlorophyll content (Porcar-Castell *et al.*, 2014; Damm *et al.*, 2015). Both terms have a dependency on observation wavelength λ. In the following, the individual terms of the Monteith-model are explained in a bit more detail.

The role of APAR The magnitude and temporal evolvement of SIF depends on changes in the fraction of incident PAR that is absorbed, i.e. on the amount of leaves and chlorophyll pigments. The expected added value of SIF with respect to spectral reflectance measurements is here that it is only sensitive to fPAR from photosynthesising material and not affected by woody material, litter or other material that contributes to absorption of PAR but not to photosynthesis.
Next, SIF - like GPP - depends on the amount of incoming PAR. Importantly, canopy structure creates differences in the light quality and quantity that penetrates the canopy. For example, the top layers of a leaf and of a canopy receive the highest intensities of

light and will contribute the most to the total signals of both(Porcar-Castell *et al.*, 2014). Taken these two terms together, SIF hence can represent a powerful proxy of absorbed radiation by photosynthesising material (green APAR), an important driver also of GPP (cf. eq. I.1). This is based on the assumption of a temporally constant $LUE_f^\lambda * \epsilon_{escape}^\lambda$.

The role of light-use-efficiency The term LUE_f represents the efficiency with which absorbed energy is quenched as fluorescence ('fluorescence yield'). At the molecular level, the quenching efficiencies of fluorescence (LUE_f) and photochemistry (LUE_p) have a light dependent relationship. Under low light, photochemical quenching and fluorescence compete for excitation energy at low NPQ. Photochemical efficiency decreases with light as more PS are closed and energy is re-emitted as fluorescence. At higher light intensities, NPQ is up-regulated, the yield of heat dissipation progressively increases and lowers the energy amounts going to both fluorescence and photochemistry. Thus, at high light intensities LUE_p and LUE_f are positively correlated (van der Tol *et al.*, 2009; Porcar-Castell *et al.*, 2014; Damm *et al.*, 2015). It needs to be emphasized that the relationship of LUE_p and LUE_f is not direct but depends on the activity of physiologically controlled heat dissipation NPQ, and the seasonal dynamics of it are not yet clearly understood (Porcar-Castell *et al.*, 2014).

The role of canopy structure Finally, when moving from the molecular level to the leaf and canopy level, canopy structural effects need to be taken into account.
Canopy structure does not only affect the penetration of solar light into the canopy, but also the emission of SIF from the canopy (and in the leaf, Porcar-Castell *et al.*, 2014; Damm *et al.*, 2015). $\epsilon_{escape}^\lambda$ describes the fraction of emitted SIF from the leaf that eventually leaves the canopy. The escape probability is essentially a function of the amount of leaves and their angular and vertical distribution in the canopy, the observation direction and the wavelength of the measurement. Red fluorescence is strongly reabsorbed in the canopy and also within a leaf. Chlorophyll content affects this process (Daumard *et al.*, 2012; Fournier *et al.*, 2012). Up to 90% of the fluorescence emission in the red wavelength region is reabsorbed (Gitelson *et al.*, 1998), with remarkable influences on the shape of the fluorescence spectrum (red fluorescence saturates compared to far-red fluorescence), on the absolute magnitude at a given wavelength as well as on the contribution of PSI and PSII to this signal. Far-red fluorescence is more strongly scattered due to the missing pigment absorption. Consequently, fluorescence in the red wavelengths mainly originates from the upper canopy layers while fluorescence at longer wavelengths will also contain information on lower layers in the canopy (Porcar-Castell *et al.*, 2014).

Taking together the similarity of the Monteith LUE-models of SIF (eq. I.2) and GPP (eq. I.1) as well as the positive relationship between the efficiencies of fluorescence and photochemical quenching at sufficient light levels like is typical for the overpass times of the satellites, the measurement of SIF might serve the following purposes: The first one is the reliable approximation of variations in the amount of APAR by only photosynthetically active pigments and without any saturation effects with respect to GPP. If the effects of APAR, fluorescence yield and structure on SIF can be disentangled as well as an understanding of the (temporally and spatially changing) effects of NPQ on the relationship between the two yields can be achieved, SIF observations might secondly also serve as an indicator of changes in photochemical efficiency (Porcar-Castell *et al.*, 2014).

It needs to be emphasised that the sensitivity of SIF to both changes in PAR and to variations in LUE_p promises that changes in plant activity and health can be detected from satellite before and without any changes in greenness (fPAR) occur. If this is found to be true, it would represent a major step forward in the state-of-the-art of Earth observation with respect to traditional spectral reflectance observations as early stress detection would become feasible. This is of particular practical importance regarding crop yields and food supply to a growing world population.

I.2.3.3.3 From theory to observations: the relationship between SIF and GPP

Linearity at ecosystem scale In contrast to the hyperbolic relationship between instantaneous chlorophyll fluorescence and carbon assimilation observed at leaf level, both are more linearly related on time scales of days to seasonal and on the canopy and ecosystem level. This has been learned from both process-based modelling exercises (Damm *et al.*, 2015; Zhang *et al.*, 2016a) as well as from model-data inter-comparisons at the global scale (Frankenberg *et al.*, 2011b; Guanter *et al.*, 2012). The simultaneous development along the season of incoming PAR and canopy structure/ fPAR linearise the relationship between SIF and GPP as does the temporal aggregation to longer time periods. The strong effect of canopy development/ structure in time is supported by several studies that stress changes in APAR as the dominant driver of SIF and find only secondary effects of carboxylation capacities (Verrelst *et al.*, 2015; Zhang *et al.*, 2016a; Migliavacca *et al.*, 2017) or physiological parameters in general (Koffi *et al.*, 2015; Norton *et al.*, 2018).

Specifics related to the ecosystem Though mostly observed to be linear, the relationship between satellite far-red SIF and best estimates of GPP is ecosystem-specific (Guanter *et al.*, 2012; Damm *et al.*, 2015). This dependency on plant functional types can be explained by differences between species in how and how strongly physiological processes and therefore the relationship between LUE_f and LUE_p are regulated (Damm *et al.*, 2015). In addition, although they possibly have similar absorption capacities (fPAR), different canopy architectures between species can create very different light environments, resulting in ecosystem-specific APAR. Further, SIF is affected by canopy and observation geometries in that it depends on the fraction of shaded and sun leaves in the field of view (Verrelst *et al.*, 2015) and the canopy gap fraction in the direction of the sensor. This is not the case for GPP which refers to the whole canopy and not only the part the canopy visible to the sensor. In contrast to that, recently, a universal relationship between GPP measured at eddy-covariance towers and satellite-retrieved SIF from the OCO-2 sensor has been shown (Sun *et al.*, 2017).

SIF changes in the absence of greenness changes As mentioned earlier, the sensitivity of SIF to the amount of incoming PAR and the relationship between LUE_p and LUE_f potentially make SIF an important indicator of early plant stress and changes in photosynthesis *before* any effects on canopy structure occur. Ground and airborne experiments have shown that passive measurements of SIF indeed relate to changes in GPP in the absence of any changes in vegetation indices (Zarco-Tejada *et al.*, 2013; Rossini *et al.*, 2015).

Limitations of SIF to indicate GPP Although SIF is intrinsically and directly linked to photosynthetic light reactions, there are also important known limitations of SIF to indicate GPP and it is still debated what the actual information content of currently available SIF data sets with respect to GPP is. The nature of SIF necessitates the separation of the contributions of APAR, LUE_f and ϵ_{esc} to an instantaneous value of which the true absolute value is not known and cannot be ground-truthed. Active research is still required to better address the following problems: 1) The true absolute value/ magnitude of SIF has large uncertainties. Despite largely consistent spatio-temporal patterns, different retrievals yield different value ranges, even if retrieved from the same sensors, because of retrieval-specific effects (related for example to the spectral retrieval window or biases, Köhler *et al.*, 2015a) and radiometric calibration of the instruments. 2) There are almost no ground truth observations available, although initiatives start to grow to put SIF sensors on eddy covariance towers (e.g. Yang *et al.*, 2015). Still, the coarse spatial resolution (compared to ecosystem spatial heterogeneity and the ground pixel sizes achievable by spectral reflectance measurements) of spaceborne SIF datasets with global coverage challenges direct comparisons between satellite and ground observations of SIF. Airborne campaigns can help bridge this spatial gap (Rascher *et al.*, 2015; Wieneke *et al.*, 2016) and be directly be compared to satellite measurements (Sun *et al.*, 2017). 3) Although the dependence of SIF on APAR, LUE_f and ϵ_{esc} represents a strong potential, it is a major challenge at the same time because it is not clear how the different contributions to the total SIF can be disentangled. 4) It is further unknown how the relationship between LUE_p and LUE_f can be characterized across time scales of days and seasons and plant functional types as it is highly variable and dependent on NPQ (e.g. Porcar-Castell *et al.*, 2014; Wieneke *et al.*, 2016). In addition, it is not clear, whether the contribution of PSI to the total SIF changes across seasons. 5) Effects of canopy structure in conjunction with the observation geometry introduce a dependency of the measured SIF on the fraction of sunlit and shaded leaves in the field of view as well as on canopy gap fractions that determine ϵ_{esc}. This does, however, not pertain to GPP. 6) Another issue is the spatio-temporal coverage and quality of available global SIF data sets which are not suitable for several types of applications. Decadal trend analysis is impossible due to the comparatively short data record. Sampling by several sensors (though not all) is discontinuous, severely challenging the representativeness of individual soundings for the final aggregated grid cell. Also, low data quality regarding signal-to-noise ratios challenges investigations in low productivity biomes (e.g. Zhang *et al.*, 2016b). These issues partly originate from the fact that the retrievals are applied to sensors that were designed for other purposes than SIF. 7) SIF measurements further represent an instantaneous value at a given time of the day with specific environmental conditions and relatively clear sky. Hence, the measured signal is only representative for this specific instance and not for the status of the ecosystem over the whole day. In case of GOME-2, the morning overpass might cause the observation of an active and healthy ecosystem, while in the afternoon potential water stress might develop. Further, in contrast to the instantaneous SIF observation, GPP usually refers to a daily integrated value with all-sky conditions (including completely cloudy). Therefore, geometrical corrections of SIF are recommended to scale the instantaneous measurement to a daily value based on the ratio between the potential incoming light at the time of the measurement and the integral across the whole day (Frankenberg *et al.*, 2011a; Zhang *et al.*, 2018). Still, this is based on the assumption that the same environmental conditions (including cloud cover) prevail over the whole day, which is never the case. Moreover,

comparisons of SIF retrieved from different sensors with different overpass times need to take into account the different illumination conditions. Similarly, when comparing to vegetation indices, observation and illumination conditions are important. A normalization of SIF accounts for illumination effects on SIF that are not contained in the vegetation indices. However, noise might get amplified by this correction.
As a consequence of missing knowledge on all these confounding and ecosystem-specific effects, currently, SIF cannot directly be translated into absolute values of GPP. Still, patterns of spatio-temporal variability of GPP can be inferred from SIF and useful constraints for terrestrial biosphere models to estimate GPP on a global scale (Parazoo *et al.*, 2014; MacBean *et al.*, 2018). In the following I summarize the most important studies on ecosystem functioning and photosynthetic activity that evaluated spaceborne SIF observations.

Summary of selected available studies that apply spaceborne SIF to infer information on GPP First global comparisons of spatio-temporal patterns between SIF and best estimates of GPP showed comparable or even better relationships between SIF and GPP than between GPP and vegetation indices. The former were found to be highly linear, while the latter saturate (Frankenberg *et al.*, 2011a; Daumard *et al.*, 2012). Good agreement between the seasonal patterns of satellite SIF and GPP inferred from eddy-covariance towers and from GPP models has been found in several biomes (e.g. Guanter *et al.*, 2014), particularly in deciduous vegetation. Biases in the length of the growing season inferred from reflectance-based approaches have been found (Joiner *et al.*, 2014; Yang *et al.*, 2015; Zhang *et al.*, 2016b). APAR, or rather $\mathrm{APAR}_{\mathrm{chlorophyll}}$, is found to merely couple SIF with GPP (Yang *et al.*, 2015; Zhang *et al.*, 2016b). Yang *et al.* (2017) observationally confirm influences of chlorophyll content, leaf area index and NDVI to canopy SIF and the high correlation between ground measurements and satellite-based canopy SIF. However, also close relationships between the yields of fluorescence and photosynthesis in both models and *in-situ* are reported (Yang *et al.*, 2015; Zhang *et al.*, 2016b). Reductions in SIF during major drought and heat events (Russian heat 2010, Great Plains drought 2012 and Texas drought 2011) were consistently found to agree with the spatio-temporal patterns in GPP. These reductions were caused by both structural changes (leaf senescence) reducing APAR, particularly in grasslands and crop lands, as well as by reductions in $\mathrm{LUE_f}$, the major effect on SIF in forests (Sun *et al.*, 2015; Yoshida *et al.*, 2015). Others have investigated the seasonality of tropical evergreen forests to address the ongoing debate on whether these forests (with an emphasis on the Amazon) are light- or water-limited during the dry season (Parazoo *et al.*, 2013; Guan *et al.*, 2015; Köhler *et al.*, 2018) and which consequences major drought events like the Amazon 2010 drought (Lee *et al.*, 2013) or the strong El Niño 2015/16 (Liu *et al.*, 2017a) have on the ecosystems. SIF apparently can indicate changes in photosynthesis in the absence of changes in greenness/ leaf area through its sensitivity to $\mathrm{LUE_f}$, which has been shown in the Russian (Yoshida *et al.*, 2015) and also in the tropical forests (Lee *et al.*, 2013) as well as in grasses treated with herbicides (Rossini *et al.*, 2015). Furthermore, satellite SIF has been employed to constrain crop GPP (Guanter *et al.*, 2014) and crop yields (Guan *et al.*, 2015). Empirically inferred GPP from SIF suggests that productivity in the major crop regions of the world is currently underestimated by 50–75% (Guanter *et al.*, 2014). Finally, assimilation of SIF observations into process-based models reduced parametric uncertainties in the estimate of global annual GPP, mostly by constraining APAR (Koffi *et al.*, 2015; Norton *et al.*, 2018)

and lead to a redistribution of GPP between the boreal and the tropical zones (Parazoo *et al.*, 2014; MacBean *et al.*, 2018). Also the timing of the modelled GPP fluxes improved after SIF assimilation (Parazoo *et al.*, 2014; Thum *et al.*, 2017).

I.2.3.4 Eddy-covariance measurements of CO_2 fluxes and empirical upscaling

I.2.3.4.1 Eddy-covariance

Measurement principle Currently, the most precise method to measure fluxes of CO_2 (and also of water and energy, here the focus is on CO_2) between the atmosphere and the land surface at ecosystem scale are eddy-covariance (EC) measurement systems. Biogenic processes in the soil and vegetation change the concentration of CO_2 in a parcel of air. Fast turbulent movements of the air in the atmospheric boundary layer will transport the different air parcels up and down. Three-dimensional sonic anemometers mounted on poles or masts can measure the three directional wind speed components with a very high frequency. Doing the same with infra-red spectral gas analysers additionally delivers high frequency information on the gas concentration in the air. Due to the eddy movements, both the vertical wind speed as well as CO_2 concentrations turbulently fluctuate around a mean value over a certain integration or sampling time. The average of the co-varying fluctuations in the vertical wind component and in the gas concentration will be proportional to the flux density of CO_2 between the land and the atmosphere. The high measurement frequency of 10 to 20 Hz and the typical measurement integration time of half to one hour allow to capture variations on all time scales from minutes to years while excluding effects of diurnal changes in atmospheric conditions. The measurements are non-invasive and cover larger footprint areas of several hundred meters up to approximately 1 km^2. However, reliable measurements of NEE are restricted to flat areas of homogeneous vegetation cover. Moreover, turbulence needs to be sufficiently strong and atmospheric conditions steady. In stable atmospheres, the air parcels do not reach the sensor fast enough compared to the measurement time but remain undetected below the sensors ('storage'). Storage additionally becomes important in high canopies like forests and during non-steady atmospheric conditions, hence in day-night transitions between respiration and GPP as well as between nighttime stable and daytime stronger convective conditions in the boundary layer. Careful corrections and post-processing of the measurements are necessary with respect to advection with the mean horizontal flow, storage, instrument placement on the tower with respect to the wind direction as well as calibration and sensor drifts. Data gaps of between 25-35% in a year occur due to system failure or maintenance, low turbulence conditions, spikes in the raw data, a too strong vertical wind component, lack of energy balance closure (i.e. often the surface net radiation is larger than the sum of turbulent fluxes of the energy and the ground heat flux) or due to management practices in agricultural areas (Baldocchi *et al.*, 2001).

Flux partitioning The measured, quality-controlled and possibly gap-filled time series of NEE measurements can be partitioned into the component fluxes gross ecosystem productivity and respiration. Different approaches have been proposed and are continuously refined for the purpose of partitioning. One method consists in exploiting the fact that at night no photosynthesis happens, but only respiration in the soil and the plants. Respiration usually depends on temperature. It also has a time dependent component that

accounts for example for the carbon supply from photosynthesis that depends amongst others on phenology/ the time of the year. Based on the night-time fluxes, a temperature sensitivity of the respiration is established that is then extrapolated to daytime using ancillary temperature measurements (e.g. Reichstein *et al.*, 2005). The difference between measured NEE and modelled respiration gives an estimate of gross ecosystem assimilation. A second approach proposed by Lasslop *et al.* (2010) mainly uses daytime EC measurements to model NEE as the sum of a light-dependent response curve including the effect of vapour pressure deficit on GPP and a temperature-based approximation of respiration. Several similar approaches and refinements exist, though, and the different methods partly give considerably different results (Reichstein *et al.*, 2005).

I.2.3.4.2 Empirical up-scaling of EC-measurements

A global network of EC sites A global network of EC sites exists that collects valuable information on the functioning and carbon balance of various ecosystem types. Data are collected and pooled in various projects and the global FLUXNET initiative aims to make these data publicly available with a standardised quality check and post-processing procedure (https://fluxnet.ornl.gov/). The locations of the sites have not been selected in a geostatistical sense but rather depend on funding, suitability as well accessability and local research interests. Therefore, the spatial distribution of EC sites is strongly biased towards Europe, the US and China. Several towers exist in Australia and South America. Africa and Asia are very much undersampled. There is barely EC data from inaccessible areas, like polar regions or the tropics. Despite the heterogeneous spatial coverage, the sites span a wide range of climatic conditions and plant functional types. Still, EC are point measurements and strictly valid only for the flux tower footprint resulting in extrapolation problems (Baldocchi *et al.*, 2001).

Empirical up-scaling the carbon fluxes to the globe For global estimates of the net and gross fluxes of carbon between the land surface and the atmosphere (as drivers of the global carbon balance) these *in-situ* observations represent a valuable basis. The information from EC sites can be exploited by trying to learn and understand the dependency of the carbon fluxes on the land surface, atmospheric, soil and nutrient conditions for different ecosystem types and to use this knowledge to spatially up-scale the fluxes from the tower to the globe. Machine learning algorithms are trained with site-level data on the fluxes and additional ancillary measurements and information on important drivers of plant activity and respiration. Global data sets of these drivers, mostly derived from satellites, subsequently serve as predictors for global estimates of GPP, respiration and NEE (Jung *et al.*, 2009; Beer *et al.*, 2010; Jung *et al.*, 2011; Tramontana *et al.*, 2016). Overall, the selection of explanatory variables has an important impact on the modelled carbon fluxes (Tramontana *et al.*, 2016). Several data sets with varying spatial (on the order of 1 km to 0.5°) and temporal resolution (daily to monthly) have been generated covering large parts of the satellite era. They generally represent seasonal patterns and variability among sites very well, with best performance for GPP (Jung *et al.*, 2011; Tramontana *et al.*, 2016). NEE is least well simulated as small errors and uncertainties in GPP and respiration can have a comparatively large effect on their difference. These up-scaled products inherently depend on the availability, quality and quantity of training data and the environmental conditions that they cover. Therefore, empirically up-scaled fluxes

naturally have higher uncertainties in regions with few or missing towers (e.g. Papale *et al.*, 2015) and do not predict anomalies well. Further, they are less representative in managed areas, as the human impact is highly dynamic, diverse and currently cannot be modelled properly for lack of explanatory data sets. Another limitation is the duration of available EC time series to cover long-term changes and interannual variability. Those are generally not well reproduced by the empirical models (Jung *et al.*, 2011; Tramontana *et al.*, 2016). Similarly, effects of disturbances, legacy effects and recovery from them are not captured well because of missing information in the training data, their localized nature and the (in-)ability of the machine learning algorithms to account for lagged effects. Next to those issues related to the spatial and temporal representativeness of the *in-situ* measurements, other sources of uncertainty arise from uncertainties in the derived empirical relationships, uncertainties, biases or gaps in driving data, uncertainties in the processing and partitioning of the EC-flux data, and missing explanatory variables (Beer *et al.*, 2010; Jung *et al.*, 2011).

The data sets used in this thesis have been produced in the FLUXCOM project (Tramontana *et al.*, 2016, http://www.fluxcom.org/). The FLUXCOM GPP serves for cross-comparing the observations and results obtained from analysing remotely sensed vegetation indices and SIF with respect to the dynamics of global vegetation cover. An ensemble of models is established to understand and limit uncertainties in the up-scaled model GPP. In that, different global meteorological reanalysis data sets are used to reduce GPP uncertainties related to uncertainties or biases in the explanatory data. In FLUXCOM, a set of different machine-learning methods is trained to get an estimate of the uncertainty effect due to the capability of the different regression algorithms to reproduce and extrapolate to different environmental conditions. Further, training is done on site-level carbon fluxes for two different partitioning methods.
Two ensemble set-ups will be introduced in the comparison in this thesis: the remote sensing (RS) runs and the meteo runs. The former are driven exclusively by spaceborne observations of land surface temperature, reflectance-based indices on greenness and water content and APAR. The RS data set has a very high spatial resolution of 1/12° and a temporal one of eight days. In contrast to that, the meteo runs are produced daily but at a coarser spatial resolution of 0.5°. They are driven by a combination of remotely sensed information on the mean seasonality of greenness and vegetation water content as well as meteorological reanalysis data on air temperature, soil moisture and global radiation. Both ensemble set-ups depend on prescribed land cover /plant functional types.

I.2.3.5 Models of plant carbon assimilation

I.2.3.5.1 Model approaches Although not employed in the work of this thesis, it needs to be mentioned that the empirical up-scaling of EC is not the only category of models to simulate exchange processes of carbon, water and energy between the land surface and the atmosphere. There are several other types of models of the terrestrial biosphere that are widely used to infer carbon fluxes of the land surface. In process-based models, the relevant biophysical and biochemical processes and functional relationships are prescribed by explicit parameterised equations. Models differ in the selection and way of process representation. Classes of models include models of enzyme kinetics (Farquhar *et al.*, 1980), of light-use-efficiency based on the Monteith-theory (cf. section I.2.2.2.2,

Monteith, 1972), or of carbon assimilation models which first calculate potential photosynthesis v_{cmax} and downscale this value based on empirical relationships with environmental conditions (Fisher *et al.*, 2014). The models can be run in a diagnostic mode assimilating ancillary information e.g. from satellites, or they can be run in a prognostic set-up.

I.2.3.5.2 The usefulness of satellite observations for the modelling of vegetation Satellite-based observations can inform the modelling in several ways. First of all, they can serve as reference data sets in model-data comparisons. Further, they can teach us about feedback mechanisms and responses of vegetation to environmental conditions. The observations can therefore help to better formulate and parameterise processes and alleviate uncertainties in process models which have uncertainties as a result of limited process understanding (Rogers *et al.*, 2017). Another aspect is related to the prescription of realistic values of light-use-efficiency, which is an important source of error in diagnostic models (e.g. Turner *et al.*, 2006). Spaceborne measurements can further be an important source of information with respect to APAR as an important controlling variable of GPP. Vegetation indices can indicate the development of leaves and pigments and hence fPAR, while SIF intrinsically depends on APAR of photosynthesising pigments. This makes them an important driver for e.g. the phenology and the seasonality of photosynthesis in models that do not predict them themselves (e.g. Luus *et al.*, 2017). At the same time, biased information from satellites can also be an important source of error in the models (Turner *et al.*, 2006). In the case of SIF, they can also be used as a direct constraint on photosynthesis parameters in process-based models (Parazoo *et al.*, 2014; Koffi *et al.*, 2015; Thum *et al.*, 2017; MacBean *et al.*, 2018; Norton *et al.*, 2018).

I.3 Objectives and research questions

In view of the previous sections it becomes obvious that photosynthesis by the terrestrial vegetation represents a key process affecting the global carbon budget and climate. Spaceborne approaches are indispensable to monitor the status of the plants on the land surface. There is no direct measurement of photosynthetic activity available. Instead, research relies on spectral reflectance as a proxy for potential photosynthesis and also a result of photosynthesis. SIF as a more direct proxy of photosynthetic activity is measurable from space, but the available datasets need to be evaluated and cross-validated. Remote sensing can also help to empirically upscale EC GPP data to the globe. This model GPP is predicted with satellite measurements as driving variables[6]. Vegetation indices are proxies for greenness, SIF and model GPP proxies of photosynthesis. This thesis explores the three complementary approaches for selected biomes and study cases and evaluates the temporal dynamics seen in them with respect to carbon fixation. The aim is to find answers to the following questions:

- Where on Earth can we find agreement between the trajectories of greenness, SIF and state-of-the-art estimates of GPP (model GPP)? In which biomes do the spatio-temporal patterns of greenness, SIF and model GPP differ and why?

[6]It needs to be emphasised that SIF is not included in the set of explanatory variables for model GPP as included in this thesis, whereas proxies of greenness are.

- Is there an added value of current satellite SIF data with respect to reflectance measurements to indicate temporal dynamics of GPP and if so, where and when?
- Can the contributions of fPAR, PAR and emission efficiency (cf. Monteith model of SIF, eq. I.2) to the observed far-red SIF be disentangled and are they plausible regarding our understanding emerging from laboratory and field experiments?

Variability patterns can be explored on various timescales. In this work, temporal dynamics will be analysed with respect to the phenological/ seasonal patterns as well as to changes to it.
The term phenology traditionally refers to periodically recurring life cycle events of plants and describes a sequence of significant eco-physiological changes. The transition from one phenological stage to another includes effects on both, the photosynthetic performance and the morphology of the plants. Here, morphological and photosynthetic phenology are distinguished. In this thesis, the term morphological phenology refers to the trajectory of greenness and hence rather to the traditional meaning of the word. Typical events of morphological phenology are bud burst, leaf unfolding, maturity, and senescence. It hence refers to the abundance and quality of leaves. Conversely, the term photosynthetic phenology describes the trajectory of photosynthetic activity or production/GPP in this thesis. It is a function of photosynthetic capacity driven by both, chlorophyll concentration and environmental conditions affecting the photosynthetic performance. Morphological and photosynthetic phenology do not necessarily co-vary. Recalling the summarising findings of Restrepo-Coupe *et al.* (2016) on the (dis-)agreement between photosynthetic potential and actual activity in Australia, a close temporal relationship between greenness and GPP is given if:

1. there is a sensible seasonality in greenness.
2. the seasonality of GPP is driven by greenness/morphological phenology
3. or meteorology is synchronous with morphological phenology and they jointly drive GPP (and GPP does not change between being controlled by morphological phenology or meteorology at different times in the year).
4. productivity is not exclusively driven by meteorology in the absence of seasonality in photosynthetic potential/greenness.

There have been observations of a temporal shift between the anatomical and the functional development of the canopy of some vegetation types, which also necessitates the differentiation between morphological and photosynthetic phenology (Richardson *et al.*, 2011; Shen *et al.*, 2014; White *et al.*, 2014; D'Odorico *et al.*, 2015). In addition, unfavourable environmental conditions cause a down-regulation of photosynthesis and a mismatch between photosynthetic and morphological dynamics.
Phenological patterns are analysed and compared for selected biomes, namely boreal forests (Chapter II) and tundra (Chapter III). Both biomes are very important and vulnerable parts of the terrestrial carbon cycle and represent major challenges for reflectance based monitoring. Boreal forests are evergreen with a small seasonality in greenness. Photosynthetic down-regulation by low temperatures and long periods of darkness and snow cover render the traditional remote sensing of photosynthetic annual cycles difficult in these forests. Tundra landscapes are characterized by low and often sparse vegetation

exhibiting a small seasonality as well. Further, many lakes, snow, ice, and frequent cloud cover confound observations of green biomass on the surface. For boreal forests and tundra specific questions are:

- Which are typical phenological dates like start, peak and end of the growing season as indicated by greenness, SIF and model GPP? How can possible differences between proxies be explained?
- Are phenological changes in photosynthetic activity traceable using SIF that do not coincide with changes in greenness?
- If so, can the observed decoupling be explained by changes in PAR and/or by changes in LUE_f?

In the third study case in this thesis (Chapter IV), the focus is on the effects of water availability on phenological patterns globally. The natural sequence of typical seasonal events might be disturbed by unusual and/or extreme environmental conditions. Also a shift in the regular timing of seasonal environmental events might shift the usual phenological event timing. Given the emerging importance of water availability for plant photosynthetic activity, specific questions to be answered are:

- Globally, which are the phenological alterations observed in different ecosystems that occur in times of changing soil moisture as indicated by greenness, SIF and model GPP?
- How can differences between ecosystems in the phenological shifts in the vegetation proxies associated with soil moisture deviations be explained?
- Can purely physiological changes be separated from greenness changes?

CHAPTER II

SATELLITE CHLOROPHYLL FLUORESCENCE MEASUREMENTS REVEAL LARGE-SCALE DECOUPLING OF PHOTOSYNTHESIS AND GREENNESS DYNAMICS IN BOREAL EVERGREEN FORESTS

Sophia Walther[1], Maximilian Voigt[1], Tea Thum[2], Alemu Gonsamo[3], Yongguang Zhang[1,4], Philipp Köhler[1], Martin Jung[5], Andrej Varlagin[6], Luis Guanter[1]

This manuscript has been submitted to *Global Change Biology* on June, 15th 2015, accepted on December, 5th 2015 and published online on December, 18th 2015. It has been published in 2016 in volume 22, number 9, pages 2979–2996, with the doi https://doi.org/10.1111/gcb.13200.

Author contributions:
LG and SW designed the research; YZ, PK, MJ and AV kindly provided data used in the analysis; SW conducted the analysis with appreciated help from MV in parts of the data processing; SW, LG, TT, AG, MJ contributed to the interpretation of the results; SW wrote the manuscript with highly valued feedback from TT, YZ, MJ, LG.

[1]GFZ German Research Centre for Geosciences, Helmholtz-Centre Potsdam, Section 1.4 Remote Sensing, Germany
[2]Finnish Meteorological Institute, Helsinki, Finland
[3]Department of Geography, University of Toronto, Canada
[4]International Institute for Earth System Sciences, Nanjing University, Nanjing, 210023, China
[5]Max-Planck-Institute for Biogeochemistry, Jena, Germany
[6]A.N. Severtsov Institute of Ecology and Evolution, Russian Academy of Sciences, Moscow, Russia

Abstract

Mid-to-high latitude forests play an important role in the terrestrial carbon cycle, but the representation of photosynthesis in boreal forests by current modeling and observational methods is still challenging. In particular the applicability of existing satellite-based proxies of greenness to indicate photosynthetic activity is hindered by small annual changes in green biomass of the often evergreen tree population and by the confounding effects of background materials like snow. As an alternative, satellite measurements of sun-induced chlorophyll fluorescence (SIF) can be used as a direct proxy of photosynthetic activity. In this study, the start and end of the photosynthetically active season of the main boreal forests are analysed using spaceborne SIF measurements retrieved from the GOME-2 instrument and compared to that of green biomass, proxied by vegetation indices including the Enhanced Vegetation Index (EVI) derived from MODIS data. We find that photosynthesis and greenness show a similar seasonality in deciduous forests. In high-latitude evergreen needleleaf forests, however, the length of the photosynthetically-active period indicated by SIF is up to six weeks longer than the green biomass changing period proxied by EVI, with SIF showing a start-of-season of approximately one month earlier than EVI. On average, the photosynthetic spring recovery as signalled by SIF occurs as soon as air temperatures exceed the freezing point (2-3 °C) and when the snow on the ground has not yet completely melted. These findings are supported by model data of gross primary production and a number of other studies which evaluated *in-situ* observations of CO_2 fluxes, meteorology and the physiological state of the needles. Our results demonstrate the sensitivity of space-based SIF measurements to light-use efficiency of boreal forests and their potential for an unbiased detection of photosynthetic activity even under the challenging conditions interposed by evergreen boreal ecosystems.

II.1 Introduction

Mid-to-high latitude forests are a substantial contributor to carbon fluxes (e.g. Beer *et al.*, 2010), constitute a large carbon pool globally (Thurner *et al.*, 2014) and are expected to react in a very sensitive way to global warming (Lenton *et al.*, 2008). Despite their important role in the global carbon cycle the modelling of the carbon fluxes between the atmosphere and the land surface is still challenging. Simulations show a large spread in the predicted magnitudes, often the timing is inaccurate and/or the models do not truly represent interannual variability (Jung *et al.*, 2011; Huntzinger *et al.*, 2012; Keenan *et al.*, 2012; Richardson *et al.*, 2012; Schaefer *et al.*, 2012; Anav *et al.*, 2015). Biases in the predicted gross primary production (GPP, gross carbon flux from the atmosphere into the plants) in early spring and late autumn make the simulations prone to errors in determining the respective start and end of the season (Schaefer *et al.*, 2012). Thus, knowledge of the seasonality of photosynthesis of the terrestrial vegetation cover gained from spatially and temporally extensive observations is highly relevant. This calls for a global, spatially resolved technique to monitor carbon fluxes and ecosystem functioning, especially in the arctic/boreal zone where *in-situ* observations are sparse and spatially biased (Schimel *et al.*, 2015).

Satellite observations of the surface reflectance are a widely used approach to infer the amount of green biomass on Earth and the photosynthetic potential of the terrestrial vege-

tation cover. Often this is done using vegetation indices (VIs), which are a combination of reflectances in different spectral bands designed to enhance the sensitivity to green vegetation (e.g. Huete *et al.*, 2002). In vegetation with large seasonal greenness changes, where leaf phenology and carbon uptake are strongly connected (Hadley *et al.*, 2009), reflectance based tracking of greenness provides good estimates of the seasonality of GPP (Shen *et al.*, 2014). However, greenness indices have a low sensitivity to short-term variations in GPP (e.g. Yang *et al.*, 2015). Another major drawback of surface reflectance measurements is that they suffer from seasonally changing contamination by shadows, snow and other canopy backgrounds, non-photosynthetically active plant materials and the atmosphere. Although greenness indices have been proven useful to delineate potential GPP for many biomes (e.g. Xiao *et al.*, 2004) the limitations to indicate photosynthetic activity become particularly evident in boreal evergreen needleleaf forests (ENF). Here greenness changes cannot be well distinguished from the signals driven by the annual snow cover (e.g. Delbart *et al.*, 2005; Beck *et al.*, 2006; Böttcher *et al.*, 2014). More than half of the annual change of greenness indices has been found to be caused by snow in many boreal evergreen areas (Delbart *et al.*, 2005; Jönsson *et al.*, 2010). In contrast to deciduous broadleaf forests (DBF), in ENF changes in biomass related to bud burst, shoot elongation, needle growth and shedding are small and slow and in sparse forests influenced by the understorey vegetation (Jönsson *et al.*, 2010; Böttcher *et al.*, 2014). Also, as opposed to photosynthesis, greenness indices are not reduced down to zero in ENF in dormant periods, hence they do not provide an unambiguous index on when actual photosynthesis starts or ends. Ongoing efforts to exploit reflectance-based observations to indicate GPP seasonality also in boreal ecosystems have lead to the development of improved vegetation indices with lower sensitivity to snow and background changes and higher consistency in the relationship to canopy development and GPP. Examples are the plant phenology index (Jin and Eklundh, 2014) or the phenology index (Gonsamo *et al.*, 2012; D'Odorico *et al.*, 2015).
Still, to monitor GPP in boreal evergreen areas, indicators of instantaneous physiological function are needed. A promising example is the photochemical reflectance index PRI (Gamon *et al.*, 1992; Peñuelas *et al.*, 1995) which has been shown to be related to photoprotective mechanisms in a leaf and hence to photosynthetic light use efficiency Φ_p (e.g. Gamon *et al.*, 1992; Peñuelas *et al.*, 1995; Gamon *et al.*, 1997; Nichol *et al.*, 2000; Barton and North, 2001; Garbulsky *et al.*, 2011; Wong and Gamon, 2014, 2015). However, there does not yet exist a global PRI data set which can be applied at ecosystem level and studies employing PRI have mostly been limited to the leaf and stand scale due to influences of background material and understorey, illumination and viewing conditions, canopy structure/LAI, nutrient status, atmospheric effects, very low temperatures and overlapping physiological effects that confound the interpretation of PRI at different temporal and spatial scales (Gamon *et al.*, 1992, 1997; Nichol *et al.*, 2000; Barton and North, 2001; Garbulsky *et al.*, 2011; Porcar-Castell *et al.*, 2012; Wong and Gamon, 2014, 2015; Damm *et al.*, 2015).

Complementarily to that, satellite measurements of sun-induced chlorophyll fluorescence (SIF) offer the possibility to monitor actual photosynthetic activity. After the first global retrievals of satellite-based SIF were accomplished in 2011 (Joiner *et al.*, 2011; Frankenberg *et al.*, 2011b), strong positive seasonal correlations between SIF retrieved from GOSAT and GOME-2 and GPP from model simulations and flux-tower estimates have empirically been found for different biomes (Frankenberg *et al.*, 2011b; Guanter *et al.*, 2012; Lee *et al.*,

2013; Parazoo *et al.*, 2013; Joiner *et al.*, 2014). Yang *et al.* (2015) report on high diurnal and seasonal correlations between satellite and ground-based SIF and tower GPP in deciduous forests. Also, first initiatives to constrain model GPP with SIF brought remarkable results in that the adapted GPP values and seasonalities are in closer agreement with flux tower measurements (Guanter *et al.*, 2014; Parazoo *et al.*, 2014; Zhang *et al.*, 2014). The exact behaviour of the positive relationship between SIF and GPP varies with retrieval wavelength, biome, canopy structure, temporal scale and stress level (e.g. Guanter *et al.*, 2012; Damm *et al.*, 2015; Rossini *et al.*, 2015).

Complex photosynthetic processes underlie the relationship between SIF and GPP. In the light reactions of photosynthesis, energy from solar photons is absorbed by pigments and transferred to reaction centres in so-called photosystems. A chain of reactions and electron transport eventually leads to the storage of the energy in chemical compounds. In the dark reactions, this energy is consumed in biochemical processes to fix carbon and produce sugars (photochemical quenching, resulting in GPP; Jones and Vaughan, 2010). What we approximate with surface reflectance measurements and VIs is the amount of absorbed photosynthetically active radiation (APAR). However, due to both, intrinsic limitations of the photosynthetic machinery and external stress factors, the APAR cannot completely be used for carbon fixation. Excess energy is re-emitted from the leaf at longer wavelengths, which is termed chlorophyll fluorescence, or dissipated as heat (non-photochemical quenching, NPQ). Chlorophyll fluorescence can be evaluated as a proxy for the activity of photosystems of type II and its electron transport rate (PSII, there exist also photosystems of type I with a rather constant but non-negligible contribution to SIF, also dependent on the wavelength of the retrieval; Maxwell and Johnson, 2000; Baker, 2008; Rossini *et al.*, 2015). The fluxes of SIF and GPP have been modelled and observed to be positively correlated, albeit with variable strength in response to environmental conditions and the activity of NPQ (van der Tol *et al.*, 2009; Frankenberg *et al.*, 2011b; Guanter *et al.*, 2012; van der Tol *et al.*, 2014; Damm *et al.*, 2015).
In ENF, which are the focus of this work, Wong and Gamon (2015) find that CO_2 exchange and the activity of PSII, or more precisely the electron transport away from it, start to recover at similar times in spring (see the beginning of the positive slope in Fig. 4 in Wong and Gamon, 2015). As SIF is a proxy for the PSII electron transport eventually leading to GPP, we expect this positive seasonal relationship between SIF and GPP to hold at the synoptic scale. As an example for ENF, Fig. II.1 shows the time series of GPP over a homogeneous spruce stand at the flux tower site Fyodorovskoye, Russia, in 8-day time resolution and sampling together with the satellite observations of SIF from the GOME-2 instrument within a radius of 30 km of the tower site. They have very similar timing of spring and autumn transitions and often even react in parallel on the short time scale of some weeks. These are compelling examples that support the assumption that SIF provides an unambiguous indication of photosynthetically active periods (Yang *et al.*, 2015).

This study focuses on the seasonality of photosynthesis in mid-to-high latitude forests. To further our understanding of the functioning of boreal forested ecosystems, even under the challenging conditions in ENF, we complementarily use the information content of greenness and satellite SIF. The obtained results are related with meteorological data sets to identify the main environmental factors driving the photosynthetic activity of boreal

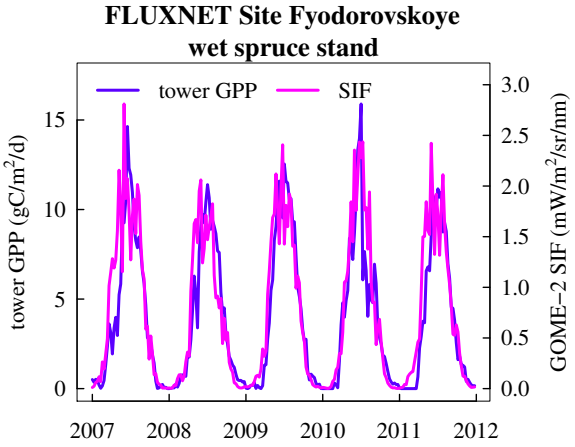

Figure II.1: Comparison of flux tower GPP observations and the satellite SIF measurements from the GOME-2 instrument (Köhler *et al.*, 2015b) within 30 km of the Russian tower site Fyodorovskoye (56.4615° N, 32.9221° E).

ecosystems, especially the evergreen ones, at synoptic scales.

II.2 Method and data

II.2.1 Data

All data sets are evaluated from January 2007 to December 2011. They are all averaged to a 0.5° grid and sampled every 8 days with an average over the 16-day period following a sampling date.

Sun-induced chlorophyll fluorescence is retrieved from measurements of the GOME-2 instrument onboard the MetOp-A satellite which crosses the equator close to 9.30 local solar time. The retrieval is done in a wavelength range between 720 and 758 nm and measurements taken with an effective cloud fraction of >50 % are discarded (Köhler *et al.*, 2015b). The resulting daily SIF data with a native pixel size of approximately 40 by 80 km^2 are gridded in 0.5° cell boxes and binned in 16-day intervals with a sampling every 8 days. Please note, that with SIF we exclusively refer to satellite retrievals of the sun-induced chlorophyll fluorescence *flux*, which is different from the fluorescence yield or efficiency (Φ_f, fluorescence flux divided by APAR) and other related fluorescence parameters often employed in *in-situ* studies with active measurement techniques.

The enhanced vegetation index EVI (Huete *et al.*, 2002) and the normalized difference vegetation index NDVI (Tucker, 1979) are calculated from NBAR surface reflectance measurements from the MODIS instrument in a 0.05° spatial resolution (MCD43C4, v005, combination of MODIS measurements onboard Terra and Aqua). NBAR means reflectances are normalized to nadir from multi-angular, cloud-free, atmospherically corrected measurements using the bidirectional reflectance distribution function for the solar angle at

local noon time[7]. The reflectances in the MCD43C4 product are a weighted average over 16 days ascribed to the first day of a corresponding 16-day period. We calculate the VIs from the NBAR reflectances instead of using the official MODIS vegetation index product in order to minimize potential seasonal effects of the illumination geometry. The resulting time series are filtered, in that only retrievals with up to 'moderate' quality (quality flag in the MODIS files 0-best/75% or more with best full inversions, 1-good/75% or more with full inversions and 2-mixed/75% or less full inversions and 25% or less fill values) are retained. As reflectances are strongly affected by the occurrence of snow, a snow correction is necessary. The snow flag provided by the MCD43C4 files indicates the percentage of sub-pixels that are covered with snow[8]. Identification of snow is done via different criteria[9] using the normalized difference snow index, band 1 and band 2 and the NDVI. This snow flag is used to identify pixels containing snow (similar to Zhang *et al.*, 2006), which are then removed from the data sets. We tested for a stricter quality filtering using only retrievals with best and good quality (flags 0 and 1) and for less strict criteria in the snow filter allowing 10% and 30% snow. The results largely remain the same (section I.1 of the supporting information).

As a complementary data source, the NDVI3g data stream has been included in the analysis (https://nex.nasa.gov/nex/projects/1349/). It is a GIMMS AVHRR time series improved for usage in high latitudes (compared to its predecessor) in native 0.0833° resolution with 15-day temporal resolution. It is a maximum value composite (MVC) with unknown exact day of acquisition and no direct correction for bidirectional reflectance effects (Guay *et al.*, 2014). We assigned a value to the first day of a possible acquisition period, i.e. days 1 and 16 of a month, as also in the MODIS files the values correspond to the 16-day period starting at the indicated date. It has been quality filtered using the flags provided in the data files. Values flagged 4, 6 or 7 (possibly containing snow or missing) have been discarded. In contrast to all other data sets NDVI3g is evaluated at the native 15-day resolution and bimonthly sampling.

Model data for GPP stem from an ensemble of statistical, remote sensing (MODIS) data-driven models used to empirically upscale flux tower measurements to the global scale (FLUXCOM, Jung et al. 2015, in prep.). These models employ machine-learning techniques and have been shown to perform well in representing seasonal patterns (Jung *et al.*, 2011). The median of 18 ensemble members (nine different machine-learning techniques and two different methods to partition flux tower measurements into GPP and respiration) is taken as representative for GPP. These model GPP data have a native resolution of 0.083° and 8 days.

Meteorological variables provided by the European Center for Medium-Range Weather Forecasts (ECMWF) ERAInterim data set (Dee *et al.*, 2011b) are used to evaluate the dependency and interaction of SIF, model GPP and the VIs with environmental conditions. We use 2 m air temperature, soil temperature, soil water content and photosynthetically active radiation arriving at the surface (PAR). ERAInterim data provide soil measures (volumetric water content and temperature) in 4 layers: 0-0.07 m depth, 0.07-0.28 m,

[7] http://landweb.nascom.nasa.gov/QA_WWW/forPage/C005_Change_BRDF.pdf
[8] There are 36 sub-pixels per 0.05°x0.05° box.
[9] http://modis.gsfc.nasa.gov/data/atbd/atbd_mod10.pdf

0.28-1.0 m and 1.0-2.89 m. Complete information on the forest conditions cannot be provided by a single layer. This is because the sensitivity of the trees to soil temperature and available water does not only depend on the vertical rooting distribution and depth but also on soil composition and the resulting hydraulic conductivity (Plamboeck *et al.*, 1999). In this analysis, we chose the second layer between 7 and 28 cm depth. The uppermost layer will not reliably indicate the available amount of water and temperature conditions to the trees as their rooting will extend to greater depth. The lowest layer will be important for the forests but it is weakly affected by meteorology and may contain the groundwater level and hence we do not expect it to be a crucial factor in (inter-)annual phenology. We use the second rather than the third layer to enlarge comparability of our results with *in-situ* ground measurements which usually are taken in 2, 5, or 10 cm depth. Qualitatively the results do only slightly change when the third layer is used as the timing of the annual peaks and minima is shifted a little (not shown). PAR is produced as an accumulated variable over a certain time range, hence the PAR values contain information on both the actual radiation arriving at the surface and the day length. The data have a spatial resolution of 0.5°. The native temporal resolution is 6 hours (or 12 hours for accumulated variables like radiation).

Identification of the forest area of interest is based on the IGBP (International Geosphere-Biosphere Programme) classification scheme and the data provided in the MODIS MCD12C1 v051 data file for 2009. We take 2009 as representative for the whole period under investigation between 2007 and 2011. The IGBP data have a spatial resolution of 0.05°. To aggregate them to 0.5°, we allocate the vegetation class to a 0.5° pixel where the majority of the underlying 0.05° subpixels belong to. To verify a certain level of homogeneity in the vegetation cover type, we only use those grid boxes in the evaluation where the frequency of subpixels belonging to a certain vegetation type is at least 75%. The threshold of 75% is chosen as a compromise between assuring high homogeneity and at the same time retaining sufficient pixels for a meaningful analysis. This correction is expected to influence and clarify the results as Klosterman *et al.* (2014) found larger biases in some satellite derived transition dates in comparison to local observations for heterogeneous pixels.

Further, we divide the forest areas classified by IGBP into ecoregions as they are delineated by Olson *et al.* (2001) [10]. Polygons are rasterized to 0.5° by again asigning the ecoregion with the largest cover fraction to a pixel.

Northern hemisphere forests are shown in Fig. II.4a. The focus in this study is on boreal forests, which we delineate as north of 50° N.

II.2.2 Method

White *et al.* (2009) compare different methods to determine key phenological dates of the growing season from the same data set and report that methods vary widely in the determined date of phenological phases, their variability, retrieval ability and their ordinal ranking. Hird and McDermid (2009) find that function fitting outperforms other noise reduction techniques in preserving the original shape of the time series (at least applied to NDVI time series). We chose the function fitting method proposed by Gonsamo *et al.*

[10] http://www.worldwildlife.org/publications/terrestrial-ecoregions-of-the-world

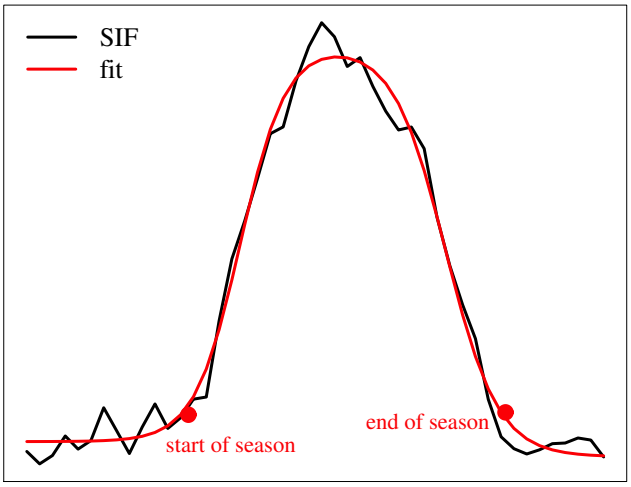

Figure II.2: Example of a real time series of satellite-based SIF data, the fitted double-logistic function and the start and end of season derived from it.

(2013) as a means to objectively quantify phenology. Here, the term phenology is used as a synonym for the research on periodically recurring events in biological life cycles in general and not limited to the study of morphological developments of plants. The method consists in fitting a double sigmoidal function to a complete cycle of vegetation development via non-linear least squares (Gonsamo *et al.*, 2013).

$$t(x) = a_1 + \frac{a_2}{1 + exp(-d_1(x - b_1))} - \frac{a_3}{1 + exp(-d_2(x - b_2))} \tag{II.1}$$

Equation (II.1) has been adapted to our time series with a maximum of 2000 iterations and a minimum step size of 10^{-6}. If no convergence is achieved, up to ten additional fitting attempts with slightly changed first guesses for the fitting parameters are done. Additionally to the weighting applied in Gonsamo *et al.* (2013), relatively smooth periods of the time series are 'rewarded'. The central point of a three-point running median is double-weighted if it is within ±25% of the median value. This is intended to deal with the relatively high noise level of SIF retrievals, especially in winter. The fitting procedure has been applied pixelwise for all five years of data availability (2007-2011). As the analysis is limited to forests in middle and high latitudes, it is sufficient to carry out the fitting procedure yearwise as only one vegetation cycle will be completed in one year. Details on the performance of the fitting can be found in section I.2 of the supporting information. To derive the starting point in time of phenological phases, Gonsamo *et al.* (2013) provide easy to apply formulae using the coefficients of the fitted function. The characteristic phases employed here are

1) start of season (SOS) or onset: $SOS = b_1 - \frac{4.562}{2d_2}$

2) end of the season (EOS) or dormancy in case of evergreens: $EOS = b_2 + \frac{4.562}{2d_2}$

The equations for the transition dates have been analytically derived from the extrema of the derivatives of the fitted functions and describe the curvature behaviour of the time series/fit. That means that they represent times when vegetation starts to progress from one state to another. Hence, the phenological markers inferred from the fitted double-sigmoidal function have biophysical meaning, which is the main reason for choosing this approach. Other possible methods to determine SOS and EOS might be unphysical. For example, the crossing of fixed thresholds of the annual amplitude as a measure for start and end of season neglects the fact that spring onset is generally a faster process than the rather gradual autumn senescence (Stöckli *et al.*, 2008; Elmore *et al.*, 2012). Fisher *et al.* (2006) discuss the short-comings of various other methods to quantify phenology and advocate the midpoint instead of the start of increase/decrease as the most robust measures for SOS/EOS. As this corresponds to the date of the most rapid growth/senescence and not to the absolute starting and ending times we decided to apply the SOS/EOS measures above by Gonsamo *et al.* (2013). Figure II.2 shows a SIF time series together with the fitted function and the transition dates inferred from it.

II.3 Results

II.3.1 Mean annual cycle and phenological transition dates

As a first step in the analysis, we spatially average the VIs, model GPP and SIF over DBF (east coast of North America, see Fig. II.4a) and ENF (whole northern hemisphere north of 50° N) and compare the median of the five annual cycles in Fig. II.3.
In Fig. II.3a we see that in DBF the seasonality of the photosynthesis proxy SIF, the model GPP data and the greenness index EVI are very similar. Sharply increasing values are observed from the start of April followed by the annual maximum by the end of May. In summer, between June and September, slightly declining photosynthetic activity and EVI are observed, before a rapid autumn shut-down follows from September to November. This decline of photosynthesis in summer has also been observed by several studies but its causes are still discussed. Wilson *et al.* (2000) find decreasing photosynthetic capacity (the maximum rate of carboxylation $v_{c_{max}}$) in summer and suggest that changing fractions of nitrogen allocated to the photosynthesis enzyme rubisco might play a major role. Bauerle *et al.* (2012) explain with the help of experiments that decreasing photosynthetic capacity in summer might be regulated by photoperiod. Yang *et al.* (2014) report on a 'summer greendown' of the canopy measured with cameras and MODIS images. EOS_{EVI} is indicated slightly later than EOS_{SIF} and EOS_{GPP} (Fig. II.3a). It has often been reported that greenness indices have a late EOS because the signal is influenced by litter, senesced or dead plant material that has not yet been abscised and NIR scattering at low illumination angles (e.g. Hadley *et al.*, 2009; Jones and Vaughan, 2010; Gonsamo *et al.*, 2012). These effects are weak here in the case of the EVI in comparison to the findings of other studies using the NDVI (e.g. Hmimina *et al.*, 2013). A high degree of variability is also observed in the time series of SIF in summer (similar to Yang *et al.*, 2015), which often parallels the behaviour of model GPP. Further details on that are shown in Fig. A.12 and discussed in the supporting information in section I.4.
The high similarity of SIF to model GPP and the EVI in DBF supports the assumption that photosynthesis and greenness are highly correlated in time and that our methodological framework combining different data sets is consistent. However, the behaviour of the

two NDVI data streams (Fig. II.3a) in DBF is inconsistent in that both tend to increase early, the MODIS NDVI only slightly, NDVI3g significantly. Also, both are characterized by a long summer plateau (in contrast to the declining values in summer in EVI, SIF and model GPP) and late autumn senescence. Similar observations hold for deciduous needleleaf forests (DNF, Fig. A.5 of the supporting information), albeit the lag between the NDVIs and the other three data streams is apparently larger here. The summer plateau can possibly be explained by the well-known saturation effects of the NDVI in high biomass canopies which is not seen in the EVI. Different sensitivities to background changes like wetness and stronger multiple NIR scattering in the canopy at low illumination angles which results in higher NDVI might play a role in the lag between NDVI and EVI from MODIS (e.g. Huete *et al.*, 2002). Diverse behaviour of the two NDVI data sets might originate from distinct compositing methods (averaging vs. maximum value composite) and sensor characteristics between MODIS and AVHRR. The following analysis will mostly focus on the EVI. This is because of the differences of the NDVI to the independent data sets of SIF, model GPP and EVI observed in deciduous forests, where high correspondence between GPP and greenness (Hadley *et al.*, 2009; Shen *et al.*, 2014) as well as low snow influence are expected. Also the EVI can handle background changes better than the NDVI (Huete *et al.*, 2002) which might become evident in a lower noise level in the EVI. Note that the VIs do not return to zero in winter.

When it comes to evergreen forests of the high northern latitudes in Fig. II.3b, the photosynthesis proxies satellite SIF and model GPP again show a very similar seasonal cycle. Both start to indicate photosynthetic activity in late March, while the EVI does not mark greenness changes before late April/beginning of May. This is the most striking difference in this mean seasonal cycle. While in summer and autumn the time series are close to each other, the EVI tends to cease to its annual minimum of about 0.2 approximately two weeks earlier than SIF. The EVI is strongly affected by the quality and snow filtering (section I.1). Apparently there are still some artefacts in the data resulting in variability in winter and early spring (dashed green line in Fig. II.3b). Restricting the MODIS reflectance data to only the ones flagged with good quality will not change the behaviour of this mean seasonal cycle (not shown). The tendency towards a broader growing season observed in deciduous forests of MODIS NDVI and NDVI3g is also present in ENF. NDVI shows a very late autumn senescence and a spring increase much earlier than the EVI increase and at similar times like the SIF and model GPP.

When identifying the SOS objectively with the approach described in the Methods section, Fig. II.4b shows that there is spatial variability in SOS_{SIF} related to latitude and continentality. For example, the SOS in the cold east Siberian DNF and mixed forests in May (DOY 128-144) is in sharp contrast to the relatively early SOS in the beginning of April (DOY 80-96) in the rather temperate ENF in southwestern Canada at the same latitude.
In Figure II.4c the difference in the commencement of photosynthetic activity (SOS_{SIF}) and green-up (SOS_{EVI}) largely exceeds one month in ENF and partly (in northern areas) also in mixed forests. In the southern parts of the mixed forests, where the fraction of deciduous species is expected to be higher, the differences decrease until they are much smaller in the range of $\pm$ 8 days in DBF and DNF. The last column in Table II.1 makes clear that spatially averaged there are no differences between SOS_{SIF} and SOS_{EVI} in DBF,

whereas they amount to approximately 30 days in the whole ENF north of 50° N averaged over all five years.
At the EOS, the map (Fig. II.4d) shows a slightly later EOS_{EVI} in the deciduous forests. However, this amounts to only 5 days in DBF (see Table A.1). At finer temporal and spatial resolution, a lag between leaf phenology/greenness and GPP seasonality has been observed (Shen *et al.*, 2014; D'Odorico *et al.*, 2015) both at the start and end of the growing season in deciduous vegetation. Although the maps in Fig. II.4c,d show a tendency of SIF towards a narrower growing season than EVI in DBF and DNF, these effects cannot reliably be resolved with the temporal and spatial resolution in this study (see also Table II.1). In the mixed forests in western Russia (Fig. II.4d), the EVI shows a delayed EOS by 2-4 weeks. In ENF and mixed forests in North America, Siberia and Fenno-Scandinavia, SIF indicates a later EOS than EVI of two to three weeks, which is in line with what we see in Fig. II.3b. It is remarkable how clear the maps of the phenological dates are able to show the transition between mixed forests and DNF, e.g. in eastern Siberia.
Comparing the length of the growing season (difference of EOS-SOS, Fig. II.4e), the results indicate that the period of photosynthetic activity is five weeks and in individual spots even longer than the 'green phase' identified from EVI in the ENF and northern parts of the mixed forests. It is approximately two to three weeks shorter in the southwestern parts of Russia. In the DBF, EVI indicates up to two weeks longer growing season than SIF.
Comparing the phenological transition dates between EVI and model GPP (Fig. A.6a of the supporting information) the patterns in ENF are similar to those between SIF and EVI, but they partly have larger amplitudes. The differences at SOS between the photosynthesis proxies and NDVI mostly have the same sign as in the comparison to the EVI (Fig. A.6b,c of the supporting information), albeit it needs to be acknowledged that their magnitude is much smaller. At the EOS the patterns observed between EVI and SIF/model GPP are mostly replicated by the NDVI.

Overall, these results show that in deciduous forests the seasonality shown by SIF, model GPP and EVI is very similar, with a slightly late EOS_{EVI}. In ENF, however, the growing season of greenness as indicated by the EVI is approximately five weeks shorter than the one of SIF and model GPP with a much later SOS_{EVI} (more than a month) and a slightly advanced EOS_{EVI} (about one to two weeks).

II.3.2 Sensitivity of SIF to the light-use efficiency of boreal forests

Following a production-efficiency model (Monteith, 1972), SIF and GPP can be approximated as the product of APAR and a yield-term describing the efficiency with which the absorbed light energy is quenched in the photochemical and fluorescence pathway (e.g. Guanter *et al.*, 2014; Joiner *et al.*, 2014).

$$GPP = APAR \cdot \Phi_p = fPAR \cdot PAR \cdot \Phi_p \sim EVI \cdot PAR \cdot \Phi_p \quad \text{(II.2)}$$

$$SIF = APAR \cdot \Phi_f \cdot \epsilon_{esc} = fPAR \cdot PAR \cdot \Phi_f \cdot \epsilon_{esc} \sim EVI \cdot PAR \cdot \Phi_f \cdot \epsilon_{esc} \quad \text{(II.3)}$$

fPAR is the fraction of the incident PAR that is absorbed and can be approximated by the EVI. ϵ_{esc} is a wavelength dependent structural factor describing the fractional escape of fluorescence from the canopy for differently organized canopies. The question arises whether APAR or Φ_f dominate the SIF signal. SIF is a good indicator for green APAR

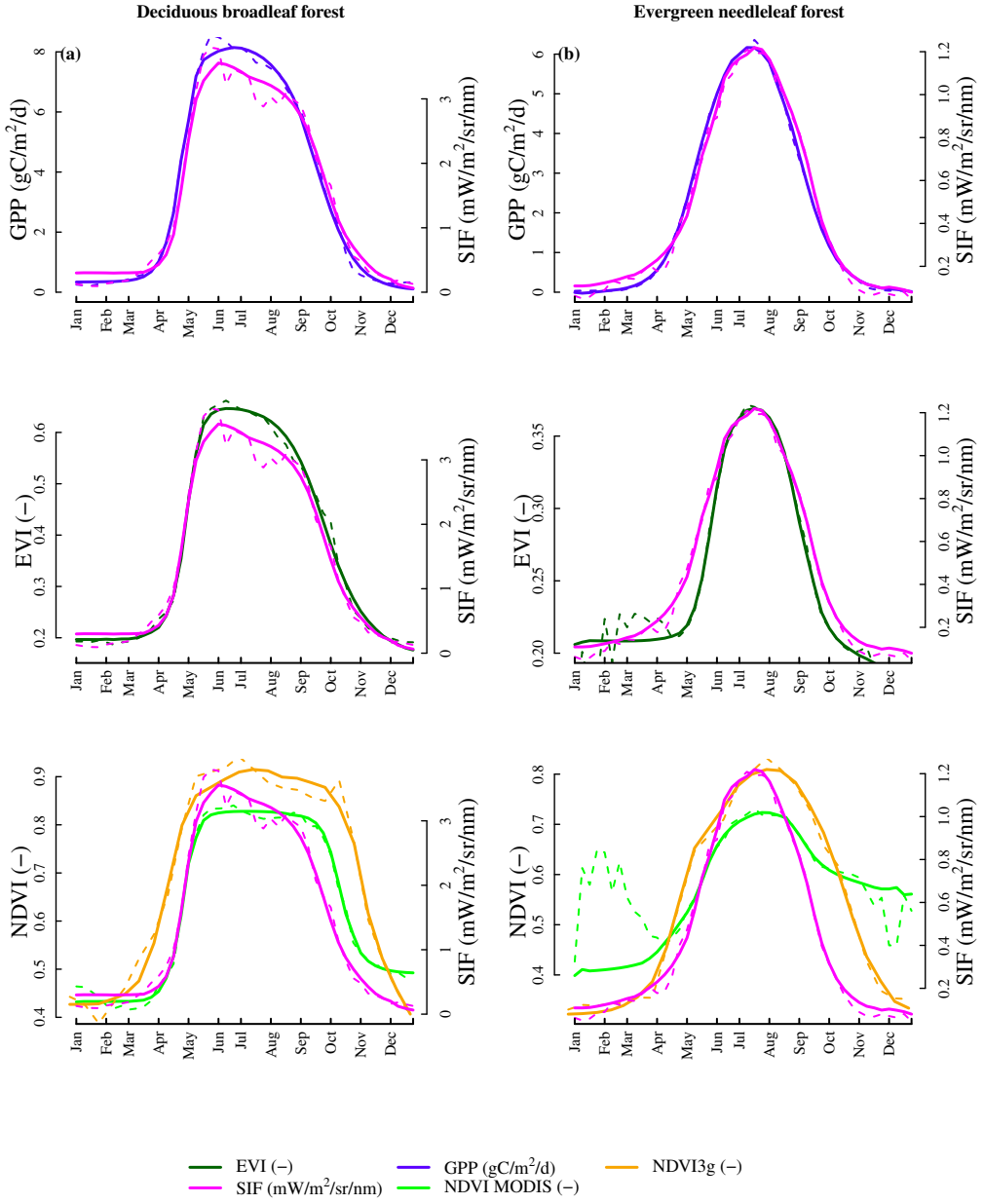

Figure II.3: Median of the annual cycles (dashed lines) and of the fitted functions (solid lines) of SIF, model GPP, EVI, NDVI and NDVI3g over **(a)** deciduous broadleaf forest and **(b)** evergreen needleleaf forest (north of 50° N). Sampling is matched between the fits and the SIF and model GPP time series, but not with the VI time series because of the many missing values in winter in the greenness indices.

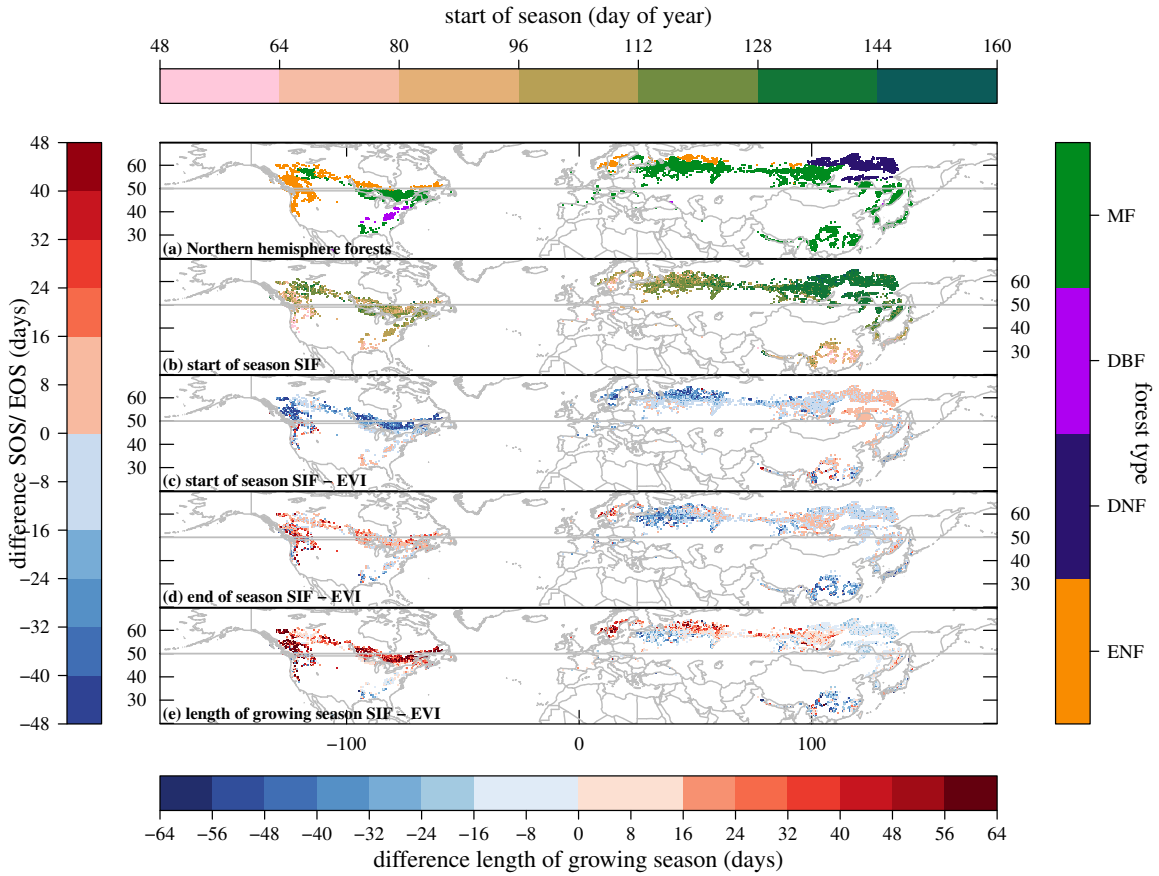

Figure II.4: **(a)**: Forest areas in 0.5° resolution as delineated by the IGBP scheme for the year 2009. ENF: evergreen needleleaf forest; DNF: deciduous needleleaf forest; DBF: deciduous broadleaf forest; MF: mixed forest. **(b)**: Mean calculated start of season for SIF in day of year (upper colour scale). **(c), (d)**: Mean differences in the calculated start and end of season dates between SIF and EVI in days. Colours refer to the left colour bar. Blue colours denote that the respective date is earlier in SIF than in EVI. The resulting average differences in the length of the growing season are shown in panel **(d)** (lower colour bar, blue colours mean a longer growing season in EVI than in SIF).

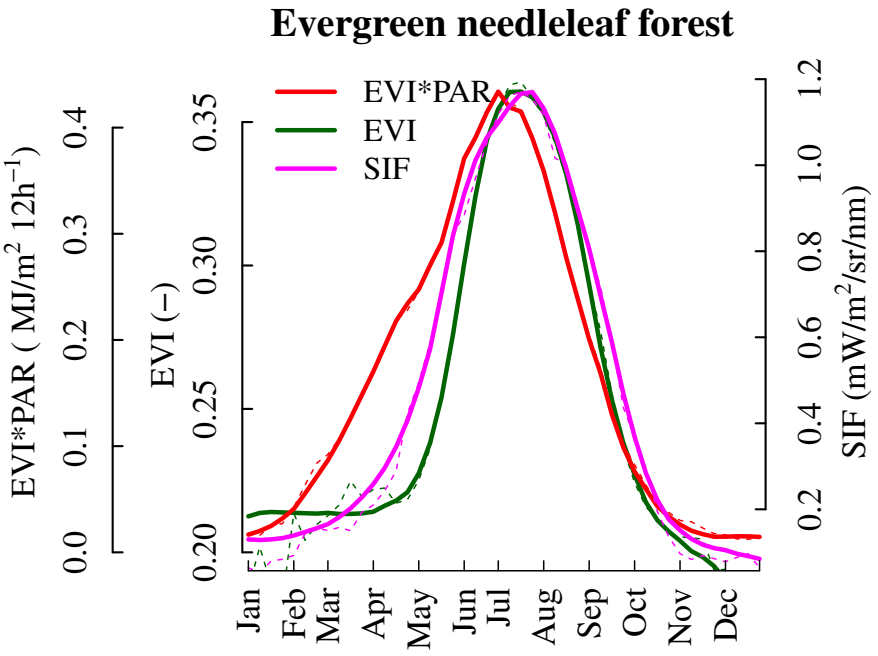

Figure II.5: Median of the annual cycles (dashed lines) and of the fitted functions (solid lines) of SIF, EVI (same as in Fig. II.3) and EVI*PAR (as a proxy for APAR) over evergreen needleleaf forest (north of 50° N). Sampling of the EVI time series is not transferred to the fits and the SIF time series because of the many missing values in winter, but sampling is matched between SIF, SIF fits, EVI fits, and EVI fits*PAR.

which might be very useful for ecosystems in which GPP is driven by canopy chlorophyll content. This may explain the good correlations found between SIF and GPP for crops where stress levels are mostly low (Guanter *et al.*, 2014). But this will not be sufficient for biomes subject to sustained stress periods like the ENF. Comparison of the mean annual cycles of SIF, EVI and EVI*PAR approximating APAR over ENF in Fig. II.5 reveals major differences between them. EVI*PAR clearly has a much advanced seasonal cycle compared to EVI with earlier spring rise, peak and autumn decrease which is also much earlier than in the case of SIF. The fact that SIF and EVI*PAR have distinct seasonal cycles suggests that SIF over ENF is not only driven by APAR but does contain major information on Φ_f. Combination of Eq. II.2 and II.3 offers the chance to deduct knowledge on Φ_p and GPP. The relationship between Φ_p and Φ_f changes gradually in response to stress and environmental conditions. They are positively correlated under NPQ dominance (in high light, most of the day, in the enzyme-limited case) and change the sign of their relationship when light becomes a limiting factor (e.g. van der Tol *et al.*, 2009; Damm *et al.*, 2015). Boreal forests in spring are normally exposed to high light conditions as will be shown in Fig. II.6 and II.7 suggesting a positive relationship between Φ_p and Φ_f. This is an important finding, especially for the carbon cycle modelling community.

II.3.3 Environmental conditions and photosynthetic activity

Having identified the main differences in the seasonal behaviour of SIF and EVI, we studied under what environmental conditions the evergreen forests leave winter dormancy and become photosynthetically active again and green up on the large scale.

As an example for the regional scale, we examine in more detail the ENF of the ecoregion of the Fenno-Scandinavian and Russian taiga (ecoregion number 706 following Olson *et al.* (2001)). This corresponds quite accurately to the ENF in Scandinavia, Finland and Russia up to 60° E (compare Fig. II.4a). The time series in Fig. II.6 confirm the late SOS_{EVI} relative to SOS_{SIF}. Comparing SOS_{SIF} with SOS_{NDVI}, there is also a lag between the commencement of photosynthesis and green-up, although their magnitudes are much smaller than in case of the EVI. Noise in the NDVI in Fig. II.6 is higher than for the EVI (despite the snow filter applied to it) which is another reason why we focus our analysis rather on the latter one.
The meteorological time series in Fig. II.6 show that at the time of SOS_{SIF}, PAR is already at 0.7-0.8 MJ m^{-2} $12h^{-1}$ which corresponds to almost two thirds of the annual PAR maximum in the Fenno-Scandinavian and Russian taiga. The snow flag is indicating that between one and two thirds of the surface are already snow free and the soil water content is reaching its annual maximum at SOS_{SIF}. Average soil temperatures in 7-28 cm depth are close to 0 °C. Mean daily mean air temperatures range between 0 ° and 5 °C and the average daily minimum temperatures (lower bound of gray shading) are just crossing the freezing point when photosynthetic activity commences. Similar observations can be made in North America in the central and mid-western shield forests, which is shown as another example in the supporting information in Fig. A.11. Here the time series also reveal short-term parallel behaviour between SIF and model GPP, e.g. short drops during cold spells in spring and summer.

The same meteorological variables have been averaged over the phenological transition dates of all five years of SIF and EVI and their spatial distribution is displayed in Fig. II.7. The start of the active period indicated by SIF occurs at mean daily air and soil temperatures between 0 ° and 5 °C in the mid-to-high latitude evergreen forests, and it becomes progressively warmer the more mixed and/or deciduous the vegetation gets. Average daily minimum temperatures are slightly negative, but average daily maximum air temperatures are markedly above 0 °C at SOS_{SIF} (shown in section I.3, Fig. A.7). Between 30 and 70% of the surface in ENF is still snow covered, so photosynthetic recovery coincides with the time of snow melt (except for the region south of the Canadian Muskwa-Slave-Lake where the surface is mostly snow free). In the mixed and deciduous forests, SOS_{SIF} takes place after complete snow melt. PAR is already higher than half the annual maximum at SOS_{SIF}. Soil water content at the SOS is highest in the northern most areas for both SIF and EVI and becomes progressively lower to the south of the investigation area (Fig. A.7). For the EVI, this meridional gradient is larger than for SIF, which becomes most apparent in the mixed forests. The conditions are similar between SIF and model GPP and between EVI and NDVI, respectively (Fig. A.8). Their small differences are consistent with the slightly earlier SOS of model GPP than SIF and NDVI than EVI.
In Table II.1 the environmental conditions averaged over the SOS of all five years in all ENF pixels north of 50° N confirm air temperatures between 1 and 3 °C, 72% of the annual illumination maximum and between 37 and 59% (with high variability) ground snow cover

at the start of photosynthesis. At SOS_{EVI} air temperatures are at 9 °C and illumination has reached 90% of its annual maximum. In DBF, SOS is marked at 13 ° C and about 80% of the annual illumination maximum for SIF, model GPP and EVI.

The differences in EOS between SIF and EVI in evergreen forests in Russia, Finland and Scandinavia (Fig. II.6) become slightly smaller than at the SOS and hence also the meteorological conditions are closer to each other. The first snow is accumulating, average daily mean air and soil temperatures are in the range of +5 °C (except 2009, both at 0 °C) and illumination has already been reduced drastically. Only around 0.2 MJ m^{-2} $12h^{-1}$ (17% of annual maximum) PAR reach the canopy at the approximate EOS.
The situation is similar in the evergreen forests in North America in Figures A.9 and A.10. Table A.1 confirms that averaged over all northern hemisphere ENF PAR is everywhere between 15 and 19% of the annual maximum, at EOS_{EVI} still a bit higher than at EOS_{SIF}. Average soil and air temperatures are again close to the freezing point (0-2 °C) at EOS for both SIF and EVI, although in North America temperatures at EOS_{SIF} are slightly lower than for EOS_{EVI}. No or very little snow has already fallen at this time of year (maximum 28% in case of EOS_{SIF}). The conditions are again similar between EOS_{SIF} and EOS_{GPP} and betwenn EOS_{EVI} and EOS_{NDVI} respectively. Striking is an exceptionally early EOS in case of NDVI north of the Great Lakes (Fig. A.7).

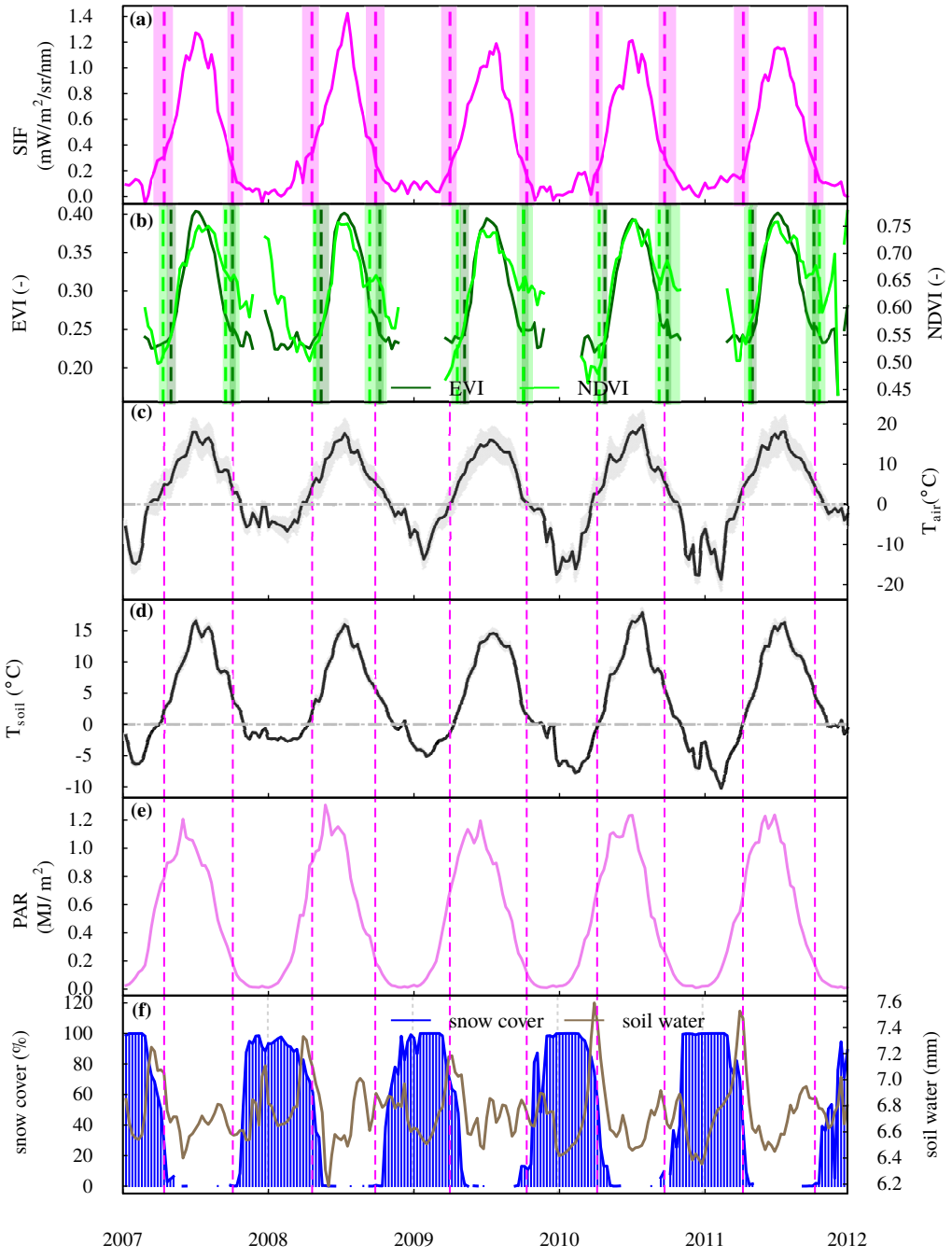

Figure II.6: Evergreen needleleaf forest in the ecoregion of Fenno-Scandinavia and the western part of Russia (ecoregion number 706 in Olson *et al.* (2001), 162 pixels in total): **(a)** Area averaged time series of SIF; dashed vertical lines mark SOS and EOS (spatial median), shaded areas indicate the interquartile range of all identified SOS/EOS in the area in the particular year. **(b)** The same as a) for MODIS EVI and NDVI. **(c, d)** Mean 2 m air and soil (7-28 cm) temperature. The shaded area indicates the range between the mean of daily minimum and the mean of daily maximum temperatures in a 16-day interval. **(e)** Average photosynthetically active radiation reaching the surface (PAR). **(f)** MODIS snow flag indicating the average snow cover in percent of the surface; soil water content in the layer between 7 and 28 cm depth. Sampling of the fits, SIF and the meteorological variables is aligned with each other. However, sampling is not matched with EVI and NDVI time series because of the many missing values in winter. The other way around the sampling of EVI/NDVI time series is aligned with the one of SIF and and the fits.

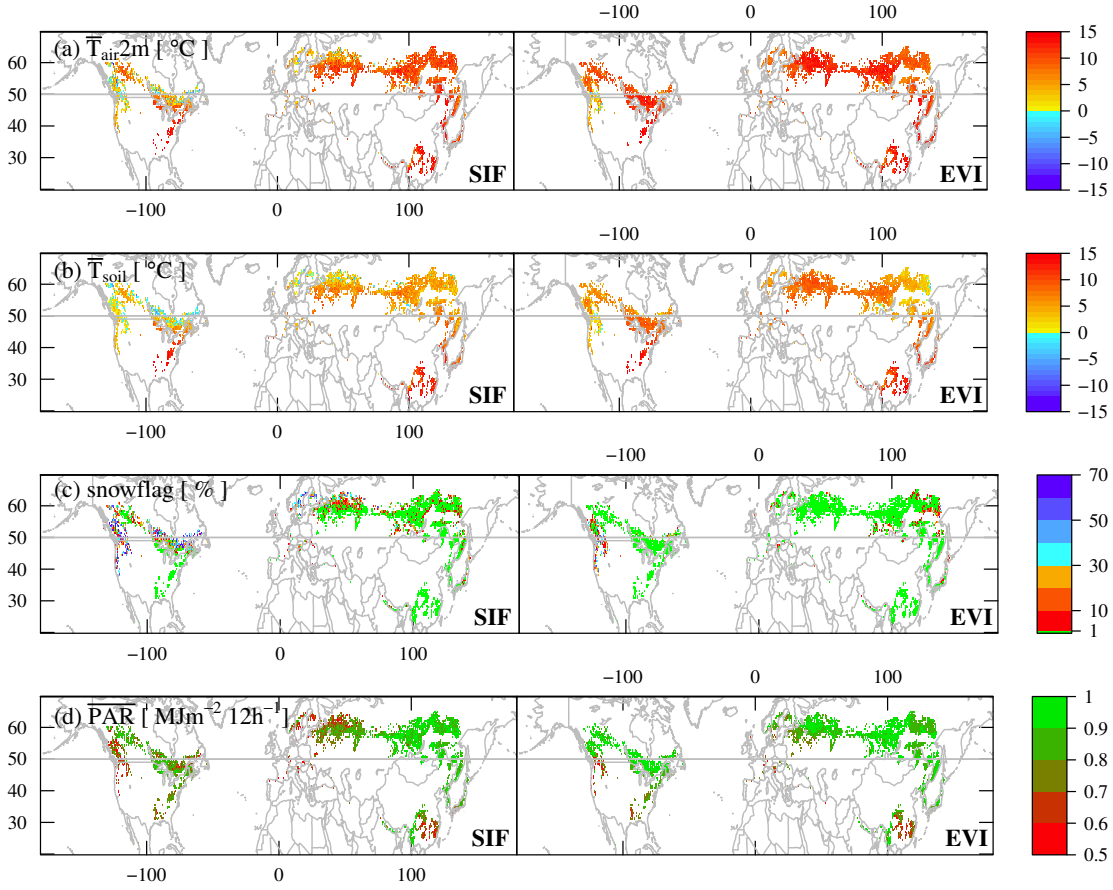

Figure II.7: The maps show the mean temperature conditions of the air and the soil in 7-28 cm depth, the MODIS snow flag and the average photosynthetically active radiation arriving at the surface at the start of season for SIF and EVI.

	$\overline{T_{2m\ air}}$ [°C]	$\overline{T^{min}_{2m\ air}}$ [°C]	$\overline{T^{max}_{2m\ air}}$ [°C]	$\overline{PAR}$ [fraction of annual max]	soil water content [mm]	$\overline{T_{soil}}$ [°C]	snow flag [%]	SOS [DOY]
ENF								
SIF	2.6±6.3	-1.6±5.9	7.1±6.5	72±24	6.8±0.6	0.9±4.4	37±42	103±31
EVI	9.2±3.5	4.5±3.2	13.8±3.9	90±13	6.5±0.5	6.1±2.8	4±16	132±19
GPP	1.2±2.8	-2.9±3	5.6±2.8	72±15	7.1±0.5	-1±2.5	59±39	98±14
DBF								
SIF	13.8±3.1	10±3.1	18.6±3.1	80±8	5.6±0.6	12.6±3	0±0	108±16
EVI	14.2±2.7	10.3±2.7	19±2.7	81±8	5.5±0.6	12.8±2.6	0±0	108±14
GPP	13±2.9	9.1±2.7	17.9±3	77±9	5.7±0.6	11.6±2.7	0±0	102±15

Table II.1: Average environmental conditions and their standard deviation at SOS for SIF, EVI and model GPP in ENF (north of 50° N) and DBF.

II.4 Discussion

II.4.1 Spring recovery in evergreen needleleaf forest

The most important finding of this study is twofold: In the high latitude ENF, green-up lags behind the commencement of photosynthesis as proxied by SIF by several weeks. Further, the seasonal behaviour of SIF is much more similar to model GPP than to APAR, which means that SIF contains information on photosynthetic light-use-efficiency Φ_p in ENF. Both findings are fully consistent with process understanding at the leaf and molecular scale and supported by model GPP data (Fig. II.3, II.4 and II.6, Table II.1) on the synoptic scale and by flux tower observations and dedicated studies at site-level.
Several small scale studies comparing CO_2-fluxes inferred from tower eddy-covariance measurements with maximum photosynthetic light use efficiency Φ_p, satellite VIs and various temperature measures confirm that physiological spring recovery commences before any change in biomass or greenness (Ottander *et al.*, 1995; Tanja *et al.*, 2003; Louis *et al.*, 2005; Arneth *et al.*, 2006; Soukupová *et al.*, 2008; Richardson *et al.*, 2011; Thum *et al.*, 2009; Jönsson *et al.*, 2010; Melaas *et al.*, 2013; Böttcher *et al.*, 2014). We find the magnitude of the temporal lag between green-up and the first signs of photosynthesis to be around one month (Fig. II.4, Table II.1 and Fig. A.6 in the supporting information). This is in accordance with site-level studies, too, as net accumulation of chlorophyll and other pigments as well as bud burst have been observed to occur approximately one month after the first photosynthetic activities (Ottander *et al.*, 1995; Soukupová *et al.*, 2008; Richardson *et al.*, 2011). Wong and Gamon (2015) describe the spring recovery of a series of leaf-level physiological indicators in coniferous species with sigmoidal functions similar to our approach. The approximation of the measurements by logistic functions offers the chance to try to directly compare our SOS on the large scale with the start of spring recovery of the several parameters in their Fig. 4 by visually identifying SOS as the point with the highest curvature change rate/the start of increase (Gonsamo *et al.*, 2013). Please note that this differs in methodology from their approach, which consists in using the half recovery time as SOS. The chlorophyll:carotenoid pigment pool ratio in Fig. 4 in Wong and Gamon (2015) starts to recover several weeks after the commencement of photosynthesis which supports the consistency of our result despite the large gap between the spatial scales.
In the absence of observations at intermediate scales, comparisons between measurements in a satellite footprint and pigments in a leaf can only be of hypothetical nature. Still, we put our second major finding - the similarity between SIF and GPP - into the context of a series of major changes of the chloroplast functioning between winter and spring. In a state of acclimation to low temperatures in winter which inhibit enzymatic and hence photosynthetic activity the trees need to keep a balance between the light energy absorbed and the energy used in carbon fixation. Mechanisms aiming to reach this balance include reduced absorption capacities as a result of lowered relative chlorophyll content (Wong and Gamon, 2015) and effective thermal energy dissipation (NPQ; Ottander *et al.*, 1995; Öquist and Huner, 2003; Ensminger *et al.*, 2004; Busch *et al.*, 2007; Porcar-Castell, 2011; Porcar-Castell *et al.*, 2014; Verhoeven, 2014). Xanthophyll and other carotenoid pigments modulate the thermal energy dissipation by the PSII. Sustained conversion of carotenoid pigments of the so-called xanthophyll cycle and increased relative carotenoid pools lead to high NPQ levels at low temperatures (e.g. Porcar-Castell, 2011; Porcar-Castell *et al.*, 2012; Verhoeven, 2014; Wong and Gamon, 2014, 2015). Next to the pigment pool sizes mentioned earlier the physiological indicators in the study by Wong and Gamon (2015)

include the reversible component of NPQ (in contrast to sustained, which is superposed on the sustained form to allow higher flexibility for the plants; Ensminger *et al.*, 2004; Porcar-Castell, 2011), photosynthetic gas exchange, electron transport rate, photosynthetic light use efficiency and PRI. Identifying again the SOS as the point in time when the values of the several indicators start to increase, their Fig. 4 suggests a close timing of the recovery of the reversible NPQ component, the activity of PSII (indicated by electron transport rate) and of the photosynthetic gas exchange. So both, the activity of PSII (approximated by SIF) and CO_2 exchange (represented by model GPP), have been shown to start to increase at very similar times in Wong and Gamon (2015) *in-situ* and in e.g. our Fig. II.3b at the continental scale which might suggest a similar underlying mechanism. Still, detailed studies are needed to identify the drivers of our observations backed up by investigations across these widely different spatial and temporal scales.

The environmental conditions at the time when SIF starts to indicate photosynthetic activity of PSII on the large scale are very similar to results in site-level studies, too. The PAR amounts incident on the canopy are already high (comparable to the conditions in August, 70% of the annual PAR maximum, Fig. II.6 and II.7, Table II.1). Temperatures, despite still being close to the freezing point (Fig. II.7, Table II.1), have partly released plants from low temperature stress. Thus, our results agree with the general notion in the literature that spring recovery of photosynthetic activity in ENF is temperature driven provided that the canopy is snow free and needles are illuminated. Wind blow, melt and snow sliding off the branches result in a snow free canopy several times during winter and spring. Recovery will not be inhibited in case the ground may still be snow covered as air temperature is the major driver (Tanja *et al.*, 2003; Arneth *et al.*, 2006; Jönsson *et al.*, 2010; Gonsamo *et al.*, 2012, , Fig. II.6, II.7c). As another example at site-level, closer examination of the conditions at the Russian flux tower site Fyodorovskoye reveals that, on average, the photosynthetic recovery commences during snow melt (decreasing snow depth) when there mostly is a uniform snow layer on the ground or the first glades are visible. While the canopy is snow free at SOS_{SIF} and SOS_{GPP}, snow depth on the ground is highly variable and can be as high as 66 cm. The time between the first appearance of snow free spots and complete snow melt ranges between 5 and 15 days at the site. Although snow melt is a gradual process highly dependent on local conditions, this is in accordance with our results on synoptic scales. Despite a decelerating effect of low soil temperatures on the rate of recovery has been reported (Ensminger *et al.*, 2008), a consistent and significant relationship between the frozen/thawed state of the soil and various indicators of photosynthesis has neither been found at site-level (Tanja *et al.*, 2003; Ensminger *et al.*, 2004) nor at the continental scale in our results. The soil temperature is around the freezing point, in some years slightly above at 3 °C, in other slightly below at -2 °C at SOS_{SIF} (Fig. II.6, Table II.1). In the uppermost soil layer (0-7 cm depth) temperatures were always at up to 5 °C, except in spring 2009 at 0 °C (not shown). At the same time the annual soil water maximum is reached or has just passed, so that water cannot be assumed to be a limiting factor at the time of the commencement of photosynthesis.

II.4.2 Limitations and uncertainties

II.4.2.1 Confounding effects of data processing

There are several factors affecting the reliability and quality of the remote sensing products as used in this study. Optical remote sensing in high latitudes is particularly influenced by high sun-zenith angles, atmospheric effects, shadows, snow cover and repeated observations in the visible are often complicated by persistent cloud cover (Stow *et al.*, 2004). Also unambiguous interpretation is confounded by canopy structure and density, contributions of background (soil, snow, wetness, understorey) and non-active plant materials, or heterogeneity of the land cover (other than the targeted one; Jones and Vaughan, 2010; Klosterman *et al.*, 2014; Damm *et al.*, 2015, and many more). Effects which are particularly relevant for the interpretation of our results are discussed in more detail below.

The IGBP land cover classification scheme with a frequency threshold was used to isolate regions with the forest type of interest while at the same time trying to make sure that only pixels with high homogeneity are used in the analysis. We checked the composition of the fine scale (0.05°) land cover classification pixels that are the basis for those 0.5° pixels that go into the analysis. Regarding landscape homogeneity, it can be said that 87.7% of the underlying 0.05° pixels are classified as ENF, 0.01% as deciduous and 4.7% as mixed forests. All other vegetation types contribute each less than 3% to the total number of ENF pixels. Further, the IGBP classification does not give any information on the density, composition, age or other details of the forest canopy. Thus our results may be affected by changing fractions of visible soil/snow background, by the activity and greenness phenology of understorey vegetation and/or of forest types other than the targeted one. From the results presented in the study by Yuan *et al.* (2014), we expect that the understorey, particularly if majorily composed of mosses, has a stronger relative effect on the seasonality of the greenness indices than on the SIF observations and model GPP. Due to the high but still limited homogeneity of the land cover deciduous species with a different leaf phenology and also photosynthetic phenology from the evergreen needleleaf forests will affect the observations. Complete elimination of confounding effects of other vegetation types and varying density cannot be achieved, especially at synoptic scales and the relatively coarse spatial resolution. The numbers above show only marginal mixing of vegetation types which is often limited to the transitional zones between different forest types (not shown).

It can be argued that the difference in start of increase between SIF and EVI is an artefact of the snow filtering procedure applied to the EVI. Although to a lesser extent than the NDVI, the EVI is unstable at the presence of snow (Huete *et al.*, 2002; Dye and Tucker, 2003; Zhang *et al.*, 2004, and Alfredo Huete, pers. comm.). If snow melt and green-up were to overlap in time, both effects could not be distinguished. In this case, it cannot be ruled out that the filtering obscure greenness changes that might occur already before the snow flag indicates that the snow on the ground has completely melted. However, to isolate the greening signal the snow filtering is imperative, and its impact on SOS_{EVI} should be small as a) snow melt cannot unequivocally be distinguished from green-up, b) green-up and snow melt were not found to overlap in time at the local scale (e.g. Böttcher *et al.*, 2014), and c) because less strict filtering thresholds of 10% and 30% surface snow cover were not found to severely affect the identified SOS_{EVI}. This might be due to the

fact that a large part of the snow melts before the ground starts to become visible and that the complete snow melt exposing the ground is very fast then (Clark *et al.*, 2006; Böttcher *et al.*, 2014). If this process proceeds faster than the temporal resolution of the data used in this study allow to see, this might explain these observations. Further discussion on this aspect can be found in the supporting information in section I.1.2. Also the MODIS snow flag gives no information on whether the snow is on the ground and/or on the canopy and on the timing of initial phases of snow melt when the thickness of the snow layer is reduced but the ground not yet visible. Its application for the snow filtering of the VIs might not be the optimum as the snow flag is known not to be perfect. We refrained from additionally applying a surface temperature threshold (similar to Zhang *et al.*, 2006) to filter out potentially snowy pixel values which are not captured by the MODIS snow flag. This might have affected the results too strongly and we trust in the fitting procedure that it can handle potential snow outliers.

Although the results of this study are very promising in the use of satellite based SIF measurements to observe vegetation activity, it needs to be acknowledged that the current satellite SIF data are still relatively noisy, especially at times with high sun-zenith angles. This mostly applies to winter times, but might affect also spring SIF values, which is of course critical in a study that aims at identifying the SOS during spring. It has been put some effort on dealing with this issue and the main outcome of this is the extended 'down-weighting' of outliers in the fitting procedure. From all available SIF data sets, in the GOME-2 data set used in this study (Köhler *et al.*, 2015b) the noise level was lowest in the investigated areas.

All datasets but the NDVI3g have been composited in the same way, meaning that averages over valid values of 16 days are assigned to the first day of a 16-day period and sampled every 8 days. Differences exist between MODIS VIs, SIF and model GPP with respect to the number of valid retrievals per 16-day period, the observation conditions (VZA, SZA, time) and the averaging method over the retrievals of 16 days (weighted vs. unweighted). NDVI3g is different from that in that it is a MVC over 15 days with unknown exact acquisition date. We assigned a value to the first day of a 15-day period with the intention to make it comparable to the other datasets. However, biases are still introduced through MVC in contrast to weighted averaging and we expect the effects of different compositing to be strongest for NDVI3g and weaker between SIF, model GPP and MODIS VIs.

II.4.2.2 Knowledge gaps in the mechanistic relationship between SIF and GPP

Earlier in the Discussion section we addressed possible processes and mechanisms on the molecular and leaf scale that might explain our observations on the large scale. However, as suitable measurements bridging the large gap to the satellite scale are not available, verification of the hypotheses is not possible. Also on the small scale there are several open questions arising from the literature regarding the processes that drive and relate SIF (PSII activity) to GPP (CO_2 fixation) and their temporal acclimation and dependence on external factors. In particular, the seasonal variations of chlorophyll fluorescence, and the relationship to NPQ and photochemical quenching of the excitation energy are not yet clear. Specifically, the strength of the positive relationship between SIF and photo-

chemical assimilation might change due to variable NPQ mechanisms and photoinhibition (Porcar-Castell *et al.*, 2014). Also, NPQ can become light-saturated and in that case PSII activity is driven by the processes that consume the energetic products of the linear electron transport (Baker, 2008). The importance of processes downstream of PSII which consume the energetic compounds formed in the light reactions to fix carbon is highlighted by several studies: Monson *et al.* (2005) report that the factor limiting spring recovery in a coniferous tree the most was the ability to use intercellular CO_2, probably as a result of slow rubisco recovery or synthesis. Soukupová *et al.* (2008) state that PSII can operate at very low temperatures while CO_2 assimilation is rather depressed at temperatures below 5 °C. This leads to seasonally changing relationships between steady-state chlorophyll fluorescence, CO_2 assimilation and the incident photon fluxes on the plant. In line with that, Thum (2009) and Kolari *et al.* (2014) find different seasonal acclimation of the light reactions (maximum electron transport rate, J_{max}) and the carbon fixation reactions ($v_{c_{max}}$). More research is clearly needed to answer the above questions and to be able to fully exploit the information content of SIF complementarily to models and reflectance measurements across the spatial and temporal scales.
Studies finding that the commencement of PSII activity and CO_2 assimilation do not necessarily occur at the same time and/or rate were conducted on fine spatial and temporal scales (Ensminger *et al.*, 2004; Soukupová *et al.*, 2008; Ensminger *et al.*, 2008; Wong and Gamon, 2015), so that this time offset can probably not be reproduced with a temporal resolution of 16 days in this work. Despite this, it needs to be mentioned that the start of increase in photosynthesis (if measured visually as start of increase and not midpoint increase) is very similar to the one of electron transport rate and the xanthophyll conversion and very different from the increase in chlorophyll content in the work of Wong and Gamon (2015), which supports the findings of this study.

II.4.3 Implications and Outlook

We initially assumed that SIF measurements can be used to track variations in GPP at the large scale. In mid-to-high latitude evergreen forests, we find that SIF contains information on photosynthetic light-use-efficiency Φ_p (Fig. II.5) and not only on APAR, which supports our initial premise. Our results confirm a lag between the spring recovery of photosynthesis and green-up that has already been reported at site-level in boreal evergreen forests. This implies that estimates of the SOS purely based on greenness indices will be biased in ENF. This will translate into errors in the spring carbon budget as values of one third to half of the annual maximum of SIF and model GPP are found at SOS_{EVI} both in our results and at site-level (Fig. II.3b, Thum *et al.*, 2009).

Our findings have strong implications for the carbon cycle modelling community, as global SIF measurements from space strongly appear to be apt to constrain parameters in these simulations related to both, leaf phenology and photosynthetic functioning. Especially in the low temperature regime in early spring and late autumn, when carbon models are inaccurate (Schaefer *et al.*, 2012), SIF might bring new insights to improve the simulation results.

For the definition of GPP out of SIF and hence the usage of SIF in carbon models, it

needs to be explained, that SIF is only able to track the light reactions of photosynthesis and therefore cannot directly be translated into GPP (see discussion on knowledge gaps in the mechanistic relationship between SIF and GPP). The scaling between SIF and GPP depends on biome (compare annual maxima of SIF and GPP in Fig. II.3 and see Guanter *et al.*, 2012) and temporal scale (Damm *et al.*, 2015). It is still uncertain to which extent SIF is sensitive to the maximum carboxylation capacity $v_{c_{max}}$ across biomes (Zhang *et al.*, 2014; Koffi *et al.*, 2015), which is an important parameter that determines the magnitude of GPP (van der Tol *et al.*, 2009; Koffi *et al.*, 2015). As discussed in Damm *et al.* (2015) many more aspects related to canopy structure (light environment and absorption, fluorescence escape mostly originates from the upper canopy layers and GPP from the whole canopy) and better process understanding need to be taken into account to translate SIF into GPP. But SIF is strongly dependent on APAR and hence chlorophyll content (at least in the far-red region where SIF is not partly reabsorbed by chlorophyll) and of course on Φ_f (Louis *et al.*, 2005; Porcar-Castell *et al.*, 2014; Koffi *et al.*, 2015), which under NPQ dominance covaries with Φ_p. If Φ_f is largely constant, the fluorescence flux SIF might be used to infer APAR, which is a controlling parameter also for GPP and an important input variable to carbon simulations (Daumard *et al.*, 2012; Koffi *et al.*, 2015). Moreover, the fact that APAR (EVI*PAR) and SIF have different seasonalities over ENF (Fig. II.5) suggests that SIF does not only contain information on APAR but also on Φ_p.

In the study by Wong and Gamon (2015) spring recovery of PRI (which is also related to Φ_p) was timed very close with photosynthesis in conifers. With future research on the confounding effects on PRI mentioned earlier - which partly also apply to SIF and greenness index observations - analysis of PRI combined with SIF and VIs might further our knowledge on vegetation activity (Gamon, 2015; Gamon *et al.*, 2015) and help understand the mechanisms that underlie our observations also at the synoptic scale.

New SIF datasets from the Orbiting Carbon Observatory-2 (launched in July 2014, Frankenberg *et al.*, 2014) and the TROPOMI instrument in the Sentinel-5-Precursor (to be launched early in 2016, Guanter *et al.*, 2015) have a 100 times increase in the number of measurements and a much higher spatial resolution against existing satellite instruments and are expected to bring further new insights into the photosynthetic seasonality, also in boreal evergreen forests.

II.5 Acknowledgements

The work by S. Walther, M. Voigt, P. Köhler and Y. Zhang was funded by the Emmy Noether Programme (GlobFluo project) of the German Research Foundation. The work of T. Thum was funded by the Academy of Finland with grant number 266803. Work by A. Varlagin was funded also by the Russian Science Foundation grant number 14-27-00065. The authors declare no conflict of interest.

CHAPTER III

ASSESSING THE DYNAMICS OF VEGETATION PRODUCTIVITY IN CIRCUMPOLAR REGIONS WITH DIFFERENT SATELLITE INDICATORS OF GREENNESS AND PHOTOSYNTHESIS

Sophia Walther[1], Luis Guanter[1], Birgit Heim[2], Martin Jung[3], Gregory Duveiller[4], Aleksandra Wolanin[1], Torsten Sachs[1]

This manuscript has been submitted to Biogeosciences Discussions on April, 18th 2018 and published as a discussion paper on April, 23rd 2018, https://doi.org/10.5194/bg-2018-196. After discussion the final paper has been accepted in Biogeosciences on August, 28th 2018 and published on October, 26th 2018, https://doi.org/10.5194/bg-15-6221-2018.

Author contributions:
SW designed and conducted the analysis with contributions from all authors. AW processed Sentinel-2 data. SW wrote the manuscript with contributions from all authors.

[1]GFZ German Research Centre for Geosciences, Helmholtz-Centre Potsdam, Section 1.4 Remote Sensing, Germany
[2]Alfred-Wegener-Institut - Helmholtz-Zentrum für Polar- und Meeresforschung Potsdam
[3]Max-Planck-Institute for Biogeochemistry, Jena, Germany
[4]European Commission, Joint Research Centre, Directorate D – Sustainable Resources - Bio-Economy Unit, Ispra, Italy

Abstract

High latitude treeless ecosystems represent spatially highly heterogeneous landscapes with small net carbon fluxes and a short growing season. Reliable observations and process understanding are critical for projections of the carbon balance of climate sensitive tundra. Spaceborne remote sensing is the only tool to obtain spatially continuous and temporally resolved information on vegetation greenness and activity in remote circumpolar areas. However, confounding effects from persistent clouds, low sun elevation angles, numerous lakes, widespread surface inundation, and the sparseness of the vegetation render it highly challenging. Productivity during the peak of the growing season importantly affects the total annual carbon uptake. Here, we conduct an extensive analysis of the timing of peak vegetation productivity as shown by satellite observations of complementary indicators of plant greenness and photosynthesis. The suite of indicators are: (1) MODIS-based vegetation indices (VIs) as proxies of the fraction of absorbed photosynthetically radiation; (2) VIs combined with estimates of absorbed photosynthetically active radiation (APAR); (3) sun-induced chlorophyll fluorescence (SIF) serving as a proxy for photosynthesis; (4) vegetation optical depth (VOD), indicative of total water content; and (5) empirically upscaled modelled gross primary productivity (GPP). Averaged over the pan-Arctic we find a clear order of the annual peak as APAR < GPP < SIF < VIs / VOD. SIF as an indicator of photosynthesis is maximized around the time of highest annual temperatures. Model GPP peaks at a similar time like APAR. The time lag of the annual peak between APAR and instantaneous SIF fluxes indicates that the SIF data do contain information on light-use efficiency of tundra vegetation, but further detailed studies are necessary to verify this. Delayed peak greenness compared to peak photosynthesis is consistently found across years and land cover classes. A particularly late peak of NDVI in regions with very small seasonality in greenness and a high amount of lakes probably originates from artefacts. Given the very short growing season in circumpolar areas, the average time difference in maximum annual photosynthetic activity and greenness/growth of 3 to 25 days (depending on the data sets chosen) is important and needs to be considered when using satellite observations as drivers in vegetation models.

III.1 Introduction

Landscapes in circumpolar regions are characterized by sparse vegetation, bare soil, rocks, large surface areas inundated by open water and a long snow covered period. Despite large carbon amounts being stored in the often permanently frozen grounds, net fluxes of carbon between the land surface and the atmosphere are small and their CO_2 balance is close to neutrality (McGuire *et al.*, 2012). Because of their strong sensitivity to environmental conditions, carbon exchange processes are highly variable in space and time (Olivas *et al.*, 2011; Pirk *et al.*, 2017; Lafleur and Humphreys, 2008; Welker *et al.*, 2004) and an ecosystem might switch between being a carbon sink or source from year to year depending on the weather conditions (Huemmrich *et al.*, 2010b).
Warming happens at accelerated rates compared to middle and lower latitudes (AMAP, 2012). The carbon budgets of both the tundra ecosystem and the Arctic boreal zone as a whole are undergoing major changes – with possibly strong positive feedbacks to climate (Pearson *et al.*, 2013). The future evolution of net ecosystem exchange (NEE) and its com-

ponent fluxes gross primary productivity (GPP) and respiration in Arctic landscapes is highly uncertain. Higher temperatures, the accompanying mineralization as well as higher atmospheric CO_2 concentrations fertilize vegetation (Yi *et al.*, 2014; Zhu *et al.*, 2016; Welker *et al.*, 2004). Accordingly, changes in species composition (Chapin *et al.*, 1995) are observed and satellite records indicate a greening in large regions in the Arctic (Jia *et al.*, 2003; Verbyla, 2008). This is interpreted as increased growth (Racine et al. in Stow *et al.*, 2004; Elmendorf *et al.*, 2012; Huemmrich *et al.*, 2010a; Chapin *et al.*, 1995) or even woody encroachment into the tundra (Racine et al. in Stow *et al.*, 2004; Dass *et al.*, 2016; Sturm *et al.*, 2001). Yet, higher leaf mass and growth do not in every case necessarily linearly translate into enhanced GPP as increased growth might also cause enhanced self-shading and lower nitrogen amounts per unit leaf area (Street *et al.*, 2007; McFadden *et al.*, 2003). A warmer climate might extend the snow free period (Myneni *et al.*, 1997) but there are contradicting indications of whether (Ueyama *et al.*, 2013b; Lund *et al.*, 2010; Kross *et al.*, 2014) or not (Gamon *et al.*, 2013; Oberbauer *et al.*, 1998; López-Blanco *et al.*, 2017; Lafleur and Humphreys, 2008) a longer growing season enhances seasonal carbon uptake and growth. Photosynthetic activity and plant growth further depend on soil moisture conditions (Gamon *et al.*, 2013; Opała-Owczarek *et al.*, 2018; Lafleur and Humphreys, 2008; Welker *et al.*, 2004) and therefore, warming and shorter and shallower snow packs do not necessarily increase productivity (Zhang *et al.*, 2008; Gamon *et al.*, 2013; Yi *et al.*, 2014; Huemmrich *et al.*, 2010b,a; Parida and Buermann, 2014). Soil warming promotes thaw and stronger drainage. Heterogeneous respiration and carbon emissions to the atmosphere are stimulated in warmer soils at lowered water table depth (Billings *et al.*, 1982; Yi *et al.*, 2014; Oechel *et al.*, 1993; Huemmrich *et al.*, 2010b; Commane *et al.*, 2017). The balance between photosynthetic carbon uptake and respirational losses is further modulated by permafrost disturbances (Cassidy *et al.*, 2016). Polar treeless regions are spatially highly heterogeneous ecosystems (Welker *et al.*, 2004) but with widespread full vegetation cover. NEE, GPP and respiration are governed by variable conditions regarding wetness and temperature, micro-topography, geomorphology and type and acidity of the soils (Kwon *et al.*, 2006; Walker *et al.*, 1998; Olivas *et al.*, 2011; Emmerton *et al.*, 2016; Pirk *et al.*, 2017). It is not clear whether, where and when the land surface in Arctic tundra actually acts as a sink or source of CO_2 (Cahoon *et al.*, 2012; McGuire *et al.*, 2012) and what the direction and magnitude of changes in altered climatic conditions will be (Oechel *et al.*, 1993; Billings, 1987; Sitch *et al.*, 2007). This has given rise to extensive and long-term project studies of the Arctic like the Arctic-Boreal Vulnerability Experiment (ABoVE, `https://above.nasa.gov/about.html`) or the Carbon in Arctic Reservoirs Vulnerability Experiment (CARVE, `https://carve.jpl.nasa.gov/Missionoverview/`), both of which are not limited to CO_2).

Observing carbon fluxes in these inaccessible and remote areas is difficult. Several long-term monitoring sites exist where phenological observations, spectral reflectance as well as gas flux measurements are conducted *in-situ*, both under natural conditions and in manipulative experiments. Many studies can be found in the literature that evaluate eddy-covariance or chamber gas flux measurements with respect to spatial patterns of NEE at a fixed point in time, or *in-situ* NEE integrated over the growing season and its variations between years (López-Blanco *et al.*, 2017; Lund *et al.*, 2010; Ueyama *et al.*, 2013a; McFadden *et al.*, 2003; Williams and Rastetter, 1999; Marushchak *et al.*, 2013; Kross *et al.*, 2014). However, only few sites exist compared to temperate regions and

observations are usually not done in a continuous manner over the complete year but during individual measurement campaigns or dedicated periods during the growing season. Even if automated instrumentation can provide more continuous measurements all along the year, it is still hampered by the difficulty of access in case of equipment failure. Compared to more temperate sites, tundra poses additional challenges on the calculation of NEE and its component fluxes GPP and respiration (Pirk *et al.*, 2017). Due to the small magnitudes of the net fluxes, different flux calculation methods might even differ in whether they indicate a source or a sink at a given time (Pirk *et al.*, 2017). Snow and soil freezing can act as a barrier for gas exchange with the atmosphere and cause a temporal decoupling between the registration at the sensors and when the gas concentrations have actually been changed by heterotrophic respiration in the soil (Arneth *et al.*, 2006) or by photosynthesis by evergreens under the snow (Starr and Oberbauer, 2003). Further, the heterogeneity of the landscape poses limits to the spatial representativeness of the relationships between the carbon fluxes and meteorological and soil conditions that have been identified *in-situ* (Pirk *et al.*, 2017; Tuovinen *et al.*, 2018). Therefore, in spatial up-scaling exercises (Ueyama *et al.*, 2013a; Marushchak *et al.*, 2013; Huemmrich *et al.*, 2013; Tramontana *et al.*, 2016) strong extrapolations are necessary. Yet, the modelling of the future evolution of the vegetation and carbon fluxes (including their timing and magnitude) in circumpolar areas requires an understanding of the component fluxes GPP and respiration as well as accurate spatially and temporally explicit observations of their drivers.

Satellite remote sensing can help to constrain the component flux of GPP and additionally to extend point observations to larger areas with repetitive coverage in time. Depending on the monitoring approach, different assets and limitations need to be considered for inferring GPP. Optical reflectance measurements can give an indication of the abundance of green plant material and hence photosynthetic potential. From spectral observations of greenness, information can be inferred on the fraction of incident photosynthetically active radiation (PAR) that is absorbed (fAPAR) and can potentially be used for carbon fixation. Following the concept of the light-use efficiency of plant productivity by Monteith (1972), the amount of absorbed radiation (APAR, the product of fAPAR and incident PAR) is an important determinant of spatial and seasonal variations in GPP (together with the efficiency with which the absorbed energy is used in carbon fixation). Site-level studies have confirmed a highly linear relationship between APAR and GPP (Huemmrich *et al.*, 2010a,b). Indeed, in the last decades, spatial extrapolations of *in-situ* observations of carbon fluxes in tundra and peatland showed the skill of indicators of greenness (leaf area index, LAI, or reflectance based indices like the NDVI or the green ratio) as a predictor for GPP and NEE (Ueyama *et al.*, 2013a,b; Chadburn *et al.*, 2017; McFadden *et al.*, 2003; Williams and Rastetter, 1999; Street *et al.*, 2007; Marushchak *et al.*, 2013). At many sites, mosses make up twice or trice the biomass of vascular plants. However, their photosynthetic capacity is much lower (Yuan *et al.*, 2014; Williams and Rastetter, 1999; Huemmrich *et al.*, 2013; Zona *et al.*, 2011), and their seasonality is often dissimilar (Gamon *et al.*, 2013) as a consequence of their different sensitivities to environmental conditions (Zona *et al.*, 2011). Micro-topography affects moisture conditions, even within small elevation changes of about one meter (Olivas *et al.*, 2011; Gamon *et al.*, 2013; Pirk *et al.*, 2017). As a consequence, distinct spatial distributions of the plant functional types and highly variable patterns of photosynthetic light-use efficiency are observed. Vascu-

lar plants prefer lower, wetter places and their growth increases biomass, productivity, NDVI, and LAI. However, when the ground becomes drier, NDVI will increase, but actual productivity decline (Olivas *et al.*, 2011; Gamon *et al.*, 2013; Buchhorn *et al.*, 2013). Consequently, the wetness of the soil confounds the interpretation of spectral reflectance with respect to productivity, which is problematic as soils are often water-saturated (Stow *et al.*, 2004). Next to the confounding effect of moisture on spectral reflectance, changes in GPP have been observed to not necessarily translate into changes in NDVI (Olivas *et al.*, 2011). In addition to these challenges, spectral reflectance observations are affected by large signals from the background and shadows cast by microtopography and vegetation itself. Snow and open water from the many small ponds and thaw lakes (globally, the highest abundance and areal coverage of lakes is between 55 and 75° N, Verpoorter *et al.*, 2014) as well as litter and dry plant material influence the spectra with seasonally changing extents. Further, persistent cloud cover, low illumination and viewing geometry (Stow *et al.*, 2004; Laidler and Treitz, 2003) and the relatively large pixel size compared to the high heterogeneity of the landscape render reflectance-based observations of circumpolar productivity difficult.

Recently, independent and complementary approaches to spectral reflectance have become available to remotely study vegetation dynamics. First, sun-induced chlorophyll fluorescence (SIF) is an electromagnetic signal emitted by chlorophyll as a 'by-product' of photosynthesis. Because it is directly related to photosynthetic activity (e.g. Porcar-Castell *et al.*, 2014) it is expected to give a more direct and accurate picture of actual photosynthesis (as compared to greenness/ growth) and is much less affected than vegetation indices by open water, snow or background effects, the heterogeneity of the land surface and plant functional types. However, the footprints of the sensors from which SIF measurements are available for several years are very large and integrate over many different growing conditions. Further, the SIF signal is generally weak in tundra regions due to the low vegetation abundance and photosynthetic rates and in combination with low illumination angles subject to high noise levels.

A second type of complementary satellite information lies in passive microwave remote sensing. Specifically, vegetation optical depth (VOD) is a radiometric variable describing the attenuation of microwave radiation emitted from the soil and the vegetation itself due to the water contained in the canopy. It can therefore be directly related to vegetation water content and biomass. VOD increases with vegetation density, but is strongly controlled by vegetation emission in very dense vegetation (Liu *et al.*, 2011). Depending on the wavelength of observation, the signal is sensitive to different depths in the canopy and objects of variable sizes (e.g. small objects like leaves versus large trunks or branches). Following Teubner *et al.* (2018), in moderately and sparsely vegetated areas, there is a chain of proportionalities from VOD to GPP. VOD indicates total water content, which is related to leaf area, which in turn is an important determinant of GPP. In their comprehensive study, Teubner *et al.* (2018) evaluated the temporal behaviour between different VOD data sets, model GPP and SIF, and found widespread high positive correlations both between the raw time series as well as patterns of anomalies globally. Although patterns in tundra vegetation have not been explored explicitly, correlations between VOD and GPP were consistently high in landscapes characterized by shrubs, grasses or sparse vegetation. Similarly, highest correlations between phenological dates derived from VOD and vegetation indices were obtained in low biomass regions (Jones *et al.*, 2011). VOD observations are insensitive to cloud cover and to variations in day light, a strong advantage in the

high latitudes of interest in our study. However, as for SIF, currently available satellite observations have a coarse spatial resolution compared to optical measurements. Further, careful corrections of effects of soil moisture, open water and frozen grounds, snow and ice, amongst others are necessary in the retrieval, and it is therefore not clear whether VOD can be a useful parameter to evaluate vegetation dynamics in the specific context of tundra.

Neither greenness nor SIF nor VOD can directly be translated into the amount of carbon taken up through photosynthesis. Nevertheless, they all represent important observation-based driving variables for the modelling of tundra carbon exchanges at landscape scale and over multiple years (e.g. Luus *et al.*, 2017). Therefore, their ability to accurately represent the timing and relative changes of photosynthetic activity and growth is of key importance for realistic model estimates of carbon fluxes. In this study, we compare the timing of the peak growing season as indicated by several satellite vegetation indices, VOD and SIF in circumpolar treeless regions. We aim at analysing their complementary information content with respect to maximum greenness and photosynthetic activity - despite all above-mentioned challenges - and relate them to environmental conditions. In addition, GPP empirically up-scaled from eddy-covariance observations using satellite measurements of different variables describing the land surface and meteorological reanalysis data (Tramontana *et al.*, 2016) is included in the study. In doing so, a comprehensive evaluation of several state-of-the-art satellite-based products is achieved in this study with a special focus on the timing of the peak growing season, as this represents the most important period with respect to total annual carbon uptake. In addition to the use of the broad array of complementary spaceborne data sets, we perform this analysis for the total circumpolar pan-Arctic treeless regions and it therefore represents an extension with respect to the majority of published tundra ecosystem studies that are mostly confined to specific regions, like Alaska.

III.2 Methods and material

III.2.1 Methods

The different vegetation proxies will be evaluated at 0.5° spatial resolution and with daily sampling. A temporal running mean in a window of 16 days is applied to all data sets. The resulting data still contain values for every day in a year, but the effective temporal resolution corresponds to 16 days. Gaps due to missing data are not aligned between data sets. The timing of the annual maximum is defined as the average day of year (DOY) of all days at which the values exceed the 95^{th} quantile of all valid values of the time series in a year in a given pixel. Because of frequently low data quality and long and intermittent data gaps in those high latitude regions of interest, we mostly base our analysis on multi-year averages of the DOYs of annual maximum (henceforth avg.peak). However, we do also compare to results based on the mean seasonal cycle.

III.2.2 Environmental variables

Air temperature at two meters height (t2m) every six hours between 2007–2016 is obtained from ERAInterim reanalysis data (Dee *et al.*, 2011a) and aggregated to 16-day temporal resolution with daily sampling.
Daily global radiation (Rg) for the years 2007-2016 is obtained from measurements of

the Clouds and the Earth's Radiant Energy System (CERES Ed4A, Wielicki *et al.*, 1996; Doelling *et al.*, 2013) onboard the Aqua and Terra satellites. From the 1° spatial resolution product (the 'SYN1deg-Day product', all-sky surface shortwave downward fluxes, initial fluxes) we disaggregate to 0.5° spatial resolution by bilinear interpolation. Subsequently, daily data are averaged in a daily moving window of 16 days.
We further include surface soil moisture (SM) model results from the GLEAM project (v3.1a, Miralles *et al.*, 2011; Martens *et al.*, 2017). GLEAM is provided at daily temporal and 0.25° spatial resolution for the years 2007–2016. For the analysis we aggregate them to 0.5° and 16-day resolution with daily sampling. In case of moisture-related variables we will explore the timing of the annual minimum as well in order to get an indication of potential moisture stress or confounding effects on reflectance measurements. Accordingly, the timing of minima are defined as the average of all DOYs at which the values are below the 5^{th} quantile of all valid values in a year in a given pixel.

III.2.3 Reflectance-based indices

We use MODIS reflectance measurements to obtain the enhanced vegetation index EVI (Huete *et al.*, 2002), the normalized difference vegetation index NDVI (Tucker, 1979), and the near infra-red reflectance of vegetation NIRv (Badgley *et al.*, 2017) as proxies of greenness for the years 2007–2016. These indices have been calculated from Nadir Bidirectional reflectance distribution function Adjusted Reflectance (NBAR) from the MODIS MCD43C4v006 product (MCD43C4: NASA LP DAAC and Science , EROS) at 0.05°. This means that the reflectance values are modelled to a value as if viewed from directly above. After quality check (only pixels with bi-directional Reflectance Distribution Function (BRDF) Quality flags 0, 1 retained) and snow filter (all pixel values containing any snow removed) the data are aggregated to 0.5° spatial resolution and left at their native temporal resolution of 16 days with daily sampling. We will refer to these throughout the manuscript as EVI, NDVI and NIRv.
As the amount of incoming photosynthetically active radiation is proportional to the total downwelling shortwave radiation we calculate an estimate of APAR as the product of global radiation and EVI (denoted EVI.Rg) or NDVI (denoted NDVI.Rg), both of which are here assumed to be a valid approximation of fAPAR. In the following we will refer to both of them together as APAR, and otherwise separate between EVI.Rg and NDVI.Rg.
We additionally include the MODIS vegetation index products of NDVI and EVI from Aqua MYD13C1v006 (MYD13C1: NASA LP DAAC and Science , EROS) and Terra MOD13C1v006 (MOD13C1: NASA LP DAAC and Science , EROS) in the analysis. In contrast to EVI, NDVI and NIRv from the MCD43C4 data, those are obtained from reflectances with different viewing angles that do not necessarily correspond to nadir. Including them in the comparison can therefore help to get an idea of the influence of directional effects on the seasonality and of the consistency of the results. From the 0.05° products generated with an 8-day frequency using a period encompassing the last eight and the following eight days of acquisitions, we removed data that do not have good quality using the VI quality indicator. We further remove pixel values that are flagged as cloudy, containing snow or ice or those that were not processed as indicated by the quality reliability flag. The remaining pixel values are aggregated to 0.5° grid cells. Throughout the manuscript we will name these EVI.VIproduct and NDVI.VIproduct or refer to both of them together as MODIS VIproduct. The data from the MODIS VIproduct are differ-

ent from all other datasets in that they are sampled every eight days, not daily.

III.2.4 Vegetation optical depth and land surface parameters

A data set of various land parameters simultaneously derived from passive microwave measurements of the AMSR-E onboard Aqua and AMSR2 onboard GCOM-W1 is used for the years 2007-2016 (v2, here called AMSR-E/2, Du *et al.*, 2017b,a). The data records are combined but not continuous. In 2011 data are available until DOY277 and restarting after that in 2012 only at DOY206. Because the peak growing season is covered in 2011, we do use data from 2011, but not from 2012. Of the observations made in descending orbits with an equatorial crossing at 1.30 AM we use VOD and volumetric surface soil moisture (0-1 cm) derived from X-band (10.7 GHz) as well as estimates of the fraction of open water. We use the descending orbit as retrievals are generally more accurate when vertical temperature gradients are low (Liu *et al.*, 2011). The retrieval specifically accounts for the effects of open water on VOD and surface soil moisture (Du *et al.*, 2017b). The accompanying quality flags are used to remove all pixel values observed under non-favourable conditions with respect to frozen soils, snow, ice or large areas of open water on the surface, very dense vegetation, precipitation, radio frequency interference or microwave signal saturation. The daily files with the native 25 km resolution data in an EASE-grid projection are first quality filtered, then reprojected to 0.25° longitude/latitude relative to WGS84 and subsequently aggregated to 0.5°. For temporal consistency we aggregate to 16 days with daily sampling as in all other data sets.
It should be noted that the GLEAM data are not fully independent from the VOD derived from AMSR-E as it is itself used in the retrieval of GLEAM SM.

III.2.5 Sun-induced chlorophyll fluorescence

Sun-induced chlorophyll fluorescence (SIF) as a proxy of photosynthetic activity is retrieved from GOME-2 measurements onboard Metop-A at 740 nm (Köhler *et al.*, 2015a, ftp://ftp.gfz-potsdam.de/home/mefe/GlobFluo/GOME-2/, it will henceforth be called SIF GFZ) for January 2007 until August 2016. We remove the individual measurements that have unfavourable observational conditions, namely those that have an effective cloud fractions of more than 50% , those that are measured before 8 o'clock or after 14 o'clock local solar time (which is important as in high latitudes during solar day additional measurements in the evening are possible but subject to high noise) or under sun-zenith angles of more than 70°, and those whose retrieval resulted a residual sum of squares larger than 2 W m^{-2} sr^{-1} μm^{-1}. The individual remaining measurements are aggregated to 0.5° resolution based on the centre coordinates of a given footprint over the 16-day intervals like in the MODIS data for each individual year to obtain a time series. Additionally, they are also directly averaged to a climatology. We added to the comparison SIF data retrieved from GOME-2 with a slightly different method (Joiner *et al.*, 2013, 2016`https://avdc.gsfc.nasa.gov/pub/data/satellite/MetOp/GOME_F/`, V26, henceforth SIF NASA). The individual measurements are filtered in the same way as for the SIF GFZ data set, except for the fact that the data are delivered filtered for an effective cloud fraction of smaller than 0.3. We then average in the same way spatially and temporally as before for the years 2007–2016.
As SIF represents an instantaneous observation at a given time of the day and a comparison

to GPP seasonality would be hampered by the fact that GPP represents an average daily value (Zhang *et al.*, 2018), additional comparisons are carried out to the SIF observations scaled to daily values (henceforth SIF.daily.int GFZ). By a geometrical approximation of incoming PAR by the cosine of the sun-zenith angle, the correction to daily values is achieved by multiplication of the instantaneous SIF with the ratio of the daily integrated (in 10-min steps) cosine of the sun-zenith angle and the cosine of the sun angle at the time of measurement. This correction is expected to account for the effects of seasonally and daily changing illumination. Caution is warranted for this correction, as it assumes that the same environmental conditions prevail over the entire day and it using such scaling factor may further amplify noise.
SIF can be approximated in a similar way like GPP following Monteith (1972) as the product of fAPAR, PAR (approximated as cos(SZA)) and the efficiency with which the energy is used in fluorescence emission. Hence, also the comparison of SIF to vegetation indices is more appropriate if one accounts for the illumination effects on SIF that are not included in the greenness indices. In that case, the SIF values are normalized by the cosine of the sun-zenith angle at the time of measurement and used in the analysis (henceforth SIF.cosSZA GFZ and SIF.cosSZA NASA). According to the SIF-Monteith model, SIF.cos(SZA) therefore represents a convolution of canopy fAPAR and the efficiency of fluorescence emission.
As a cross check of the plausibility of the GOME-2 SIF additional comparisons to SIF at 757nm retrieved from OCO-2 are done using the OCO-2 SIF lite files (B8100r) from September 2014 to mid October 2017 (OCO-2 Science Team/Michael Gunson, 2017; Frankenberg *et al.*, 2014; Sun *et al.*, 2018). We filter all measurements taken with a sun-zenith angle of less than 70°, in nadir mode and over regions whose IGBP land cover is not water, forest, crops, urban or mosaic. Samplings of OCO-2 SIF (henceforth OCO2) and OCO-2 SIF corrected for illumination conditions by division by cos(SZA) in the same way as for the GOME-2 measurements (henceforth OCO2.cosSZA, OCO2 and GOME-2 have different overpass times and therefore different instantaneous illumination at the time of measurement) are averaged to a climatology based on 16-day averages sampled daily as a spatial average over different smaller regions of interest. The regional averaging is necessary as OCO-2 has no continuous sampling like GOME-2.

III.2.6 FLUXCOM model GPP

A different indicator of photosynthetic activity is provided by the GPP model simulations from the FLUXCOM initiative (http://www.fluxcom.org/products.html, Tramontana *et al.*, 2016). Relationships between land surface and environmental variables and land-atmosphere energy and carbon fluxes learned at FLUXNET eddy-covariance sites in the La-Thuile data set (http://fluxnet.fluxdata.org/data/la-thuile-dataset/) are spatially up-scaled to the globe using a set of machine-learning techniques. FLUXCOM GPP is generated in two set-ups, the 'remote sensing set-up (RSGPP)' and the 'meteorology + remote sensing (METGPP)' set-up. The former one uses satellite-observed land surface conditions to estimate GPP at 8-daily temporal resolution and 1/12° and we use the years 2007–2015. The METGPP represents an ensemble of GPP where the mean annual cycle of land surface conditions and additional information on actual meteorological conditions from reanalysis is used in the prediction at 0.5° and daily resolution. We restrict the MET-

GPP data to the years 2007–2010 as for those years simulation results from all ensemble members are available. We aggregate to 16-day averages sampled every day, consistent with the MODIS sampling in the MCD43C4v006 data. The RSGPP is linearly interpolated to daily values at 1/12°. Subsequent aggregation to 0.5° and running means over 16 days match the spatio-temporal resolution to all other data sets. Together RSGPP and METGPP are referred to as model GPP.

III.2.7 Land cover

We use the ESA CCI land cover classification and aggregate it to broader classes of moss, bare/sparse, grass/herbaceous, woody, water and other. The ESA CCI provides a tool to convert discrete land cover classes to continuous vegetation fractions (`http://maps.elie.ucl.ac.be/CCI/viewer/download/ESACCI-LC-Ph2-PUGv2_2.0.pdf` and Poulter *et al.*, 2015) and we use it to obtain land cover fractions from the native 300 m pixels in 0.5° pixels for the period 2008-2012 (Fig. B.1). The distribution of mosses in these products is expected to be problematic because it is a complicated class to characterise for global land cover products. Being partly based on regional maps with varying thematic detail in their legends, it is possible that this moss class in the ESA CCI is not always accurately identified over certain regions, explaining why moss cover is barely indicated in Siberia.

III.2.8 The study area

Land cover data sets exhibit substantial differences in the classes they assign to circumpolar regions. We compared the ESA CCI land cover, GlobeLand30 by Chen *et al.* (2015) and the IGBP classification from MODIS MCD12C1 and found that classification of the same area can range from barren to grasslands to open shrub lands, depending on the chosen dataset (not shown). A clear and generally accepted delineation of a class 'tundra' is not given. We therefore define our study area based on tree cover as 'polar treeless regions'.

Global data on annual forest cover gain and loss have been provided by (Hansen *et al.*, 2013) based on Landsat images. We take 2009 as representative for the period of investigation. Based on information on the global tree cover in 2000, the yearly losses until 2009 and the gains until 2009 (assuming a linear growth between 2000 and 2012), global tree cover in 2009 is estimated. We aggregated from the original 30 arcsec resolution to 0.5°. Regions with less than 5 % tree cover north of 55° N are fixed as our study area (cf. Fig. III.1). In Hansen et al.'s data, a tree is defined to have a minimum height of 5 m which is tall for circumpolar areas. The studied area will therefore include parts of the taiga-tundra transition zone, tundra as well as polar deserts.

The landscape in this study area exhibits complex microtopography caused by polygons and is characterized by abundant (thaw) lakes. Though vegetation often fully covers the ground (Stow *et al.*, 2004), it is sparse and with one to three months the growing season and carbon uptake period are short in high-latitude tundra. The RGB images from Sentinel-2 for selected spots in Fig. III.1 give examples of what tundra landscapes and the tundra-taiga transition can look like. Further, for small areas on the Alaskan North Slope and the root of the Taimyr Peninsula (the corresponding places are indicated in Fig.III.1),

the climatologies of environmental conditions in Fig. III.2 and Fig. III.3 illustrate the annual cycles of environmental conditions together with Sentinel-2 images at given points in time during the growing season. Temperatures rise above the zero degree Celsius line in late May and snow melt is often only completed in June. GLEAM soil moisture is usually highest at the time of the start of the growing season and also illumination is close to maximum. Temperatures keep increasing until July (ice layers on lakes can persist until July, cf. Fig. III.1, example of tundra close to the Laptev Strait). GLEAM soil moisture is lowest at the time of highest temperatures, while areas of open water are largest. Light conditions are already diminishing. Temperatures fall below the freezing point in late September or October. During this short period of favourable growing conditions vegetation phenology rapidly develops (cf. temporal sequences of RGBs in Fig. III.2, III.3 and Arneth *et al.*, 2006).

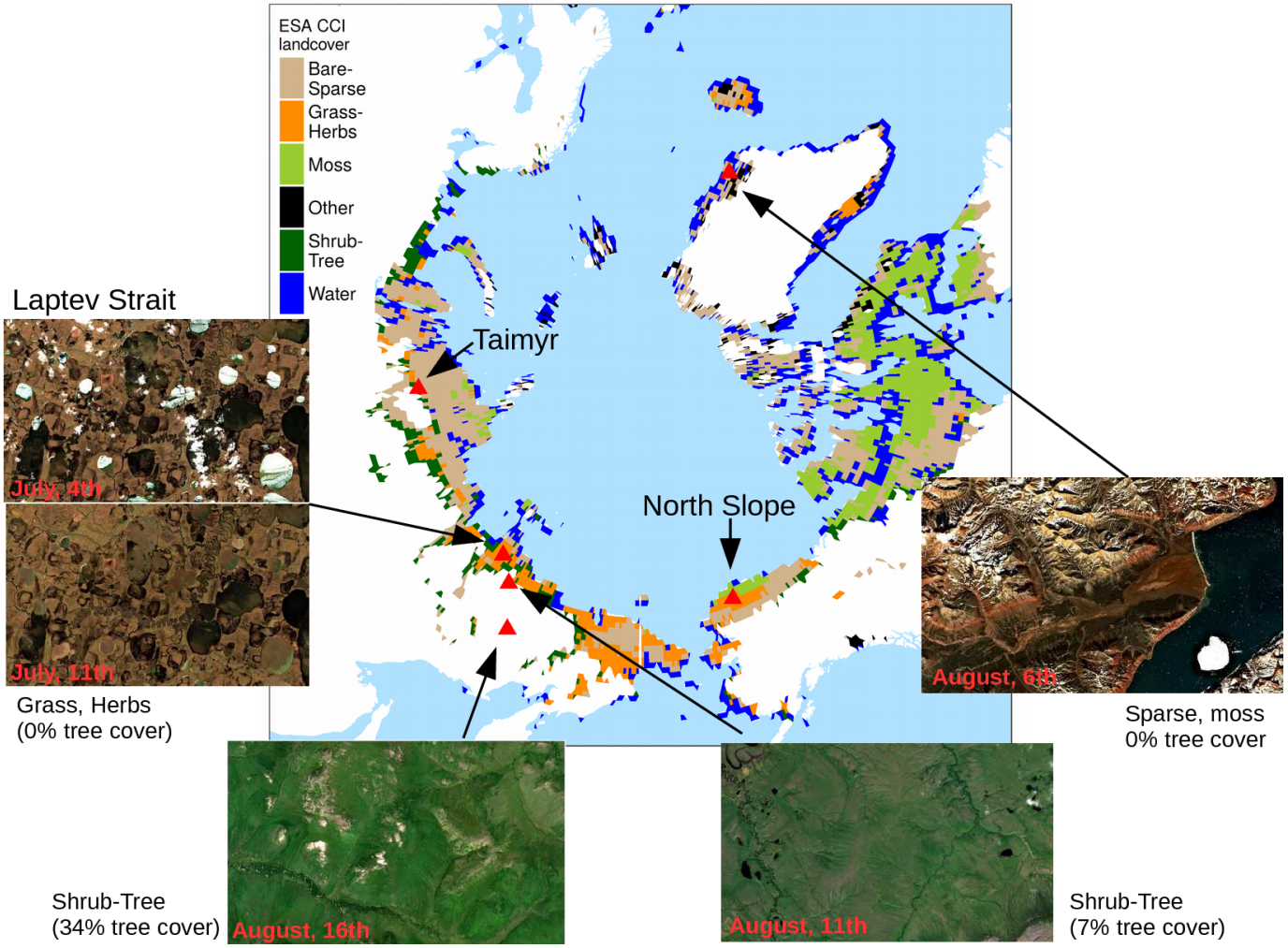

Figure III.1: ESA CCI land cover in regions with less than 5% tree cover according to Hansen *et al.* (2013). Atmospherically corrected true colour images are from Sentinel-2 taken at different dates in 2017. For the region shown in each image the majority land cover is given and the tree cover percentage according to Hansen *et al.* (2013).

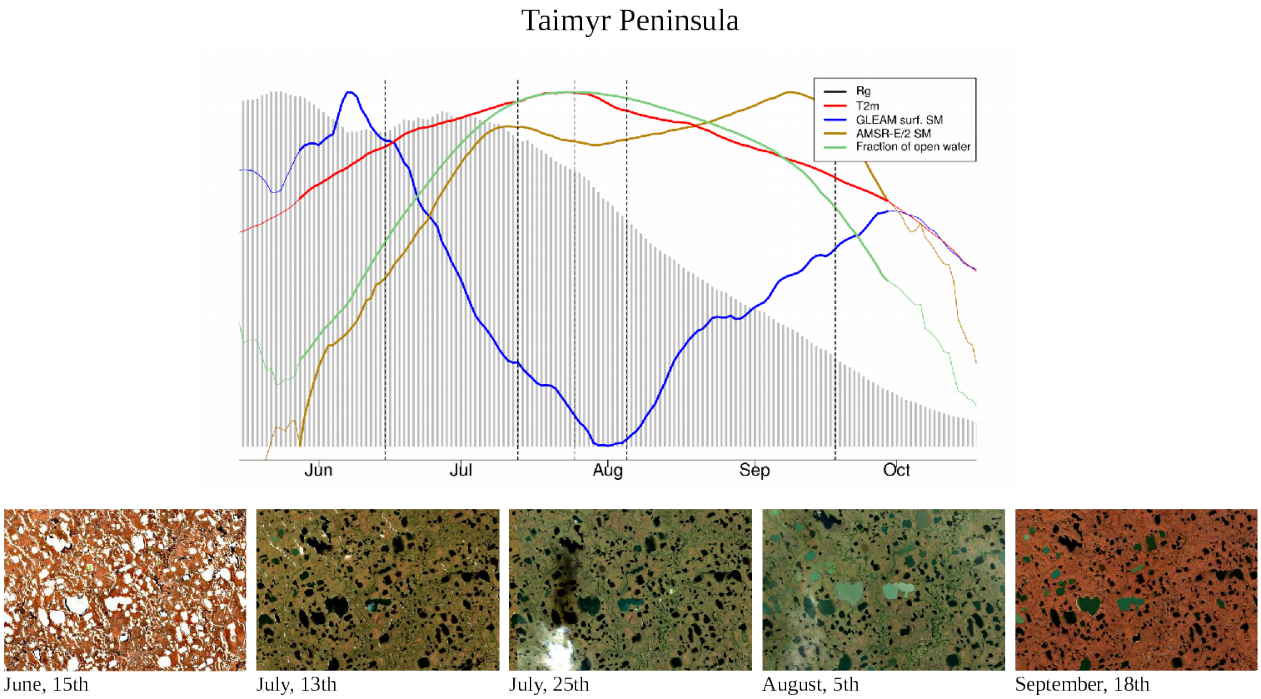

Figure III.2: Climatologies of different atmospheric and land surface variables for a small area on the Taimyr Peninsula/ Russia indicated in Fig. III.1. Bold lines indicate the time period when air temperatures are above the freezing point. Vertical dashed lines indicate the time of the year when the Sentinel-2 images shown in the second panel were taken. Sentinel-2 images are atmospherically corrected and taken in 2017.

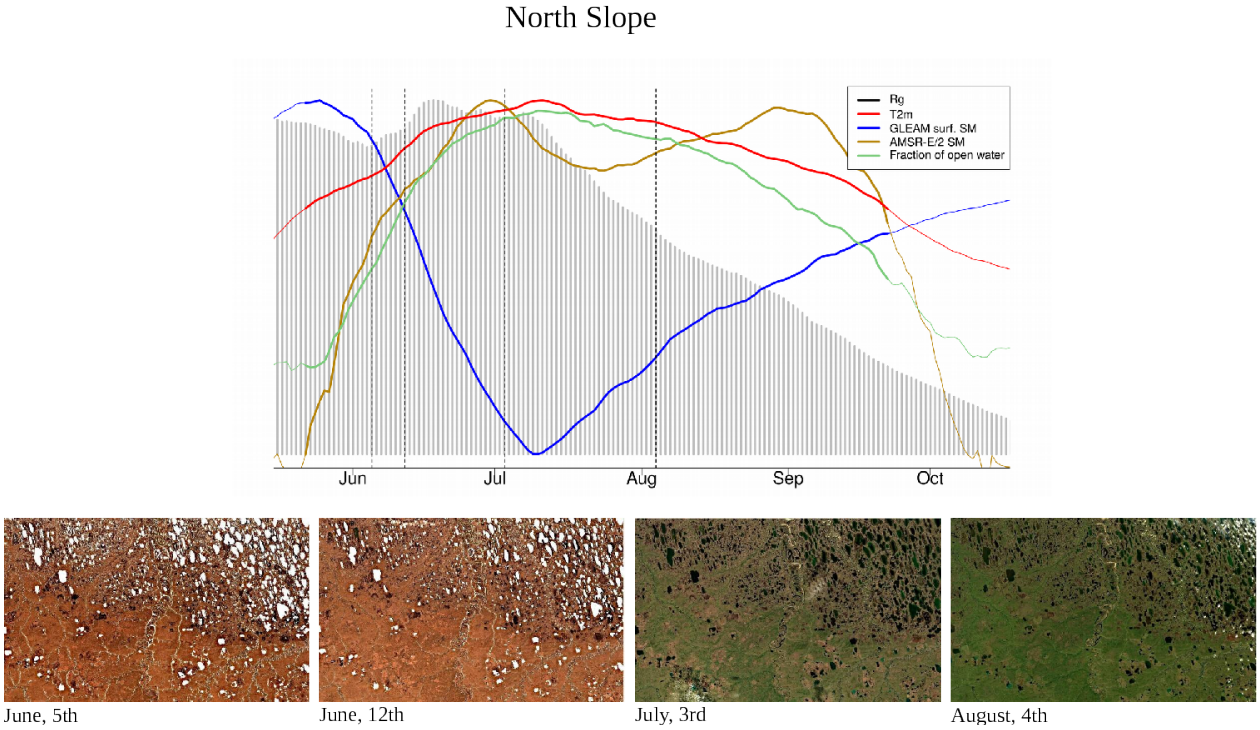

Figure III.3: Climatologies of different atmospheric and land surface variables for a small area in the North Slope/ Alaska indicated in Fig. III.1. Bold lines indicate the time period when air temperatures are above the freezing point. Vertical dashed lines indicate the time of the year when the Sentinel-2 images shown in the second panel were taken. Sentinel-2 images are atmospherically corrected and taken in 2017.

III.3 Results

III.3.1 Timing of the annual peak in vegetation activity and greenness

The distribution of the timing of the annual maximum in polar treeless regions (Fig. III.4, regionally and over years) shows a distinct order of the satellite vegetation proxies. All proxies indicate highest plant activity and biomass after the summer solstice. While APAR is highest around DOY191 (July, 10th), METGPP indicates maximum photosynthetic activity at a similar time, RSGPP four days later. It is the time when surface soil moisture is almost at minimum according to GLEAM (Fig. B.2). The SIF GFZ peaks only about one week later (four days later in case of SIF.daily.int GFZ) around DOY202 (July, 21th). The observations show that the SIF GFZ peak, potentially indicative of highest photosynthesis, is reached in close synchrony with the annual temperature peak. In contrast to that, SIF NASA on average peaks only on July, 28th (DOY 209), at a similar time when surface inundation by open water is highest (Fig. B.2, although both the SIF NASA and AMSR-E/2 data indicate a large range). Removing the effect of incoming radiation from the SIF measurement (by dividing by cos(sun zenith angle)) shifts the annual maximum for SIF.cosSZA GFZ compared to SIF GFZ by six days, and by eleven days for SIF.cosSZA NASA compared to SIF NASA and there is comparatively large scatter. The yearly maximum in vegetation indices occurs in late July/ early August, where EVI and NIRv peak around July, 31st (DOY212), one and a half weeks after the temperature and SIF GFZ maxima. VOD peaks on average in close temporal agreement with EVI and NIRv. Finally, up to five days later the MODIS VIproduct as well the NDVI reach their maxima in the first week of August. Grouping indicators based on the similarity of their intrinsic properties (e.g. RSGPP and METGPP, SIF GFZ and SIF NASA, EVI and NIRv) shows such groups have a consistent behaviour and follow a certain pattern: APAR indices < model GPP < SIF < fAPAR (with EVI, NIRv,VOD < NDVI).

III.3.2 Spatial patterns of the annual maxima of the satellite vegetation proxies and of the lags between them

Overlaid on the general order of the different groups of proxies, there is considerable spatial variability in the timing of the maximum of the mean annual cycle for each satellite indicator (Fig. III.5). In areas close to the date line (i.e. easternmost Siberia and Alaska), most proxies peak slightly earlier than in northern Canada (mainland and islands) or the coasts of western and central Siberia (i.e. Taimyr Peninsula and regions of the Lena Delta and the Laptev Strait). In general, the spatial pattern of the timing of the annual maximum of the satellite indicators qualitatively closely corresponds to the dynamics seen in air temperature and partly in the surface soil moisture (GLEAM). Incoming light shows partly reversed patterns with earlier maximum irradiance in northern Canada and western-central Siberia.

We test whether the annual maximum is shifted systematically between proxies or whether there are spatial gradients in the peak lag between proxies, and plot maps of the average lag between the peaks of selected proxies and NDVI. We take the NDVI because it is the most widely used vegetation index for productivity studies, both from the satellite as well as in ground-based observations, particularly in polar tundra. Figure III.6 confirms the general pattern of a shifted annual peak of NDVI as compared to NDVI.Rg, RSGPP, SIF

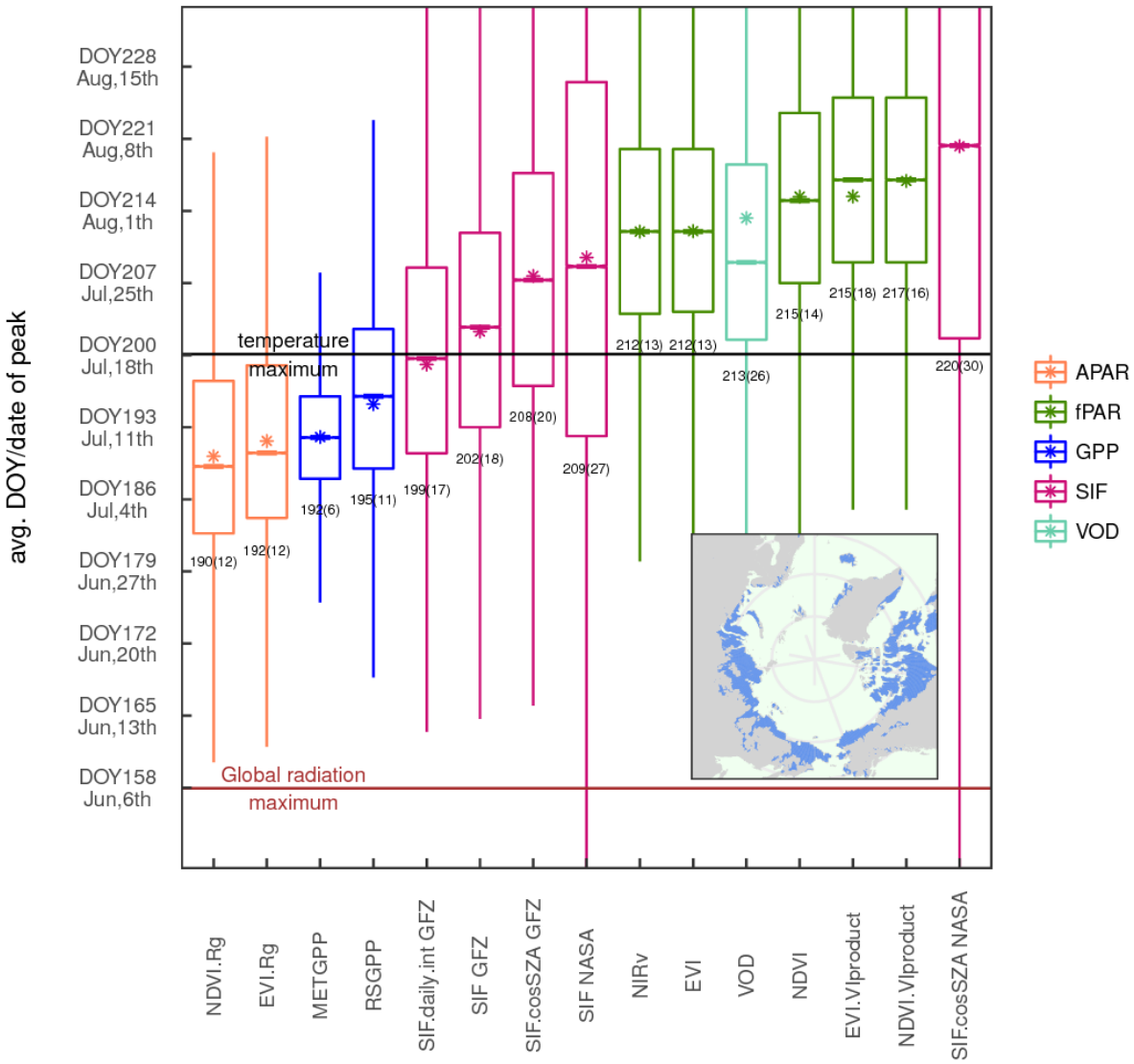

Figure III.4: Distribution of the DOY of the peak of the different vegetation proxies over the study region and between years (spatial sampling matched between data sets for each year). Bars in the boxes indicate the median, stars the mean, the numbers below the bars denote the spatio-temporal mean (standard deviation). Colours of the bars denote grouping of the different variables according to the families of fAPAR, APAR, model GPP, SIF, VOD.

GFZ, VOD and the similar timing like EVI all over the study area. It further shows that the lag is not homogeneous in space, but that it is largest in vast areas in northern Canada, on Iceland and in the northern part of the Siberian Taimyr Peninsula. Interestingly, the tundra regions that exhibit the largest time difference of the annual maximum between the individual vegetation proxies and NDVI tend to correspond to those where the annual maximum is reached comparatively late (Fig. III.5). In contrast to the denser vegetation cover on the Siberian coast, very sparse vegetation (i.e. devoid of shrubs/ woody vegetation) characterizes the northern Canadian regions, both the islands and the mainland, as well as the northern part of the Taimyr Peninsula (cf. Fig. B.1, and also Walker *et al.* (2005, their Fig. 1)). In addition, there is a comparatively high amount of lakes and high fractions of barren regions in the areas of large NDVI lags in the central Siberian coastal areas (close to the Laptev Strait), coastal Alaskan North Slope and in mainland Canada northwest of Hudson Bay. Similar results are obtained for EVI.Rg, METGPP, SIF.daily.int GFZ (Fig. B.3). Next to these general observations, VOD indicates a much later peak in smaller, but contiguous areas in northwestern Canada as well as in lake-rich regions on the Siberian coast (again the coast close to Laptev Strait). NDVI lags to METGPP are generally slightly larger than to RSGPP. No outstanding region emerges for the lags compared to SIF NASA. The illumination correction of SIF (SIF.cosSZA) reduces the time difference to the NDVI compared to the instantaneous SIF as expected.

III.3.3 Spatial patterns of peak timing and of peak lags to the NDVI in relation to environmental variables

Putting the annual maximum of the NDVI into relation with the one of the environmental variables, partly similar spatial patterns emerge like for the vegetation proxies (Fig. III.6). Precisely, air temperature and soil moisture (GLEAM minimum) peak earlier everywhere and have the largest time difference to the NDVI in the sparsely vegetated areas on Iceland, northern Canada and parts of the Taimyr. Conversely for the microwave retrievals of the amount of open water on the surface, where mixed temporal relationships with the NDVI peak are observed. Most water is present after the time of NDVI peak in large parts of northern Canada, Greenland and in land masses close to the date line, while NDVI is at maximum after the fraction of open water in all other regions. Summer precipitation might influence the microwave fraction of open water as typically highest surface inundation is expected to happen immediately after snow melt.
It is further interesting to test whether a certain temporal relationship between the maximum in photosynthesis or greenness and the dynamics of the environmental conditions holds across years. In Figure III.7, the environmental variable with the highest absolute value of the rank correlation with the timing of the maximum of the given satellite proxy across years and in a spatial moving window is displayed. The important role of energy-related variables, mostly temperature, for vegetation activity and growth is highlighted by widespread highest correlations with temperature and radiation for RSGPP, SIF GFZ, EVI and NDVI. Interesting to note are the contiguous regions of exceptions with higher relationships with moisture related variables for RSGPP, EVI and NDVI in northwestern Canada and parts of the Taimyr. VOD and NDVI.Rg do show a strong relationship with the annual temperature maximum less frequently and more often a higher importance of soil moisture or open water on the surface.

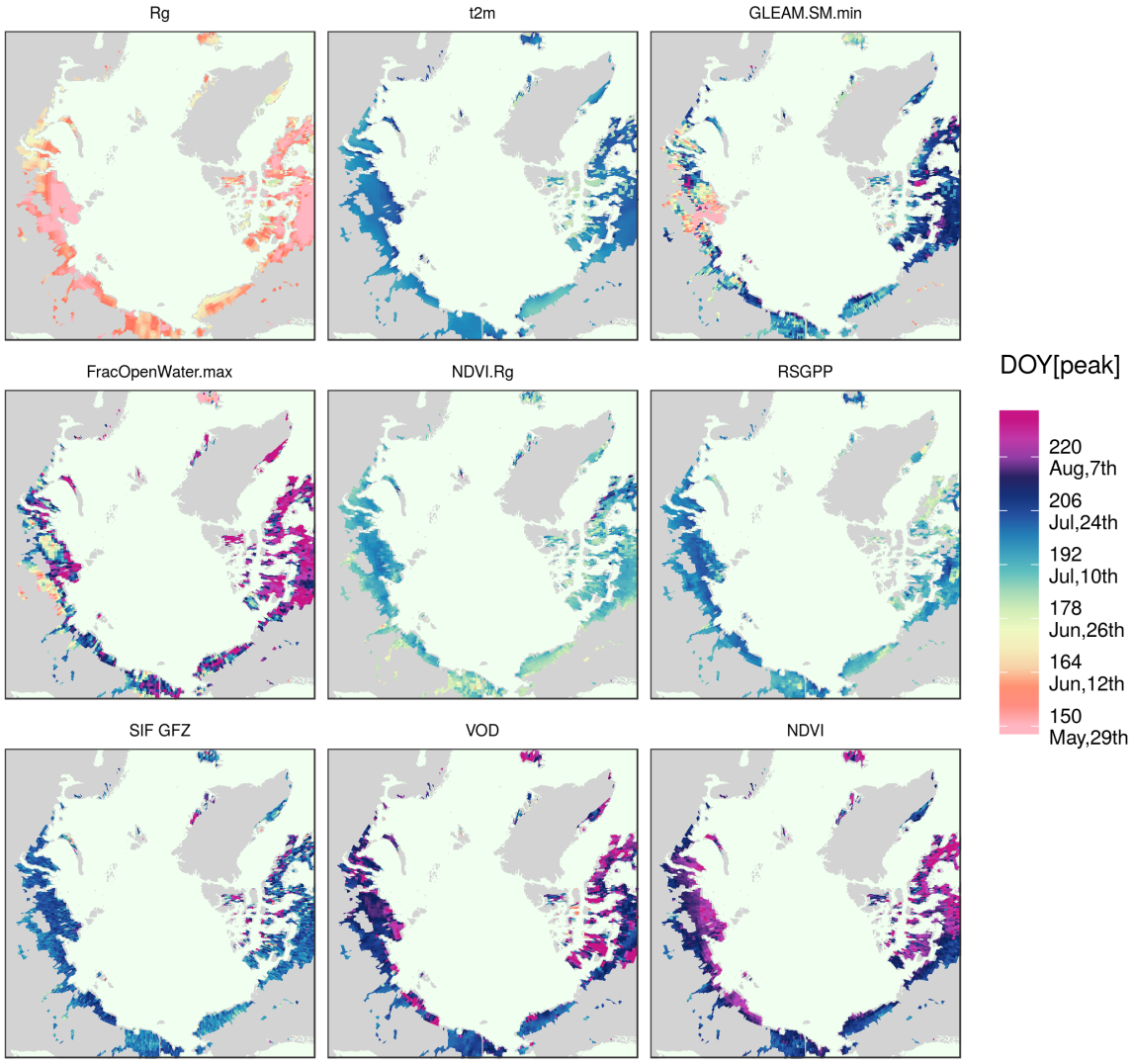

Figure III.5: DOY of the annual maximum averaged over all years as indicated by selected vegetation proxies.

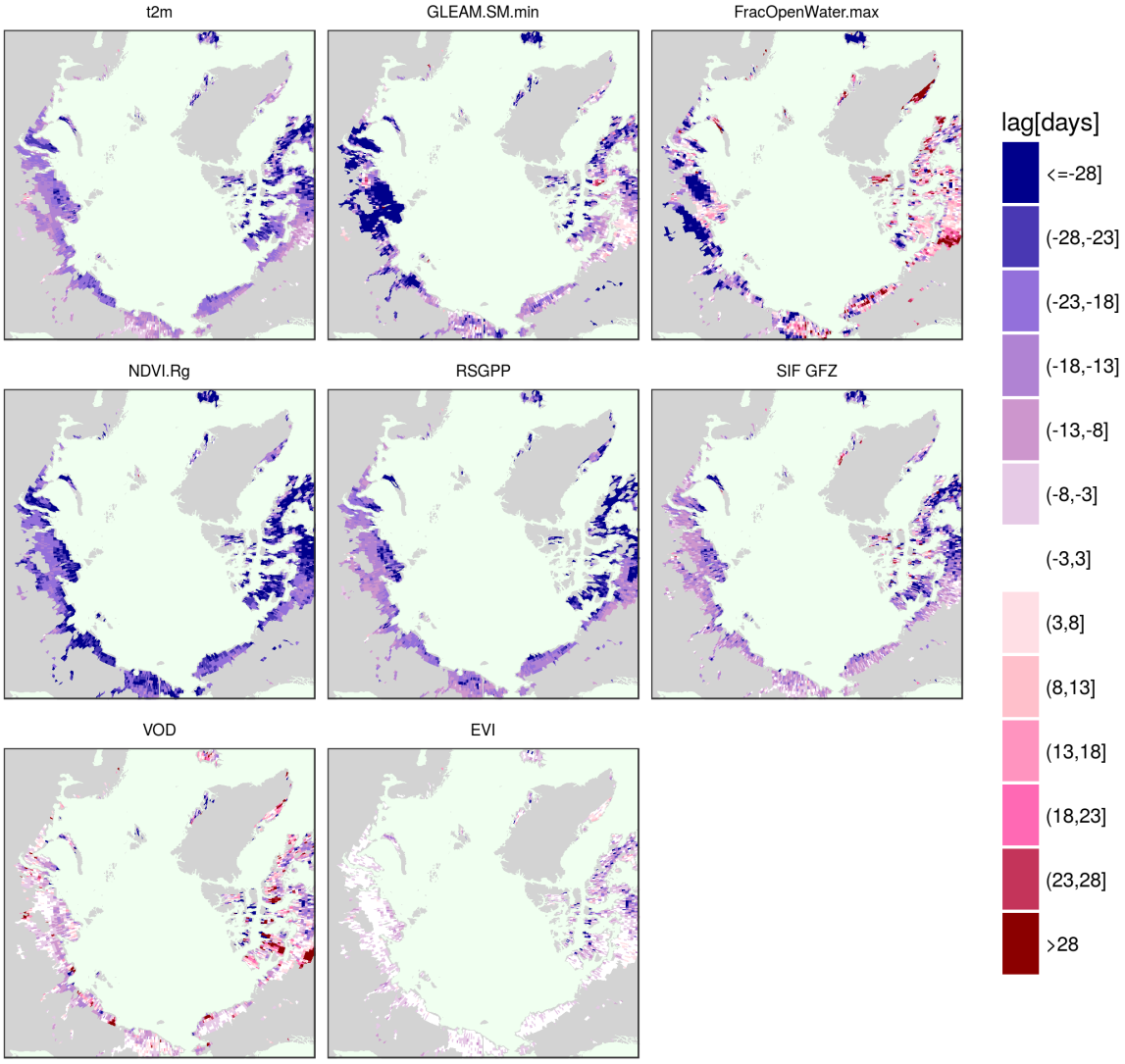

Figure III.6: Average time difference of the maximum across years of selected vegetation proxies and the NDVI.

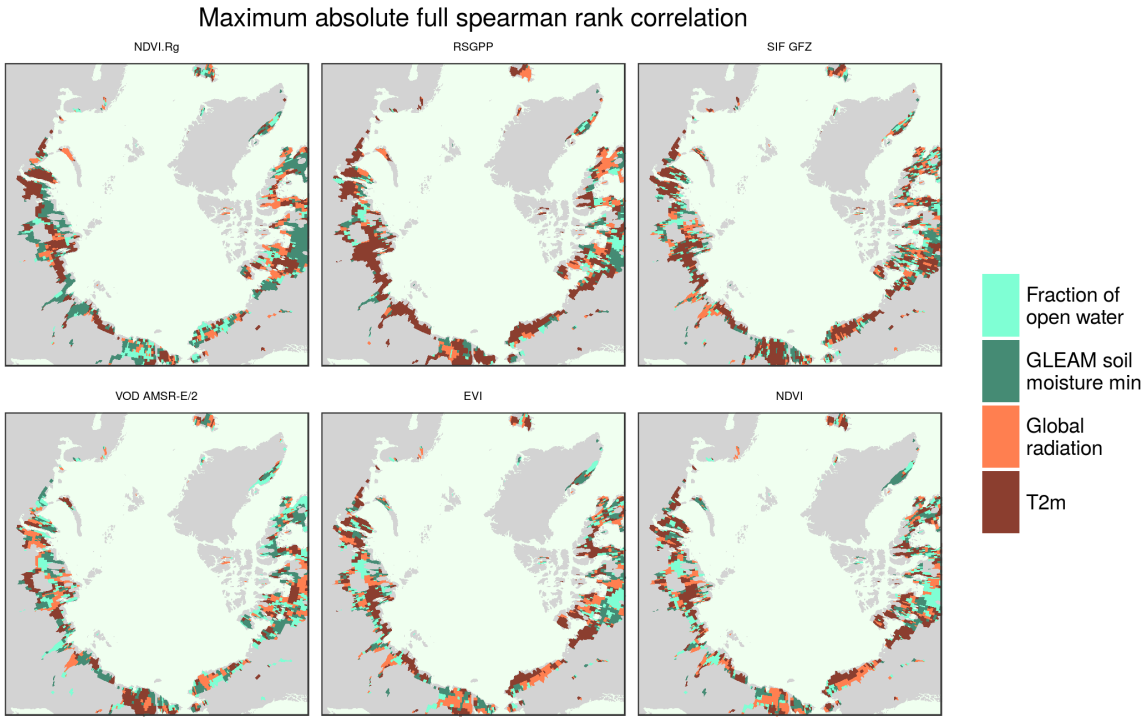

Figure III.7: Spearman rank correlation between the peak DOY of the vegetation proxies across years and the peak DOY of environmental variables in spatial moving windows of 1.5° (so 9 spatial pixels times 10 years at most, correlated only if more than 20 data points available). Plotted here is the variable with the highest absolute correlation. Full correlations have been calculated (no partial correlations).

III.3.4 Consistency of the annual peak lags between different land covers and across years

The fact that there is spatial variability in the shift between the annual peaks of the satellite proxies relative to the NDVI suggests that the proxies differ in how strongly they indicate the spatial gradients in the peak DOY. We test to what extent the shift of the annual maximum holds across different years and whether there is a dependency on the land cover. Fig. III.8 (and Fig. B.4) shows the peak lags as a function of land cover based on ESA CCI and for all years in the study period separately. Peak lags to the NDVI per proxy are generally similar between land covers, although there is a tendency in several proxies (excluding the VIproducts of MxD13C1, METGPP, SIF NASA) for larger lags in regions classified as moss. According to Fig. III.1, this largely corresponds to the sparsely vegetated areas in northern Canada with also high cover fractions of water and barren. The smallest lags of RSGPP and SIF GFZ are shown for shrubs and trees. There is also some variability between years which is largest for the timing of the moisture related variables of maximum extent of open water and GLEAM soil moisture minimum. Conversely, variability of the peak lag per land cover is smaller for the vegetation proxies between years.

III.4 Discussion

Despite the considerable challenges for remote sensing applications in high latitudes, the differences in the peak timing of families or groups of key satellite indicators of plant productivity are fairly clear in polar tundra. Absorbed energy (APAR, both EVI.Rg and NDVI.Rg) is maximized roughly one month after peak irradiance in early July. Regarding model GPP and SIF as indicators of photosynthetic activity, there is a time lag between them of four days to two and a half weeks, depending on the combination of data sets. Model GPP peaks at a similar time like APAR. SIF GFZ reaches maximum one to one and a half weeks after (July, 21st), but SIF NASA only in the end of July (DOY 209, July, 28th). Greenness (EVI and NIRv) culminates three weeks after APAR and one and a half weeks after SIF GFZ. NDVI maximum is delayed on average three more days. The indication of peak vegetation water content by VOD at a similar time like EVI and NIRv corroborates the usefulness of VOD to indicate vegetation biomass also in tundra.

Vegetation activity is highly (though not exclusively) temperature-driven in tundra (e.g. Jia et al. in Stow *et al.*, 2004; May *et al.*, 2017; Chapin, 1987). In the beginning of the growing season, light is abundant and plants rely on rhizome nutrient and carbohydrate reserves to rapidly increase photosynthetic activity (Arneth *et al.*, 2006) and growth (Chapin, 1987) by exposed mosses, lichens and evergreens after snow melt and rapid leaf out of deciduous plants. The fact that the photosynthesis seasonal maximum is reached in close temporal agreement with air temperature adds plausibility to the observed patterns in model GPP and SIF. As the time of favourable environmental conditions for growth is short, several plant types strongly invest into their photosynthetic capacity until late in the growing season to make use of the available light and temperature (Rogers *et al.*, 2017). At the time when greenness is at maximum, photosynthetic rates are decreasing as PAR is already strongly reduced and also the temperature peak has passed. The peak timing of SIF before greenness might hence indicate that although photosynthetic

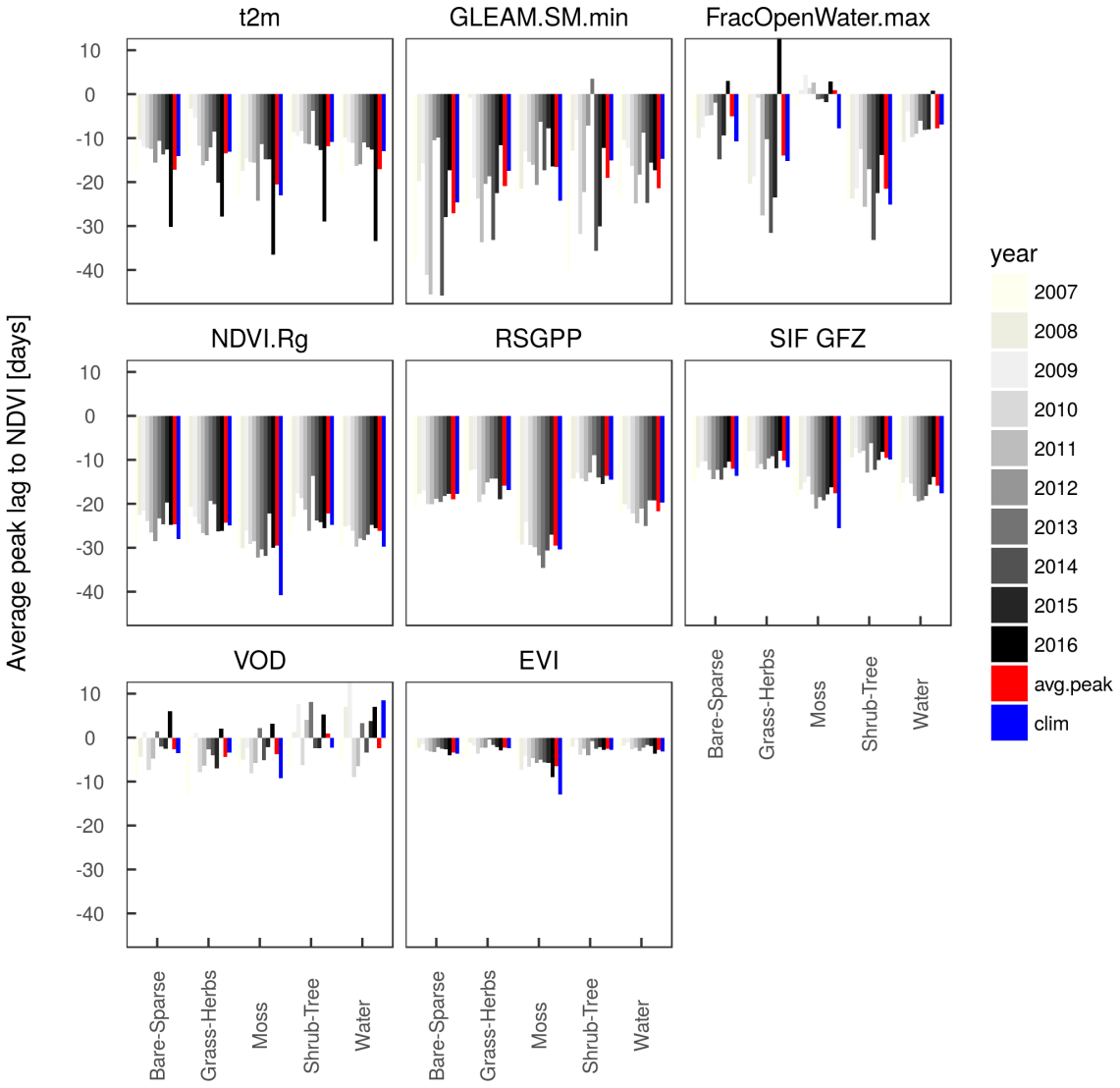

Figure III.8: Average of the time difference between the peaks of one selected variable per family (APAR, fAPAR, SIF, GPP, VOD) and the NDVI as a reference, weighted with fractional cover per vegetation type (based on ESA CCI) and per year. 'clim' denotes the peak lags between the mean seasonal cycles and 'avg.peak' represents the average of the lags across the individual years.

potential (fAPAR) is not yet fully developed, plants profit from the still higher amounts of light and maximal temperature in the year to reach peak photosynthetic rates in the second half of July. Prolonged investment of photosynthates into plant tissue result in a delayed maximum of green biomass. The coordinated dynamics of annual maximum photosynthetic activity and the resulting peak photosynthetic potential (fAPAR) with temperature are also supported by the widespread agreement between greenness proxies and photosynthesis proxies in high correlations with the temperature maximum across years and space (Fig. III.7). At the site-level, gas flux measurements find a similar timing of maximum GPP in the first half/mid-July (Emmerton *et al.*, 2016) and at the time of the annual temperature peak (Kross *et al.*, 2014; Welker *et al.*, 2004). Similarly for Lafleur and Humphreys (2008) who report on largest annual site-level NEE after summer solstice near the annual temperature maximum between DOYs190–210 and a dominant role of GEP in driving these dynamics. Also the results of Chadburn *et al.* (2017) indicate that in Earth system models, GPP rather depends on LAI in the first part of the growing season until the end of July. After that, GPP is more driven by light and always depends on temperature.

An interesting aspect of the general time lags between proxies is the one of eleven days between peak APAR and peak SIF. According to the Monteith model for SIF, the observation of a time difference of peak APAR and peak SIF suggests that SIF might contain information on temporal dynamics of actual photosynthetic light-use-efficiency of tundra vegetation. Circumarctic vegetation is adapted to low light intensities to allow photosynthesis also at low irradiance (Chapin, 1987; Rogers *et al.*, 2017, and references therein). Consequently, photosynthesis will rapidly become light-saturated, a situation that calls for high levels of non-photochemical quenching in order to avoid photodamage and inhibition by excess energy. Under these conditions, the efficiencies of carbon fixation and fluorescence emission are positively correlated (Porcar-Castell *et al.*, 2014). Consequently, our results indicate a potential benefit of using also SIF in modelling photosynthetic carbon uptake in circumpolar tundra for its apparent sensitivity to both APAR and photosynthetic light-use-efficiency. Although they did not report on results on GPP, Luus *et al.* (2017) found higher agreement between modelled NEE and eddy-covariance derived NEE when phenology is prescribed by SIF instead of EVI in tundra in Alaska.

In our results, NDVI and the MODIS VIproducts are the latest greenness proxies and peak around DOY216 (August, 4th). The NDVI is a widely used indicator of productivity and comparing to ground-based measurements as well as satellite observations with the AVHRR instrument shows mostly support for NDVI peak in very late July or the beginning of August. Ground NDVI along a transect in Alaska by Huemmrich et al. in Stow *et al.* (2004) agree with the MODIS NDVI in that the seasonal maximum is observed at DOY218 in the beginning of August. In a second year there is even a second peak at DOY230 in ground-based NDVI. Huemmrich *et al.* (2010a) show time series of ground-based NDVI in Alaska that reaches the peak about two weeks earlier (at DOY203) than the average MODIS NDVI in our results but remains high until the end of August. However, May *et al.* (2017) report on peak dates of in-situ measured NDVI in Alaska roughly one week to two weeks earlier (DOY 199-207) and tell about the beginning of senescence after the first sunset in late July or the beginning of August. Finally, satellite-based bi-weekly NDVI from the AVHRR instrument is shown to peak between July, 22nd and August, 4th (Jia et al. in

Stow *et al.*, 2004; Zhou *et al.*, 2001). Still, the onset and the peak timing of MODIS-based NDVI has also been found to not be consistent with ground based observations of NDVI (Gamon *et al.*, 2013) which might suggest partly questionable reliability of satellite NDVI.

While the reported ground observations were all conducted in Alaska, Fig. III.6 and B.3 show that the NDVI largely agrees with the other vegetation indices EVI and NIRv and only peaks later in the northeasternmost parts of Canada. In addition to the Taimyr and coastal North Slope Alaska, these are the same regions where also the NDVI lags to all other proxies are largest. According to the ESA CCI land cover, those regions are characterized by moss (Fig. III.1). Moss often has no clear seasonal cycle in greenness making a peak identification difficult. Moreover, vegetation is particularly sparse in the form of prostrate dwarf shrubs and there are extensive barren areas with rich lake cover in those northern Canadian areas (Fig. B.1, Walker *et al.*, 2005, their Fig. 1, 2e and 3). This renders the reflectance based observation particularly sensitive to background conditions, especially without a clear seasonality in greenness (Walker *et al.*, 2005, their Fig. 2f). Confirmation for this hypothesis of strong contamination of the NDVI signal is given by the sharp transition from the very large lags in northeastern mainland Canada (eastern Barren Grounds) to lower albeit still negative lags to the northwestern part of mainland Canada (Fig. III.6 and B.3, corresponding to the land cover transition between bare-sparse in the western parts of the Barren Grounds to moss in the more easterly regions of the Barren Grounds in Fig. III.1). Similar like the northern Canadian islands and northeastern mainland, northwestern Canada is characterized by many lakes (Walker *et al.*, 2005) and ESA CCI land cover reports on sparse vegetation with much moss and open water as well (Fig. B.1). However, in these more western areas, vegetation changes to rather erect dwarf shrubs and graminoids (Walker *et al.*, 2005, their Fig.3) which exhibit a clearer seasonality than the very sparse vegetation in the eastern parts with prostrate shrubs. To illustrate this point, Fig. B.5 shows the mean annual cycles of the different vegetation indices averaged over smaller regions in northern tundra. While most regions show a relatively clear seasonality, the time series of the Canadian Archipelago (northern mainland and islands), northeastern Canada and Iceland are particularly flat with no clear annual maximum period. The Canadian time series also show increasing values at the beginning and at the end of the growing season that are partly even higher than the summer maximum and severely affect the identification of the annual peak. These problems are much less pronounced in the sub-panel showing northwestern Canada with rather erect dwarf shrubs/ graminoids. We speculate that possible explanations for this might be an increasing effect of low SZA late in the growing season (Kobayashi *et al.*, 2016) affecting low NDVI in particularly sparse vegetation heavily. NDVI might also be strongly decreased by standing surface water (Gamon *et al.*, 2013) from snow melt or intermittent precipitation that has not yet drained or evaporated until later in the growing season. Only upon drying, will the NDVI increase due to the missing water absorption of the NIR, and this might affect the trajectory of NDVI strongest in the sparsely vegetated regions with the largest peak lags.

Although model GPP, SIF GFZ and SIF NASA are indicators of photosynthetic activity, they indicate different peak timing. There are several possible explanations for this: SIF might be influenced by seasonal cloud cover that affects SIF values both physiologically at the leaf level and on its way from the canopy to the satellite. However, empirical anal-

yses have shown that choosing different thresholds of cloud cover does not strongly affect temporal patterns of SIF (Köhler *et al.*, 2015a) and also in our tests with a lower cloud cover threshold no consistent patterns emerged (not shown). Further, undetected sub-pixel clouds can influence the seasonality (Köhler *et al.*, 2018). Although data availability becomes problematic in the case of OCO-2, resulting in discontinuous climatologies , there is largely agreement with OCO-2 SIF when averaged of larger regions (Fig. B.6). This is another indication that the peak timing obtained from GOME-2 SIF GFZ observations is reliable. However, the relatively large inconsistency between SIF GFZ and SIF NASA remains unclear. Figure B.7 shows the time series of both together with the illumination correction. We argue that the NASA data set is more prone to noise (for example for retrievals over bright surfaces when there is partial snow cover) due to the generally lower absolute values that result from a narrower retrieval window and that this severely affects the identification of the annual peak. This is indicated by the large spread in Fig. III.4, by the less pronounced spatial patterns in Fig. III.6, and by the time series examples in Fig. B.7. Further, the illumination correction amplifies noise in the time series. This is thus an example for the degradation of the signal by the division by cos(SZA) and calls for caution in applying it.
SIF GFZ might be better capturing the actual peak of photosynthesis in tundra than model GPP. Since the SIF maximum is reached in close temporal agreement with air temperature, it might indicate that SIF shows higher sensitivity of photosynthetic rates to temperature. The earlier peak of model GPP might be explained by a possible higher sensitivity to radiation as it is challenging to model effects of water table depth or temperature acclimation. This is especially true for the METGPP that culminates slightly earlier than RSGPP and that is driven by a mean seasonal cycle and not temporally resolved greenness. Furthermore, FLUXCOM GPP might not accurately represent GPP in tundra due to the small size of training data. FLUXCOM GPP is trained at FLUXNET sites and according to Tramontana *et al.* (2016) there are eleven sites north of 55° that are not classified as forest or temperate and serve the modelling of GPP in our study area. Five of them are located north of 65° and the three training sites classified as Arctic are all located in Alaska. Generally, model performance of model GPP is reduced in extreme climates (Tramontana *et al.*, 2016).
Overall it needs to be stated that gaps in the data and the short growing season with often small seasonality and high noise levels challenge the reliable identification of phenological dates in all data sets.

III.5 Conclusions

We analysed and compared satellite-based indicators of plant productivity with respect to the timing of their maximum in Arctic treeless regions. Over the whole study area, peak productivity is generally reached in July with a clear order of APAR culminating in the first half of July together with model GPP followed by SIF GFZ in the second third of July in synchrony with highest annual temperatures. SIF NASA is delayed by one week. EVI and NIRv indicate maximum greenness in the end of July, together with VOD as a proxy for vegetation water content. NDVI and MODIS VIproducts peak only in the first week of August. We interpret this sequence as an investment into growth of leaf tissue and pigments also after optimal conditions for assimilation regarding light and temperature have passed. Peak photosynthesis occurs earlier at a time when full photo-

synthetic potential has not yet developed but when light is still abundant and temperature favourable. Largest lags between NDVI and photosynthesis indicators are found in regions with particularly sparse vegetation without a clear seasonality in spectral reflectance that can heavily be confounded by low sun angles and the high abundance of lakes.
To our knowledge, satellite-based remote sensing of tundra vegetation has so far been based on spectral reflectance. A-priori it was questionable whether current satellite-based SIF data sets are useful for tundra vegetation considering the very large footprints, high susceptibility to noise and very small signals from the sparse vegetation. However, the spatial patterns of peak productivity of SIF are qualitatively similar to the ones seen in model GPP and reflectance-based observations. Furthermore, the fact that the SIF maximum is reached in close temporal agreement with air temperature indicates a benefit for photosynthesis from highest temperatures. The general time difference between proxies of APAR and SIF suggest that there is information on light-use-efficiency contained in the SIF observations. Still, further studies are needed to verify this. The results of our study confirm the important separation between indicators of greenness and photosynthesis and non-negligible differences between data sets of the same indicators. Upon data availability in the future, similar cross-comparisons to the chlorophyll-carotenoid index (Gamon *et al.*, 2016) and the photochemical reflectance index (Gamon *et al.*, 1992) in tundra might add yet additional complementary information on circumpolar vegetation dynamics.

III.6 Acknowledgements

We thank Guido Ceccherini e Fabio Cresto-Aleina for help on polarstereographic plotting, Ulrich Weber for processing of GlobeLand30 data and FLUXCOM data, Alessandro Cescatti for discussion and Ramdane Alkama for processing Hansen forest cover data.

CHAPTER IV

SATELLITE OBSERVATIONS OF THE CONTRASTING RESPONSE OF TREES AND GRASSES TO VARIATIONS IN WATER AVAILABILITY

Sophia Walther[1,2], Gregory Duveiller[2], Martin Jung[3], Luis Guanter[1], Alessandro Cescatti[2], Gustau Camps-Valls[4]

A modified version of this manuscript has been accepted for publication in *Geophysical Research Letters* and has been published on January, 25th 2019, https://doi.org/10.1029/2018GL080535.

Author contributions:
All authors contributed to the design of the research, SW conducted the analysis. SW wrote the manuscript with contributions from all authors, GD and AC finalized the manuscript.

A large part of the work on this project has been done during two research stays at the Joint Research Centre of the European Commission, Ispra, Italy. One has been supported by a research grant of DAAD, during the second one I received a work contract in Italy.

[1]GFZ German Research Centre for Geosciences, Helmholtz-Centre Potsdam, Section 1.4 Remote Sensing, Germany
[2]European Commission, Joint Research Centre, Directorate D – Sustainable Resources - Bio-Economy Unit, Ispra, Italy
[3]Max-Planck-Institute for Biogeochemistry, Jena, Germany
[4]Universitat de València, Image Processing Laboratory (IPL), València, Spain

Abstract

Global variations in ecosystem primary productivity are dominated by water availability. Until recently, characterizing the global photosynthetic response of different ecosystems to anomalies in soil moisture was hampered by observational limitations. Here we use a number of satellite-based proxies for productivity, including spectral indices, sun-induced chlorophyll fluorescence and data-driven estimates ofgross primary production (GPP), to re-evaluate the relationship between terrestrial photosynthesis and water. In contrast to non-woody vegetation, we find a global resilience of forested ecosystems in times of reduced soil water content. Both SIF and data-driven GPP indicate an increase in photosynthesis as a result of the accompanying higher amounts of light. Conversely, traditional remote sensing indicators of greenness reach their detection limit and largely remain stable. Our study thus highlights the differential responses of ecosystems along a tree cover gradient and illustrates the importance of differentiating indicators of plant greenness from those of photosynthesis for the monitoring and understanding of ecosystems.

IV.1 Introduction

Several recent studies stress the dominant role of water availability in driving the variability of photosynthetic activity and land carbon uptake at global scale(Jung *et al.*, 2011; Vicente-Serrano *et al.*, 2013; Poulter *et al.*, 2014; Jung *et al.*, 2017). Water deficit has been reported to cause major reductions in photosynthesis(Barber *et al.*, 2000; Barr *et al.*, 2002; Ciais *et al.*, 2005; Peng *et al.*, 2011; Schwalm *et al.*, 2012; Zscheischler *et al.*, 2014; Sun *et al.*, 2015; Yoshida *et al.*, 2015), particularly in semi-arid regions(Ahlström *et al.*, 2015; Huang *et al.*, 2016). Anomalies in precipitation caused by strong phases of the El Niño/Southern Oscillation are associated with large variability in the land carbon uptake in the semi-arid(Poulter *et al.*, 2014) and in the tropics (Liu *et al.*, 2017b). For tropical ecosystems in particular, there has been a long debate on the degree of water-limitation of photosynthesis(Nemani *et al.*, 2003; Huete *et al.*, 2006; Myneni *et al.*, 2007; Saleska *et al.*, 2007; Asner and Alencar, 2010; Brando *et al.*, 2010; Morton *et al.*, 2014; Guan *et al.*, 2015; Wu *et al.*, 2018). Also for temperate forests, negative impacts of individual events of water deficit (and heat) on GPP are reported. Those occur as a result of carry-over effects of enhanced evapotranspiration and soil moisture depletion in spring(Barr *et al.*, 2002; Angert *et al.*, 2005; le Maire *et al.*, 2010; Buermann *et al.*, 2013; Piao *et al.*, 2014; Dass *et al.*, 2016; Sippel *et al.*, 2017) and might even develop into heat- and drought-induced forest mortality(van Mantgem *et al.*, 2009; Allen *et al.*, 2010; Peng *et al.*, 2011). With climate change driving the reduction in snow packs and the anticipation of spring phenology such observations might become more frequent. However, neither the ecosystem strategies to cope with water stress (like the degree of isohydricity, enzymatic changes, carbon allocation, structural changes of the canopy) nor the possible mechanisms overrunning drought resistance and resilience capacities (e.g. cavitation, carbon starvation, critical soil moisture thresholds) are fully understood yet(van der Molen *et al.*, 2011; Fisher *et al.*, 2017). This is partly because our observational capabilities are limited and allow only indirect diagnosis of terrestrial photosynthetic activity across large spatial domains.

Advances in satellite Earth observation that occurred in the last decades offer the means to systematically examine the state of vegetation structure and function at the proper spatial and temporal scales. Traditionally this is done using vegetation indices based on

red and near-infrared reflectances, such as the enhanced vegetation index (EVI)(Huete *et al.*, 2002), that serve as proxies for photosynthetic potential and relate to plant structure and chlorophyll content (i.e. green biomass). However, such indices, on which much literature is based upon, do not respond to short-term reductions in water availability if these do not generate a reduction of green biomass. On the other hand, GPP estimations from flux tower eddy-covariance measurements do capture such effects of non-destructive water stress, but are only available over a spatially-biased selection of sites (Schimel *et al.*, 2015). This has led efforts to generate spatially explicit simulations of GPP by training machine learning algorithms to upscale site-level empirical relationships between flux tower GPP and environmental and land surface properties derived from satellite observations(Tramontana *et al.*, 2016). In parallel, a new avenue for assessing GPP directly from space at global scale has opened using SIF. It is a weak electromagnetic signal emitted by photosynthesising plants that relates to both the amount of radiation absorbed by chlorophyll and the efficiency with which it is used in carbon assimilation(Meroni *et al.*, 2009; Zarco-Tejada *et al.*, 2013; Porcar-Castell *et al.*, 2014; Joiner *et al.*, 2011; Frankenberg *et al.*, 2011a). The contributions of both to the total SIF signal across time and the explicit coupling to GPP yet remain to be clarified(Porcar-Castell *et al.*, 2014).
Our assessment is based on a simultaneous evaluation of all three indicators of photosynthesis (SIF and estimated GPP) and greenness (EVI). Anomalies in water availability are represented as meteorological events, defined as an integration of consecutive negative or positive deviations in soil water content (see Methods). After factoring out trends and normalizing the deviations from the mean seasonal cycle for all productivity and water availability indicators, we analyse how productivity varies globally with both positive and negative events of various intensities in soil moisture content along a tree cover gradient.

IV.2 Results

IV.2.1 Contrasting patterns of vegetation productivity associated with below average soil water content between forested and non-forested ecosystems

A spatial diagnostic of the average vegetation deviation associated with periods of below average soil moisture illustrates how both photosynthesis (represented by SIF and model GPP) and greenness (EVI) strongly decrease in large parts of the world (see Fig. IV.1). These areas mainly correspond to semi-arid regions where the vegetation cover is dominated by grassland, savannah and cropland, with little or no trees (Fig. IV.1d). In such areas, vegetation activity heavily depends on water availability and is therefore highly variable(Poulter *et al.*, 2014; Ahlström *et al.*, 2015) (cf. supplementary Fig. C.1, C.2), and strongly coupled to the atmosphere(Koster *et al.*, 2004; Zscheischler *et al.*, 2015). On the contrary, in cold or warm-humid climates with medium-to-high tree cover, results show a relative increase in photosynthesis in periods of reduced water availability. To better analyse this pattern, Fig. IV.2 displays the deviations from the mean in productivity and greenness along a tree cover gradient and across a range of different intensities in anomalies in water availability. For non-forested ecosystems, the three vegetation proxies consistently show the expected synchronous patterns of reduced/increased photosynthesis and greenness in times of decreased/enhanced soil water content. Furthermore, the magnitude of the vegetation anomaly increases with the strength of the departure of soil moisture from

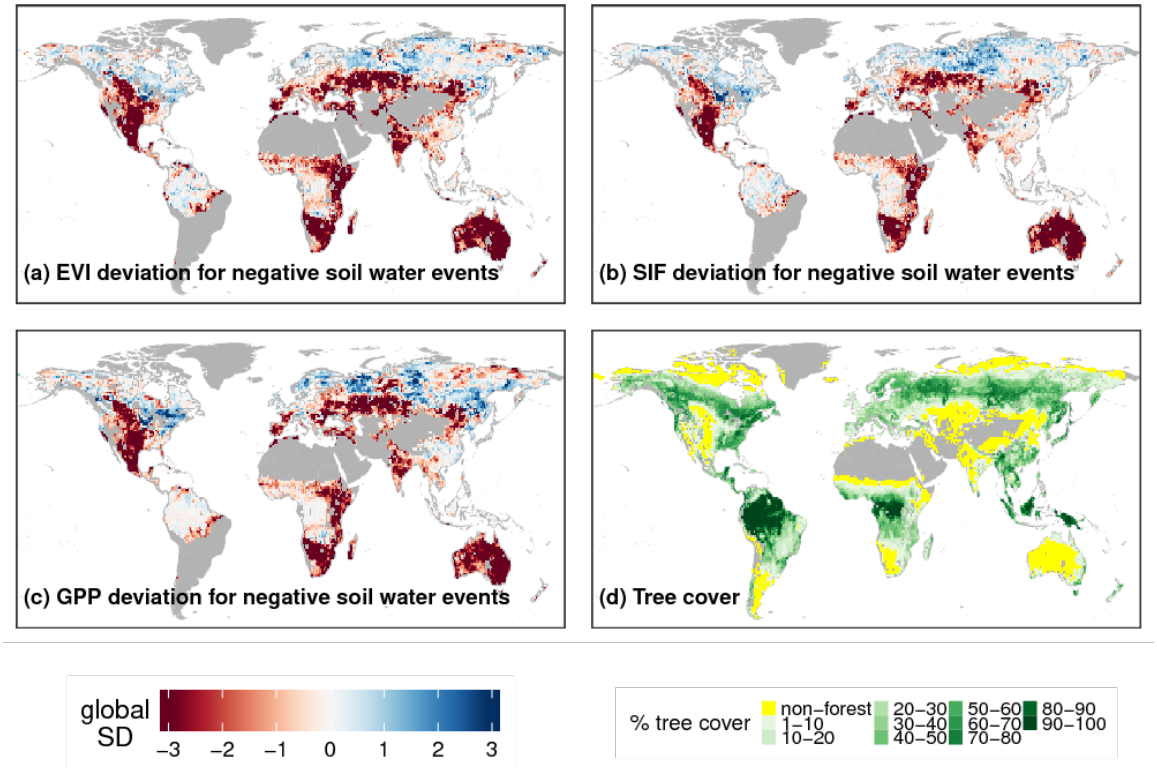

Figure IV.1: Typical vegetation reaction to below average soil water content: a-c) Deviations seen in the vegetation observations averaged across all events of reduced soil moisture. Units are given in 'global SD', meaning the standard deviation in space and time across the data cube of deviations (see methods). d) Average amount of tree cover in a pixel.

the mean, as expected. The situation changes along the tree cover gradient as both SIF and modelled GPP detect a clear reversal in the sign of the deviations in photosynthesis co-occurring with strong anomalies in water content. Here, water deficits are actually associated with increased photosynthesis whereas wetter-than-usual periods lower it. This effect is persistent even when considering soil moisture anomalies at different soil depths (see supplementary Fig. C.3). Interestingly, the traditional satellite based greenness index (EVI) is not markedly enhanced during periods of reduced soil moisture. These regional patterns of enhanced photosynthesis are in contrast to the established perception that reduced water availability has a generally negative impact on the primary productivity of terrestrial ecosystems (Zhao and Running, 2010; Liu *et al.*, 2013; Schwalm *et al.*, 2012; Reichstein *et al.*, 2013).

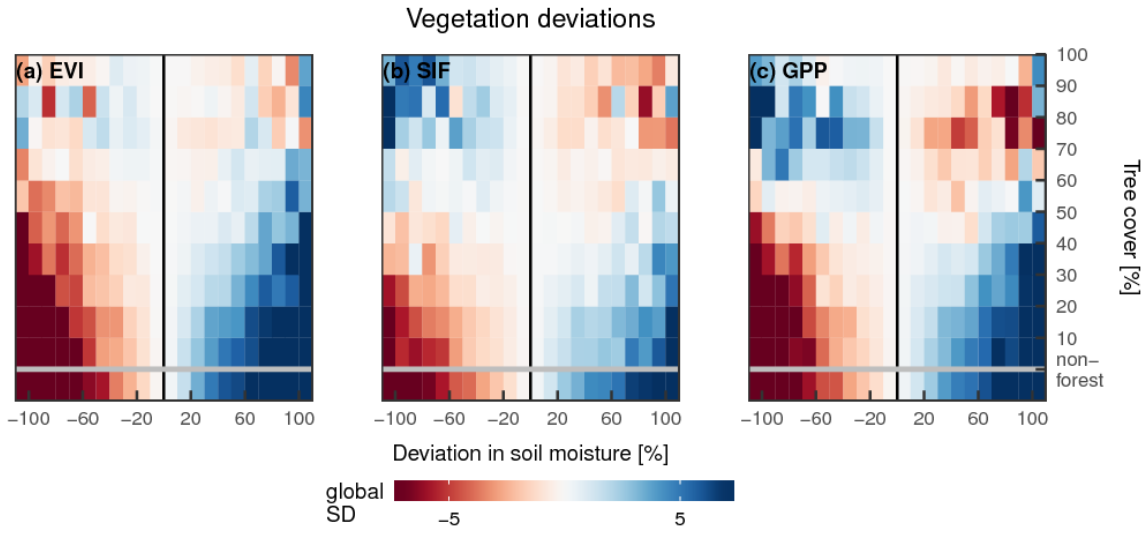

Figure IV.2: Average patterns of vegetation greenness and photosynthesis associated with water availability along a tree cover gradient: Average deviation seen in the vegetation proxies for a given anomaly in the soil water content and as a function of the amount of trees in the given pixel.

IV.2.2 The roles of light and tree density in determining the photosynthetic response to soil moisture

To explore the mechanism behind the differential response of greenness and photosynthesis to altered water availability, we examine the co-variation of temperature, incoming radiation and soil moisture with those vegetation proxies directly derived from satellite. Figure IV.3 presents the partial correlations in time of deviations in SIF and EVI with respect to either temperature, incoming radiation or soil moisture, whilst controlling for the remaining two. Soil moisture is the variable showing the largest partial correlations for both SIF and EVI in regions with little or no tree cover. This confirms that variations in soil water content affect non-forested ecosystems mainly by causing plant structural and pigment changes(Zhang *et al.*, 2016c) (i.e. chlorophyll content, leaf area), which translate into the observed variability in both greenness and photosynthesis. For intermediate fractions of tree cover, temperature becomes the component explaining the temporal variations of both EVI and SIF best, while the partial correlations with soil moisture decrease to zero. For dense forests, however, partial correlations of SIF and EVI with both soil moisture and temperature drop and radiation becomes the single-most important driver of variability in SIF, while EVI remains negatively correlated to radiation. This pattern indicates that, in dense forests, primary productivity is primarily controlled by incoming radiation (cf. the consistent results for model GPP in supplementary Fig. C.4) and the resulting temporal dynamics of photosynthesis can be tracked consistently by satellite-based SIF retrievals. The increase in photosynthesis also raises transpiration(Koirala *et al.*, 2017), which would result in a reduction of soil water content that is less likely to be replenished by precipitation due to lower cloud cover. Such mechanisms can explain the marked patterns of concurrent increases in photosynthesis and soil water reduction in densely forested areas shown in Fig. IV.2.

This effect of increased photosynthesis under conditions of decreased soil moisture typically occurs in colder humid climates where water is not the main factor limiting photosynthesis. It poses the question of whether the patterns observed in Fig. IV.2 are an artefact of the global distribution of forests, which favours comparatively humid regions, or is there an intrinsic inter-dependence between the amount of trees in an ecosystem and how it responds to variations in soil moisture(De Keersmaecker *et al.*, 2015)? We find widespread regions with a negative relationship between soil moisture and photosynthetic activity when tree cover is higher (i.e. the higher the tree cover the stronger is the association of lower soil water content with increased photosynthesis and vice versa, red regions in Fig. C.5). The occurrence of these regions in all climate zones proves that it is not the distribution of forests in rather humid climates alone that drives the response of forests to meteorological variations, but that it is the intrinsic structural and physiological differences of trees and grasses causing the observed differential responses between them(Sims *et al.*, 2014). The most reasonable explanations for this behaviour are the greater rooting depth of trees(Canadell *et al.*, 1996), their water storage capacity in the stems (Matheny *et al.*, 2015) and different strategies of water conservation between grasses and trees(Teuling *et al.*, 2010; Kelliher *et al.*, 1993). One possible reason why we do not clearly observe the pattern in tropical forests is the low data coverage from remote sensing due to clouds.

IV.2.3 The importance of greenness versus photosynthesis to assess variability in ecosystem productivity

The regular co-occurrence of increased forest photosynthesis at reduced soil water content (and vice versa), as consistently indicated by SIF and model GPP, cannot reliably be identified using satellite observations of EVI. Compared to SIF and model GPP, the EVI shows the smallest positive deviations in forests in times of reduced soil moisture (cf. Fig. IV.1). The EVI anomalies across gradients in tree cover and soil moisture deviations of both signs (Fig. IV.2a) are noisy and weak in ecosystems with more than 60% tree cover. The reason of the discrepancy between SIF and EVI in areas with a high abundance of trees is probably due to their different sensitivity to the amount of radiation absorbed in the photosynthetic process. Fluctuations in absorbed light, that mostly drive variability in photosynthesis here, can be effectively tracked by SIF but not by EVI when changes in greenness are largely absent (Fig. IV.3a). This explains the different response of EVI (greenness) from SIF and modelled GPP (photosynthesis) in forests. These patterns proved to be replicable with different greenness indices and another data set of SIF(Joiner *et al.*, 2013) (cf. MODIS NDVI(Tucker, 1979), NIRv(Badgley *et al.*, 2017) and NASA SIF in supplementary Fig. C.6, C.7). They are also robust with respect to another soil moisture data set used to define meteorological events (ERAInterim and GLEAM, supplementary Fig. C.8) and across climate zones (supplementary Fig. C.9). They even hold for some very large soil moisture deviations (Fig. IV.2, supplementary Fig. C.10). Confirmation for the negative co-variations of light with soil moisture in driving the fluctuations in forest photosynthesis is provided by consistent patterns in the variability in an estimate of absorbed radiation (cf. the product of EVI and global radiation (EVI.Rg) in supplementary Fig. C.11). Interestingly, we find different thresholds of inversion of the sensitivity along the tree cover gradient between EVI and both SIF and model GPP. We hypothesise that herbaceous dry-down strongly affects the spectral greenness signal in

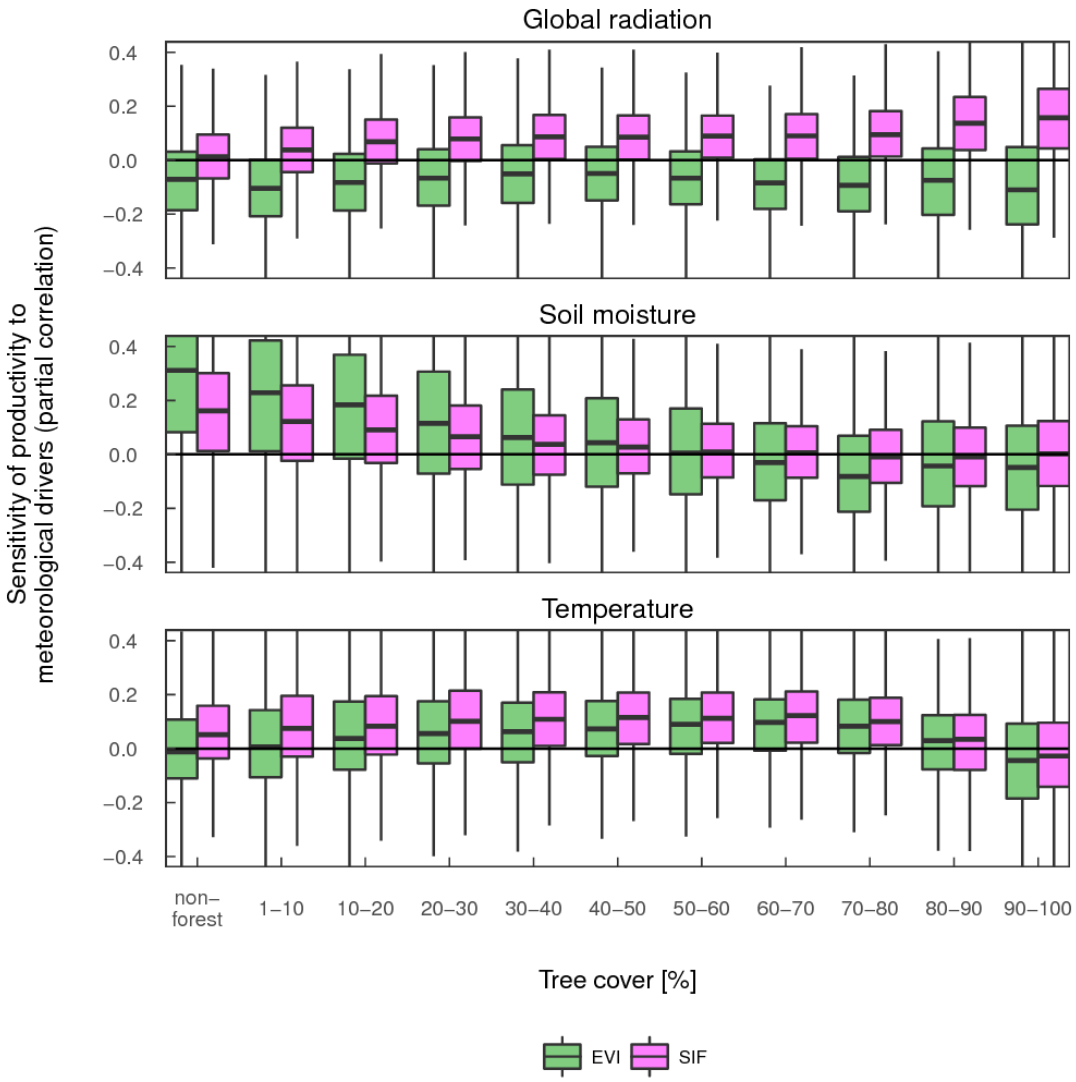

Figure IV.3: The strength of the relationship between vegetation greenness or photosynthesis and anomalies in meteorology for different amounts of tree cover: Partial correlations in time between temporal fluctuations in vegetation proxies and global radiation, temperature or soil moisture with the effects of the corresponding other two meteorological variables removed. Partial correlations are summarized as a function of tree coverage based here on 0.5° resolution data.

these mixed ecosystems. At the same time, the trees are not yet water-limited but their activity benefits from the additional radiation. That way they could balance the signal in SIF and model GPP but not in EVI. This observation reinforces the importance of the differentiation between greenness and photosynthesis in any kind of ecosystem study.

IV.3 Discussion

While the similar patterns of average variability among Earth observation products of greenness on the one hand and among various indicators of photosynthesis on the other hand build confidence in our results, they represent average patterns based on a limited number of occurrences of soil moisture fluctuations of all magnitudes. The photosynthesis enhancement in forest during periods of high radiation and reduced soil water content, as observed on average in our results, has also been reported for some very extreme events like for the strong drought in temperate forests in the US in 2012(Wolf *et al.*, 2016) or forested areas in Russia during the heat wave in 2010(Flach *et al.*, 2018). In the literature, contradictory responses of forest greenness to reduced soil moisture are reported. Observations range from negative deviations in the absence of structural changes, via no or only small(Sims *et al.*, 2014; Vicca *et al.*, 2016) greenness changes for extreme drought events, to an apparent green-up under conditions of decreased soil water content(Sims *et al.*, 2014) or under extreme heat(Zhang *et al.*, 2015). These inconsistent patterns highlight the clear need for advanced observational capabilities of the phenomena at large spatial scale. The results of our study suggest that satellite derived SIF may be a valuable asset in such a refined observational system, which is facilitated by SIF's sensitivity to instantaneous photosynthetic functioning, its direct link to plant chlorophyll content, or both. It demonstrates the capacity to inform on short-term responses of vegetation to meteorological anomalies where traditional greenness observations reach their detection limit that results from the intrinsic difference between photosynthesis and greenness.

The main conclusion to take from our study is twofold: i) The instantaneous deviations in vegetation greenness and photosynthesis that are associated with times of rapidly fluctuating soil moisture differ in sign between ecosystems with higher or lower abundances of trees; and ii) Estimates of greenness and photosynthesis show contrasting average responses in regions with higher tree cover. Our results confirm the importance of water for vegetation productivity that has emerged from a large body of literature. Non-woody semi-arid ecosystems strongly respond to the availability of soil water. At the same time, our findings show that - although apparently obvious - any surplus of water will not necessarily be beneficial for photosynthesis everywhere. Specifically, photosynthesis in ecosystems with more than 50% tree cover is more strongly affected by the co-variations in light and temperature than by soil moisture itself. In contrast to photosynthesis, greenness does barely change in those areas.
These patterns have both ecological and methodological implications. First, the differential relationship of forested and non-forested ecosystems with soil moisture has important consequences for the functioning of ecosystems in regions with extensive ongoing de- or afforestation. Man-made changes in forest cover modify the degree to which carbon uptake by vegetation is limited and consequently affected by water or light (or temperature). Also the related fluxes of energy and water will likely be altered (Teuling *et al.*, 2010; Forzieri *et al.*, 2017; Duveiller *et al.*, 2018). In addition, modifications in vegetation-

atmosphere feedbacks might cause fundamental shifts between a possible intensification or a mitigation of meteorological anomalies of all magnitudes, including extremes such as droughts (Seneviratne *et al.*, 2010; Miralles *et al.*, 2016; Green *et al.*, 2017; Zscheischler *et al.*, 2015). Second, we highlight the intrinsic but often neglected crucial difference between plant greenness and photosynthetic activity. In the absence of more direct proxies of productivity, a large part of the available research on ecosystem productivity in relation to environmental factors has relied exclusively on greenness or related variables. This is straight-forward in non-woody vegetation where greenness and photosynthesis often change concomitantly. The fluctuations in forest photosynthesis in the absence of strong greenness changes, however, call for a clearer differentiation in ecosystem and climate research between both and one might consider revisiting a part of the available literature under this aspect.

Acknowledgements

We would like to thank Michele Meroni and Markus Reichstein for valuable discussion and Ramdane Alkama for processing the Hansen forest cover map. Thanks also to Ulrich Weber for providing processed CERES data. SW and LG are funded by the Emmy Noether Programme of the German Research Foundation(GU 1276/1-1). SW acknowledges financial support through a scholarship from the German Academic Exchange Service (DAAD). MJ acknowledges support from the EU H2020 BACI project (grant no. 640176). GCV work has been supported by EU under the ERC consolidator grant SEDAL-647423.

Author Contributions

All authors contributed to the design of the research, SW conducted the analysis. SW wrote the manuscript with contributions from all authors, GD and AC finalized the manuscript.

Competing Financial Interests statement

The authors declare no competing financial interest.

IV.4 Methods

To investigate the global patterns in temporal variability of vegetation primary productivity and its relation to climate drivers, we use data sets aggregated to 1° spatial and 16 days temporal resolution (sampled every 8 days) from their native resolution. For the analysis of the effect of tree cover on the vegetation response to changes in soil water we use 0.5° spatial resolution data. The study period comprises the years from 2007 to 2015.

Sun-induced chlorophyll fluorescence. Sun-induced chlorophyll fluorescence (SIF) is an electro-magnetic signal emitted in the red and far-red wavelength region by photosynthesising plants. Its magnitude co-varies with the light energy used for carbon fixation in the plants and is the most direct proxy of GPP available on the satellite scale(Porcar-Castell *et al.*, 2014). We concentrate here on the far-red SIF (740 nm) and will not look at SIF in the red wavelength range since the retrievals in the far-red are more mature, since it is still not clear how re-absorption affects the satellite signal in the red wavelength region and because water stress in particular has been shown to be better detectable in the far-red than in the red SIF(Ač *et al.*, 2015; Daumard *et al.*, 2010; Middleton *et al.*, 2016). The longest available far-red SIF data records originate from measurements of the GOME-2 instrument on-board the MetOp-A satellite. They are available from January 2007 on, and currently two statistically-based retrieval methods have produced global far-red SIF data sets, in the following referred to as the GFZ (L2, `ftp://ftp.gfz-potsdam.de/home/mefe/GlobFluo/GOME-2/ungridded/` Köhler *et al.*, 2015a, shown in the main manuscript) and the NASA data set (L2 data v26, `https://avdc.gsfc.nasa.gov/pub/data/satellite/MetOp/GOME_F/` Joiner *et al.*, 2013, 2016, giving consistent results, shown in the supporting information). From the individual soundings of both data sets those measured under sun zenith angles larger than 70°, after 2 p.m. or before 8 a.m. local solar time were excluded. In order to remove too cloudy scenes, the effective cloud fraction was used to filter out observations with cloud fractions larger than 50% (larger than 30% in case of NASA SIF). The remaining valid observations were gridded to 1° spatial and 16 days temporal resolution.

Greenness indices and land cover. Greenness indices EVI (Huete *et al.*, 2002), NDVI (Tucker, 1979) and NIRv (Badgley *et al.*, 2017) have been calculated from MODIS nadir surface reflectance measurements. MCD43C4v005 data were retrieved from the online Reverb, courtesy of the NASA EOSDIS Land Processes Distributed Active Archive Center (LP DAAC), USGS/Earth Resources Observation and Science (EROS) Center, Sioux Falls, South Dakota, `https://lpdaac.usgs.gov/dataset_discovery/modis/modis_products_table/mcd43c4`. The surface reflectances gridded at 0.05° have been filtered for snow and good quality retrievals (quality flags 0 and 1 admitted, meaning at least 75% with full or best inversions), the vegetation indices have been calculated, and then aggregated to 1° spatial resolution.
Furthermore, information on land cover according to the IGBP classification has been retrieved from the MCD12C1 file for 2009 (we take this year as representative for the whole study period) in order to exclude regions from the analysis that are covered by water, ice or that are barren. We aggregated it to 1° spatial resolution by assigning the land cover class with the most frequent occurrence in all sub-pixels of 0.05°.

Data-driven GPP model simulations. Additional comparisons are carried out with model results of GPP from the FLUXCOM simulations (Tramontana *et al.*, 2015 http://www.fluxcom.org/products.html). Different machine-learning techniques are used to spatially up-scale the empirical relationship between GPP and various land surface variables learned at FLUXNET eddy-covariance tower locations to the globe. Only remotely sensed variables (plant functional type, EVI, NDVI, middle infrared reflectance, leaf area index, normalized difference water index, land surface temperature during day and night, global radiation) inferred from MODIS measurements are used as explanatory variables. We use the median of an ensemble of simulations that come with a native resolution of 1/12° and 8 days.

Meteorological data and soil water content. To study the environmental effects on vegetation, we look at temperature and water conditions using the air temperature in two meters height and the volumetric soil water content in the four layers between 0-7 cm, 7-28 cm, 28-100 cm and 100-289 cm depth from ERAInterim reanalysis data(Dee *et al.*, 2011a). We convert the volumetric soil water content in m^3/m^3 to mm and additionally take an average across all four soil layers weighted by the layer thickness.
To avoid a possible dependence of the results on the choice of the soil moisture data set, we additionally use information on soil water in the surface and the root zone layers obtained from the GLEAM v3.1a data (Miralles *et al.*, 2011; Martens *et al.*, 2017). We intentionally do not use precipitation or vapour pressure deficit but soil water in order to get an estimate of the amount of water that is effectively available to the plants rather than the potential supply or atmospheric demand which are more strongly decoupled from the vegetation and potential stressing factors.
To have an estimate of the incoming radiation, we use all-sky surface fluxes of downward shortwave radiation (global radiation) computed from observed top-of-atmosphere fluxes that are distributed at 1° spatial and daily temporal resolution (the 'SYN1deg-Day product') by the Clouds and the Earth's Radiant Energy System (CERES)(Doelling *et al.*, 2013) onboard the Aqua and Terra satellites. The data cover the period 2007–2014, so all analyses including global radiation data are based only on those years and do exclude information from 2015.
Tree cover and Köppen climate classification. Information on the amount of tree cover is inferred from the global maps of global forest cover gain and loss by Hansen et al. (Hansen *et al.*, 2013) based on Landsat images. The global forest cover in 2009 (with tree cover defined as the areal coverage with canopies of more than 5 m height) has been obtained by combining information on the global tree cover in 2000, the yearly losses until 2009 and the gains until 2009 assuming a linear growth between 2000 and 2012. This information on forest cover in 2009 has subsequently been aggregated from the native 30 arcsec resolution to 1° to be used in this study.
Climate classification is based on the latest release of the global map of the Köppen-Geiger classification (Rubel *et al.*, 2017; Kottek *et al.*, 2006) representative for the period 1986–2010.
It is a known issue that SIF measurements suffer from noise contamination in South America due to high cosmic particle fluxes in the region of the South Atlantic Anomaly(Köhler *et al.*, 2015a). We therefore excluded this region (Transcom region 4, all of South America except larger Amazonia) from all analyses.

Data processing

Deviations from the average behaviour. All data streams of vegetation proxies and of meteorological and soil moisture conditions are treated in the same way in that they are linearly de-trended pixelwise (over the whole period 2007–2015) if a reliable estimate of the linear trend can be obtained. This means that more than half of the data points must be available over the period analysed and the trend has to be significant at the 5% level in a given pixel. This procedure is intended to remove possible tiny artefacts/trends due to sensor degradation that have been reported for the MODIS C5 NBAR surface reflectances (Lyapustin *et al.*, 2014) and that might have translated into the calculation of our vegetation indices from the MODIS sensor. The resulting de-trended time series is deseasonalized by removing the mean seasonal cycle (MSC). This procedure is complicated by the fact that we include in our analysis retrievals of SIF from the GOME-2 instrument onboard MetOp-A. Several orbit manoeuvres of MetOp-A have been done between the end of 2011 and the beginning of 2013, mostly in 2012, and it is not clear to what extent those might have artificially affected the time series. There is a tendency towards lower values in both, the GFZ and the NASA SIF data, particularly against the end of the data record. According to our tests, those decreasing values are best corrected for by computing the MSC separately for the period 2007-2011 and 2012-2015. In order to be consistent between data sets, this is not only done in case of SIF but for all data streams. The resulting deviations from the average temporal behaviour originate from shifts in phenology and will be a natural reaction of the vegetation to meteorological variations. They do not describe anomalous (in the sense of unexpected) behaviour of the plants. In order to exclude cumulative effects resulting from comparatively large deviations caused by noise in phases when vegetation is dormant or absent, we only take into account observations when there is green vegetation (EVI$\geq$0.1) and during the growing season (roughly approximated by EVI$\geq$30% of annual maximum). We apply the same growing season filter to all data sets and also match the spatio-temporal sampling, so that the same points in time and space are taken into account for each vegetation proxy. A standardization of each data set by its area weighted standard deviation across the whole data cube (weigh a given pixel value by the cosine of the latitude of the pixel and take the standard deviation across all pixel values) will make the deviations comparable between vegetation proxies as well as their ranges and units. Hence the resulting deviations from the average vegetation behaviour are measured in units of 'global (spatio-temporal) standard deviations (global SD)'.

Event-based analysis. The link between meteorology and vegetation variability is studied from a driver perspective. That means that we search for deviations from climatology in one meteorological variable and define events based on that. Then, the corresponding deviation in the vegetation proxies is analysed for each event. We use deviations in the soil water content to define a meteorological event as a period of consecutive positive (negative) deviations in a given pixel. We then sum the deviations of a given vegetation proxy in the same pixel over the duration of a given event and will obtain the integrated deviation (or event size) as the immediate vegetation response to the soil moisture event. Iterating over all pixels and events we will thus obtain integrated vegetation deviations that can be compared across proxies in a consistent way, as for every vegetation proxy the meteorological events are the same. We show integrated event sizes of relative deviations in soil moisture (deviation at a given time step divided by the multi-year average value

at this time of the year) in order to make deviations in soil moisture comparable across space. For summary plots other than maps the deviations are weighted by their areal contributions to the average (again, a pixel value is weighted with the cosine of the latitude). If a meteorological event has no effect on the vegetation, this method will still work. However, lagged and longer lasting vegetation responses(Braswell *et al.*, 1997; Smith, 2011; Frank *et al.*, 2015) to meteorological variations are not taken into account. Limiting the analysis to the immediate responses of the vegetation leaves an important ecological time period uncovered, which might be particularly severe in case of forested ecosystems. Furthermore, co-limitation of plant activity by more that one meteorological variable (compound events), e.g. heat and drought, cannot explicitly be identified with this approach. Methods to detect extreme events(Zscheischler *et al.*, 2013, 2014; Mahecha *et al.*, 2017) or coincidence analysis of extremes in environmental conditions and the vegetation response(e.g. Donges *et al.*, 2016; Rammig *et al.*, 2015; Baumbach *et al.*, 2017) have intentionally not been employed in this study, as we are interested in the general response of vegetation to environmental fluctuations rather than in the most extreme ones. Except for applying the quite crude growing season filter, we do not analyse the vegetation reactions separately for different times during the year. This represents an important limitation of our study as differing responses and sensitivities might be expected for different seasons. For example, in the mid-latitudes vegetation is generally rather temperature-limited in spring and rather sensitive to precipitation in summer with changing sensitivities with latitude throughout a year(le Maire *et al.*, 2010; Wu *et al.*, 2012; Ceccherini *et al.*, 2014). The overstory in a savannah ecosystem has been shown to be light-limited during the wet season and water-limited during the dry season(Moore *et al.*, 2016), the same for southeast Asian tropical forests(Zhang *et al.*, 2016d). Further, the detectability of the meteorological impacts on the vegetation does not only change between the types of satellite observation (greenness or SIF), but also with the season and the phasing between the meteorological driver and the phenology of the vegetation proxy(Vicca *et al.*, 2016; Zhang *et al.*, 2016d). Our approach is limited to give information on the average behaviour across all times of the growing season. We cannot infer whether observed sensitivities are rather due to changes in the length of the growing season or due to effects during the peak seasonal cycle(Zhou *et al.*, 2016). Splitting for various periods during a year will result in too few events and results will become barely representative and reliable. With more years of available satellite observations future investigations should consider analysing seasonally changing responses.

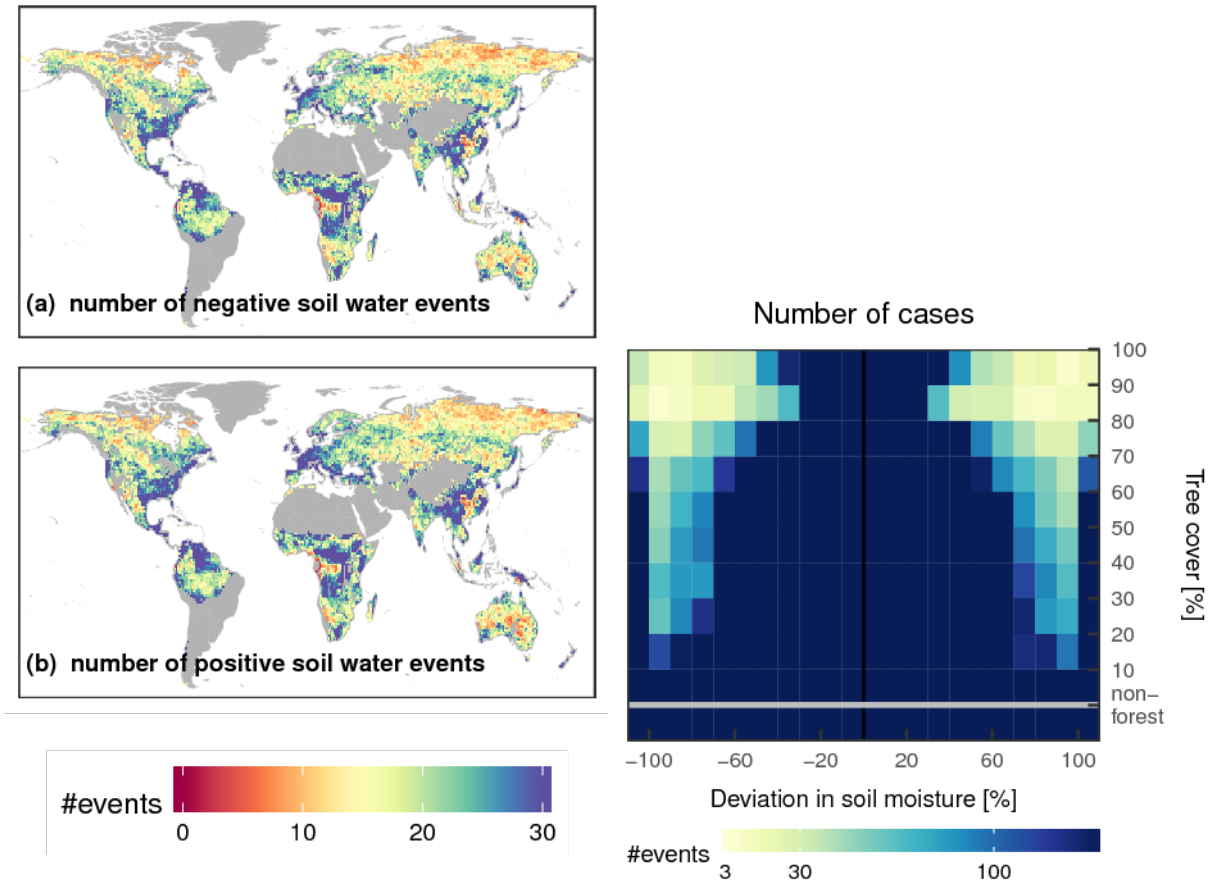

Figure IV.4: Number of events going into an average.

CHAPTER V

SYNTHESIS AND OUTLOOK

The objective of this thesis was the joint evaluation of temporal patterns of various indicators of vegetation photosynthetic activity derived from spacebased measurements. In this context, phenological behaviour has been inferred and compared between reflectance-based vegetation indices as proxies of greenness/ photosynthetic potential and SIF as a proxy of actual photosynthetic activity. In addition, estimates of GPP based on empirical models that ingests information from both *in-situ* EC measurements and satellite-based information on the state of the land surface are used. Phenological patterns were analysed for boreal forests and tundra as well as phenological shifts related to soil water availability globally. In the following, answers to the specific research questions are given for each case study separately before summarizing the main objectives of this thesis based on all three case studies:

Chapter II highlights the intrinsic differences between photosynthetic activity and greenness in the timing of the start and the end of the annual cycles in boreal evergreen forests.

- Which are typical phenological dates like start, peak and end of the growing season as indicated by greenness, SIF and model GPP? How can possible differences between proxies be explained?

  The photosynthetic spring recovery as indicated by both SIF and model GPP coincides with the rise of air temperatures above the freezing point and precedes increases in greenness by approximately four weeks. This is in agreement with knowledge from leaf-level and laboratory studies who had found an earlier commencement of photosynthesis than changes in chlorophyll concentration and emerging of shoots. In contrast to that, the start and end of the the growing season in deciduous broadleaf forest has been found to be largely consistent.

- Are phenological changes in photosynthetic activity traceable using SIF that do not coincide with changes in greenness?

  The results have shown that SIF is capable of indicating variability in photosynthesis when greenness is largely constant, both in evergreen forests during spring recovery

as well as in deciduous forests during the peak growing season. It needs to be noted that as a consequence of the data processing, in evergreen needleleaf forest, possible early signs of green-up after winter dormancy may be masked for snow. However, testing of several snow cover thresholds and comparison with *in-situ* observations indicate that a significant effect on the results is improbable.

- If so, can the decoupling be explained by changes in PAR and/or by changes in LUE_f?

  Comparison of a proxy of APAR with SIF suggests that changes in photosynthesis in evergreens can be explained by the effects of both PAR and LUE_f in spring. Conversely, in deciduous forests, changes in incoming PAR mainly drive variability in SIF and model GPP during the peak growing season when greenness is relatively stable.

Chapter III presents an evaluation of the timing of the peak growing season in circumpolar treeless regions by a comprehensive comparison of various indicators of greenness and photosynthesis and demonstrates a lag of on average one week between both.

- Which are typical phenological dates like start, peak and end of the growing season as indicated by greenness, SIF and model GPP? How can possible differences between proxies be explained?

  There is a distinct order of the time in the year when the annual maximum values of the different vegetation proxies are reached: APAR $\leq$ model GPP $<$ SIF $<$ vegetation indices and VOD. This sequence is explained as the result of best conditions for photosynthesis by peak temperatures and much incoming PAR, while the full built-up of new plant material is extended until late in the short growing season. It is possible that relatively high uncertainties in NDVI and SIF due to low illumination angles affect the results. NDVI additionally is influenced by background conditions. The study further hypothesises on a too strong sensitivity of model GPP to radiation resulting in an earlier peak compared to SIF. Data availability and partly very small seasonal cycles in combination with relatively high noise levels introduce uncertainties in the analysis. Therefore, average patterns over multiple years are analysed.

- Are phenological changes in photosynthetic activity traceable using SIF that do not coincide with changes in greenness?

  There is a lag between annual peak photosynthesis and greenness. However, both of them change during the short growing season and greenness is not constant, but asynchronous.

- If so, can the observed decoupling be explained by changes in PAR and/or by changes in LUE_f?

  SIF is strongly driven by the amount of incoming light. Still, there is a temporal mismatch between estimates of APAR and SIF maxima. This indicates that LUE_f also affects the timing of the annual maximum of SIF and delays it with respect to APAR towards the period of highest annual temperatures.

Chapter IV elaborates on the phenological shifts as observed from space that are associated with periods of deviations in soil moisture. Investigated are global ecosystems along a tree cover gradient.

- Globally, which are the phenological alterations observed in different ecosystems that occur in times of changing soil moisture as indicated by greenness, SIF and model GPP?

  Patterns of deviations from the mean seasonal cycle in the vegetation proxies are evaluated for a range of events of soil moisture anomalies. Regions characterized by low tree cover on average show strong reductions in greenness and photosynthesis proxies in times of reduced soil moisture (and vice versa for elevated soil water content). Conversely, ecosystems with tree cover of more than 50 % show increases in photosynthesis proxies but barely in greenness. Further, the tree cover threshold at which the inversion of the proxies' sensitivity to soil water occurs differs between proxies of greenness and of photosynthesis.

- How can differences between ecosystems in the phenological shifts in the vegetation proxies associated with soil moisture deviations be explained?

  This can be explained by the fact that non-forested ecosystems intrinsically do not follow a water conservative strategy. Conversely for forested areas, where trees usually have access to deeper soil layers and stored reserves in the stems. Even though a certain level of soil moisture is necessary, it seems that forest activity is not actively regulated by soil water on the time scales under investigation but rather by the associated co-variations in light. The different tree cover threshold of the inversion of the sensitivity of greenness versus photosynthesis in mixed tree-grass-ecosystems is interpreted as a stronger signal of water changes in spectral reflectance than in actual photosynthesis.

- Can purely physiological changes be separated from greenness changes?

  While in non-forested ecosystems the vegetation responses are driven by changes in greenness (leaf drying and senescence or leaf flushing), forests indicate only negligible anomalies in greenness on the investigated time scales. PAR is the most important driving variable for photosynthesis in forests, as indicated by the qualitatively similar response of APAR to SIF and model GPP. It needs to be noted, that the average of vegetation anomalies of all sizes have been evaluated. Hence the signal that is interpreted corresponds to the average pattern of phenological shifts of all magnitudes, including but not limited to extreme events. This implies that for individual events the vegetation responses can differ significantly depending on the complex interplay of external factors that influence the ecosystem activity.

Following the joint assessment of vegetation dynamics from space as done for these three selected study cases the overall objectives that have been achieved in this thesis can be summarized as follows:

- Where on Earth can we find agreement between the trajectories of greenness, SIF and state-of-the-art estimates of GPP (model GPP)? In which biomes do the spatio-temporal patterns of greenness, SIF and model GPP differ and why?

  The trajectories of spectral greenness indices and photosynthesis as indicated by SIF and model GPP are generally synchronous in times and places where photosynthesis is primarily driven by greenness. This is often the case for deciduous vegetation with respect to the length of the growing season where no photosynthesis can take place before leaves have emerged or after they have senescened. Similarly, morphological phenology in non-forested ecosystems is heavily affected by shifts in environmental conditions, particularly by fluctuations in soil moisture availability. Fast flushing of grasses with precipitation and senescence with water deficit cause synchronous changes in greenness and photosynthesis.
  Asynchrony between the dynamics of photosynthesis and greenness is observed when green biomass is present but photosynthesis is more strongly driven by environmental limitations. This is illustrated with the examples of the photosynthetic spring recovery in evergreen needleleaf forests upon temperature increase above the freezing point before new pigments and shoots are built, or with the example of the light-driven fluctuations in photosynthesis in deciduous forests during the peak growing season. Also in circumpolar tundra do the trajectories of greenness and photosynthesis indicators partly disagree in that a lag of the annual maxima is observed. This is interpreted as being the consequence of a longer built-up of plant material also after optimal conditions for photosynthesis regarding temperature and light have passed. As a last example, in mixed tree-non tree ecosystems, it appears that the spectral reflectance signal is much stronger influenced by environmental changes like water availability than actual photosynthesis. A possible explanation is the stronger contribution of trees as a structurally more stable ecosystem component to the photosynthesis signal than to the spectral signal. There might be a brown-down of grass during water deficit but possibly light-enhanced photosynthesis by the trees in the ecosystem who do not suffer from water shortage yet.

- Is there an added value of current satellite SIF data with respect to reflectance measurements to indicate temporal dynamics of GPP and if so, where and when?

  Cross-consistency of the temporal patterns of SIF and model GPP support SIF as a reliable indicator of fluctuations in photosynthesis, also in the case of differing greenness dynamics. Therefore, under the conditions of constant or asynchronous greenness dynamics, SIF has been shown to represent an asset for the space-based monitoring of photosynthesis compared to reflectance-based measurements. The results emphasize that a clear distinction between greenness and photosynthetic activity is necessary when exploring plant productivity, particularly in places where their dynamics are asynchronous. In the absence of more direct proxies of photosynthesis in the past, several studies exclusively used greenness indicators to estimate ecosystem dynamics. Those might partly need to be revisited. However, this thesis is limited to the cross-comparison of the temporal patterns in several vegetation proxies and their interpretation with respect to environmental conditions and knowledge from field and laboratory studies. It is no direct validation or translation of the pat-

terns into GPP. Hypotheses on the process-attribution of the observed patterns are given based on comparisons to field observations and physiological knowledge, but due to the coarse spatial scale of investigation consolidated mechanistic explanations are not possible. Moreover, only selected environmental variables (often based on models) were taken into account in the interpretation where other factors might have affected the vegetation (vapour pressure deficit, nutrients, lagged effects etc.) or the measured signals (canopy structure, observation geometry, etc.) as well. Finally, due to data quality and availability all analyses are limited to a temporal resolution of 16 days which might have obscured shorter term variations in photosynthesis.

- Can the contributions of fPAR, PAR and emission efficiency (cf. Monteith model of SIF, eq. I.2) to the observed far-red SIF be disentangled and are they plausible regarding what has been found in laboratory and field experiments?

  In order to separate the contributions of fPAR, PAR and LUE_f to the total SIF, additional information is required which represents an important error source for the contributing factors of interest. The sensitivity of SIF to incoming PAR is one of the advantages of SIF compared to traditional reflectance-based monitoring from space. The photosynthetic variations in forests that can be attributed to light where effects of fPAR, soil moisture or temperature are of minor importance are a good example of this. Further, in one measurement, SIF incorporates the total amount of energy that is absorbed by chlorophyll and can potentially be used for carbon fixation. Although this same term, $APAR_{green}$, can as well be approximated by the product of any vegetation index and PAR, this would necessitate two measurements, of which the one of fPAR will mostly not be $fPAR_{green}$ but $fPAR_{total\ scene}$.
  Still, also the dynamics of SIF and estimates of APAR are not always synchronous. This indicates that the value of SIF to track photosynthesis does not only result from its sensitivity to PAR but also to changes in LUE_f. This has been demonstrated in this thesis for the photosynthetic spring onset in evergreen needleleaf forests and could be explained with the available literature on physiological mechanisms of photosynthetic downregulation in winter. As another example further to the north in circumpolar tundra, SIF reaches its annual peak only when air temperature is most favourable despite that absorbed energy peaks already earlier which is potentially indicative of effects of LUE_f in the dynamics of total SIF.
  In summary, SIF has been shown to be a reliable indicator of variability in photosynthesis through its consistency with model GPP, also in places and at times when greenness shows a different behaviour. For the three study cases of this thesis, SIF was shown to be useful through its sensitivity to all terms of the SIF Monteith model (eq. I.2).

The work presented here is a joint assessment and cross-comparison of satellite proxies of greenness and photosynthesis. Their agreement with each other or with expectations from knowledge gained from leaf-level studies adds confidence to their performance for the space-based monitoring of photosynthesis. However, the studies do not represent a validation of the different data sets - a critical step that needs further attention in future research. The value of SIF to indicate *variations* in GPP is a restriction at the same time as a direct translation into GPP is not possible. Besides the limitations of SIF to indicate GPP given in section I.2.3.3, it needs to be stated that research on the driving variables

of SIF and its relationship to GPP, including the ratio of LUE_p/LUE_f, for various situations and ecosystems is necessary. Moreover, the scale mismatch between leaf-level or field campaigns and the satellite footprint needs to be bridged for research activities that are directed rather towards validation than to comparison. This could be achieved by airborne measurements (HyPlant and CFIS, Rascher *et al.*, 2015; Sun *et al.*, 2017) and/ or new space instruments that are capable of monitoring fluorescence. Very promising in this respect is the recently launched Sentinel-5 Precursor TROPOMI (TROPOspheric Monitoring Instrument). Globally continuous coverage with ground footprints of 7 x 7 km size at nadir view and five-fold sampling compared to GOME-2 will be achieved across the full SIF spectrum (Guanter *et al.*, 2015). This will allow finer resolution studies in both space and time. The spatio-temporal resolution of current GOME-2 data[1], the most widely analysed ones with continuous global coverage, represents a major limitation for certain applications. With global data at finer spatial and temporal resolution new opportunities for carbon cycle-related studies will be given. Next to TROPOMI, the ESA Earth Explorer Mission FLEX will be the first dedicated mission to observe fluorescence from space (ESA, 2015; Drusch *et al.*, 2017). The remarkably fine spatial resolution of 300 m will allow studies on scales that are unprecedented for space-based SIF. The concurrent measurement of land surface temperature, spectral reflectance and SIF in both emission peaks is expected to allow an important advancement in the understanding of processes governing SIF. A major limitation of FLEX is however the revisit time of 27 days at the equator (increasing sampling towards higher latitudes) allowing temporal investigations at monthly time scale under the assumption of cloud-free conditions at consecutive overpasses.

A very exciting new avenue is the monitoring of vegetation at sub-daily resolution by retrieving SIF from geostationary satellite instruments. This would allow very high temporal resolution studies of diurnal dynamics of photosynthesis instead of being limited to a snapshot at a given time of the day, including short-term fluctuations of LUE and many more. Several missions are planned like Sentinel-4, TEMPO or GeoCARB. At the same time, initiatives are underway to also empirically upscale EC measurements to the globe at sub-daily time steps (Bodesheim *et al.*, 2018). Cross-comparisons of these products with geostationary SIF observations promise to significantly extend our understanding of the relationship between SIF and GPP and further illuminate under which conditions or at what time during the day the two are possibly decoupled.

Active research is currently also happening to address photosynthesis dynamics from the complementary approach of measuring reflectances in wavelengths that are affected by changes in pigment pool sizes and states. Specifically, the ratio of the pool sizes of carotenoids and chlorophylls determines the ability to both absorb energy and quench it photochemically on the one hand and to quench it in a non-photochemical way on the other hand. Moreover, carotenoids are chemically changed in the xanthophyll cycle according to the environmental conditions, and the different states of the carotenoids are associated with different capabilities of NPQ. These pigment changes affect photochemical quenching and fluorescence and change the reflective properties of the leaves. The chlorophyll-carotenoid index (CCI, Gamon *et al.*, 2016) is a promising example of a new index that apparently reliably tracks photosynthesis dynamics in evergreens and deciduous species by being sensitive to structural effects and pigment changes (Springer *et al.*, 2017). Moreover, the photochemical reflectance index (PRI, Gamon *et al.*, 1992, 1997;

[1] 40 x 80 km and 1.5 days revisit time, since July 2013 40 x 40 km, three days revisit time

Wong and Gamon, 2014; Gamon *et al.*, 2015) is employed in analyses as an indicator of the combined dynamics in pigment pool sizes and xanthophylls. However, both indices seem to be influenced by the appearance of snow (Springer *et al.*, 2017) and hitherto no global data sets are available for CCI or PRI.
Finally, research of merging the complementary information in greenness and SIF and of exploiting the assets of both is starting to grow. Downscaling exercises of coarse SIF data to finer spatial resolution using reflectance data showed promising temporal agreement with EC GPP (Duveiller and Cescatti, 2016). Also data sets of proxies of $fPAR_{chlorophyll}$ statistically obtained from MODIS data trained on GOME-2 SIF have been published recently (Gentine and Alemohammad, 2018). Those approaches allow studies in a higher spatial resolution based on records that span several years which is not possible in a non-synergistic use of the data sources.
With this wealth of upcoming new data sources of SIF and new reflectance-based indices with potential future global application, extensive further analyses of the assets and limitations of SIF, reflectance-based approaches and model GPP will be possible as well as an improved understanding of global ecosystem functioning and carbon uptake.

Appendices

APPENDIX A

SUPPORTING INFORMATION FOR THE PUBLICATION "SATELLITE CHLOROPHYLL FLUORESCENCE MEASUREMENTS REVEAL LARGE-SCALE DECOUPLING OF PHOTOSYNTHESIS AND GREENNESS DYNAMICS IN BOREAL EVERGREEN FORESTS IN SPRING"

I.1 Effects of EVI quality and snow filtering

Different thresholds in the quality and snow filtering of the EVI preprocessing were tested. The filtering has been done in the native 0.05° resolution, hence before the spatial aggregation to 0.5°. It has been tested for the influence of the strictness of the quality filtering in that in one experiment all MODIS surface reflectances with MODIS quality flags inferior to 0 (best,75% or more with best full inversions) and 1 (good,75% or more with full inversions) were discarded. In a second version additionally pixels having mixed quality (flag 2, 75% or less full inversions and 25% or less fill values) were admitted. Similarly, a strict snow filter has been applied, meaning that all pixels containing any snow according to the snow flag were removed and two less strict versions allowing 10% and 30% snow cover. This has also been compared to the results of a completely unfiltered EVI.

I.1.1 Quality filtering

Figure A.1 shows the effect of the quality filtering on the obtained SOS, EOS, relative RMSE and the number of years where the fitting was successful. Except for western Russia, the data set with up to mixed quality overall has a somewhat narrower growing season than with the strict quality filter, meaning a slightly later SOS and a slightly earlier EOS. The mixed quality EVI also has a slightly higher relative RMSE, especially in western Russia, but there also higher success in the fitting (measured in years in which a fit was possible). In the rest of the mid-to-high latitude forests the number of fitted years does not depend on the quality filtering. These observations are independent of the snow threshold chosen. When no threshold is chosen and the snow influence on the EVI is not removed, the effects of the quality filtering are strongest and partly change their sign. The influence of the quality filter on the coefficient of determination is only very

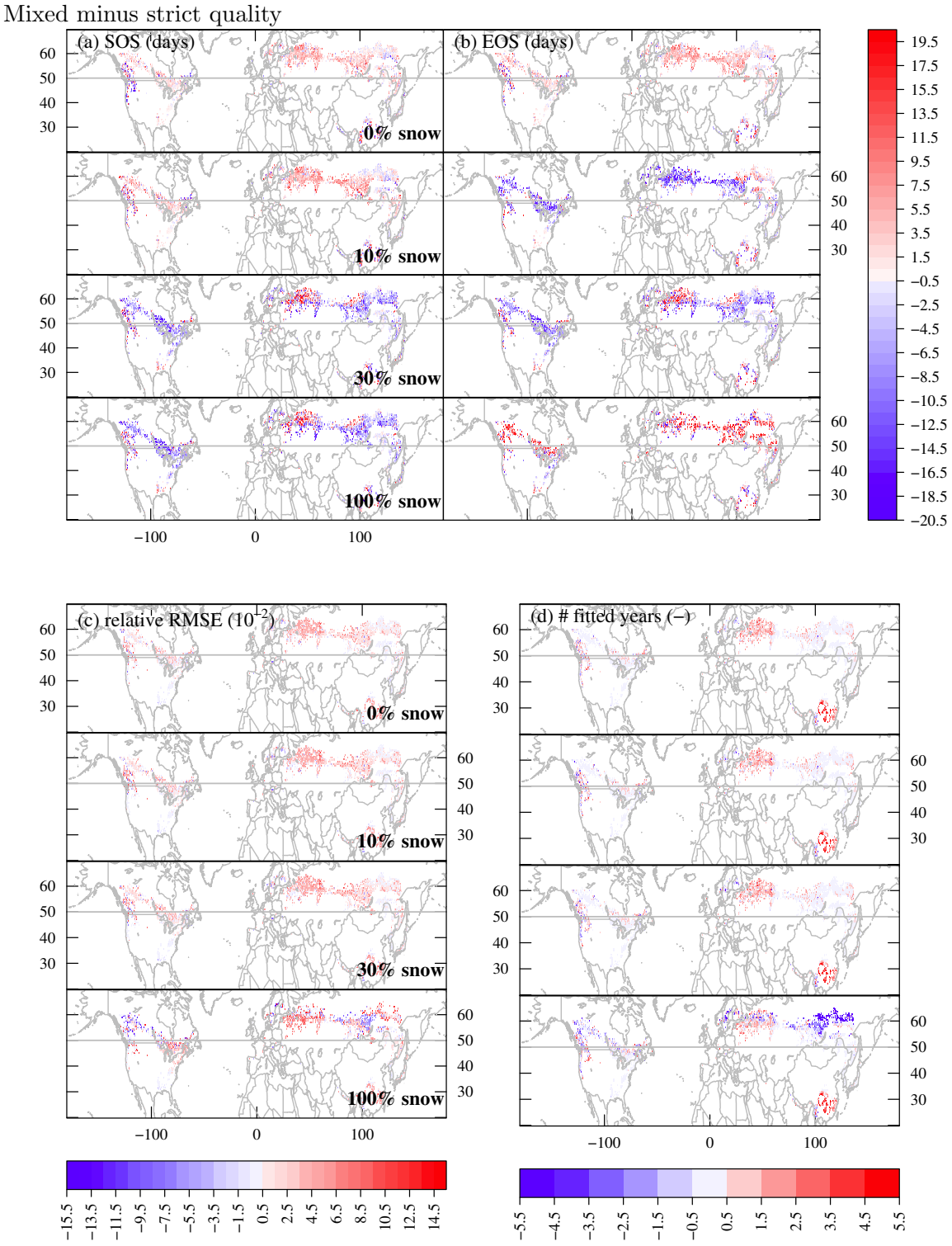

Figure A.1: Effect of the strictness of the quality filtering of the EVI on the identified SOS **(a)**, EOS **(b)**, relative RMSE **(c)** and the number of years where the fitting was successful **(d)** for different thresholds of the snow filter (100% means no snow filter applied). Displayed are the differences between the mixed quality (quality flags up to 2) and the good quality only (quality flags 0 and 1) data sets.

marginal (strict quality filtering has a r^2 of at most 0.055 higher than the mixed quality in the case without snow filter, not shown). It has been decided for the less strict quality filtering in order to retain more points for the fitting procedure, which results in a higher number of successful SOS and EOS identifications and should make the obtained average phenological dates more robust. This is an important aspect, particularly as only five years of data go into the analysis.

I.1.2 Snow filtering

In Figure A.2 the median annual cycles of the EVI are shown for ENF, DNF and DBF and in a version containing 100% snow (no snow filter applied), containing no snow (all snowy pixels removed) and the corresponding fitted functions. The effect of snow on the time series is clear in the ENF and DNF and only marginally visible in the temperate DBF. The presence of snow advances the increase of the EVI, and the increase might be the signal of its melting. A snow filter is crucial to reliably identify the annual cycle of the EVI which is only caused by greenness changes and not by the occurrence of snow. In Figure A.3 the effects of the different snow filter thresholds on SOS, EOS, relative RMSE and the number of years in which a successful fitting was possible is shown for the EVI with mixed quality. The maps will qualitatively look the same with the strict quality filtering with quantitatively slightly smaller differences (not shown). The level of the snow filter threshold does not have any influence on SOS and EOS. This might be due to the fact already stated in the main text that a large part of the snow melts in a phase of decreasing snow depth before the ground starts to become visible and that the complete snow melt exposing the ground is very fast then (Clark *et al.*, 2006; Böttcher *et al.*, 2014). The effects of a missing snow filter are a wider growing season (earlier SOS, later EOS), a higher relative RMSE and much less success in the fitting (up to four years less). This can be understood by looking at the time series in Fig. A.2 where averaged over these large forest regions the EVI increase commences earlier in the case without snow filter. Taken all this together it has been decided for the strict snow filter removing all EVI values containing *any* snow as i) a snow filter is absolutely necessary, ii) the absolute value of the snow filter does not influence the results (at least in a range of up to 30% ground snow cover), and iii) in order to be as consistent and correct as possible and remove any effect unrelated to greenness.

I.2 The fitting procedure

We fitted a double-sigmoidal function (Eq. II.1 of the main text; Gonsamo *et al.*, 2013) to the time series of SIF, EVI, model GPP, MODIS NDVI and NDVI3g in order to identify the main starting and ending times of the annual cycles from them (SOS,EOS). Overall the fitting was quite successful. In Figure A.4 high values close to 1 of the coefficients of determination between the time series and the fits are shown. The lowest values of down to 0.8 in case of SIF (and partly MODIS NDVI) are found in the northernmost areas of the investigation area. The relative root mean squared error in those regions is up to 18%, mostly however at 10-12% in case of SIF. This is still double as high as the average relative RMSE of both EVI and model GPP. This can be explained by the higher variability in the SIF time series. The less smooth behaviour is due to noise, especially in winter. In summer probably clouds influence the signal in both a physiological (greater

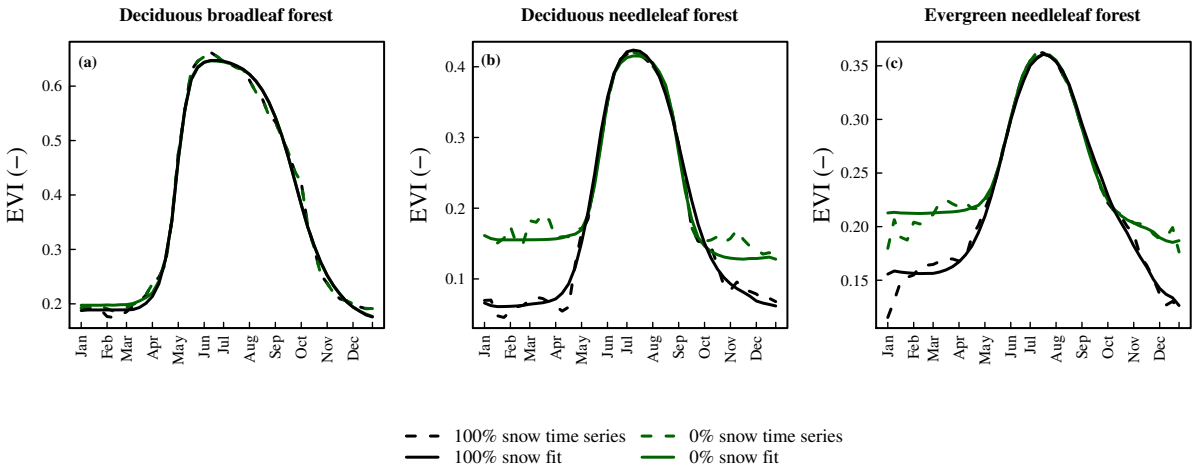

Figure A.2: Average time series of the EVI spatially averaged over DBF **(a)**, DNF **(b)**, and ENF **(c)** without snow filter (black dashed line), with all snowy pixels removed (green dashed line) and the fitted functions (solid lines, respectively). Sampling not matched between data sets.

fraction of diffuse vs. direct radiation causes different physiological reactions and light-use-efficiencies; Gu *et al.*, 1999; Jenkins *et al.*, 2007) and a technical way (thick clouds may scatter the SIF signal away from the sensor direction). For EVI and model GPP generally very high r^2 and low relative RMSE are found.

I.3 Additional results

Time series spatially averaged at the ecosystem level are again compared to meteorological conditions. In order to avoid duplication, the ecoregion of Fenno-Scandianavia and Russia is not again shown but instead the spatially averaged time series of ENF in the ecoregions of the Central and Midwestern Canadian Shield Forests (ecoregion numbers 361 and 368 in Olson *et al.* (2001)), the main part of which are situated between Lake Winnipeg and Lake Superior. They are combined with each other because of their strong similarity and can been seen in Fig. A.11. Although the MODIS NDVI annual amplitude is three times as high as the one of the EVI in these Canadian forests, its seasonal cycle is not as clear. Outside the main growing season it is characterized by spurious peaks and dips. This behaviour is unexpected and remains unclear as these artefacts cannot be explained with residual snow in the scene as NDVI would increase both with snow melt and green-up. In 2009 and 2010 striking dips in mid summer can be seen. Relatively high noise is also affecting the SIF time series in winter and spring which might also affect the identification of SOS, although the weighting procedure is intended to reduce the noise effects here. In general the seasonal cycle is again very similar to the one of model GPP and both, SIF and model GPP, have an earlier SOS than EVI. What is different in these ecoregions compared to the one presented in the main text in Fenno-Scandinavia, is that snow melt seems to be slightly more abrupt than in northern Europe as the shoulder of the time series of the snow flag during melt is steeper. This might explain, why air temperatures

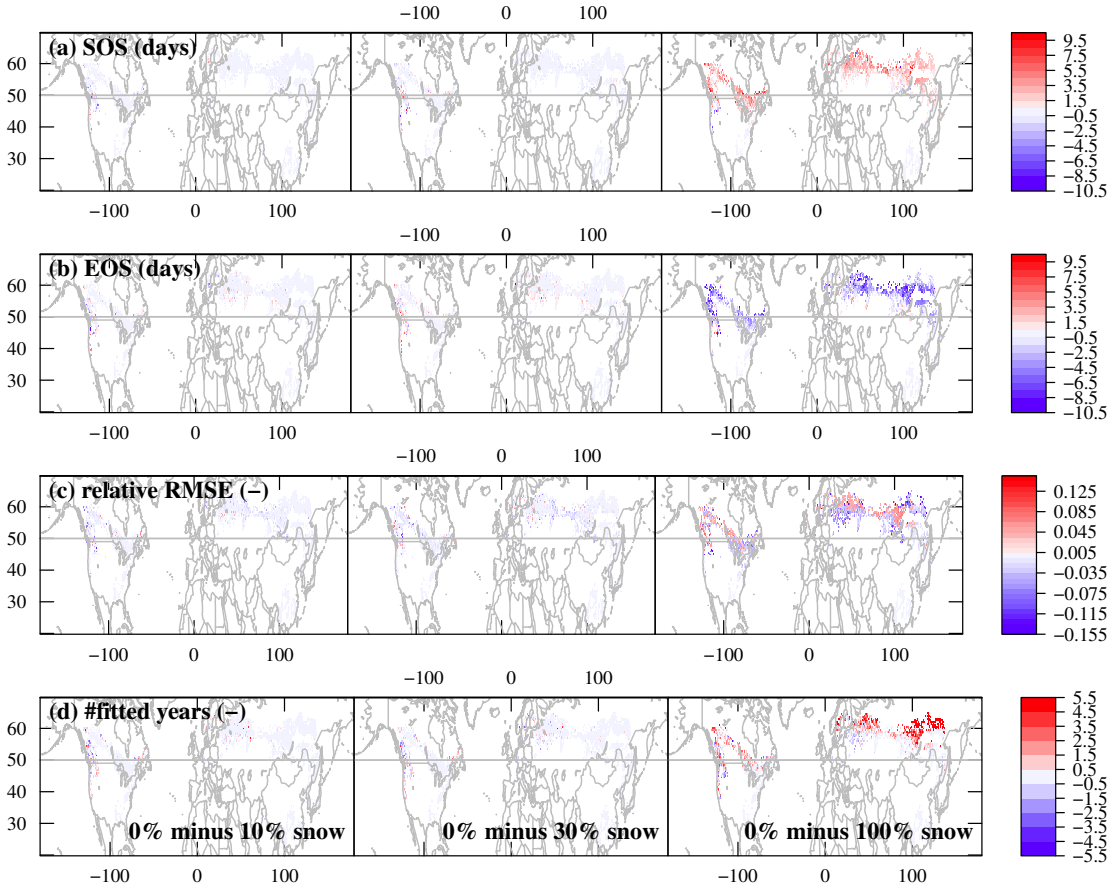

Figure A.3: Effect of the different snow filter thresholds on the SOS **(a)**, EOS **(b)**, relative RMSE **(c)** and the number of fitted years **(d)**. Results are only shown for the mixed quality case. 0% snow: EVI values flagged by the MODIS snow flag as containing non-zero snow are removed; 10%/ 30% snow: pixel values with snow flag higher than 10%/ 30% are discarded. Additional comparison to a completely unfiltered data set is also shown (100% snow).

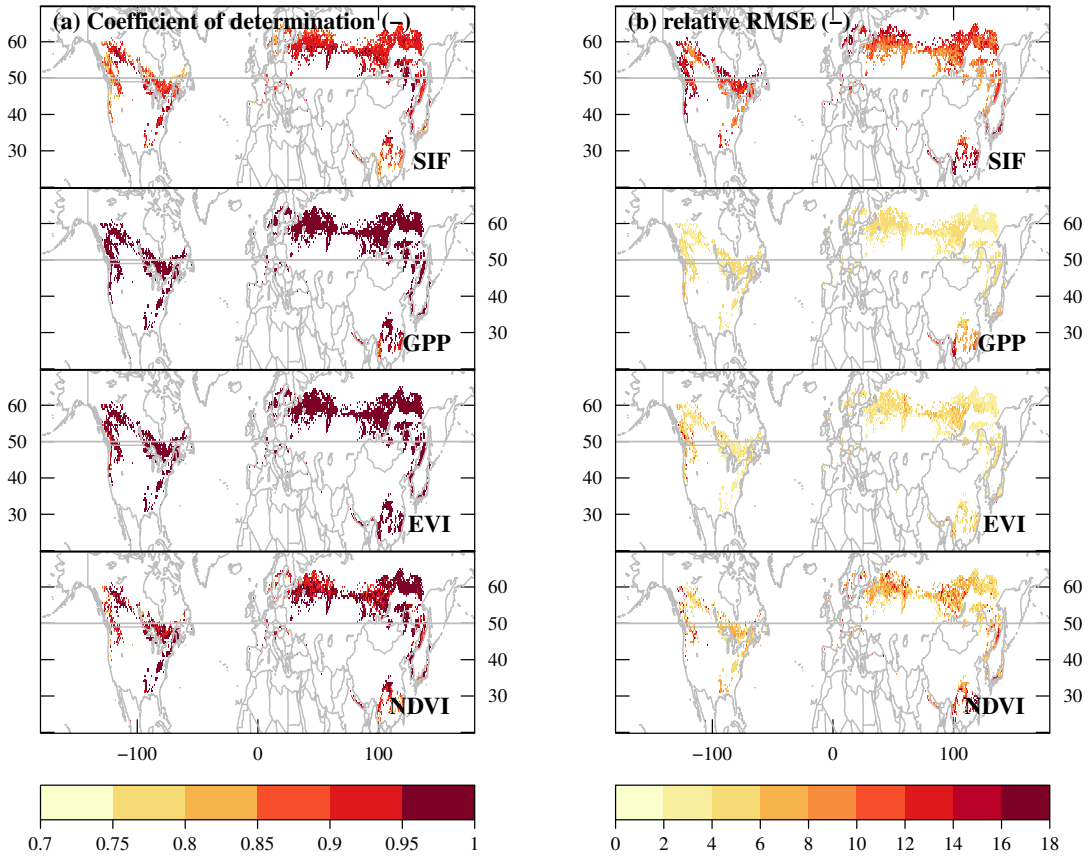

Figure A.4: **a):** The maps show the coefficient of determination r^2 between the time series and the corresponding fits over all five years for SIF, GPP, EVI and MODIS NDVI. **(b)** The same for the root mean squared error between the time series and the corresponding fits relative to the annual amplitude.

are closer to 0 °C at SOS_{SIF} and average daily minimum temperatures markedly below the freezing point. Remarkable is further the qualitative similarity between SIF and GPP in small details, like the small peaks in summer 2008 and 2009 and the short breaks in spring increase in 2009 and 2010 and autumn decrease in 2010, which are probably caused by the corresponding air temperature conditions.

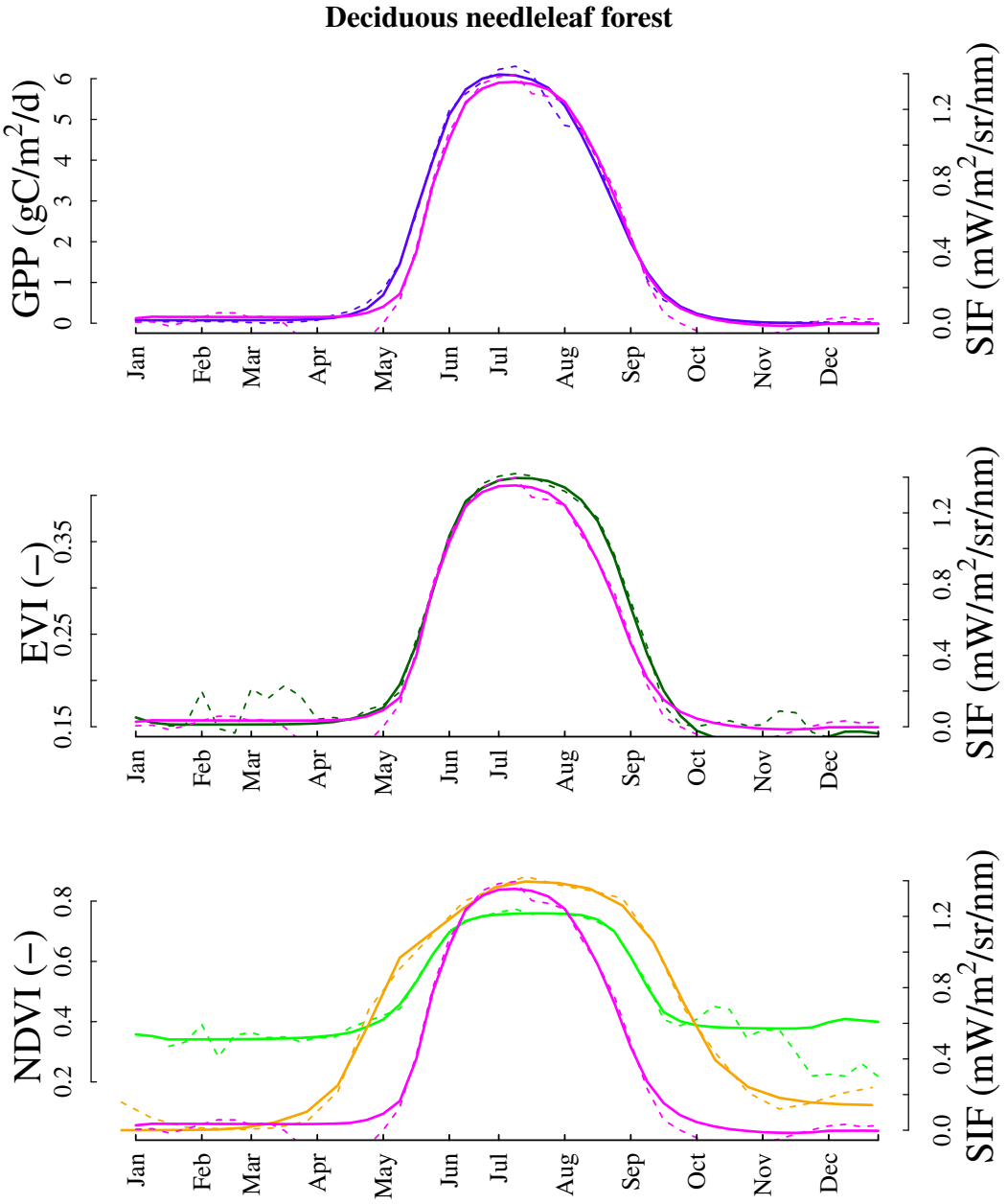

Figure A.5: Median of the annual cycles (dashed lines) and of the fitted functions (solid lines) of SIF, model GPP, EVI, NDVI and NDVI3g over deciduous needleleaf forest. Sampling is matched between the fits and the SIF and model GPP time series, but not with the VI time series because of the many missing values in winter in the VIs.

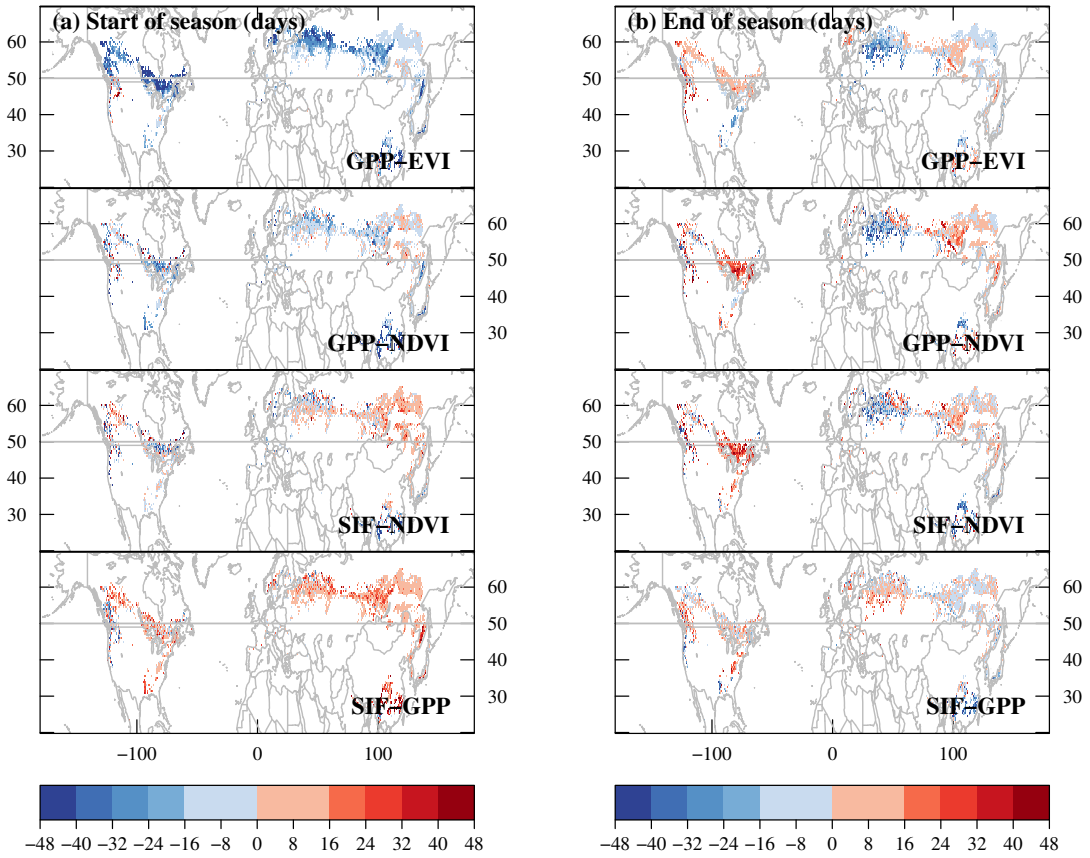

Figure A.6: Mean differences in the calculated start and end of season dates between SIF, EVI, GPP and MODIS NDVI in days.

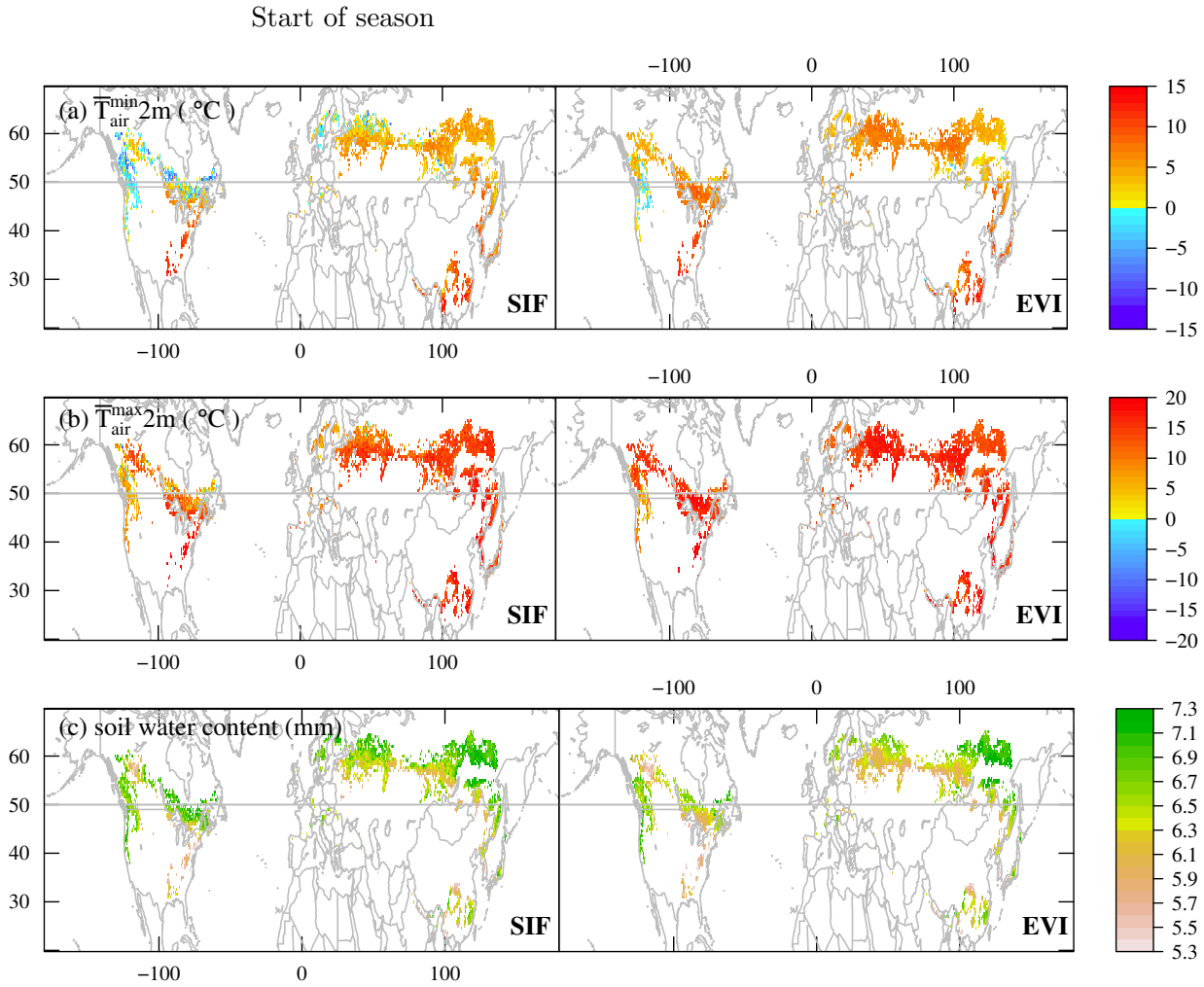

Figure A.7: The maps show the mean of daily minimum **(a)** and maximum temperature **(b)** conditions of the air and the soil water content in the soil layer between 7 and 28 cm depth **(c)** at the start of season for SIF and EVI.

Start of season

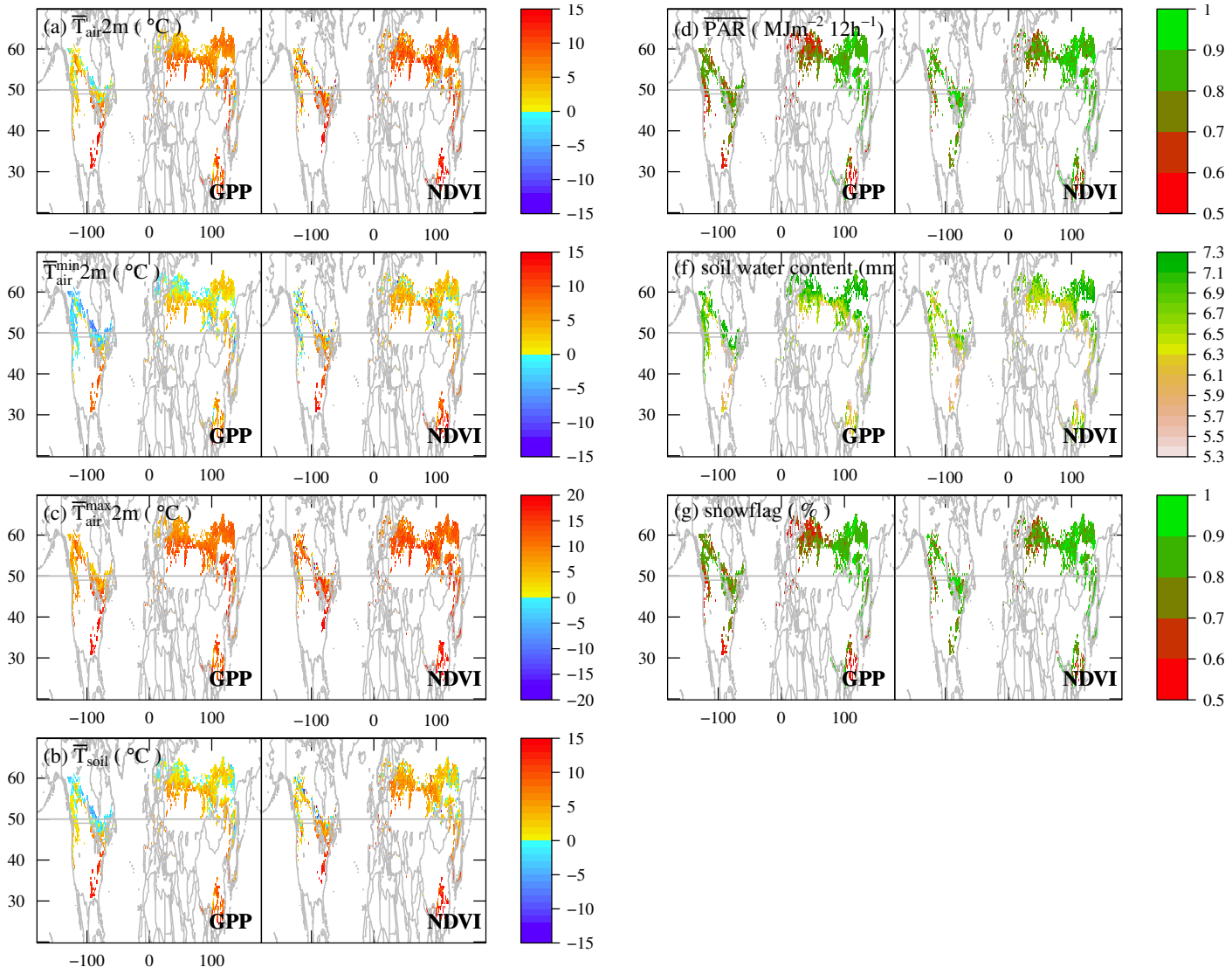

Figure A.8: The maps show the temperature conditions of the air **(a,b,c)** and the soil in 7-28 cm depth **(d)**, the average photosynthetically active radiation arriving at the surface **(e)**, the soil water content **(f)** and the MODIS snow flag **(g)** and at the start of season for GPP and NDVI.

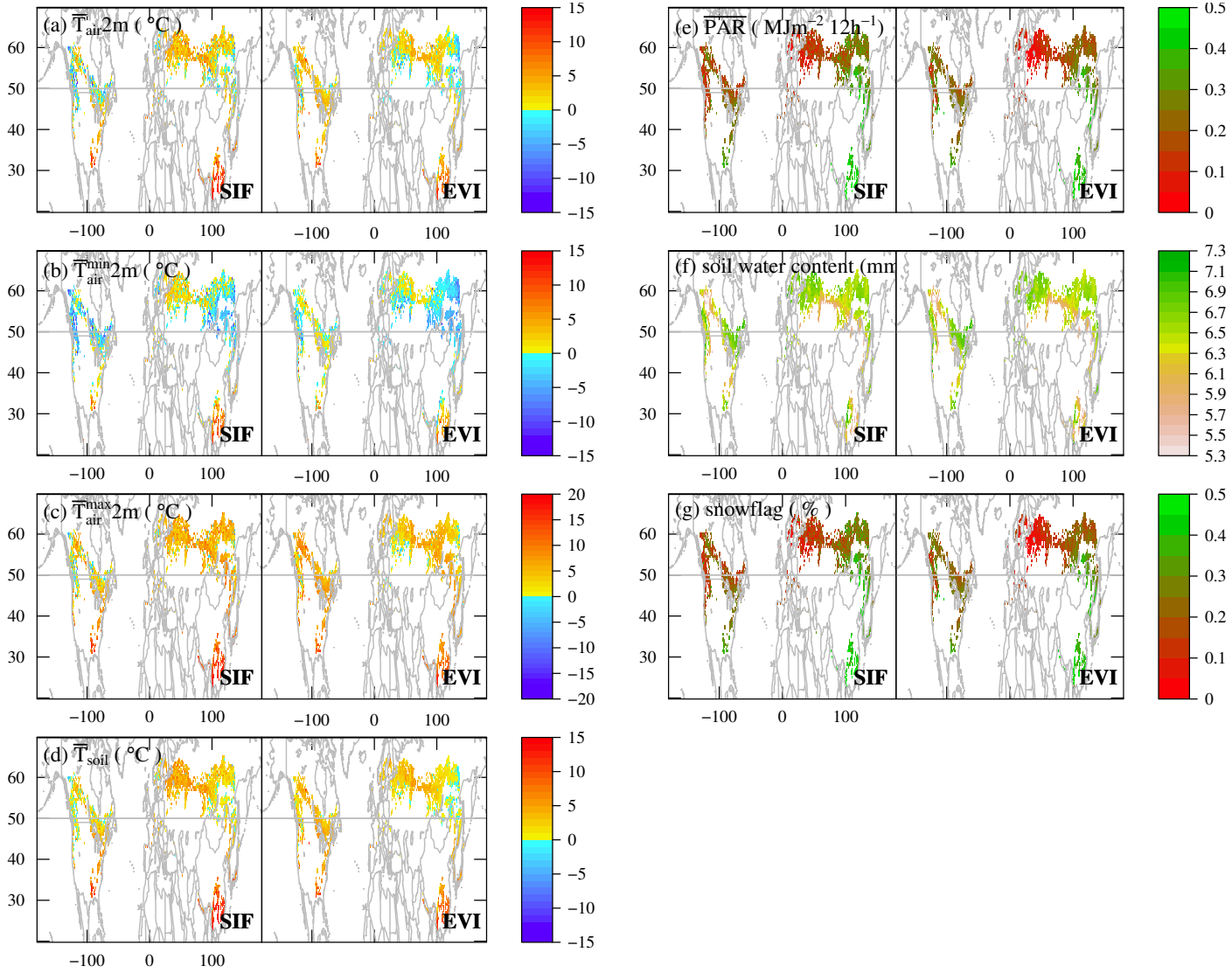

Figure A.9: The maps show the temperature conditions of the air **(a,b,c)** and the soil in 7-28 cm depth **(d)**, the average photosynthetically active radiation arriving at the surface **(e)**, the soil water content **(f)** and the MODIS snow flag **(g)** and at the end of season for SIF and EVI.

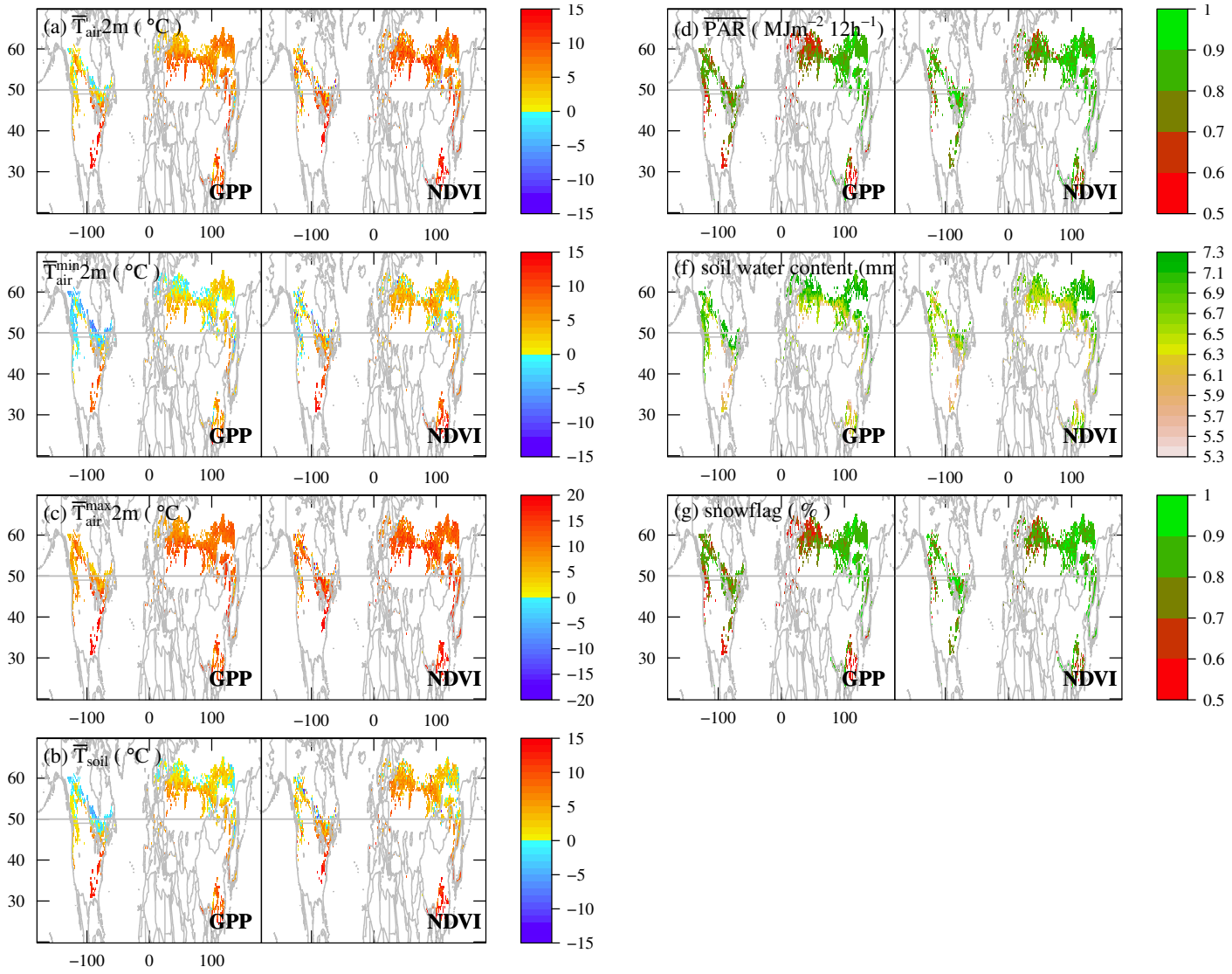

Figure A.10: The maps show the temperature conditions of the air **(a,b,c)** and the soil in 7-28 cm depth **(d)**, the average photosynthetically active radiation arriving at the surface **(e)**, the soil water content **(f)** and the MODIS snow flag **(g)** and at the end of season for GPP and NDVI.

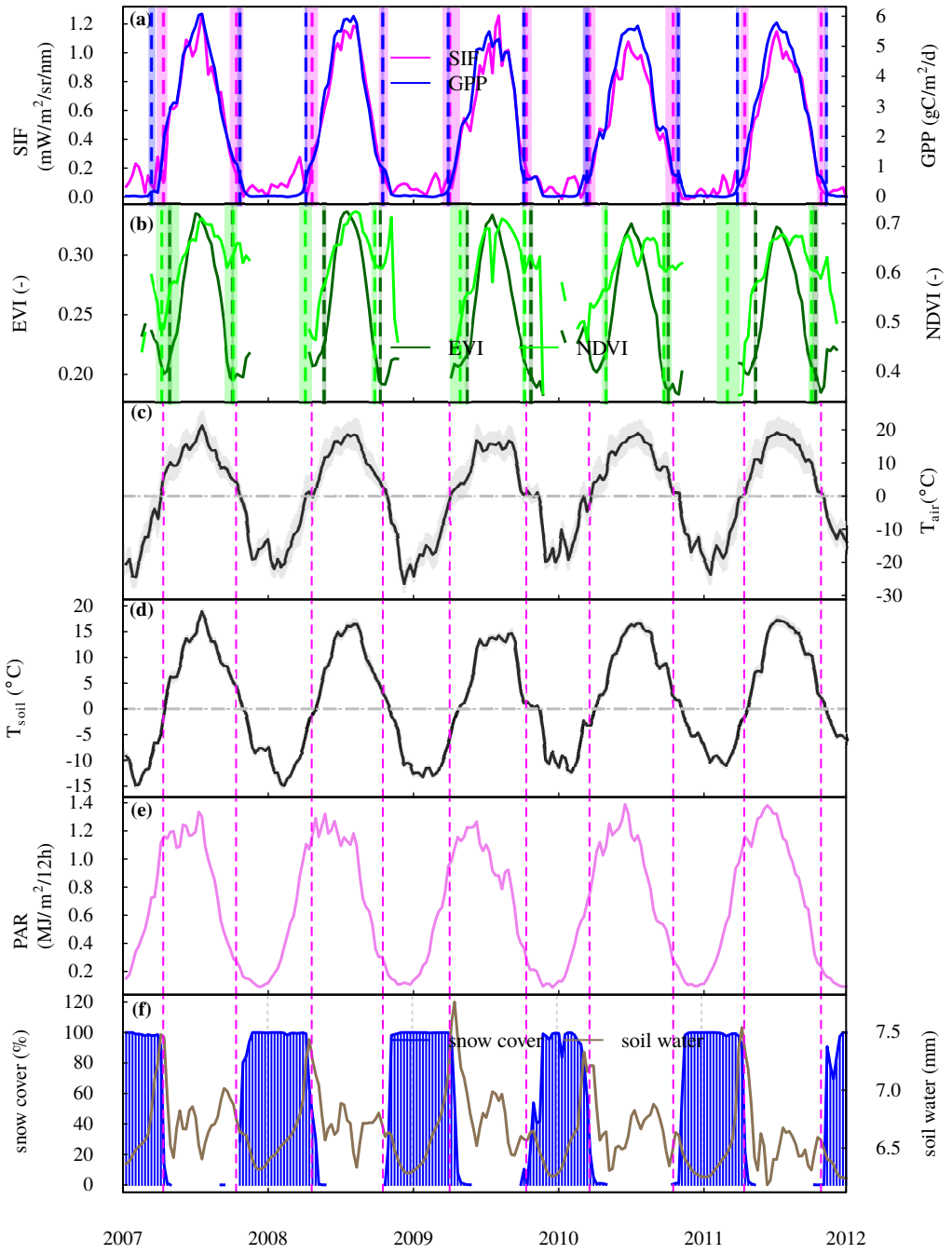

Figure A.11: ENF in the Midwestern and Central Canadian Shield forests (ecoregions 361 and 368 in Olson *et al.* (2001), 91 pixels in total) : **(a)** Area averaged time series of SIF and GPP; dashed vertical lines mark SOS/EOS (spatial median), shaded areas indicate the interquartile range of all identified SOS/EOS in the area. **(b)** the same as in a) but for MODIS EVI and NDVI. **(c,d)** Mean 2 m air and soil (7-28 cm) temperature. The shaded area indicates the range between the mean of daily minimum and the mean of daily maximum temperatures in a 16-day interval. **(e)** Photosynthetically active radiation reaching the surface (PAR). **(f)** Average snow cover in percent of the surface (MODIS snow flag); soil water content in the layer between 7 and 28 cm depth. Sampling of SIF, GPP and the meteorological variables is aligned with each other, but not with EVI/NDVI because of the many missing values in winter. The other way around the sampling of EVI/NDVI are aligned with the one of SIF.

	$\overline{T_{2m\ air}}$ [°C]	$\overline{T^{min}{}_{2m\ air}}$ [°C]	$\overline{T^{max}{}_{2m\ air}}$ [°C]	$\overline{PAR}$ [fraction of annual max]	soil water content [mm]	$\overline{T_{soil}}$ [°C]	snow flag [%]	EOS [DOY]
ENF								
SIF	-0.2±5.8	-2.3±5.8	2.3±6	16±10	6.5±0.5	1.8±3.5	28±40	296±27
EVI	2.1±3.9	-0.2±3.7	4.9±4.3	19±10	6.5±0.5	2.9±2.6	11±27	288±19
GPP	0.1±3.4	-1.8±3.4	2.5±3.4	15±6	6.5±0.5	1.5±2	18±31	295±15
DBF								
SIF	4.5±4.4	1.6±3.8	8.3±5.1	27±8	6.1±0.6	5.7±3.6	0±2	328±21
EVI	3.2±3.4	0.5±3	6.8±3.9	24±6	6.3±0.5	4.7±2.6	1±6	333±15
GPP	6.9±2.9	3.6±2.5	11.3±3.5	31±7	5.8±0.6	7.8±2.4	0±0	312±14

Table A.1: Average environmental conditions and their standard deviation at EOS for SIF, EVI, model GPP in ENF (north of 50° N) and DBF.

I.4 Deciduous broadleaf forest

In DBF significant differences in the seasonality between greenness measurements and photosynthetic activity are not expected in data with a temporal resolution of 16 days as in this study. In the main text it has been shown that the SOS is very similar between EVI, NDVI, SIF and model GPP and that temperature conditions are markedly above 0 °C. EVI generally indicates later EOS than the photosynthesis proxies model GPP and SIF. The time series in Fig. A.12 reveal unexpected and interesting features that remain obscure when only looking at the transition dates:

i) There is a gradual *summer greendown* observable from EVI, SIF, model GPP, i.e. decreasing values in summer before the steeper autumn senescence is initiated and before the annual temperature peak is reached. This is not seen in MODIS NDVI and NDVI3g and has been shortly discussed in the main text. There exist different studies that have identified a period of decreasing values of both, photosynthetic capacity ($v_{c_{max}}$) at the leaf and plot scale (Wilson *et al.*, 2000; Bauerle *et al.*, 2012; Yang *et al.*, 2014) and vegetation indices (EVI, NDVI and green chromatic corrdinate=G/(R+B+G)) at the canopy (camera) and satellite scale (Jenkins *et al.*, 2007; Elmore *et al.*, 2012; Yang *et al.*, 2014). Several authors have termed this period between the end of June/ early July and the beginning of autumn senescence *summer greendown*. During this period no major changes in LAI or leaf mass are expected and also have not been observed (Wilson *et al.*, 2001; Yang *et al.*, 2014). However, a decline in the NIR reflectance relative to the visible has been reported several times (Jenkins *et al.*, 2007; Elmore *et al.*, 2012; Yang *et al.*, 2014) and is ascribed to leaf aging or changes in leaf internal structures (Yang *et al.*, 2014). At the leaf and plot scale decreases in the maximum carboxylation capacity $v_{c_{max}}$ and electron transport rate J_{max} of plants have been identified during the same phase, despite rather constant chlorophyll and leaf nitrogen amounts (Wilson *et al.*, 2000, 2001; Bauerle *et al.*, 2012; Yang *et al.*, 2014). The reasons for these observations are still unclear. Bauerle *et al.* (2012) suggest, that decreasing photoperiod might induce changes in the photosynthetic apparatus, as in experiments with artificially prolonged photoperiod the photosynthetic rates did not decrease as much as under natural illumination. Figure A.12 shows the parallel behaviour of SIF, model GPP and EVI with the seasonal cycle of PAR. This, too, strongly suggests light availability as a cause for this summer greendown (meaning now both, a decrease in greenness and photosynthetic activity). The seasonal variation in $v_{c_{max}}$ is observed in several species and may reflect seasonally changing fractions of nitrogen allocated to the carbon-fixing enzyme rubisco (Wilson *et al.*, 2000) which leads to decreasing $v_{c_{max}}$. Wilson *et al.* (2000) further hypothesise that starch accumulation with time might create negative feedbacks to rubisco generation and/or that the rubisco-$v_{c_{max}}$ relationship is temporally constant but that with increasing leaf age the mesophyll conductance for CO_2 decreases due to increasing lignin concentrations. This results in the same observations as if $v_{c_{max}}$ and rubisco were not seasonally constant.

ii) This summer greendown is overlaid with high summer variability in the cases of SIF and model GPP, but not for EVI. SIF parallels model GPP strongly. This indicates variable rates of photosynthesis in summer which are not accompanied by changes in greenness, hence LAI and/or chlorophyll content. Figure A.12 makes clear that this variability is very similar to changes in the amount of photosynthetically active radiation arriving at the surface and suggests that these changes are light-driven, too, which is also studied in Yang *et al.* (2015). Changes in PAR can only be caused by clouds at approximately constant

day length. Both, the amount and the optical thickness of the clouds are importantly influencing PAR. PAR only represents variations in the absolute amount of radiation arriving at the surface and because SIF and model GPP strongly go together with PAR, we suggest that on the large scale this decisively determines photosynthesis. However, not only the amount, but also the quality, meaning the ratio of diffuse and direct radiation, is crucial for photosynthesis. Studies have shown that net ecosystem exchange is higher under diffuse than under direct illumination at the same or even lower radiation level, meaning that the gain in photosynthesis due to higher diffuse PAR can be greater than the decrease due to lower direct PAR (Gu *et al.*, 1999). Jenkins *et al.* (2007) ascribe daily light use efficiency (Φ_p) changes with constant fAPAR to variations in the ratio of diffuse/direct downwelling radiation and rather not PAR or other meteorological variables. Less direct light leads to less saturation in the top of canopy leaves and to less shadowing in the canopy, which leads to a higher canopy Φ_p. With the available data a detailed analysis of SIF and this mechanism is not possible. However, we tend to say, that this effect plays a minor role compared to photosynthesis reduction due to lower PAR amounts at the temporal and spatial scale that we are observing in this work. Although it can be ruled out that this signal of summer variability is a sampling problem, it cannot be completely verified that this signal is purely of physiological nature and not caused by scattering of the SIF signal by clouds. The GPP model is also remote sensing data driven and might suffer from a similar cloud problem, although we regard this as very unlikely.

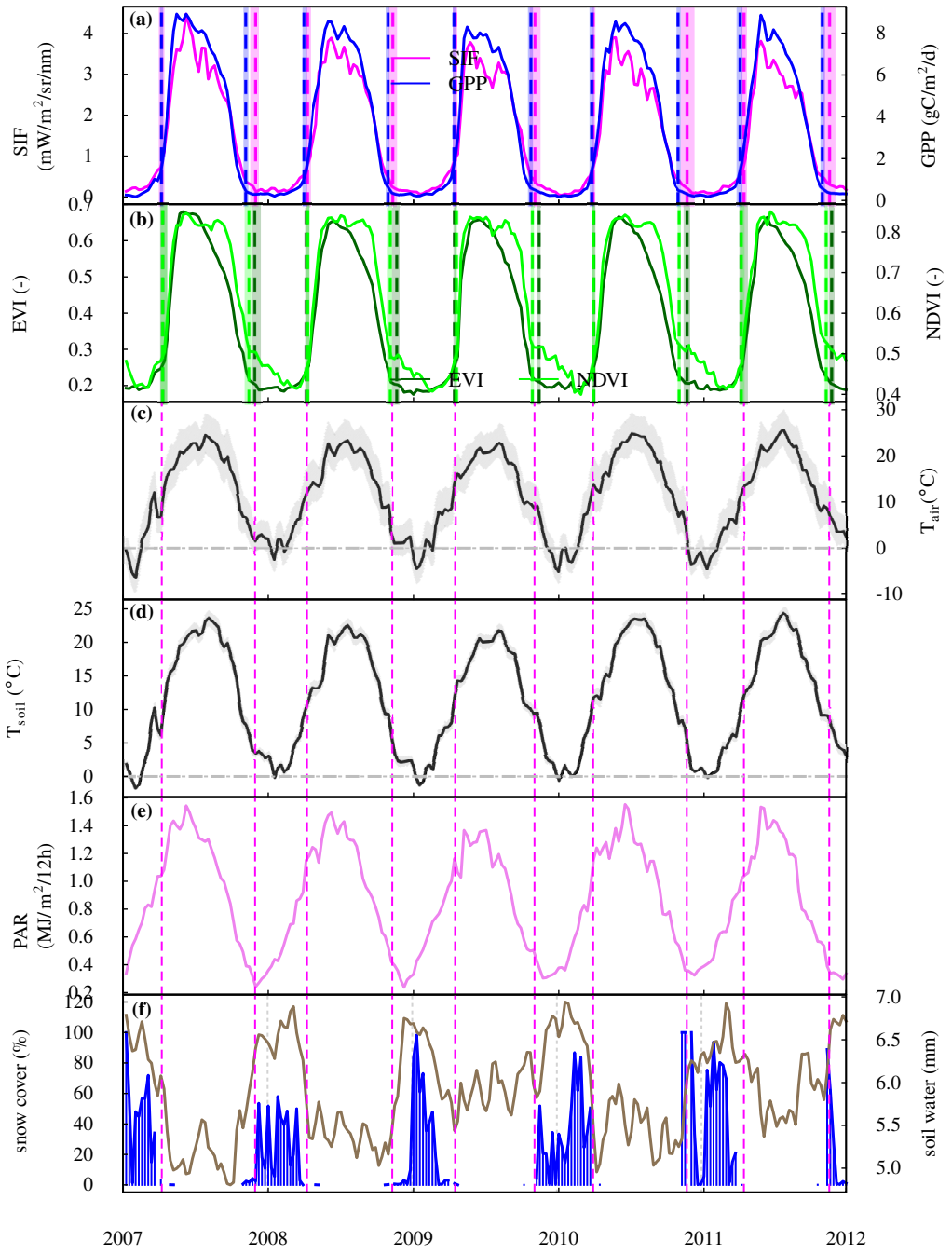

Figure A.12: Deciduous broadleaf forest (74 pixels in total): **(a)** Area averaged time series of SIF and GPP; dashed vertical lines mark SOS and EOS (spatial median), shaded areas indicate the interquartile range of all identified SOS/ EOS in the area in the particular year. **(b)** the same as in a) but for EVI and MODIS NDVI. **(c,d)** Mean 2 m air and soil (7-28 cm) temperature. The shaded area indicates the range between the mean of daily minimum and the mean of daily maximum temperatures in a 16-day interval. **(e)** Photosynthetically active radiation reaching the surface (PAR). **(f)** MODIS snow flag indicating the average snow cover in percent of the surface; soil water content in the layer between 7 and 28 cm depth. Meteorological variables are from the ERAInterim Reanalysis. Sampling of SIF, GPP and the meteorological variables is aligned with each other, but not with EVI/NDVI because of the many missing values in winter. The other way around the sampling of EVI/NDVI are aligned with the one of SIF.

APPENDIX B

SUPPORTING INFORMATION FOR THE PUBLICATION "ASSESSING THE DYNAMICS OF VEGETATION PRODUCTIVITY IN CIRCUMPOLAR REGIONS WITH DIFFERENT SATELLITE INDICATORS OF GREENNESS AND PHOTOSYNTHESIS"

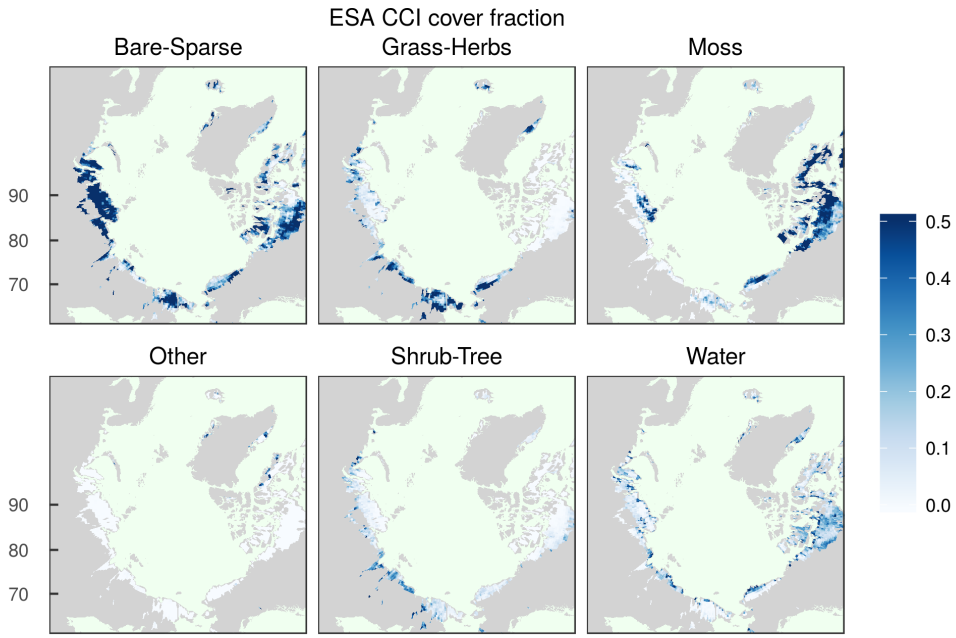

Figure B.1: Fractions of the aggregated land cover classes for the ESA CCI land cover data set. The aggregated classes comprise 'moss' (class 100 in the ESA CCI classification), 'bare/ sparse' (classes 28-30,35-37, fractions of 16 and 19), 'grass/ herbaceous' (classes 26, fractions of 13,16,19,21–25, 33), 'woody' (shrubs and trees, classes 10–12,14,15,17,18,20, fractions of 13,16,19,21–25,31–33), 'water' (class 38, fractions of 31–33) and 'other' (remaining classes and fractions).

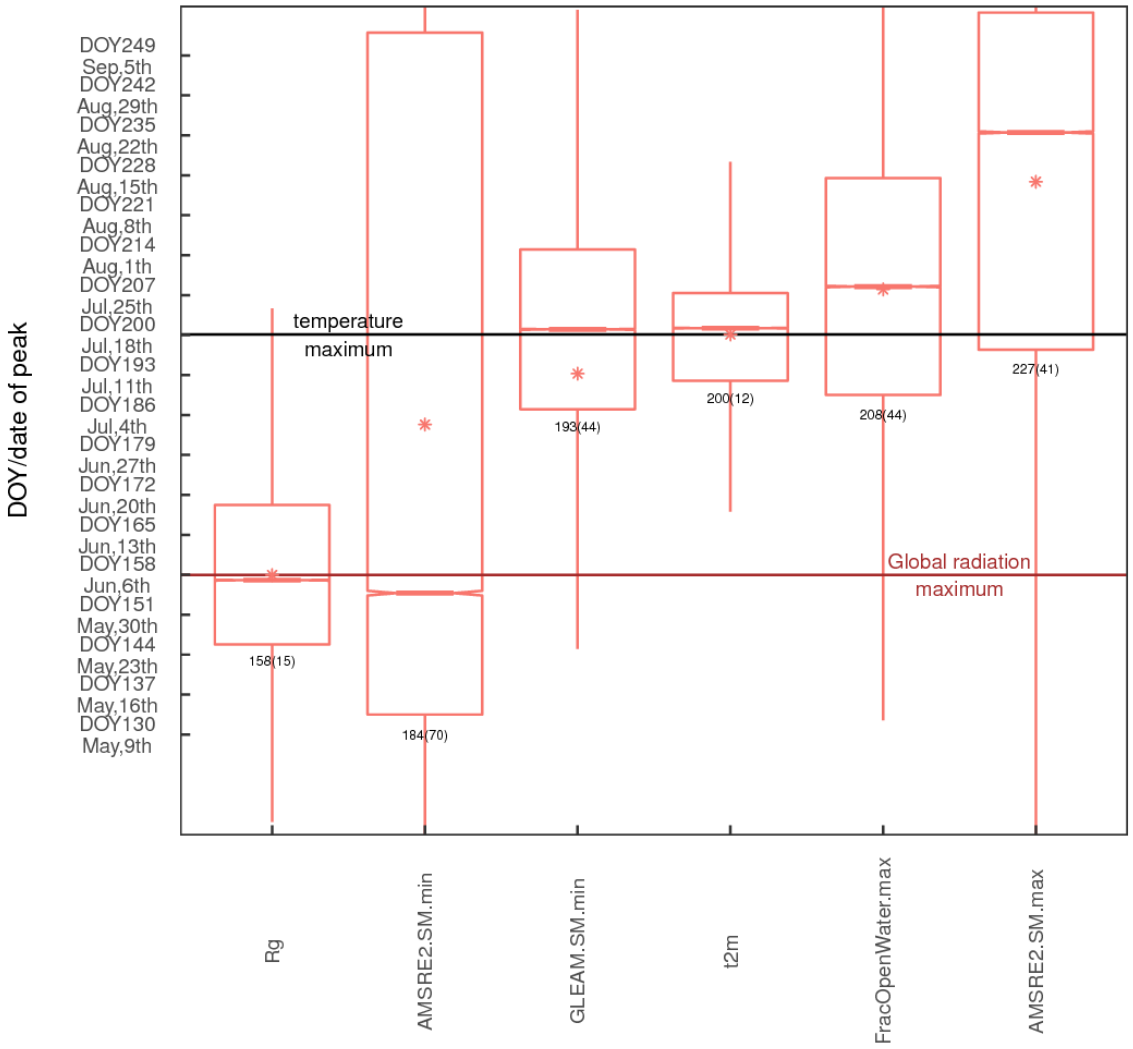

Figure B.2: Distribution of the DOY of the peak of the different environmental variables over the study region and between years (spatial sampling matched between data sets for each year). Bars in the boxes indicate the median, stars the mean, the numbers below the bars denote the spatial mean (standard deviation).

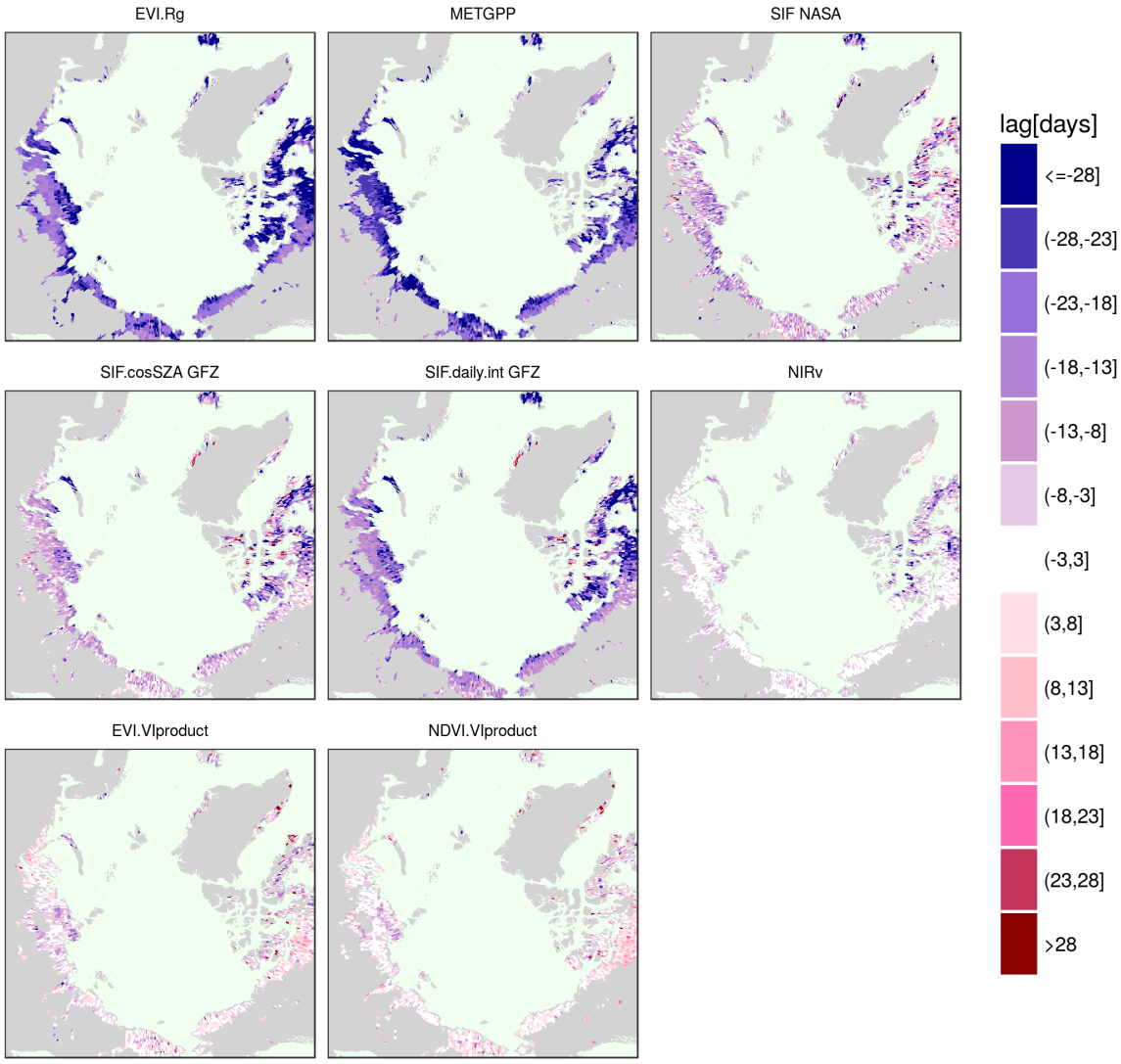

Figure B.3: Average time difference of the maximum across years of selected vegetation proxies and the NDVI.

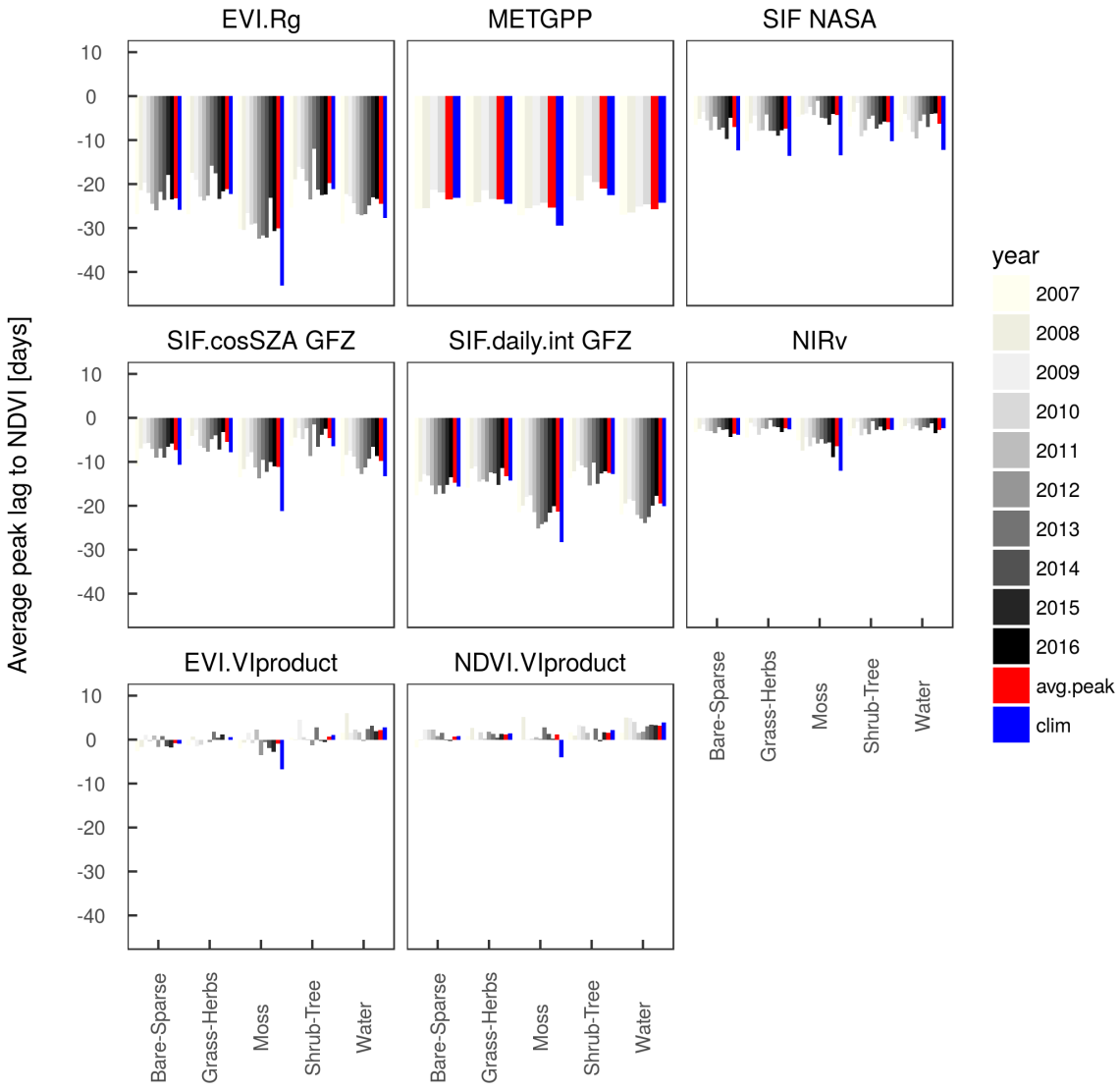

Figure B.4: Average of the time difference between the peaks of various variables and the NDVI as a reference per vegetation type (based on ESA CCI) and per year. 'clim' denotes the peak lags between the mean seasonal cycles and 'avg.peak' represents the average of the lags in the individual years.

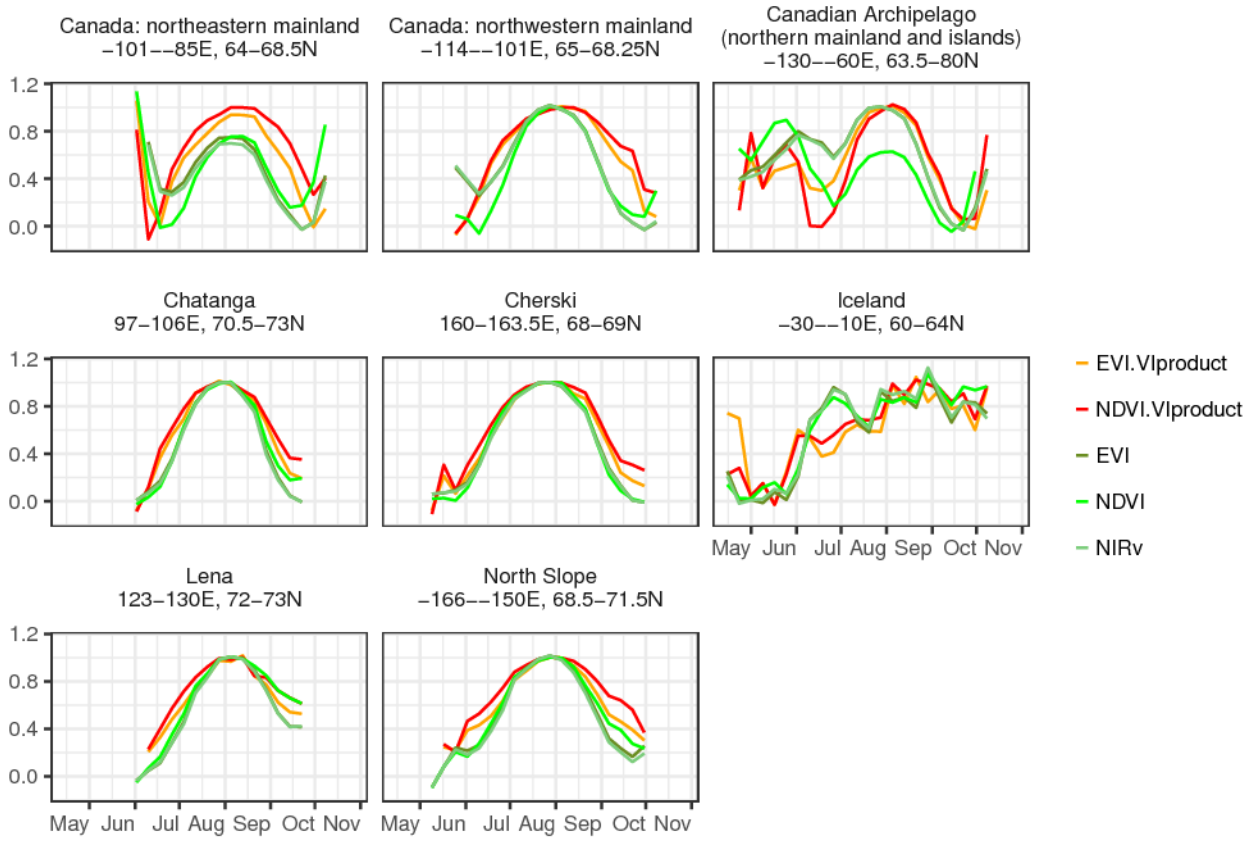

Figure B.5: Mean seasonal cycles of MODIS vegetation indices calculated from NBAR reflectances (MCD43C4) and as provided by the MODIS VIproduct (MxD13C1). Values are scaled to 0/1.

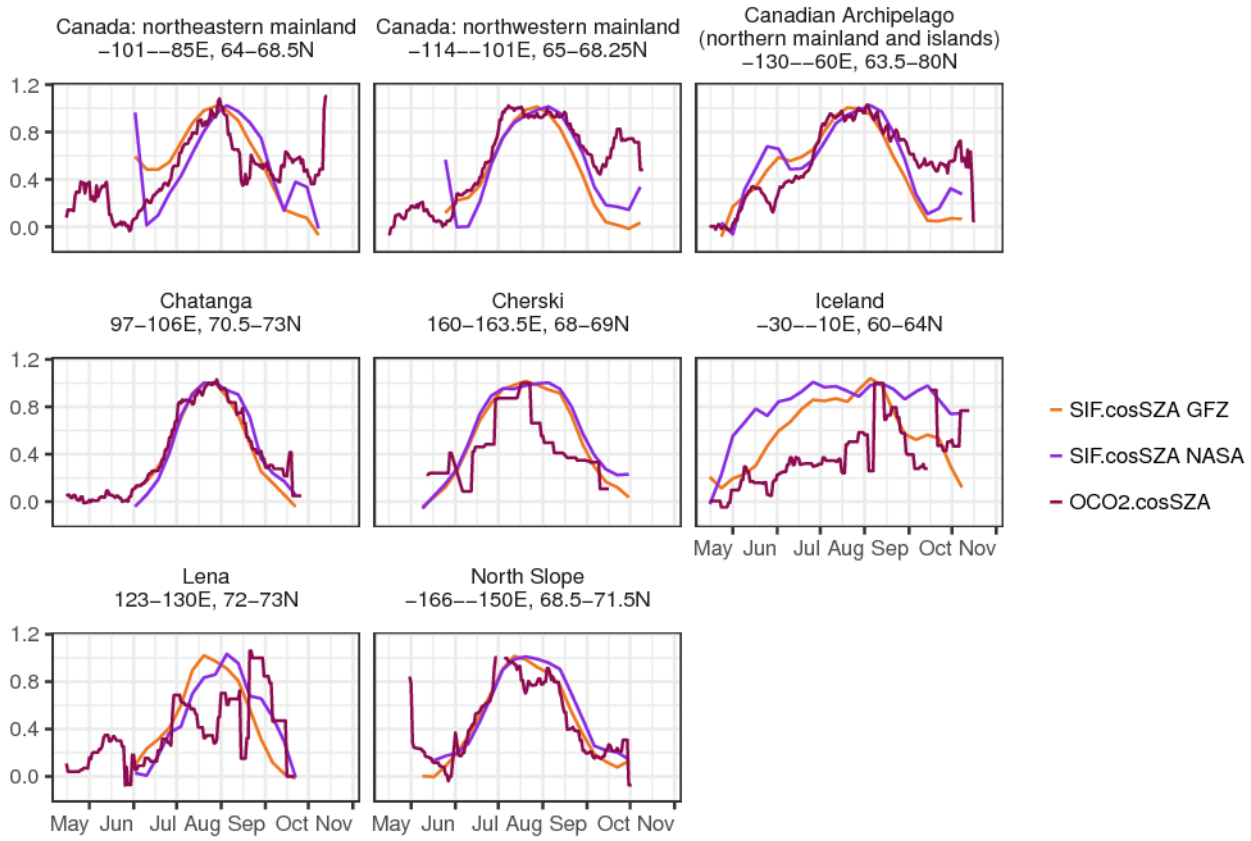

Figure B.6: Mean seasonal cycles of SIF data from GOME-2 and OCO-2 as a comparison. Values are scaled to 0/1.

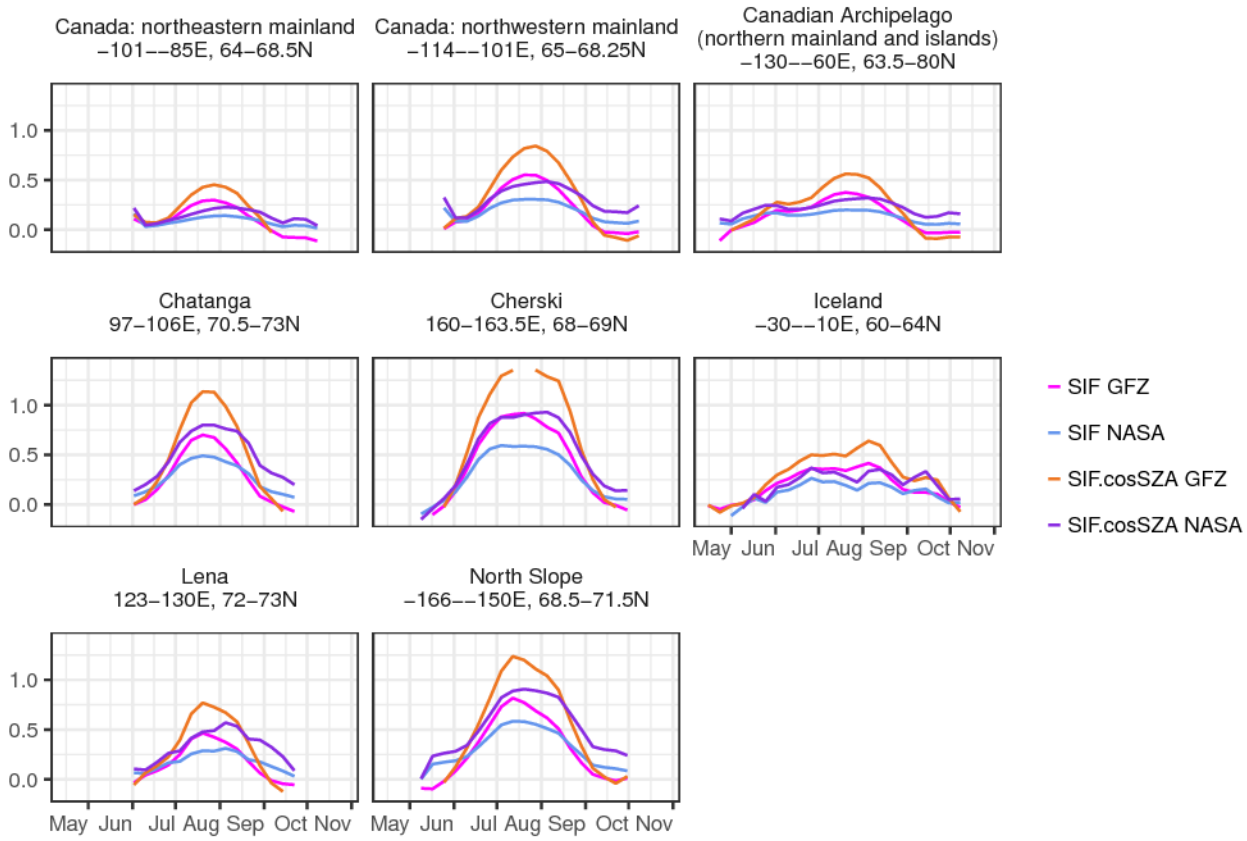

Figure B.7: Mean seasonal cycles of SIF data from GOME-2 for the two retrievals GFZ and NASA. Values are given in mW/(m2 sr nm).

APPENDIX C

SUPPORTING INFORMATION FOR THE MANUSCRIPT "SATELLITE OBSERVATIONS OF THE CONTRASTING RESPONSE OF TREES AND GRASSES TO VARIATIONS IN WATER AVAILABILITY"

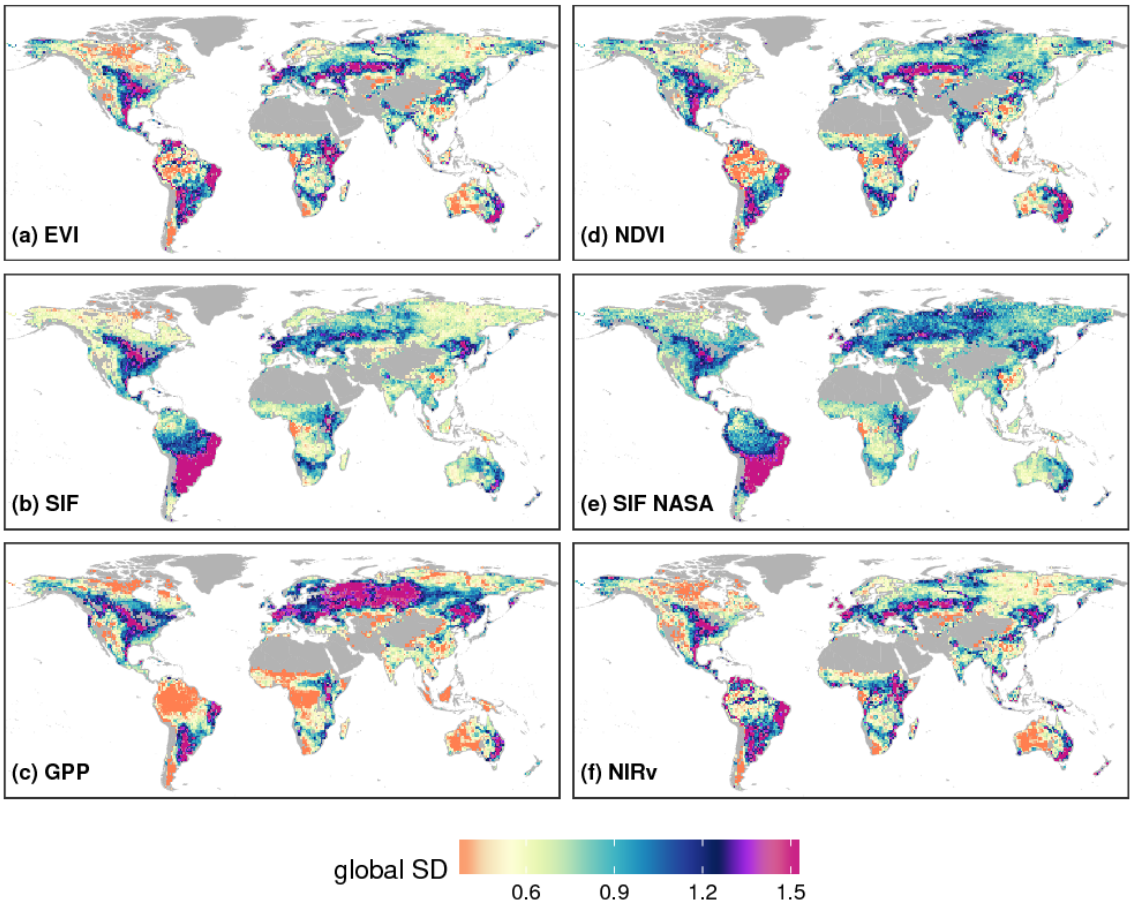

Figure C.1: Hotspots of variability in vegetation greenness and photosynthetic activity. Average absolute deviations from the mean seasonal cycle of the detrended time series.

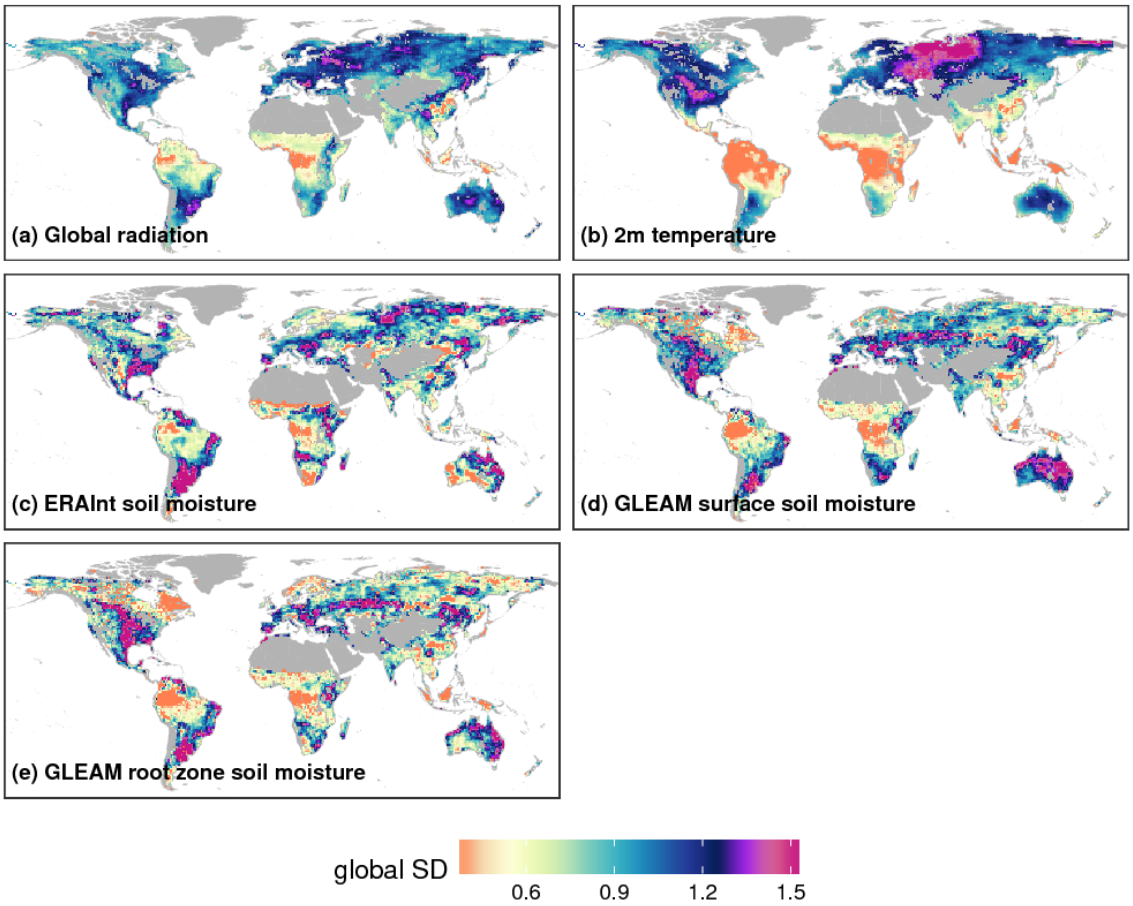

Figure C.2: Variability in meteorology. Average absolute deviations from the mean seasonal cycle of the detrended time series.

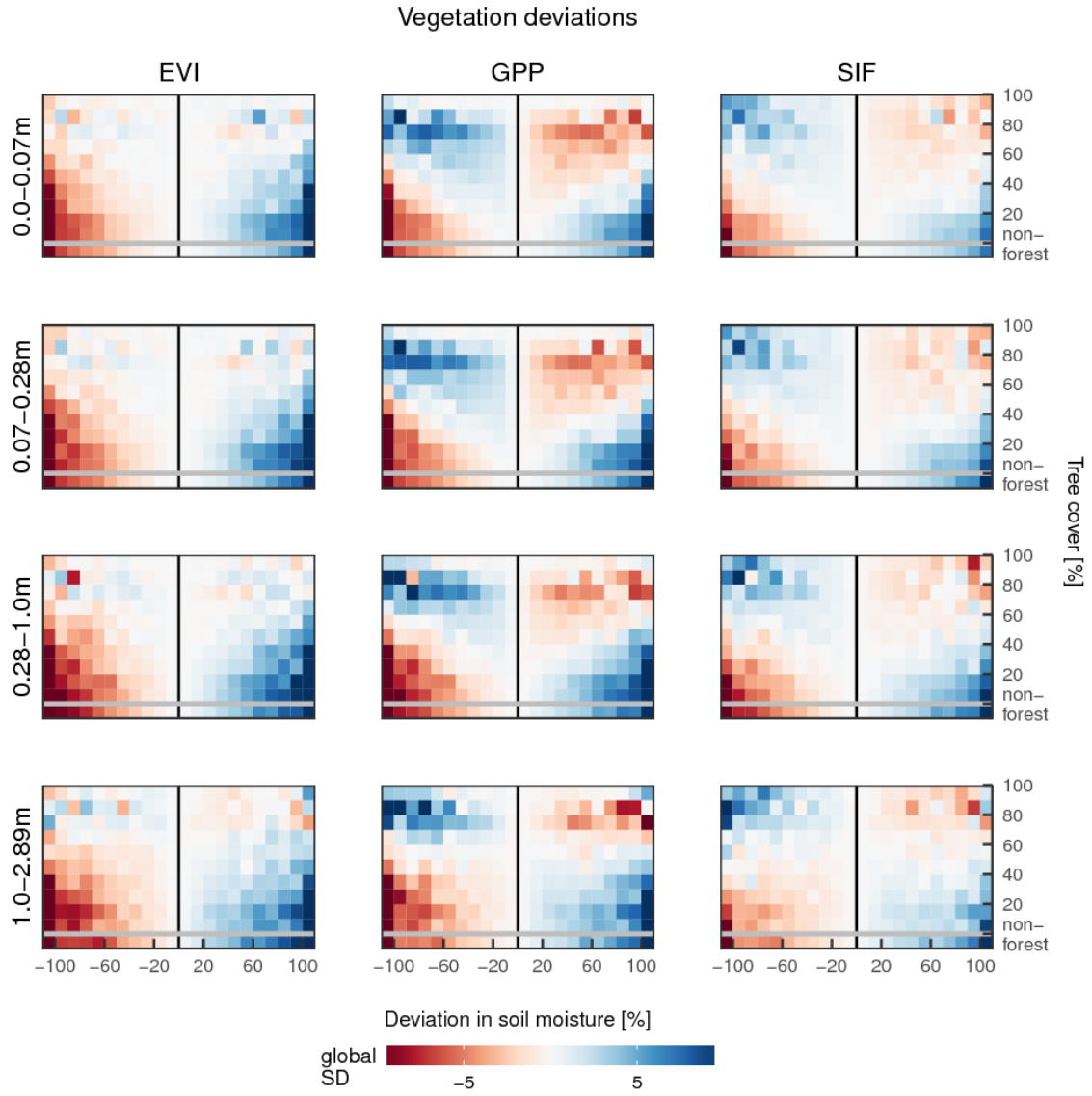

Figure C.3: Typical patterns of vegetation greenness and photosynthesis associated with water availability along a tree cover gradient and separately for different soil layers: Average deviation seen in the vegetation proxies for a given anomaly in the soil water content and as a function of the amount of trees in the different depths.

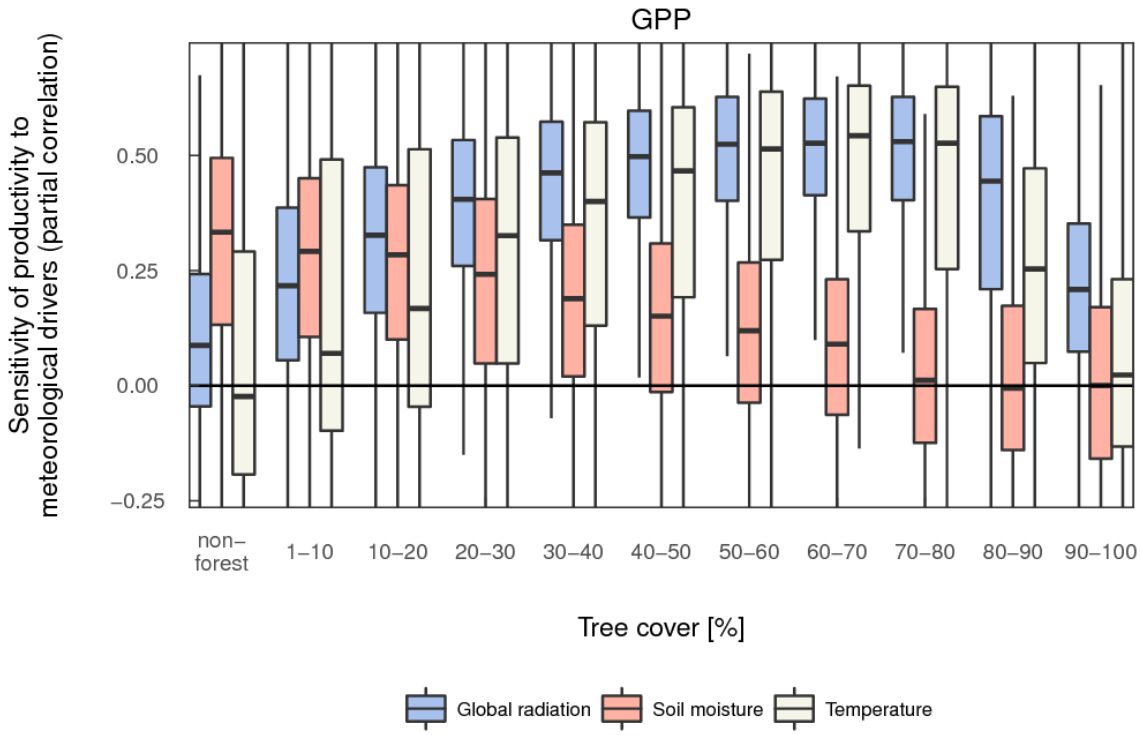

Figure C.4: Partial correlations in time between meteorological anomalies and model GPP anomalies, controlling for the remaining other meteorological variables as a function of tree cover.

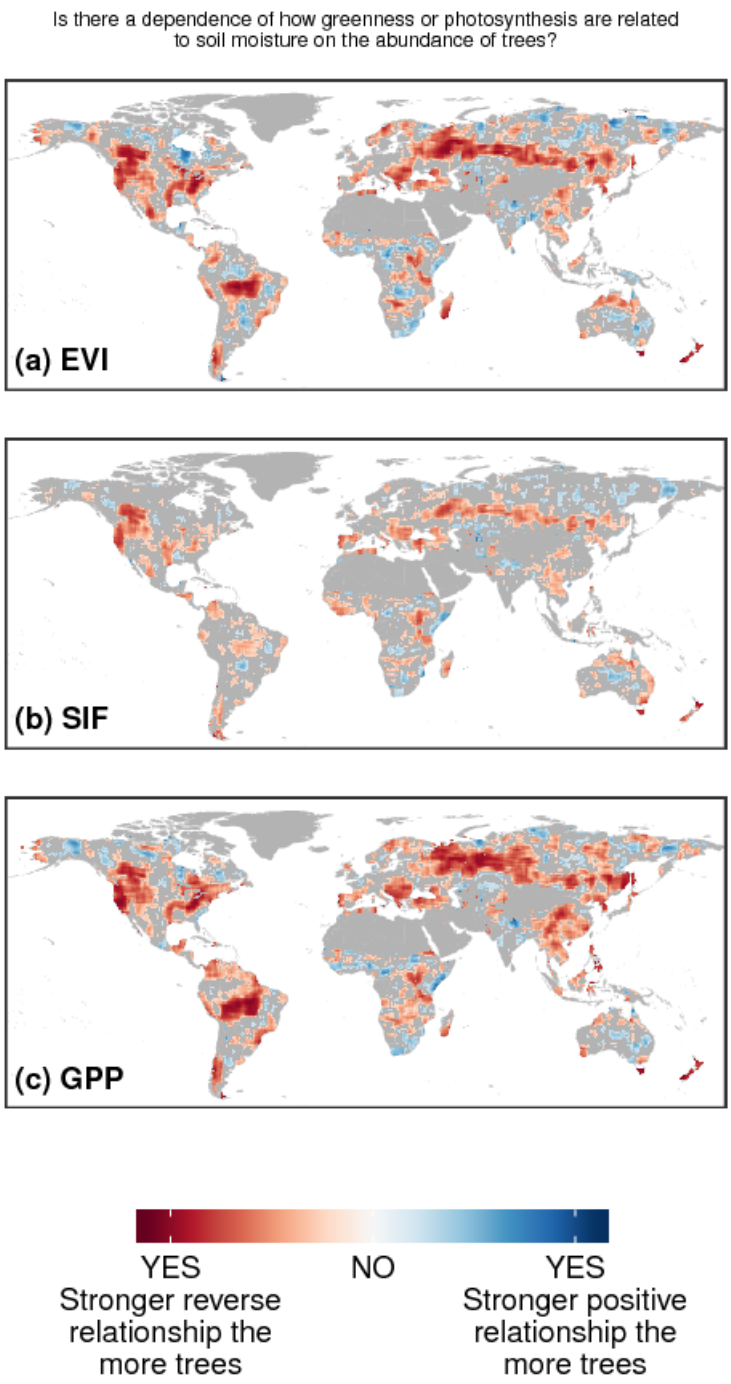

Figure C.5: Relationship between tree cover and the effect of soil moisture on vegetation as observed by EVI, model GPP and SIF: Spatial partial correlation between tree cover and the partial correlation in time between the vegetation proxies and soil moisture in time (with the effects of variations in global radiation and temperature removed) in a moving window of 5.5°. The effect of spatial gradients in average temperature has been removed in the spatial partial correlation. For this analysis data of 0.5° resolution have been used. Only significant (95%) spatial partial correlations are shown. Colour scale extents from -1 (red) to 1 (blue).

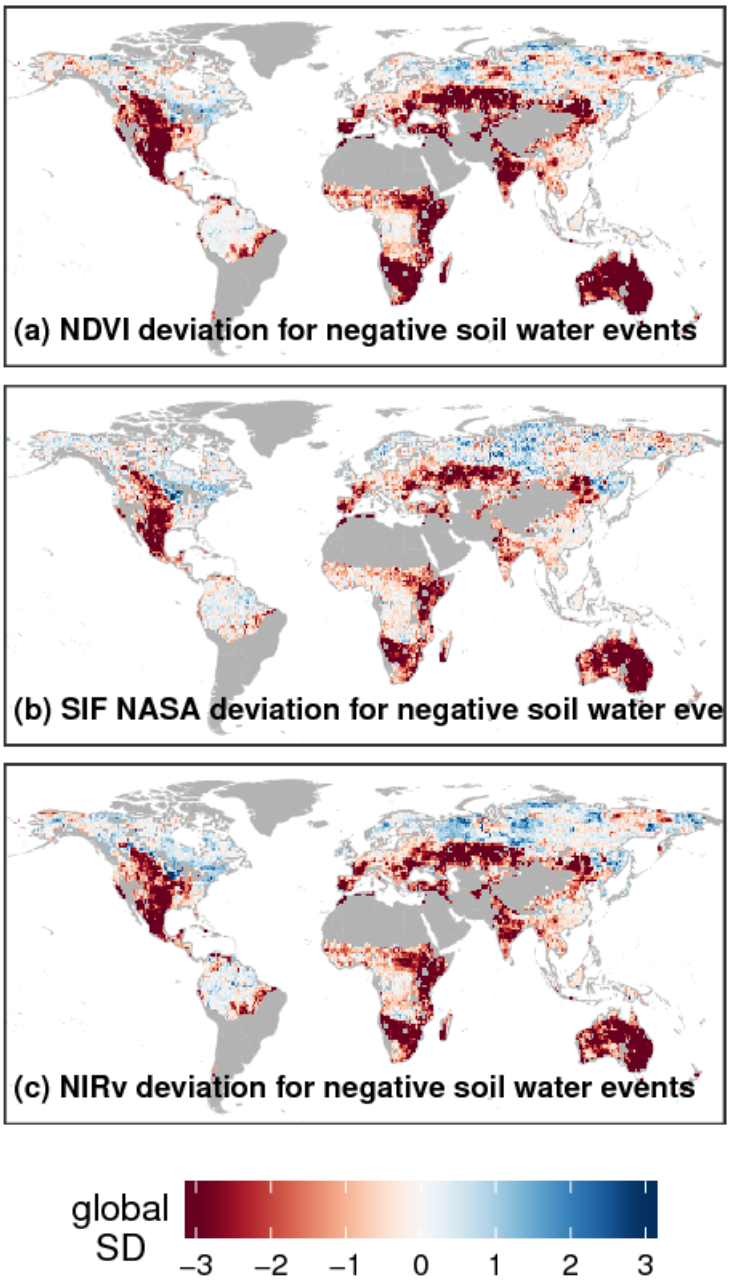

Figure C.6: Deviations seen in the vegetation observations averaged across all events of decreased soil moisture. Units are given in 'global SD', meaning the standard deviation in space and time across the data cube of deviations (see methods).

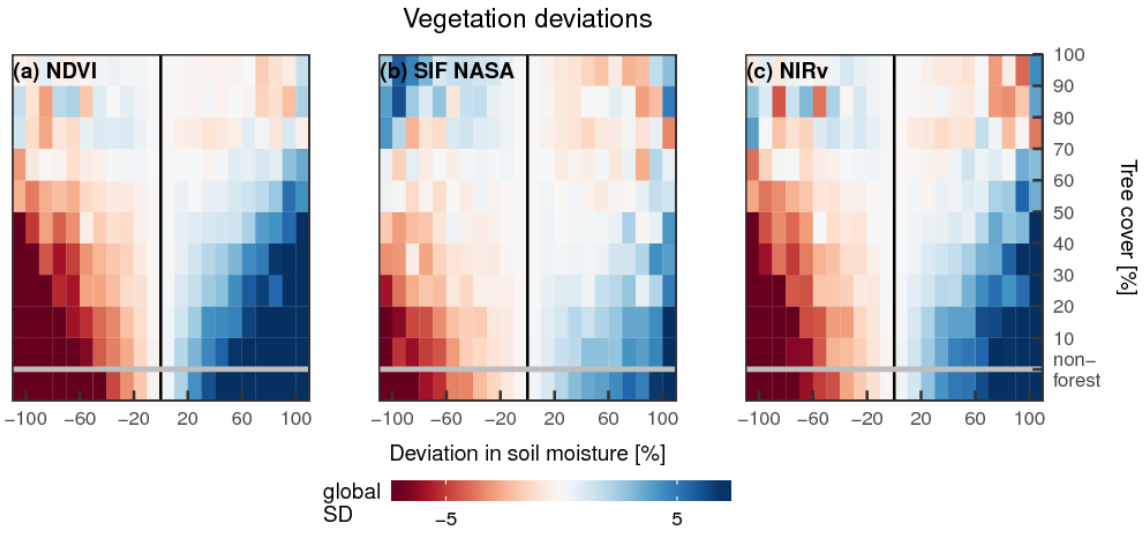

Figure C.7: Typical patterns of vegetation greenness and photosynthesis associated with water availability along a tree cover gradient: Average deviation seen in the vegetation proxies for a given anomaly in the soil water content and as a function of the amount of trees.

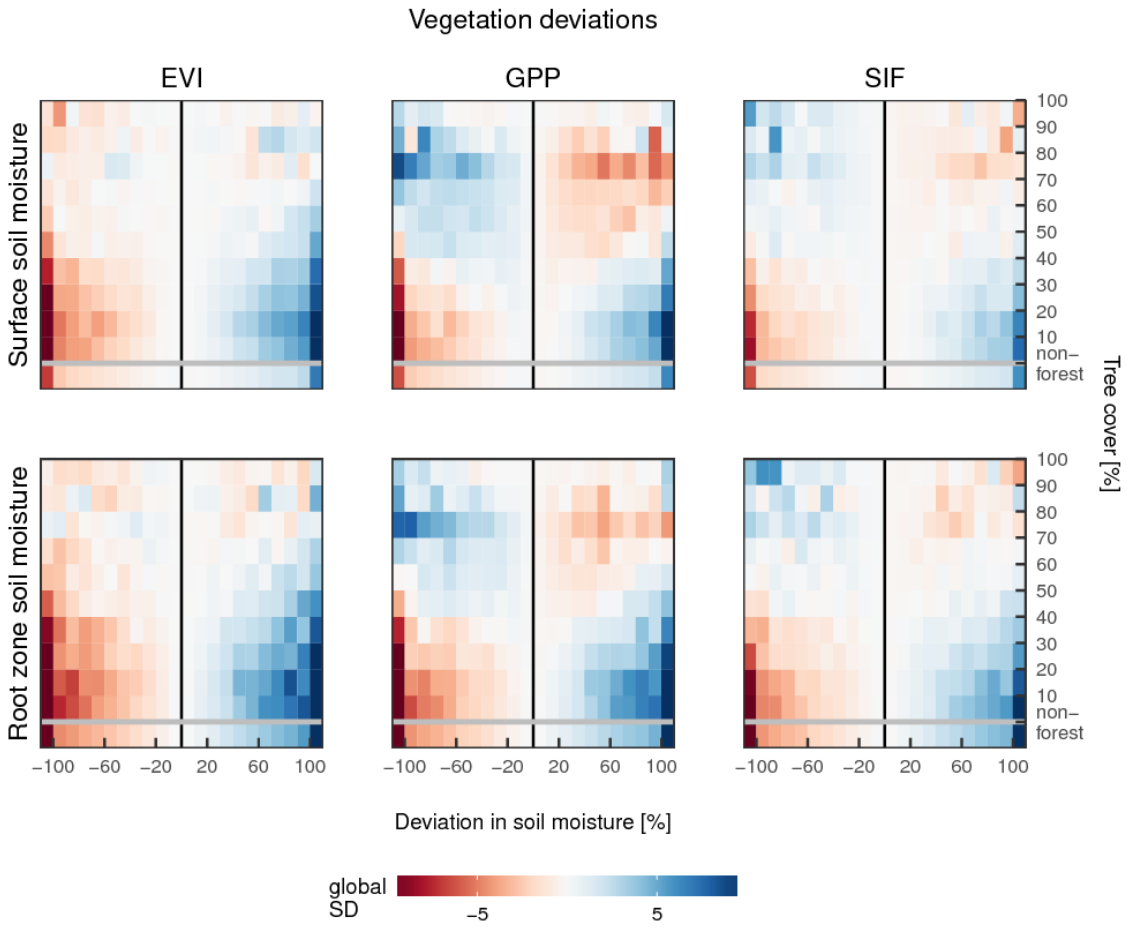

Figure C.8: Typical patterns of vegetation greenness and photosynthesis associated with water availability along a tree cover gradient: Average deviation seen in the vegetation proxies for a given anomaly in the soil water content and as a function of the amount of trees with meteorological events being defined by deviations in soil moisture in the GLEAM data set instead of ERAInterim.

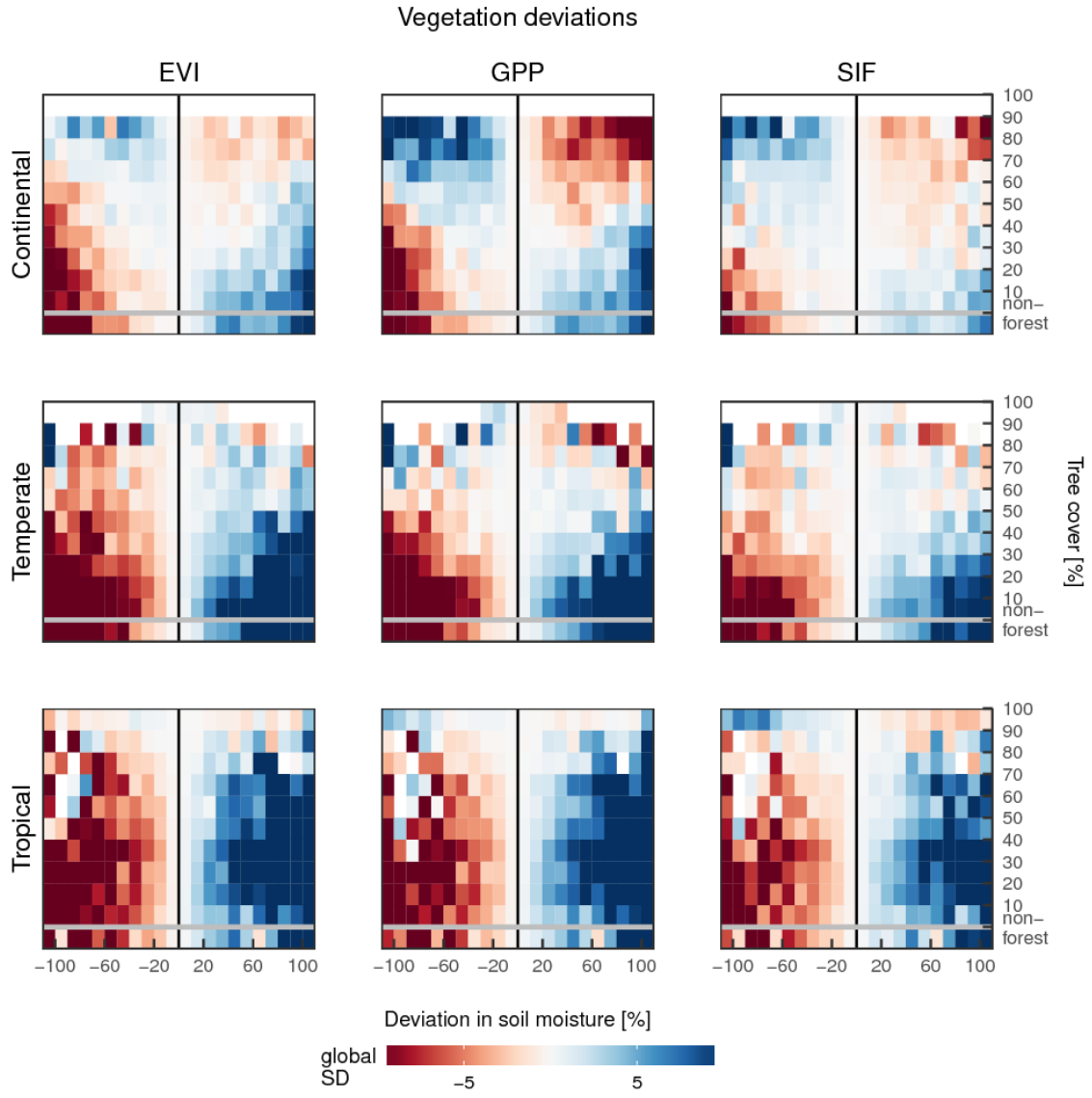

Figure C.9: Typical patterns of vegetation greenness and photosynthesis associated with water availability along a tree cover gradient and separately for different climate classes: Average deviation seen in the vegetation proxies for a given anomaly in the soil water content and as a function of the amount of trees in the different climate classes according to the Koeppen climate classification.

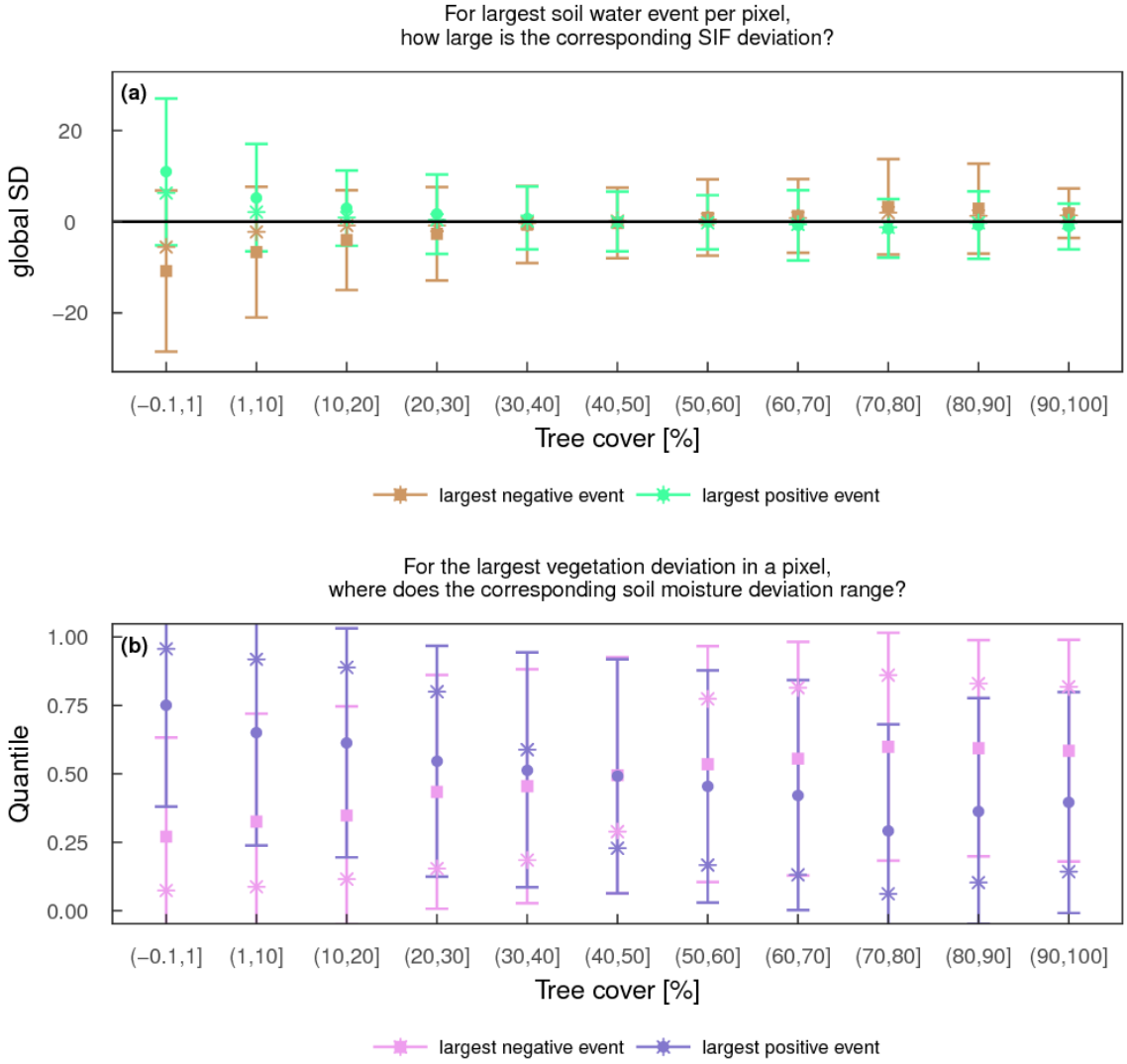

Figure C.10: Correspondence between largest deviations in vegetation and soil moisture as a function of forest cover: a) What deviations are seen in photosynthesis as indicated by SIF in each pixel for the largest positive and largest negative deviations in soil moisture as a function of forest cover? b) Where in the range of all events of soil water deviations in a pixel does the soil moisture deviation range that co-occurs with the largest positive deviation in photosynthesis and the largest negative one? Filled symbols represent the mean, stars the median across pixels and the error bars represent one standard deviation.

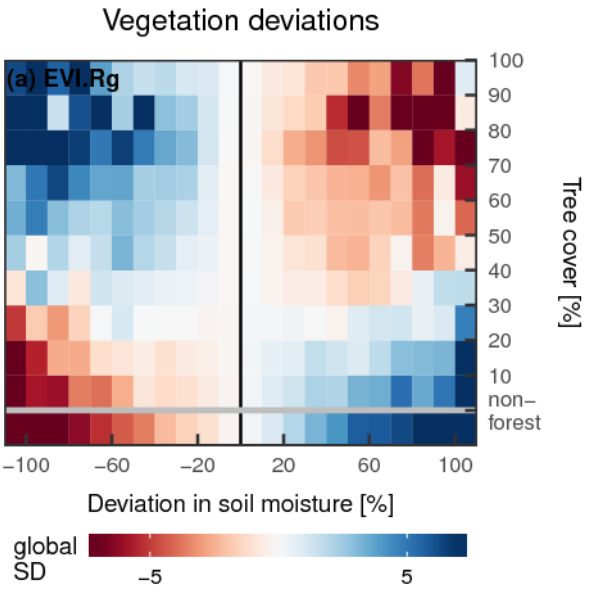

Figure C.11: Typical patterns of a proxy of APAR associated with water availability along a tree cover gradient: Average deviation seen in the product of EVI and global radiation for a given anomaly in the soil water content and as a function of the amount of trees in a given pixel.

Bibliography

Ahlström, A., Raupach, M. R., Schurgers, G., *et al.* (2015), The dominant role of semi-arid ecosystems in the trend and variability of the land CO2 sink, *Science*, **348**(6237) 895–899, doi:10.1126/science.aaa1668.

Alkama, R. and Cescatti, A. (2016), Biophysical climate impacts of recent changes in global forest cover, *Science*, **351** 600–604, doi:10.1126/science.aac8083.

Allen, C. D., Macalady, A. K., Chenchouni, H., *et al.* (2010), A global overview of drought and heat-induced tree mortality reveals emerging climate change risks for forests, *Forest Ecology and Management*, **259**(4) 660–684, doi:10.1016/j.foreco.2009.09.001.

AMAP (2012), Arctic Climate Issues 2011: Changes in Arctic Snow, Water, Ice and Permafrost. SWIPA 2011 Overview Report, Arctic Monitoring and Assessment Programme (AMAP), Oslo.

Anav, A., Friedlingstein, P., Beer, C., *et al.* (2015), Spatiotemporal patterns of terrestrial gross primary production: A review, *Reviews of Geophysics*, doi:10.1002/2015RG000483.

Anderegg, W. R. L., Ballantyne, A. P., Smith, W. K., *et al.* (2015), Tropical nighttime warming as a dominant driver of variability in the terrestrial carbon sink, *Proceedings of the National Academy of Sciences*, **112**(51) 15591–15596, doi:10.1073/pnas.1521479112.

Angert, A., Biraud, S., Bonfils, C., Henning, C. C., Buermann, W., Pinzon, J., Tucker, C. J., and Fung, I. (2005), Drier summers cancel out the CO2 uptake enhancement induced by warmer springs, *PNAS*, **102**(31) 10823–10827, doi:10.1073/pnas.0501647102.

Arneth, A., Lloyd, J., Shibistova, O., Sogachev, A., and Kolle, O. (2006), Spring in the boreal environment: observations on pre- and post-melt energy and CO2 fluxes in two central Siberian ecosystems, *Boreal Environment Research*, **1**(4) 311–328.

Asner, G. P. and Alencar, A. (2010), Drought impacts on the Amazon forest: the remote sensing perspective, *New Phytologist*, **187**(3) 569–578, doi:10.1111/j.1469-8137.2010.03310.x.

Ač, A., Malenovský, Z., Olejníčková, J., Gallé, A., Rascher, U., and Mohammed, G. (2015), Meta-analysis assessing potential of steady-state chlorophyll fluorescence for remote sensing detection of plant water, temperature and nitrogen stress, *Remote Sensing of Environment*, **168** 420–436, doi:https://doi.org/10.1016/j.rse.2015.07.022.

Badgley, G., Field, C. B., and Berry, J. A. (2017), Canopy near-infrared reflectance and terrestrial photosynthesis, *Science Advances*, **3**(3), doi:10.1126/sciadv.1602244.

Baker, N. R. (2008), Chlorophyll Fluorescence: A Probe of Photosynthesis In Vivo, *Annual Review of Plant Biology*, **59**(1) 89–113, doi:10.1146/annurev.arplant.59.032607.092759.

Baldocchi, D., Falge, E., Gu, L., *et al.* (2001), FLUXNET: A New Tool to Study the Temporal and Spatial Variability of Ecosystem-Scale Carbon Dioxide, Water Vapor, and Energy Flux Densities, *Bulletin of the American Meteorological Society*, **82**(11) 2415–2434, doi:10.1175/1520-0477(2001)082⟨2415:FANTTS⟩2.3.CO;2.

Baldocchi, D., Ryu, Y., and Keenan, T. (2016), Terrestrial Carbon Cycle Variability [version 1; referees: 2 approved], *F1000Research*, **5**(2371), doi:10.12688/f1000research.8962.1.

Ballantyne, A., Smith, W., Anderegg, W., *et al.* (2017), Accelerating net terrestrial carbon uptake during the warming hiatus due to reduced respiration, *Nature Climate Change*, **7**(148–152), doi:10.1038/nclimate3204.

Ballantyne, A. P., Alden, C. B., Miller, J. B., Tans, P. P., and White, J. W. C. (2012), Increase in observed net carbon dioxide uptake by land and oceans during the past 50 years, *Nature*, **488**(70–72), doi:10.1038/nature11299.

Barber, V. A., Juday, G. P., and Finney, B. P. (2000), Reduced growth of Alaskan white spruce in the twentieth century from temperature-induced drought stress, *Nature*, **405** 319–326.

Barr, A. G., Griffis, T. J., Black, T. A., Lee, X., Staebler, R. M., Fuentes, J. D., Chen, Z., and Morgenstern, K. (2002), Comparing the carbon budgets of boreal and temperate deciduous forest stands, *Canadian Journal of Forest Research*, **32**(5) 813–822, doi:10.1139/x01-131.

Bartholomé, E. and Belward, A. S. (2005), GLC2000: a new approach to global land cover mapping from Earth observation data, *International Journal of Remote Sensing*, **26**(9) 1959–1977, doi:10.1080/01431160412331291297.

Barton, C. V. M. and North, P. R. J. (2001), Remote sensing of canopy light use efficiency using the photochemical reflectance index: Model and sensitivity analysis, *Remote Sensing of Environment*, **78**(3) 264–273, doi:http://dx.doi.org/10.1016/S0034-4257(01)00224-3.

Bastos, A., Janssens, I. A., Gouveia, C. M., *et al.* (2016), European land CO2 sink influenced by NAO and East-Atlantic Pattern coupling, *Nature Communications*, **7**(10315), doi:10.1038/ncomms10315.

Bauerle, W. L., Oren, R., Way, D. A., *et al.* (2012), Photoperiodic regulation of the seasonal pattern of photosynthetic capacity and the implications for carbon cycling, *Proceedings of the National Academy of Sciences*, **109**(22) 8612–8617, doi:10.1073/pnas.1119131109.

Baumbach, L., Siegmund, J. F., Mittermeier, M., and Donner, R. V. (2017), Impacts of temperature extremes on European vegetation during the growing season, *Biogeosciences*, **14**(21) 4891–4903, doi:10.5194/bg-14-4891-2017.

Beck, P. S. A., Atzberger, C., Høgda, K. A., Johansen, B., and Skidmore, A. K. (2006), Improved monitoring of vegetation dynamics at very high latitudes: A new method using MODIS NDVI , *Remote Sensing of Environment*, **100**(3) 321–334, doi:http://dx.doi.org/10.1016/j.rse.2005.10.021.

Beer, C., Reichstein, M., Tomelleri, E., *et al.* (2010), Terrestrial Gross Carbon Dioxide Uptake: Global Distribution and Covariation with Climate, *Science*, **329**(5993) 834–838, doi:10.1126/science.1184984.

Billings, W., Luken, J., Mortensen, D., and Peterson, K. (1982), Arctic Tundra: A Source or Sink for Atmospheric Carbon Dioxide in a Changing Environment?, *Oecologia*, **5** 5–1.

Billings, W. D. (1987), Carbon balance of Alaskan tundra and taiga ecosystems: past, present and future, *Quaternary Science Reviews*, **6**(2) 165–177, doi:https://doi.org/10.1016/0277-3791(87)90032-1.

Blankenship, R. E. (2014), Molecular Mechanisms of Photosynthesis, second edition edition, Wiley Blackwell.

Bodesheim, P., Jung, M., Gans, F., Mahecha, M. D., and Reichstein, M. (2018), Upscaled diurnal cycles of land-atmosphere fluxes: a new global half-hourly data product, *Earth System Science Data Discussions*, **2018** 1–47, doi:10.5194/essd-2017-130.

Bonan, G. (2008), Ecological Climatology - Concepts and Applications, second edition edition, Cambridge University Press.

Böttcher, K., Aurela, M., Kervinen, M., *et al.* (2014), MODIS time-series-derived indicators for the beginning of the growing season in boreal coniferous forest — A comparison with CO2 flux measurements and phenological observations in Finland , *Remote Sensing of Environment*, **140**(0) 625–638, doi:http://dx.doi.org/10.1016/j.rse.2013.09.022.

Brando, P. M., Goetz, S. J., Baccini, A., Nepstad, D. C., Beck, P. S. A., and Christman, M. C. (2010), Seasonal and interannual variability of climate and vegetation indices across the Amazon, *Proceedings of the National Academy of Sciences*, **107**(33) 14685–14690, doi:10.1073/pnas.0908741107.

Braswell, B. H., Schimel, D. S., Linder, E., and Moore, B. (1997), The Response of Global Terrestrial Ecosystems to Interannual Temperature Variability, *Science*, **278**(5339) 870–873, doi:10.1126/science.278.5339.870.

Buchhorn, M., Walker, D. A., Heim, B., Raynolds, M. K., Epstein, H. E., and Schwieder, M. (2013), Ground-Based Hyperspectral Characterization of Alaska Tundra Vegetation along Environmental Gradients, *Remote Sensing*, **5**(8) 3971–4005, doi:10.3390/rs5083971.

Buermann, W., Parida, R. B., Jung, M., Burn, D. H., and Reichstein, M. (2013), Earlier springs decrease peak summer productivity in North American boreal forests, *Environmental Research Letters*, **8**(2) 024027.

Busch, F., Hüner, N. P. A., and Ensminger, I. (2007), Increased air temperature during simulated autumn conditions does not increase photosynthetic carbon gain but affects the dissipation of excess energy in seedlings of the evergreen conifer Jack pine, *Plant physiology*, **143**(3) 1242–1251.

Busch, F. A., Sage, R. F., and Farquhar, G. D. (2018), Plants increase CO2 uptake by assimilating nitrogen via the photorespiratory pathway, *Nature Plants*, **4**(1) 46–54, doi:10.1038/s41477-017-0065-x.

Cahoon, S. M. P., Sullivan, P. F., Shaver, G. R., Welker, J. M., and Post, E. (2012), Interactions among shrub cover and the soil microclimate may determine future Arctic carbon budgets, *Ecology Letters*, **15**(12) 1415–1422, doi:10.1111/j.1461-0248.2012.01865.x.

Canadell, J., Jackson, R. B., Ehleringer, J. B., Mooney, H. A., Sala, O. E., and Schulze, E.-D. (1996), Maximum rooting depth of vegetation types at the global scale, *Oecologia*, **108**(4) 583–595, doi:10.1007/BF00329030.

Cassidy, A. E., Christen, A., and Henry, G. H. R. (2016), The effect of a permafrost disturbance on growing-season carbon-dioxide fluxes in a high Arctic tundra ecosystem, *Biogeosciences*, **13**(8) 2291–2303, doi:10.5194/bg-13-2291-2016.

Ceccherini, G., Gobron, N., and Migliavacca, M. (2014), On the Response of European Vegetation Phenology to Hydroclimatic Anomalies, *Remote Sensing*, **6**(4) 3143–3169, doi:10.3390/rs6043143.

Chadburn, S. E., Krinner, G., Porada, P., *et al.* (2017), Carbon stocks and fluxes in the high latitudes: using site-level data to evaluate Earth system models, *Biogeosciences*, **14**(22) 5143–5169, doi:10.5194/bg-14-5143-2017.

Chapin, F. S., Shaver, G., Giblin, A., Nadelhoffer, K., and Laundre, J. (1995), Responses of Arctic Tundra to Experimental and Observed Changes in Climate, *Ecology*, **76**(3) 694–711, doi:10.2307/1939337.

Chapin, F. S. I. (1987), Environmental controls over growth of tundra plants, *Ecological Bulletins*, **38** 69–76.

Chen, J., Chen, J., Liao, A., *et al.* (2015), Global land cover mapping at 30m resolution: A POK-based operational approach, *ISPRS Journal of Photogrammetry and Remote Sensing*, **103** 7–27, doi:https://doi.org/10.1016/j.isprsjprs.2014.09.002, global Land Cover Mapping and Monitoring.

Ciais, P., Reichstein, M., Viovy, N., *et al.* (2005), Europe-wide reduction in primary productivity caused by the heat and drought in 2003, *Nature letters*, **437** 529–533, doi:10.1038/nature03972.

Ciais, P., Sabine, C., Bala, G., *et al.* (2013), Carbon and Other Biogeochemical Cycles, in Climate Change 2013: The Physical Science Basis. Contribution of Working Group I to the Fifth Assessment Report of the Intergovernmental Panel on Climate Change [Stocker, T.F., D. Qin, G.- K. Plattner, M. Tignor, S.K. Allen, J. Boschung, A. Nauels, Y. Xia, V. Bex and P.M. Midgley (eds.), 465–570, Cambridge University Press, Cambridge, United Kingdom and New York, NY, USA, doi:10.1017/CBO9781107415324.015.

Clark, M. P., Slater, A. G., Barrett, A. P., Hay, L. E., McCabe, G. J., Rajagopalan, B., and Leavesley, G. H. (2006), Assimilation of snow covered area information into hydrologic and land-surface models, *Advances in Water Resources*, **29**(8) 1209–1221, doi:http://dx.doi.org/10.1016/j.advwatres.2005.10.001.

Commane, R., Lindaas, J., Benmergui, J., *et al.* (2017), Carbon dioxide sources from Alaska driven by increasing early winter respiration from Arctic tundra, *Proceedings of the National Academy of Sciences*, **114**(21) 5361–5366, doi:10.1073/pnas.1618567114.

Damm, A., Guanter, L., Paul-Limoges, E., *et al.* (2015), Far-red sun-induced chlorophyll fluorescence shows ecosystem-specific relationships to gross primary production: An assessment based on observational and modelling approaches, *Remote Sensing of Environment*, **166** 91–105, doi:http://dx.doi.org/10.1016/j.rse.2015.06.004.

Dass, P., Rawlins, M. A., Kimball, J. S., and Kim, Y. (2016), Environmental controls on the increasing GPP of terrestrial vegetation across northern Eurasia, *Biogeosciences*, **13**(1) 45–62, doi:10.5194/bg-13-45-2016.

Daumard, F., Champagne, S., Fournier, A., Goulas, Y., Ounis, A., Hanocq, J. F., and Moya, I. (2010), A Field Platform for Continuous Measurement of Canopy Fluorescence, *IEEE TRANSACTIONS ON GEOSCIENCE AND REMOTE SENSING*, **48**(9) 3358–3368, doi:10.1109/TGRS.2010.2046420.

Daumard, F., Goulas, Y., Champagne, S., Fournier, A., Ounis, A., Olioso, A., and Moya, I. (2012), Continuous monitoring of canopy level sun-induced chlorophyll fluorescence during the growth of a sorghum field, *Geoscience and Remote Sensing, IEEE Transactions on*, **50**(11) 4292–4300.

De Keersmaecker, W., Lhermitte, S., Tits, L., Honnay, O., Somers, B., and Coppin, P. (2015), A model quantifying global vegetation resistance and resilience to short-term climate anomalies and their relationship with vegetation cover, *Global Ecology and Biogeography*, **24**(5) 539–548, doi:10.1111/geb.12279.

Dee, D. P., Uppala, S. M., Simmons, A. J., *et al.* (2011a), The ERA-Interim reanalysis: configuration and performance of the data assimilation system, *Quarterly Journal of the Royal Meteorological Society*, **137**(656) 553–597, doi:10.1002/qj.828.

Dee, D. P., Uppala, S. M., Simmons, A. J., *et al.* (2011b), The ERA-Interim reanalysis: configuration and performance of the data assimilation system, *Quarterly Journal of the Royal Meteorological Society*, **137**(656) 553–597, doi:10.1002/qj.828.

Delbart, N., Kergoat, L., Le Toan, T., Lhermitte, J., and Picard, G. (2005), Determination of phenological dates in boreal regions using normalized difference water index, *Remote Sensing of Environment*, **97**(1) 26–8, doi:http://dx.doi.org/10.1016/j.rse.2005.03.011.

D'Odorico, P., Gonsamo, A., Gough, C. M., *et al.* (2015), The match and mismatch between photosynthesis and land surface phenology of deciduous forests, *Agricultural and Forest Meteorology*, **214–215** 25–38, doi:http://dx.doi.org/10.1016/j.agrformet.2015.07.005.

Doelling, D. R., Loeb, N. G., Keyes, D. F., *et al.* (2013), Geostationary Enhanced Temporal Interpolation for CERES Flux Products, *Journal of Atmospheric and Oceanic Technology*, **30**(6) 1072–1090, doi:10.1175/JTECH-D-12-00136.1.

Donges, J., Schleussner, C.-F., Siegmund, J., and Donner, R. (2016), Event coincidence analysis for quantifying statistical interrelationships between event time series, *The European Physical Journal Special Topics*, **225**(3) 471–487, doi:10.1140/epjst/e2015-50233-y.

Drusch, M., Moreno, J., Del Bello, U., *et al.* (2017), The FLuorescence EXplorer Mission Concept – ESA's Earth Explorer 8, *IEEE Transactions on Geoscience and Remote Sensing*, **55**(3) 1273–1284, doi:10.1109/TGRS.2016.2621820.

Du, J., Jones, L. A., and Kimball, J. S. (2017a), Daily Global Land Parameters Derived from AMSR-E and AMSR2, Version 2 [GeoTIFF 2007-2016], doi:http://dx.doi.org/10.5067/RF8WPYOPJKL2, accessed in March 2018.

Du, J., Kimball, J. S., Jones, L. A., Kim, Y., Glassy, J., and Watts, J. D. (2017b), A global satellite environmental data record derived from AMSR-E and AMSR2 microwave Earth observations, *Earth System Science Data*, **9**(2) 791–808, doi:10.5194/essd-9-791-2017.

Duveiller, G. and Cescatti, A. (2016), Spatially downscaling sun-induced chlorophyll fluorescence leads to an improved temporal correlation with gross primary productivity, *Remote Sensing of Environment*, **182** 72–89, doi:https://doi.org/10.1016/j.rse.2016.04.027.

Duveiller, G., Hooker, J., and Cescatti, A. (2018), The mark of vegetation change on Earth's surface energy balance, *Nature Communications*, **9**(679), doi:10.1038/s41467-017-02810-8.

Dye, D. G. and Tucker, C. J. (2003), Seasonality and trends of snow-cover, vegetation index, and temperature in northern Eurasia, *Geophysical Research Letters*, **30**(7), doi:10.1029/2002GL016384, 1405.

Elmendorf, S. C., Henry, G. H. R., Hollister, R. G., R. D.and Björk, *et al.* (2012), Plot-scale evidence of tundra vegetation change and links to recent summer warming, *Nature Climate Change*, **2** 453–457, doi:10.1038/NCLIMATE1465.

Elmore, A. J., Guinn, S. M., Minsley, B. J., and Richardson, A. D. (2012), Landscape controls on the timing of spring, autumn, and growing season length in mid-Atlantic forests, *Global Change Biology*, **18**(2) 656–674, doi:10.1111/j.1365-2486.2011.02521.x.

Emmerton, C. A., St. Louis, V. L., Humphreys, E. R., Gamon, J. A., Barker, J. D., and Pastorello, G. Z. (2016), Net ecosystem exchange of CO2 with rapidly changing high Arctic landscapes, *Global Change Biology*, **22**(3) 1185–1200, doi:10.1111/gcb.13064.

Ensminger, I., Schmidt, L., and Lloyd, J. (2008), Soil temperature and intermittent frost modulate the rate of recovery of photosynthesis in Scots pine under simulated spring conditions, *New Phytologist*, **177**(2) 428–442, doi:10.1111/j.1469-8137.2007.02273.x.

Ensminger, I., Sveshnikov, D., Campbell, D. A., Funk, C., Jansson, S., Lloyd, J., Shibistova, O., and Öquist, G. (2004), Intermittent low temperatures constrain spring recovery of photosynthesis in boreal Scots pine forests, *Global Change Biology*, **10**(6) 995–1008, doi:10.1111/j.1365-2486.2004.00781.x.

ESA (2015), Report for Mission Selection - An Earth Explorer to observe vegetation fluorescence, FLEX, esa sp-1330/2 (2 volume series) edition, European Space Agency,Noordwijk, The Netherlands.

Farquhar, G. D., von Caemmerer, S., and Berry, J. A. (1980), A biochemical model of photosynthetic CO2 assimilation in leaves of C3 species, *Planta*, **149**(1) 78–90, doi:10.1007/BF00386231.

Feng, S. and Fu, Q. (2013), Expansion of global drylands under a warming climate, *Atmospheric Chemistry and Physics*, **13**(19) 10081–10094, doi:10.5194/acp-13-10081-2013.

Fisher, J. B., Huntzinger, D. N., Schwalm, C. R., and Sitch, S. (2014), Modeling the Terrestrial Biosphere, *Annual Review of Environment and Resources*, **39**(1) 91–123, doi:10.1146/annurev-environ-012913-093456.

Fisher, J. B., Melton, F., Middleton, E., *et al.* (2017), The future of evapotranspiration: Global requirements for ecosystem functioning, carbon and climate feedbacks, agricultural management, and water resources, *Water Resources Research*, **53**(4) 2618–2626, doi:10.1002/2016WR020175.

Fisher, J. I., Mustard, J. F., and Vadeboncoeur, M. A. (2006), Green leaf phenology at Landsat resolution: Scaling from the field to the satellite, *Remote Sensing of Environment*, **100**(2) 265–279, doi:http://dx.doi.org/10.1016/j.rse.2005.10.022.

Flach, M., Sippel, S., Gans, F., Bastos, A., Brenning, A., Reichstein, M., and Mahecha, M. D. (2018), Contrasting biosphere responses to hydrometeorological extremes: revisiting the 2010 western Russian Heatwave, *Biogeosciences Discussions*, **2018** 1–21, doi:10.5194/bg-2018-130.

Forkel, M., Carvalhais, N., Rödenbeck, C., Keeling, R., Heimann, M., Thonicke, K., Zaehle, S., and Reichstein, M. (2016), Enhanced seasonal CO2 exchange caused by amplified plant productivity in northern ecosystems, *Science*, **351**(6274) 696–699, doi:10.1126/science.aac4971.

Forzieri, G., Alkama, R., Miralles, D. G., and Cescatti, A. (2017), Satellites reveal contrasting responses of regional climate to the widespread greening of Earth, *Science*, **356**(6343) 1180–1184, doi:https://doi.org/10.1126/science.aal1727.

Fournier, A., Daumard, F., Champagne, S., Ounis, A., Goulas, Y., and Moya, I. (2012), Effect of canopy structure on sun-induced chlorophyll fluorescence, *ISPRS Journal of Photogrammetry and Remote Sensing*, **68** 112–120, doi:https://doi.org/10.1016/j.isprsjprs.2012.01.003.

Frank, D., Reichstein, M., Bahn, M., *et al.* (2015), Effects of climate extremes on the terrestrial carbon cycle: concepts, processes and potential future impacts, *Global Change Biology*, **21**(8) 2861–2880, doi:10.1111/gcb.12916.

Frankenberg, C., Fisher, J. B., Worden, J., *et al.* (2011a), New global observations of the terrestrial carbon cycle from GOSAT: Patterns of plant fluorescence with gross primary productivity, *Geophysical Research Letters*, **38**(17) n/a–n/a, doi:10.1029/2011GL048738, l17706.

Frankenberg, C., Fisher, J. B., Worden, J., *et al.* (2011b), New global observations of the terrestrial carbon cycle from GOSAT: Patterns of plant fluorescence with gross primary productivity, *Geophysical Research Letters*, **38**(17), doi:10.1029/2011GL048738, l17706.

Frankenberg, C., O'Dell, C., Berry, J., Guanter, L., Joiner, J., Köhler, P., Pollock, R., and Taylor, T. E. (2014), Prospects for chlorophyll fluorescence remote sensing from the Orbiting Carbon Observatory-2, *Remote Sensing of Environment*, **147** 1–12, doi:http://dx.doi.org/10.1016/j.rse.2014.02.007.

Frankenberg, C., O'Dell, C., Guanter, L., and McDuffie, J. (2012), Remote sensing of near-infrared chlorophyll fluorescence from space in scattering atmospheres: implications for its retrieval and interferences with atmospheric CO_2 retrievals, *Atmospheric Measurement Techniques*, **5**(8) 2081–2094, doi:10.5194/amt-5-2081-2012.

Friedlingstein, P., Cox, P., Betts, R., *et al.* (2006), Climate–Carbon Cycle Feedback Analysis: Results from the C4MIP Model Intercomparison, *Journal of Climate*, **19**(14) 3337–3353, doi:10.1175/JCLI3800.1.

Gamon, J., Huemmrich, K., Stone, R., and Tweedie, C. (2013), Spatial and temporal variation in primary productivity (NDVI) of coastal Alaskan tundra: Decreased vegetation growth following earlier snowmelt, *Remote Sensing of Environment*, **129** 144 – 153, doi:http://dx.doi.org/10.1016/j.rse.2012.10.030.

Gamon, J. A. (2015), Reviews and Syntheses: optical sampling of the flux tower footprint, *Biogeosciences*, **12**(14) 4509–4523, doi:10.5194/bg-12-4509-2015.

Gamon, J. A., Huemmrich, K. F., Wong, C. Y. S., Ensminger, I., Garrity, S., Hollinger, D. Y., Noormets, A., and Peñuelas, J. (2016), A remotely sensed pigment index reveals photosynthetic phenology in evergreen conifers, *Proceedings of the National Academy of Sciences*, **113**(46) 13087–13092, doi:10.1073/pnas.1606162113.

Gamon, J. A., Kovalchuck, O., Wong, C. Y. S., Harris, A., and Garrity, S. R. (2015), Monitoring seasonal and diurnal changes in photosynthetic pigments with automated PRI and NDVI sensors, *Biogeosciences*, **12**(13) 4149–4159, doi:10.5194/bg-12-4149-2015.

Gamon, J. A., nuelas, J. P., and Field, C. B. (1992), A narrow-waveband spectral index that tracks diurnal changes in photosynthetic efficiency, *Remote Sensing of Environment*, **41**(1) 35 – 44, doi:http://dx.doi.org/10.1016/0034-4257(92)90059-S.

Gamon, J. A., Serrano, L., and Surfus, J. S. (1997), The photochemical reflectance index: an optical indicator of photosynthetic radiation use efficiency across species, functional types, and nutrient levels, *Oecologia*, **112**(4) 492–501, doi:10.1007/s004420050337.

Garbulsky, M. F., Peñuelas, J., Gamon, J., Inoue, Y., and Filella, I. (2011), The photochemical reflectance index (PRI) and the remote sensing of leaf, canopy and ecosystem radiation use efficiencies: A review and meta-analysis, *Remote Sensing of Environment*, **115**(2) 281–297, doi:http://dx.doi.org/10.1016/j.rse.2010.08.023.

Gentine, P. and Alemohammad, S. H. (2018), Reconstructed Solar-Induced Fluorescence: A Machine Learning Vegetation Product Based on MODIS Surface Reflectance to Reproduce GOME-2 Solar-Induced Fluorescence, *Geophysical Research Letters*, **0**(0), doi:10.1002/2017GL076294.

Gitelson, A. A., Buschmann, C., and Lichtenthaler, H. K. (1998), Leaf chlorophyll fluorescence corrected for re-absorption by means of absorption and reflectance measurements, *Journal of Plant Physiology*, **152**(2) 283–296, doi:https://doi.org/10.1016/S0176-1617(98)80143-0.

Glenn, E. P., Huete, A. R., Nagler, P. L., and Nelson, S. G. (2008), Relationship Between Remotely-sensed Vegetation Indices, Canopy Attributes and Plant Physiological Processes: What Vegetation Indices Can and Cannot Tell Us About the Landscape, *Sensors*, **8** 2136–2160, doi:10.3390/s8042136.

Glenn, E. P., Neale, C. M. U., Hunsaker, D. J., and Nagler, P. L. (2011), Vegetation index-based crop coefficients to estimate evapotranspiration by remote sensing in agricultural

and natural ecosystems, *Hydrological Processes*, **25**(26) 4050–4062, doi:10.1002/hyp.8392.

Gonsamo, A., Chen, J. M., and D'Odorico, P. (2013), Deriving land surface phenology indicators from CO2 eddy covariance measurements , *Ecological Indicators*, **29**(0) 203–207, doi:http://dx.doi.org/10.1016/j.ecolind.2012.12.026.

Gonsamo, A., Chen, J. M., Price, D. T., Kurz, W. A., and Wu, C. (2012), Land surface phenology from optical satellite measurement and CO2 eddy covariance technique, *Journal of Geophysical Research: Biogeosciences*, **117**(G3), doi:10.1029/2012JG002070, g03032.

Graven, H. D., Keeling, R. F., Piper, S. C., *et al.* (2013), Enhanced Seasonal Exchange of CO2 by Northern Ecosystems Since 1960, *Science*, **341**(6150) 1085–1089, doi:10.1126/science.1239207.

Green, J. K., Konings, A. G., Alemohammad, S. H., Berry, J., Entekhabi, D., Kolassa, J., Lee, J.-E., and Gentine, P. (2017), Regionally strong feedbacks between the atmosphere and terrestrial biosphere, *Nature Geoscience*, **10** 410–414, doi:10.1038/ngeo2957.

Gu, L., Fuentes, J. D., Shugart, H. H., Staebler, R. M., and Black, T. A. (1999), Responses of net ecosystem exchanges of carbon dioxide to changes in cloudiness: Results from two North American deciduous forests, *Journal of Geophysical Research: Atmospheres*, **104**(D24) 31421–31434, doi:10.1029/1999JD901068.

Guan, K., Berry, J. A., Zhang, Y., Joiner, J., Guanter, L., Badgley, G., and Lobell, D. B. (2015), Improving the monitoring of crop productivity using spaceborne solar-induced fluorescence, *Global Change Biology*, n/a–n/a, doi:10.1111/gcb.13136.

Guanter, L., Aben, I., Tol, P., *et al.* (2015), Potential of the TROPOspheric Monitoring Instrument (TROPOMI) onboard the Sentinel-5 Precursor for the monitoring of terrestrial chlorophyll fluorescence, *Atmospheric Measurement Techniques*, **8**(3) 1337–1352, doi:10.5194/amt-8-1337-2015.

Guanter, L., Alonso, L., Gómez-Chova, L., Amorós-López, J., Vila, J., and Moreno, J. (2007), Estimation of solar-induced vegetation fluorescence from space measurements, *Geophysical Research Letters*, **34**(8) n/a–n/a, doi:10.1029/2007GL029289, l08401.

Guanter, L., Frankenberg, C., Dudhia, A., Lewis, P. E., Gómez-Dans, J., Kuze, A., Suto, H., and Grainger, R. G. (2012), Retrieval and global assessment of terrestrial chlorophyll fluorescence from GOSAT space measurements, *Remote Sensing of Environment*, **121** 236–251, doi:https://doi.org/10.1016/j.rse.2012.02.006.

Guanter, L., Zhang, Y., Jung, M., *et al.* (2014), Global and time-resolved monitoring of crop photosynthesis with chlorophyll fluorescence, *Proceedings of the National Academy of Sciences*, **111**(14) E1327–E1333, doi:10.1073/pnas.1320008111.

Guay, K. C., Beck, P. S. A., Berner, L. T., Goetz, S. J., Baccini, A., and Buermann, W. (2014), Vegetation productivity patterns at high northern latitudes: a multi-sensor satellite data assessment, *Global Change Biology*, **20**(10) 3147–3158, doi:10.1111/gcb.12647.

Hadley, J. L., O'Keefe, J., Munger, J. W., Hollinger, D. Y., and Richardson, A. D. (2009), Phenology of Forest-Atmosphere Carbon Exchange for Deciduous and Coniferous Forests in Southern and Northern New England, in A. Noormets, editor, Phenology of Ecosystem Processes, 119–141, Springer New York, doi:10.1007/978-1-4419-0026-5_5.

Hansen, M. C., Potapov, P. V., Moore, R., *et al.* (2013), High-Resolution Global Maps of 21st-Century Forest Cover Change, *Science*, **342**(6160) 850–853, doi:10.1126/science.1244693.

Harris, A. and Dash, J. (2010), The potential of the MERIS Terrestrial Chlorophyll Index for carbon flux estimation, *Remote Sensing of Environment*, **114**(8) 1856–1862, doi:https://doi.org/10.1016/j.rse.2010.03.010.

Heinsch, F. A., Zhao, M., Running, S. W., *et al.* (2006), Evaluation of remote sensing based terrestrial productivity from MODIS using regional tower eddy flux network observations, *IEEE Transactions on Geoscience and Remote Sensing*, **44**(7) 1908–1925, doi:10.1109/TGRS.2005.853936.

Hird, J. N. and McDermid, G. J. (2009), Noise reduction of NDVI time series: An empirical comparison of selected techniques, *Remote Sensing of Environment*, **113**(1) 248–258, doi:http://dx.doi.org/10.1016/j.rse.2008.09.003.

Hmimina, G., Dufrêne, E., Pontailler, J.-Y., *et al.* (2013), Evaluation of the potential of MODIS satellite data to predict vegetation phenology in different biomes: An investigation using ground-based NDVI measurements , *Remote Sensing of Environment*, **132**(0) 145–158, doi:http://dx.doi.org/10.1016/j.rse.2013.01.010.

Hoffer, R. M. (1984), CHAPTER 5: Remote Sensing to Measure the Distribution and Structure of Vegetation, in G. M. Woodwell, editor, The Role of Terrestrial Vegetation in the Global Carbon Cycle: Measurement by Remote Sensing, 131–159, SCOPE: John Wiley & Sons Ltd.

horti daily (n.d.), Absorption spectra of pigments, http://www.hortidaily.com/article/13755/Absorption-spectra-versus-Action-spectra, accessed: February, 17th 2018.

Houghton, R. A. (2000), Interannual variability in the global carbon cycle, *Journal of Geophysical Research: Atmospheres*, **105**(D15) 20121–20130, doi:10.1029/2000JD900041.

Huang, J., Yu, H., Guan, X., Wang, G., and Guo, R. (2015), Accelerated dryland expansion under climate change, *Nature Climate Change*, **6** 166–171, doi:10.1038/nclimate2837.

Huang, L., He, B., Chen, A., Wang, H., Liu, J., Lü, A., and Chen, Z. (2016), Drought dominates the interannual variability in global terrestrial net primary production by controlling semi-arid ecosystems, *Scientific Reports*, **6**, doi:10.1038/srep24639.

Huemmrich, K., Gamon, J., Tweedie, C., Campbell, P., Landis, D., and Middleton, E. (2013), Arctic Tundra Vegetation Functional Types Based on Photosynthetic Physiology and Optical Properties, *IEEE Journal of Selected Topics in Applied Earth Observations and Remote Sensing*, **6**(2) 265–275, doi:10.1109/JSTARS.2013.2253446.

Huemmrich, K., Gamon, J., Tweedie, C., *et al.* (2010a), Remote sensing of tundra gross ecosystem productivity and light use efficiency under varying temperature and moisture conditions, *Remote Sensing of Environment*, **114**(3) 481 – 489, doi:http://dx.doi.org/10.1016/j.rse.2009.10.003.

Huemmrich, K. F., Kinoshita, G., Gamon, J. A., Houston, S., Kwon, H., and Oechel, W. C. (2010b), Tundra carbon balance under varying temperature and moisture regimes, *J. Geophys. Res*, **115**, doi:10.1029/2009JG001237, g00I02.

Huete, A., Didan, K., Miura, T., Rodriguez, E., Gao, X., and Ferreira, L. (2002), Overview of the radiometric and biophysical performance of the MODIS vegetation indices, *Remote Sensing of Environment*, **83** 195–213, pII: S0034-4257(02)00096-2 .

Huete, A. R., Didan, K., Shimabukuro, Y. E., *et al.* (2006), Amazon rainforests green-up with sunlight in dry season, *Geophysical Research Letters*, **33**(6), doi:10.1029/2005GL025583.

Huntzinger, D., Post, W., Wei, Y., *et al.* (2012), North American Carbon Program (NACP) regional interim synthesis: Terrestrial biospheric model intercomparison, *Ecological Modelling*, **232**(0) 144–157, doi:http://dx.doi.org/10.1016/j.ecolmodel.2012.02.004.

Jackson, R. D. and Huete, A. R. (1991), Interpreting vegetation indices, *Preventive Veterinary Medicine*, **11** 185–200.

Jenkins, J. P., Richardson, A. D., Braswell, B. H., Ollinger, S. V., Hollinger, D. Y., and Smith, M. L. (2007), Refining light-use efficiency calculations for a deciduous forest canopy using simultaneous tower-based carbon flux and radiometric measurements, *Agricultural and Forest Meteorology*, **143**(1-2) 69–79, doi:http://dx.doi.org/10.1016/j.agrformet.2006.11.008.

Jia, G. J., Epstein, H. E., and Walker, D. A. (2003), Greening of arctic Alaska, 1981–2001, *Geophysical Research Letters*, **30**(20), doi:10.1029/2003GL018268.

Jin, H. and Eklundh, L. (2014), A physically based vegetation index for improved monitoring of plant phenology, *Remote Sensing of Environment*, **152** 512–525, doi:http://dx.doi.org/10.1016/j.rse.2014.07.010.

Joiner, J., Guanter, L., Lindstrot, R., *et al.* (2013), Global monitoring of terrestrial chlorophyll fluorescence from moderate-spectral-resolution near-infrared satellite measurements: methodology, simulations, and application to GOME-2, *Atmospheric Measurement Techniques*, **6**(10) 2803–2823, doi:10.5194/amt-6-2803-2013.

Joiner, J., Yoshida, Y., Guanter, L., and Middleton, E. M. (2016), New methods for the retrieval of chlorophyll red fluorescence from hyperspectral satellite instruments: simulations and application to GOME-2 and SCIAMACHY, *Atmospheric Measurement Techniques*, **9**(8) 3939–3967, doi:10.5194/amt-9-3939-2016.

Joiner, J., Yoshida, Y., Vasilkov, A. P., Yoshida, Y., Corp, L. A., and Middleton, E. M. (2011), First observations of global and seasonal terrestrial chlorophyll fluorescence from space, *Biogeosciences*, **8**(3) 637–651, doi:10.5194/bg-8-637-2011.

Joiner, J., Yoshida, Y., Vasilkov, A. P., *et al.* (2014), The seasonal cycle of satellite chlorophyll fluorescence observations and its relationship to vegetation phenology and ecosystem atmosphere carbon exchange, *Remote Sensing of Environment*, **152**(0) 375–391, doi:http://dx.doi.org/10.1016/j.rse.2014.06.022.

Jones, H. G. and Vaughan, R. A. (2010), Remote sensing of vegetation - principles, technologies and applications, Oxford University Press.

Jones, M. O., Jones, L. A., Kimball, J. S., and McDonald, K. C. (2011), Satellite passive microwave remote sensing for monitoring global land surface phenology, *Remote Sensing of Environment*, **115**(4) 1102–1114, doi:https://doi.org/10.1016/j.rse.2010.12.015.

Jönsson, A. M., Eklundh, L., Hellström, M., Bärring, L., and Jönsson, P. (2010), Annual changes in MODIS vegetation indices of Swedish coniferous forests in relation to snow dynamics and tree phenology, *Remote Sensing of Environment*, **114**(11) 2719–2730, doi:http://dx.doi.org/10.1016/j.rse.2010.06.005.

Jung, M., Reichstein, M., and Bondeau, A. (2009), Towards global empirical upscaling of FLUXNET eddy covariance observations: validation of a model tree ensemble approach using a biosphere model, *Biogeosciences*, **6**(10) 2001–2013, doi:10.5194/bg-6-2001-2009.

Jung, M., Reichstein, M., Margolis, H. A., *et al.* (2011), Global patterns of land-atmosphere fluxes of carbon dioxide, latent heat, and sensible heat derived from eddy covariance, satellite, and meteorological observations, *Journal of Geophysical Research: Biogeosciences*, **116**(G3), doi:10.1029/2010JG001566, g00J07.

Jung, M., Reichstein, M., Schwalm, C. R., *et al.* (2017), Compensatory water effects link yearly global land CO2 sink changes to temperature, *Nature*, **541** 516–520, doi:10.1038/nature20780.

Keeling, C. D., Whorf, T. P., Wahlen, M., and van der Plichtt, J. (1995), Interannual extremes in the rate of rise of atmospheric carbon dioxide since 1980, *Nature*, **375** 666 – 670, doi:10.1038/375666a0.

Keenan, T., Baker, I., Barr, A., *et al.* (2012), Terrestrial biosphere model performance for inter-annual variability of land-atmosphere CO2 exchange, *Global Change Biology*, **18**(6) 1971–1987, doi:10.1111/j.1365-2486.2012.02678.x.

Keenan, T. F., Prentice, I. C., Canadell, J. G., Williams, C. A., Wang, H., Raupach, M., and Collatz, G. J. (2016), Recent pause in the growth rate of atmospheric CO2 due to enhanced terrestrial carbon uptake, *Nature Communications*, **7**(13428), doi:10.1038/ncomms13428.

Kelliher, F. M., Leuning, R., and Schulze, E. D. (1993), Evaporation and canopy characteristics of coniferous forests and grasslands, *Oecologia*, **95**(2) 153–163, doi:10.1007/BF00323485.

Klosterman, S. T., Hufkens, K., Gray, J. M., *et al.* (2014), Evaluating remote sensing of deciduous forest phenology at multiple spatial scales using PhenoCam imagery, *Biogeosciences*, **11**(16) 4305–4320, doi:10.5194/bg-11-4305-2014.

Kobayashi, H., Yunus, A. P., Nagai, S., *et al.* (2016), Latitudinal gradient of spruce forest understory and tundra phenology in Alaska as observed from satellite and ground-based data, *Remote Sensing of Environment*, **177** 160–170, doi:http://dx.doi.org/10.1016/j.rse.2016.02.020.

Koffi, E. N., Rayner, P. J., Norton, A. J., Frankenberg, C., and Scholze, M. (2015), Investigating the usefulness of satellite derived fluorescence data in inferring gross primary productivity within the carbon cycle data assimilation system, *Biogeosciences Discussions*, **12**(1) 707–749, doi:10.5194/bgd-12-707-2015.

Köhler, P., Guanter, L., and Joiner, J. (2015a), A linear method for the retrieval of sun-induced chlorophyll fluorescence from GOME-2 and SCIAMACHY data, *Atmospheric Measurement Techniques*, **8**(6) 2589–2608, doi:10.5194/amt-8-2589-2015.

Köhler, P., Guanter, L., and Joiner, J. (2015b), A linear method for the retrieval of sun-induced chlorophyll fluorescence from GOME-2 and SCIAMACHY data, *Atmospheric Measurement Techniques*, **8**(6) 2589–2608, doi:10.5194/amt-8-2589-2015.

Köhler, P., Guanter, L., Kobayashi, H., Walther, S., and Yang, W. (2018), Assessing the potential of sun-induced fluorescence and the canopy scattering coefficient to track large-scale vegetation dynamics in Amazon forests, *Remote Sensing of Environment*, **204** 769–785, doi:https://doi.org/10.1016/j.rse.2017.09.025.

Koirala, S., Jung, M., Reichstein, M., *et al.* (2017), Global distribution of groundwater-vegetation spatial covariation, *Geophysical Research Letters*, **44**(9) 4134–4142, doi:10.1002/2017GL072885.

Kolari, P., Chan, T., Porcar-Castell, A., Bäck, J., Nikinmaa, E., and Juurola, E. (2014), Field and controlled environment measurements show strong seasonal acclimation in photosynthesis and respiration potential in boreal Scots pine, *Frontiers in Plant Science*, **5**(717), doi:10.3389/fpls.2014.00717.

Koster, R. D., Dirmeyer, P. A., Guo, Z., *et al.* (2004), Regions of Strong Coupling Between Soil Moisture and Precipitation, *Science*, **305**(5687) 1138 – 1140, doi:10.1126/science.1100217.

Kottek, M., Grieser, J., Beck, C., Rudolf, B., and Rubel, F. (2006), World Map of the Köppen-Geiger climate classification updated, *Meteorologische Zeitschrift*, **15**(3) 259–263, doi:10.1127/0941-2948/2006/0130.

Krause, G. H. and Weis, E. (1991), Chlorophyll Fluorescence and Photosynthesis: The Basics, *Annual Review of Plant Physiology and Plant Molecular Biology*, **42**(1) 313–349, doi:10.1146/annurev.pp.42.060191.001525.

Kross, A. S. E., Roulet, N. T., Moore, T. R., Lafleur, P. M., Humphreys, E. R., Seaquist, J. W., Flanagan, L. B., and Aurela, M. (2014), Phenology and its role in carbon dioxide exchange processes in northern peatlands, *Journal of Geophysical Research: Biogeosciences*, **119**(7) 1370–1384, doi:10.1002/2014JG002666, 2014JG002666.

Kwon, H.-J., Oechel, W. C., Zulueta, R. C., and Hastings, S. (2006), Effects of climate variability on carbon sequestration among adjacent wet sedge tundra and moist tussock

tundra ecosystems, *Journal of Geophysical Research: Biogeosciences*, **111**(G3), doi:10.1029/2005JG000036, g03014.

Lafleur, P. M. and Humphreys, E. R. (2008), Spring warming and carbon dioxide exchange over low Arctic tundra in central Canada, *Global Change Biology*, **14**(4) 740–756, doi:10.1111/j.1365-2486.2007.01529.x.

Laidler, G. J. and Treitz, P. (2003), Biophysical remote sensing of arctic environments, *Progress in Physical Geography*, **27**(1) 44–68, doi:10.1191/0309133303pp358ra.

Lasslop, G., Reichstein, M., Papale, D., *et al.* (2010), Separation of net ecosystem exchange into assimilation and respiration using a light response curve approach: critical issues and global evaluation, *Global Change Biology*, **16**(1) 187–208, doi:10.1111/j.1365-2486.2009.02041.x.

le Maire, G., Delpierre, N., Jung, M., *et al.* (2010), Detecting the critical periods that underpin interannual fluctuations in the carbon balance of European forests, *Journal of Geophysical Research: Biogeosciences*, **115**(G3) n/a–n/a, doi:10.1029/2009JG001244, g00H03.

Le Quéré, C., Andrew, R. M., Friedlingstein, P., *et al.* (2017), Global Carbon Budget 2017, *Earth System Science Data Discussions*, **2017** 1–79, doi:10.5194/essd-2017-123.

Le Quéré, C., Raupach, M. R., Canadell, J. G., *et al.* (2009), Trends in the sources and sinks of carbon dioxide, *Nature Geoscience*, **2** 831–836, doi:10.1038/ngeo689.

Lee, J.-E., Frankenberg, C., van der Tol, C., *et al.* (2013), Forest productivity and water stress in Amazonia: observations from GOSAT chlorophyll fluorescence, *Proceedings of the Royal Society of London B: Biological Sciences*, **280**(1761), doi:10.1098/rspb.2013.0171.

Lenton, T. M., Held, H., Kriegler, E., Hall, J. W., Lucht, W., Rahmstorf, S., and Schellnhuber, H. J. (2008), Tipping elements in the Earth's climate system, *Proceedings of the National Academy of Sciences*, **105**(6) 1786–1793, doi:10.1073/pnas.0705414105.

Liu, G., Liu, H., and Yin, Y. (2013), Global patterns of NDVI-indicated vegetation extremes and their sensitivity to climate extremes, *Environmental Research Letters*, **8**(2) 025009.

Liu, J., Bowman, K. W., Schimel, D. S., *et al.* (2017a), Contrasting carbon cycle responses of the tropical continents to the 2015–2016 El Niño, *Science*, **358**(6360), doi:10.1126/science.aam5690.

Liu, J., Bowman, K. W., Schimel, D. S., *et al.* (2017b), Contrasting carbon cycle responses of the tropical continents to the 2015–2016 El Niño, *Science*, **358**(6360,), doi:10.1126/science.aam5690.

Liu, Y., J., P. A., Kumar, M., W., H. C., Katul, G. G., and Porporato, A. (2017c), Increasing atmospheric humidity and CO2 concentration alleviate forest mortality risk, *Proceedings of the National Academy of Sciences of the United States of America PNAS*, **114**(37) 9918–9923, doi:10.1073/pnas.1704811114.

Liu, Y. Y., de Jeu, R. A. M., McCabe, M. F., Evans, J. P., and van Dijk, A. I. J. M. (2011), Global long-term passive microwave satellite-based retrievals of vegetation optical depth, *Geophysical Research Letters*, **38**(18), doi:10.1029/2011GL048684, l18402.

López-Blanco, E., Lund, M., Williams, M., Tamstorf, M. P., Westergaard-Nielsen, A., Exbrayat, J.-F., Hansen, B. U., and Christensen, T. R. (2017), Exchange of CO_2 in Arctic tundra: impacts of meteorological variations and biological disturbance, *Biogeosciences*, **14**(19) 4467–4483, doi:10.5194/bg-14-4467-2017.

Louis, J., Ounis, A., Ducruet, J. M., *et al.* (2005), Remote sensing of sunlight-induced chlorophyll fluorescence and reflectance of Scots pine in the boreal forest during spring recovery, *Remote Sensing of Environment*, **96**(1) 37–48, doi:10.1016/j.rse.2005.01.013.

Lund, M., Lafleur, P. M., Roulet, N. T., *et al.* (2010), Variability in exchange of CO2 across 12 northern peatland and tundra sites, *Global Change Biology*, **16**(9) 2436–2448, doi:10.1111/j.1365-2486.2009.02104.x.

Luus, K. A., Commane, R., Parazoo, N. C., *et al.* (2017), Tundra photosynthesis captured by satellite-observed solar-induced chlorophyll fluorescence, *Geophysical Research Letters*, **44**(3) 1564–1573, doi:10.1002/2016GL070842, 2016GL070842.

Lyapustin, A., Wang, Y., Xiong, X., *et al.* (2014), Scientific impact of MODIS C5 calibration degradation and C6+ improvements, *Atmospheric Measurement Techniques*, **7**(12) 4353–4365, doi:10.5194/amt-7-4353-2014.

Ma, X., Huete, A., Cleverly, J., *et al.* (2016), Drought rapidly diminishes the large net CO2 uptake in 2011 over semi-arid Australia, *Scientific Reports*, **6**(37747) 2036–2052, doi:10.1038/srep37747.

Ma, X., Huete, A., Moran, S., Ponce-Campos, G., and Eamus, D. (2015), Abrupt shifts in phenology and vegetation productivity under climate extremes, *Journal of Geophysical Research: Biogeosciences*, **120**(10) 2036–2052, doi:10.1002/2015JG003144.

Ma, X., Huete, A., Yu, Q., *et al.* (2013), Spatial patterns and temporal dynamics in savanna vegetation phenology across the North Australian Tropical Transect, *Remote Sensing of Environment*, **139** 97–115, doi:https://doi.org/10.1016/j.rse.2013.07.030.

MacBean, N., Maignan, F., Bacour, C., *et al.* (2018), Strong constraint on modelled global carbon uptake using solar-induced chlorophyll fluorescence data, *Scientific Report*, **8**(1973) 2037–2051, doi:10.1038/s41598-018-20024-w.

Mahecha, M. D., Gans, F., Sippel, S., *et al.* (2017), Detecting impacts of extreme events with ecological in situ monitoring networks, *Biogeosciences*, **14**(18) 4255–4277, doi:10.5194/bg-14-4255-2017.

Marcolla, B., Rödenbeck, C., and Cescatti, A. (2017), Patterns and controls of inter-annual variability in the terrestrial carbon budget, *Biogeosciences*, **14**(16) 3815–3829, doi:10.5194/bg-14-3815-2017.

Martens, B., Miralles, D. G., Lievens, H., *et al.* (2017), GLEAM v3: satellite-based land evaporation and root-zone soil moisture, *Geoscientific Model Development*, **10**(5) 1903–1925, doi:10.5194/gmd-10-1903-2017.

Marushchak, M. E., Kiepe, I., Biasi, C., *et al.* (2013), Carbon dioxide balance of subarctic tundra from plot to regional scales, *Biogeosciences*, **10**(1) 437–452, doi: 10.5194/bg-10-437-2013.

Matheny, A. M., Bohrer, G., Garrity, S. R., Morin, T. H., Howard, C. J., and Vogel, C. S. (2015), Observations of stem water storage in trees of opposing hydraulic strategies, *Ecosphere*, **6**(9) 1–13, doi:10.1890/ES15-00170.1, art165.

Maxwell, K. and Johnson, G. N. (2000), Chlorophyll fluorescence—a practical guide, *Journal of Experimental Botany*, **51**(345) 659–668, doi:10.1093/jexbot/51.345.659.

May, J. L., Healey, N. C., Ahrends, H. E., Hollister, R. D., Tweedie, C. E., Welker, J. M., Gould, W. A., and Oberbauer, S. F. (2017), Short-Term Impacts of the Air Temperature on Greening and Senescence in Alaskan Arctic Plant Tundra Habitats, *Remote Sensing*, **9**(12), doi:10.3390/rs9121338.

MCD43C4: NASA LP DAAC, U. E. R. O. and Science (EROS) Center, S. D., Sioux Falls (n.d.), MCD43C4: MODIS/Terra and Aqua Nadir BRDF-Adjusted Reflectance Daily L3 Global 0.05Deg CMG V006, https://dx.doi.org/10.5067/MODIS/MCD43C4.006, accessed in November 2017.

McFadden, J. P., Eugster, W., and Chapin, F. S. (2003), A REGIONAL STUDY OF THE CONTROLS ON WATER VAPOR AND CO2 EXCHANGE IN ARCTIC TUNDRA, *Ecology*, **84**(10) 2762–2776, doi:10.1890/01-0444.

McGuire, A. D., Christensen, T. R., Hayes, D., *et al.* (2012), An assessment of the carbon balance of Arctic tundra: comparisons among observations, process models, and atmospheric inversions, *Biogeosciences*, **9**(8) 3185–3204, doi:10.5194/bg-9-3185-2012.

Melaas, E. K., Richardson, A. D., Friedl, M. A., Dragoni, D., Gough, C. M., Herbst, M., Montagnani, L., and Moors, E. (2013), Using FLUXNET data to improve models of springtime vegetation activity onset in forest ecosystems, *Agricultural and Forest Meteorology*, **171-172**(0) 46–56, doi:http://dx.doi.org/10.1016/j.agrformet.2012.11.018.

Meroni, M., Rossini, M., Guanter, L., Alonso, L., Rascher, U., Colombo, R., and Moreno, J. (2009), Remote sensing of solar-induced chlorophyll fluorescence: Review of methods and applications, *Remote Sensing of Environment*, **113**(10) 2037–2051, doi:https://doi.org/10.1016/j.rse.2009.05.003.

Middleton, E. M., Huemmrich, K. F., Landis, D. R., Black, T. A., Barr, A. G., and McCaughey, J. H. (2016), Photosynthetic efficiency of northern forest ecosystems using a MODIS-derived Photochemical Reflectance Index (PRI), *Remote Sensing of Environment*, **187** 345–366, doi:https://doi.org/10.1016/j.rse.2016.10.021.

Migliavacca, M., Perez-Priego, O., Rossini, M., *et al.* (2017), Plant functional traits and canopy structure control the relationship between photosynthetic CO2 uptake and far-red sun-induced fluorescence in a Mediterranean grassland under different nutrient availability, *New Phytologist*, doi:10.1111/nph.14437, 2016-22970.

Miralles, D., Nieto, R., McDowell, N. G., *et al.* (2016), Contribution of water-limited ecoregions to their own supply of rainfall, *Environmental Research Letters*, **11**(12) 124007.

Miralles, D. G., Holmes, T. R. H., De Jeu, R. A. M., Gash, J. H., Meesters, A. G. C. A., and Dolman, A. J. (2011), Global land-surface evaporation estimated from satellite-based observations, *Hydrology and Earth System Sciences*, **15**(2) 453–469, doi:10.5194/hess-15-453-2011.

MOD13C1: NASA LP DAAC, U. E. R. O. and Science (EROS) Center, S. D., Sioux Falls (n.d.), MOD13C1: MODIS/Terra Vegetation Indices 16-Day L3 Global 0.05 Deg CMG V006, https://dx.doi.org/10.5067/MODIS/MOD13C1.006, accessed in December 2017.

Monson, R. K., Sparks, J. P., Rosenstiel, T. N., *et al.* (2005), Climatic Influences on Net Ecosystem CO2 Exchange during the Transition from Wintertime Carbon Source to Springtime Carbon Sink in a High-Elevation, Subalpine Forest, *Oecologia*, **146**(1) 130–147.

Monteith, J. L. (1972), Solar Radiation and Productivity in Tropical Ecosystems, *Journal of Applied Ecology*, **9**(3) 747–766.

Moore, C. E., Beringer, J., Evans, B., Hutley, L. B., McHugh, I., and Tapper, N. J. (2016), The contribution of trees and grasses to productivity of an Australian tropical savanna, *Biogeosciences*, **13**(8) 2387–2403, doi:10.5194/bg-13-2387-2016.

Morton, J., D. C. Nagol, Carabajal, C. C., Rosette, J., Palace, M., Cook, B. D., Vermote, E. F., Harding, D. J., and North, P. R. J. (2014), Amazon forests maintain consistent canopy structure and greenness during the dry season, *Nature*, **506**, doi:10.1038/nature13006.

Mueller, N. D., Butler, E. E., McKinnon, K. A., Rhines, A., Tingley, M., Holbrook, N. M., and Huybers, P. (2016), Cooling of US Midwest summer temperature extremes from cropland intensification, *Nature Climate Change*, **6** 317–322, doi:10.1038/nclimate2825.

MYD13C1: NASA LP DAAC, U. E. R. O. and Science (EROS) Center, S. D., Sioux Falls (n.d.), MYD13C1: MODIS/Aqua Vegetation Indices 16-Day L3 Global 0.05 Deg CMG V006, https://dx.doi.org/10.5067/MODIS/MYD13C1.006, accessed in December 2017.

Myneni, R. B., Keeling, C. D., Tucker, C. J., Asrar, G., and Nemani, R. R. (1997), Increased plant growth in the northern high latitudes from 1981 to 1991, *Nature*, **386**, doi:10.1038/386698a0.

Myneni, R. B., Yang, W., Nemani, R. R., *et al.* (2007), Large seasonal swings in leaf area of Amazon rainforests, *Proceedings of the National Academy of Sciences*, **104**(12) 4820–4823, doi:10.1073/pnas.0611338104.

Nemani, R. R., Keeling, C. D., Hashimoto, H., Jolly, W. M., Piper, S. C., Tucker, C. J., Myneni, R. B., and Running, S. W. (2003), Climate-Driven Increases in Global Terrestrial Net Primary Production from 1982 to 1999, *Science*, **300** 1560–1563, doi:10.1126/science.1082750.

Nichol, C. J., Huemmrich, K. F., Black, T. A., Jarvis, P. G., Walthall, C. L., Grace, J., and Hall, F. G. (2000), Remote sensing of photosynthetic-light-use efficiency of boreal forest, *Agricultural and Forest Meteorology*, **101**(2–3) 131–142, doi:http://dx.doi.org/10.1016/S0168-1923(99)00167-7.

Norton, A. J., Rayner, P. J., Koffi, E. N., and Scholze, M. (2018), Assimilating solar-induced chlorophyll fluorescence into the terrestrial biosphere model BETHY-SCOPE v1.0: model description and information content, *Geoscientific Model Development*, **11**(4) 1517–1536, doi:10.5194/gmd-11-1517-2018.

Oberbauer, S. F., Starr, G., and Pop, E. W. (1998), Effects of extended growing season and soil warming on carbon dioxide and methane exchange of tussock tundra in Alaska, *Journal of Geophysical Research*, **103**(D22) 29,075–29,082.

OCO-2 Science Team/Michael Gunson, A. E. (2017), OCO2 L2 Lite SIF; OCO-2 Level 2 bias-corrected solar-induced fluorescence and other select fields from the IMAP-DOAS algorithm aggregated as daily files, version 8, NASA Goddard Earth Science Data and Information Services Center (GES DISC), Greenbelt, MD, USA, accessed in October 2017.

Oechel, W. C., Hastings, S. J., Vourlrtis, G., Jenkins, M., Riechers, G., and Grulke, N. (1993), Recent change of Arctic tundra ecosystems from a net carbon dioxide sink to a source, *Nature*, **361** 520–523, doi:10.1038/361520a0.

Olivas, P. C., Oberbauer, S. F., Tweedie, C., Oechel, W. C., Lin, D., and Kuchy, A. (2011), Effects of Fine-Scale Topography on CO2 Flux Components of Alaskan Coastal Plain Tundra: Response to Contrasting Growing Seasons, *Arctic, Antarctic, and Alpine Research*, **43**(2) 256–266, doi:https://doi.org/10.1657/1938-4246-43.2.256.

Olson, D. M., Dinerstein, E., Wikramanayake, E. D., *et al.* (2001), Terrestrial Ecoregions of the World: A New Map of Life on Earth: A new global map of terrestrial ecoregions provides an innovative tool for conserving biodiversity, *BioScience*, **51**(11) 933–938, doi:10.1641/0006-3568(2001)051[0933:TEOTWA]2.0.CO;2.

Opała-Owczarek, M., Pirożnikow, E., Owczarek, P., *et al.* (2018), The influence of abiotic factors on the growth of two vascular plant species (Saxifraga oppositifolia and Salix polaris) in the High Arctic, *CATENA*, **163** 219–232, doi:https://doi.org/10.1016/j.catena.2017.12.018.

Öquist, G. and Huner, N. P. A. (2003), Photosynthesis of overwintering evergreen plants, *Annual Review of Plant Biology*, **54**(1) 329–355, doi:10.1146/annurev.arplant.54.072402.115741.

Ottander, C., Campbell, D., and Öquist, G. (1995), Seasonal changes in photosystem II organisation and pigment composition in *Pinus sylvestris*, *Planta*, **197**(1) 176–183, doi:10.1007/BF00239954.

Papagiannopoulou, C., Miralles, D. G., Dorigo, W., Verhoest, N., Depoorter, M., and Waegeman, W. (2017), Vegetation anomalies caused by antecedent precipitation in most of the world, *Environmental Research Letters*.

Papale, D., Black, T. A., Carvalhais, N., *et al.* (2015), Effect of spatial sampling from European flux towers for estimating carbon and water fluxes with artificial neural networks, *Journal of Geophysical Research: Biogeosciences*, **120**(10) 1941–1957, doi:10.1002/2015JG002997, 2015JG002997.

Parazoo, N. C., Bowman, K., Fisher, J. B., *et al.* (2014), Terrestrial gross primary production inferred from satellite fluorescence and vegetation models, *Global Change Biology*, **20**(10) 3103–3121, doi:10.1111/gcb.12652.

Parazoo, N. C., Bowman, K., Frankenberg, C., *et al.* (2013), Interpreting seasonal changes in the carbon balance of southern Amazonia using measurements of XCO2 and chlorophyll fluorescence from GOSAT, *Geophysical Research Letters*, **40**(11) 2829–2833, doi:10.1002/grl.50452.

Parida, B. R. and Buermann, W. (2014), Increasing summer drying in North American ecosystems in response to longer nonfrozen periods, *Geophysical Research Letters*, **41**(15) 5476–5483, doi:10.1002/2014GL060495.

Peñuelas, J., Ciais, P., Canadell, J. G., *et al.* (2017), Shifting from a fertilization-dominated to a warming-dominated period, *Nature Ecology & Evolution*, **1** 1438–1445, doi:10.1038/s41559-017-0274-8.

Peñuelas, J., Filella, I., and Gamon, J. A. (1995), Assessment of photosynthetic radiation-use efficiency with spectral reflectance, *New Phytologist*, **131**(3) 291–296, doi:10.1111/j.1469-8137.1995.tb03064.x.

Pearson, R. G., Phillips, S. J., Loranty, M. M., Beck, P. S. A., Damoulas, T., Knight, S. J., and Goetz, S. J. (2013), Shifts in Arctic vegetation and associated feedbacks under climate change, *Nature Climate Change*, **3** 673–677, doi:10.1038/nclimate1858.

Peng, C., Ma, Z., Lei, X., *et al.* (2011), A drought-induced pervasive increase in tree mortality across Canada's boreal forests, *Nature Climate Change*, **1** 467–471, doi:10.1038/nclimate1293.

Perez-Priego, O., Guan, J., Rossini, M., *et al.* (2015), Sun-induced chlorophyll fluorescence and photochemical reflectance index improve remote-sensing gross primary production estimates under varying nutrient availability in a typical Mediterranean savanna ecosystem, *Biogeosciences*, **12**(21) 6351–6367, doi:10.5194/bg-12-6351-2015.

Piao, S., Ciais, P., Friedlingstein, P., *et al.* (2008), Net carbon dioxide losses of northern ecosystems in response to autumn warming, *Nature*, **451** 49–52, doi:10.1038/nature06444.

Piao, S., Nan, H., Huntingford, C., *et al.* (2014), Evidence for a weakening relationship between interannual temperature variability and northern vegetation activity, *Nature Communications*, **5**(5018), doi:10.1038/ncomms6018.

Piao, S., Sitch, S., Ciais, P., *et al.* (2013), Evaluation of terrestrial carbon cycle models for their response to climate variability and to CO2 trends, *Global Change Biology*, **19**(7) 2117–2132, doi:10.1111/gcb.12187.

Pirk, N., Sievers, J., Mertes, J., Parmentier, F.-J. W., Mastepanov, M., and Christensen, T. R. (2017), Spatial variability of CO_2 uptake in polygonal tundra: assessing low-frequency disturbances in eddy covariance flux estimates, *Biogeosciences*, **14**(12) 3157–3169, doi:10.5194/bg-14-3157-2017.

Plamboeck, A. H., Grip, H., and Nygren, U. (1999), A hydrological tracer study of water uptake depth in a Scots pine forest under two different water regimes, *Oecologia*, **119**(3) 452–460, doi:10.1007/s004420050807.

Porcar-Castell, A. (2011), A high-resolution portrait of the annual dynamics of photochemical and non-photochemical quenching in needles of *Pinus sylvestris*, *Physiologia Plantarum*, **143**(2) 139–153, doi:10.1111/j.1399-3054.2011.01488.x.

Porcar-Castell, A., Garcia-Plazaola, J. I., Nichol, C. J., *et al.* (2012), Physiology of the seasonal relationship between the photochemical reflectance index and photosynthetic light use efficiency, *Oecologia*, **170**(2) 313–323, doi:10.1007/s00442-012-2317-9.

Porcar-Castell, A., Tyystjärvi, E., Atherton, J., *et al.* (2014), Linking chlorophyll a fluorescence to photosynthesis for remote sensing applications: mechanisms and challenges, *Journal of Experimental Botany*, **65**(15) 4065–4095, doi:10.1093/jxb/eru191.

Poulter, B., Frank, D., Ciais, P., *et al.* (2014), Contribution of semi-arid ecosystems to interannual variability of the global carbon cycle, *Nature*, **509** 600–603, doi:10.1038/nature13376.

Poulter, B., MacBean, N., Hartley, A., *et al.* (2015), Plant functional type classification for earth system models: results from the European Space Agency's Land Cover Climate Change Initiative, *Geoscientific Model Development*, **8**(7) 2315–2328, doi:10.5194/gmd-8-2315-2015.

Rammig, A., Donges, J. F., Babst, F., von Bloh, W., Frank, D., Thonicke, K., and Mahecha, M. D. (2015), Coincidences of climate extremes and anomalous vegetation responses: comparing tree ring patterns to simulated productivity, *Biogeosciences*, **12**(2) 373.

Rascher, U., Alonso, L., Burkart, A., *et al.* (2015), Sun-induced fluorescence – a new probe of photosynthesis: First maps from the imaging spectrometer HyPlant, *Global Change Biology*, **21**(12) 4673–4684, doi:10.1111/gcb.13017.

Raven, P. H., Evert, R. F., and Eichhorn, S. E. (1999), Biology of Plants, sixth edition edition, W. H. Freeman and Company Worth Publishers.

Reichstein, M., Bahn, M., Ciais, P., *et al.* (2013), Climate extremes and the carbon cycle, *Nature*, **500**(7462) 287–295, doi:10.1038/nature12350.

Reichstein, M., Falge, E., Baldocchi, D., *et al.* (2005), On the Separation of Net Ecosystem Exchange into Assimilation and Ecosystem Respiration: Review and Improved Algorithm, *Global Change Biology*, **11** 1424–1439.

Restrepo-Coupe, N., Huete, A., Davies, K., *et al.* (2016), MODIS vegetation products as proxies of photosynthetic potential along a gradient of meteorologically and biologically driven ecosystem productivity, *Biogeosciences*, **13**(19) 5587–5608, doi:10.5194/bg-13-5587-2016.

Reuter, M., Buchwitz, M., Hilker, M., *et al.* (2017), How Much CO2 Is Taken Up by the European Terrestrial Biosphere?, *Bulletin of the American Meteorological Society*, **98**(4) 665–671, doi:10.1175/BAMS-D-15-00310.1.

Richardson, A. D., Anderson, R. S., Arain, M. A., *et al.* (2012), Terrestrial biosphere models need better representation of vegetation phenology: results from the North American Carbon Program Site Synthesis, *Global Change Biology*, **18**(2) 566–584, doi:10.1111/j.1365-2486.2011.02562.x.

Richardson, A. D., Andy Black, T., Ciais, P., *et al.* (2010), Influence of spring and autumn phenological transitions on forest ecosystem productivity, *Philosophical Transactions of the Royal Society B: Biological Sciences*, **365**(1555) 3227–3246, doi:10.1098/rstb.2010.0102.

Richardson, A. D., Braswell, B. H., Hollinger, D. Y., Jenkins, J. P., and Ollinger, S. V. (2011), Near-surface remote sensing of spatial and temporal variation in canopy phenology, *Ecological Applications*, **19**(6) 1417–1428, doi:10.1111/j.1399-3054.2011.01488.x.

Rogers, A., Medlyn, B. E., Dukes, J. S., *et al.* (2017), A roadmap for improving the representation of photosynthesis in Earth system models, *New Phytologist*, **213**(1) 22–42, doi:10.1111/nph.14283.

Rossini, M., Nedbal, L., Guanter, L., *et al.* (2015), Red and far red Sun-induced chlorophyll fluorescence as a measure of plant photosynthesis, *Geophysical Research Letters*, **42**(6) 1632–1639, doi:10.1002/2014GL062943.

Rubel, F., Brugger, K., Haslinger, K., and Auer, I. (2017), The climate of the European Alps: Shift of very high resolution Köppen-Geiger climate zones 1800–2100, *Meteorologische Zeitschrift*, **26**(2) 115–125, doi:10.1127/metz/2016/0816.

Saleska, S. R., Didan, K., Huete, A. R., and da Rocha, H. R. (2007), Amazon Forests Green-Up During 2005 Drought, *Science*, **318**(5850) 612–612, doi:10.1126/science.1146663.

Schaefer, K., Schwalm, C. R., Williams, C., *et al.* (2012), A model-data comparison of gross primary productivity: Results from the North American Carbon Program site synthesis, *Journal of Geophysical Research: Biogeosciences*, **117**(G3), doi:10.1029/2012JG001960, g03010.

Schimel, D., Pavlick, R., Fisher, J. B., *et al.* (2015), Observing terrestrial ecosystems and the carbon cycle from space, *Global Change Biology*, **21**(5) 1762–1776, doi:10.1111/gcb.12822.

Schimel, D. S., House, J. I., Hibbard, K. A., *et al.* (2001), Recent patterns and mechanisms of carbon exchange by terrestrial ecosystems, *Nature Progress*, **414** 169–172, doi:10.1038/35102500.

Schlaepfer, D. R., Bradford, J. B., Lauenroth, W. K., *et al.* (2017), Climate change reduces extent of temperate drylands and intensifies drought in deep soils, *Nature Communications*, **8**(14196), doi:10.1038/ncomms14196.

Schneising, O., Reuter, M., Buchwitz, M., Heymann, J., Bovensmann, H., and Burrows, J. P. (2014), Terrestrial carbon sink observed from space: variation of growth rates and seasonal cycle amplitudes in response to interannual surface temperature variability, *Atmospheric Chemistry and Physics*, **14**(1) 133–141, doi:10.5194/acp-14-133-2014.

Schwalm, C. R., Williams, C. A., Schaefer, K., *et al.* (2012), Reduction in carbon uptake during turn of the century drought in western North America, *Nature Geoscience*, **5** 551–556, doi:10.1038/ngeo1529.

Seevers, P. M. and Ottmann, R. W. (1994), Evapotranspiration estimation using a normalized difference vegetation index transformation of satellite data, *Hydrological Sciences Journal*, **39**(4) 333–345, doi:10.1080/02626669409492754.

Seneviratne, S., Nicholls, N., Easterling, D., *et al.* (2012), Changes in climate extremes and their impacts on the natural physical environment, Cambridge University Press, Cambridge, UK, and New York, NY, USA, in: Managing the Risks of Extreme Events and Disasters to Advance Climate Change Adaptation [Field, C.B., V. Barros, T.F. Stocker, D. Qin, D.J. Dokken, K.L. Ebi, M.D. Mastrandrea, K.J. Mach, G.-K. Plattner, S.K. Allen, M. Tignor, and P.M. Midgley (eds.)]. A Special Report of Working Groups I and II of the Intergovernmental Panel on Climate Change (IPCC).

Seneviratne, S. I., Corti, T., Davin, E. L., Hirschi, M., Jaeger, E. B., Lehner, I., Orlowsky, B., and Teuling, A. J. (2010), Investigating soil moisture–climate interactions in a changing climate: A review, *Earth-Science Reviews*, **99**(3–4) 125–161, doi:10.1016/j.earscirev.2010.02.004.

Shen, M., Tang, Y., Desai, A. R., Gough, C., and Chen, J. (2014), Can EVI-derived land-surface phenology be used as a surrogate for phenology of canopy photosynthesis?, *International Journal of Remote Sensing*, **35**(3) 1162–1174, doi:10.1080/01431161.2013.875636.

Sims, D. A., Brzostek, E. R., Rahman, A., Dragoni, D., and Phillips, R. P. (2014), An improved approach for remotely sensing water stress impacts on forest C uptake, *Global Change Biology*, **20**(9) 2856–2866, doi:10.1111/gcb.12537.

Sims, D. A., Rahman, A. F., Cordova, V. D., *et al.* (2006), On the use of MODIS EVI to assess gross primary productivity of North American ecosystems, *Journal of Geophysical Research: Biogeosciences*, **111**(G4), doi:10.1029/2006JG000162.

Sippel, S., Forkel, M., Rammig, A., *et al.* (2017), Contrasting and interacting changes in simulated spring and summer carbon cycle extremes in European ecosystems, *Environ. Res. Lett.*, **12**.

Sitch, S., McGuire, A. D., Kimball, J., *et al.* (2007), Assessing the carbon balance of circumpolar arctic tundra using remote sensing and process modeling, *Ecological Applications*, **17**(1) 213–234, doi:10.1890/1051-0761(2007)017[0213:ATCBOC]2.0.CO;2.

Smith, M. D. (2011), An ecological perspective on extreme climatic events: a synthetic definition and framework to guide future research, *Journal of Ecology*, **99**(3) 656–663, doi:10.1111/j.1365-2745.2011.01798.x.

Soukupová, J., Cséfalvay, L., Urban, O., Košvancová, M., Marek, M., Rascher, U., and Nedbal, L. (2008), Annual variation of the steady-state chlorophyll fluorescence emission of evergreen plants in temperate zone, *Functional Plant Biology*, **35** 63–76.

Springer, K. R., Wang, R., and Gamon, J. A. (2017), Parallel Seasonal Patterns of Photosynthesis, Fluorescence, and Reflectance Indices in Boreal Trees, *Remote Sensing*, **9**(7), doi:10.3390/rs9070691.

Starr, G. and Oberbauer, S. F. (2003), PHOTOSYNTHESIS OF ARCTIC EVERGREENS UNDER SNOW: IMPLICATIONS FOR TUNDRA ECOSYSTEM CARBON BALANCE, *Ecology*, **84**(6) 1415–1420, doi:10.1890/02-3154.

Stöckli, R., Rutishauser, T., Dragoni, D., O'Keefe, J., Thornton, P. E., Jolly, M., Lu, L., and Denning, A. S. (2008), Remote sensing data assimilation for a prognostic phenology model, *Journal of Geophysical Research: Biogeosciences*, **113**(G4), doi:10.1029/2008JG000781.

Stow, D. A., Hope, A., McGuire, D., *et al.* (2004), Remote sensing of vegetation and land-cover change in Arctic Tundra Ecosystems, *Remote Sensing of Environment*, **89**(3) 281 – 308, doi:http://dx.doi.org/10.1016/j.rse.2003.10.018.

Street, L., Shaver, G. R., Williams, M., and Van Wijk, M. T. (2007), What is the relationship between changes in canopy leaf area and changes in photosynthetic CO2 flux in arctic ecosystems?, *Journal of Ecology*, **95** 139–150, doi:10.1111/j.1365-2745.2006.01187.x.

Sturm, M., Racine, C., and Tape, K. (2001), Increasing shrub abundance in the Arctic, *Nature*, **411** 546.

Sun, Y., Frankenberg, C., Jung, M., Joiner, J., Guanter, L., Köhler, P., and Magney, T. (2018), Overview of Solar-Induced chlorophyll Fluorescence (SIF) from the Orbiting Carbon Observatory-2: Retrieval, cross-mission comparison, and global monitoring for GPP, *Remote Sensing of Environment*, **209** 808–823, doi:https://doi.org/10.1016/j.rse.2018.02.016.

Sun, Y., Frankenberg, C., Wood, J. D., *et al.* (2017), OCO-2 advances photosynthesis observation from space via solar- induced chlorophyll fluorescence, *Science*, **358**(189), doi:10.1126/science.aam5747.

Sun, Y., Fu, R., Dickinson, R., Joiner, J., Frankenberg, C., Gu, L., Xia, Y., and Fernando, N. (2015), Drought onset mechanisms revealed by satellite solar-induced chlorophyll fluorescence: Insights from two contrasting extreme events, *Journal of Geophysical Research: Biogeosciences*, **120**(11) 2427–2440, doi:10.1002/2015JG003150.

Taiz, L. and Zeiger, E. (1991), Plant Physiology, The Benjamin/ Cummings Publishing Company, Inc.

Tanja, S., Berninger, F., Vesala, T., *et al.* (2003), Air temperature triggers the recovery of evergreen boreal forest photosynthesis in spring, *Global Change Biology*, **9**(10) 1410–1426, doi:10.1046/j.1365-2486.2003.00597.x.

Teubner, I. E., Forkel, M., M.and Jung, Liu, Y. Y., *et al.* (2018), Assessing the relationship between microwave vegetation optical depth and gross primary production, *International Journal of Applied Earth Observation and Geoinformation*, **65** 79–91, doi:https://doi.org/10.1016/j.jag.2017.10.006.

Teuling, A. J., Seneviratne, S. I., Stöckli, R., *et al.* (2010), Contrasting response of European forest and grassland energy exchange to heatwaves, *Nature Geoscience*, **3** 722–727, doi:10.1038/ngeo950.

Teuling, A. J., Taylor, C. M., Meirink, J. F., *et al.* (2017), Observational evidence for cloud cover enhancement over western European forests, *Nature communications*, **8**, doi:10.1038/ncomms14065.

Thum, T. (2009), Modelling boreal forest CO2 exchange and seasonality, Dissertation, University of Helsinki, Faculty of Science, Department of Physics, Division of Atmospheric Sciences and Geophysics.

Thum, T., Aalto, T., Laurila, T., Aurela, M., Hatakka, J., Lindroth, A., and Vesala, T. (2009), Spring initiation and autumn cessation of boreal coniferous forest CO2 exchange assessed by meteorological and biological variables, *Tellus B*, **61**(5) 701–717, doi:10.1111/j.1600-0889.2009.00441.x.

Thum, T., Zaehle, S., Köhler, P., *et al.* (2017), Modelling sun-induced fluorescence and photosynthesis with a land surface model at local and regional scales in northern Europe, *Biogeosciences*, **14**(7) 1969–1987, doi:10.5194/bg-14-1969-2017.

Thurner, M., Beer, C., Santoro, M., *et al.* (2014), Carbon stock and density of northern boreal and temperate forests, *Global Ecology and Biogeography*, **23**(3) 297–310, doi:10.1111/geb.12125.

Tramontana, G., Ichii, K., Camps-Valls, G., Tomelleri, E., and apale, D. (2015), Uncertainty analysis of gross primary production upscaling using Random Forests, remote sensing and eddy covariance data, *Remote Sensing of Environment*, **168**("") 360–373, doi:http://dx.doi.org/10.1016/j.rse.2015.07.015, "".

Tramontana, G., Jung, M., Schwalm, C. R., *et al.* (2016), Predicting carbon dioxide and energy fluxes across global FLUXNET sites with regression algorithms, *Biogeosciences*, **13**(14) 4291–4313, doi:10.5194/bg-13-4291-2016.

Tucker, C. J. (1979), Red and photographic infrared linear combinations for monitoring vegetation, *Remote sensing of Environment*, **8**(2) 127–150.

Tuovinen, J.-P., Aurela, M., Hatakka, J., *et al.* (2018), Interpreting eddy covariance data from heterogeneous Siberian tundra: land cover-specific methane fluxes and spatial representativeness, *Biogeosciences Discussions*, **2018** 1–36, doi:10.5194/bg-2018-155.

Turner, D. P., Rifts, W. D., Cohen, W. B., *et al.* (2006), Evaluation of MODIS NPP and GPP products across multiple biomes, *Remote sensing of Environment*, **102** 282–292, doi:10.10161j.rse.2006.02.017.

Ueyama, M., Ichii, K., Iwata, H., *et al.* (2013a), Upscaling terrestrial carbon dioxide fluxes in Alaska with satellite remote sensing and support vector regression, *Journal of Geophysical Research: Biogeosciences*, **118**(3) 1266–1281, doi:10.1002/jgrg.20095.

Ueyama, M., Iwata, H., Harazono, Y., Euskirchen, E. S., Oechel, W. C., and Zona, D. (2013b), Growing season and spatial variations of carbon fluxes of Arctic and boreal

ecosystems in Alaska (USA), *Ecological Applications*, **23**(8) 1798–1816, doi:10.1890/11-0875.1.

van der Molen, M. K., Dolman, A. J., Ciais, P., *et al.* (2011), Drought and ecosystem carbon cycling, *Agricultural and Forest Meteorology*, **151**(7) 765–773, doi:10.1016/j.agrformet.2011.01.018.

van der Tol, C., Berry, J. A., Campbell, P. K. E., and Rascher, U. (2014), Models of fluorescence and photosynthesis for interpreting measurements of solar-induced chlorophyll fluorescence, *Journal of Geophysical Research: Biogeosciences*, **119**(12) 2312–2327, doi:10.1002/2014JG002713, 2014JG002713.

van der Tol, C., Verhoef, W., and Rosema, A. (2009), A model for chlorophyll fluorescence and photosynthesis at leaf scale, *Agricultural and Forest Meteorology*, **149**(1) 96–105, doi:http://dx.doi.org/10.1016/j.agrformet.2008.07.007.

van Mantgem, P. J., Stephenson, N. L., Byrne, J. C., *et al.* (2009), Widespread Increase of Tree Mortality Rates in the Western United States, *Science*, **323**(5913) 521–524, doi:10.1126/science.1165000.

Verbyla, D. (2008), The greening and browning of Alaska based on 1982–2003 satellite data, *Global Ecol. Biogeogr.*, **17** 547–555, doi:10.1111/j.1466-8238.2008.00396.x.

Verhoeven, A. (2014), Sustained energy dissipation in winter evergreens, *New Phytologist*, **201**(1) 57–65, doi:10.1111/nph.12466.

Verpoorter, C., Kutser, T., Seekell, D. A., and Tranvik, L. J. (2014), A global inventory of lakes based on high-resolution satellite imagery, *Geophysical Research Letters*, **41**(18) 6396–6402, doi:10.1002/2014GL060641.

Verrelst, J., Rivera, J. P., van der Tol, C., Magnani, F., Mohammed, G., and Moreno, J. (2015), Global sensitivity analysis of the {SCOPE} model: What drives simulated canopy-leaving sun-induced fluorescence?, *Remote Sensing of Environment*, **166** 8–21, doi:http://dx.doi.org/10.1016/j.rse.2015.06.002.

Vicca, S., Balzarolo, M., Filella, I., *et al.* (2016), Remotely-sensed detection of effects of extreme droughts on gross primary production, *Scientific Reports*, **6**, doi:10.1038/srep28269.

Vicente-Serrano, S. M., Gouveia, C., Camarero, J. J., *et al.* (2013), Response of vegetation to drought time-scales across global land biomes, *Proceedings of the National Academy of Sciences of the United States of America*, **110**(1) 52–57, doi:http://doi.org/10.1073/pnas.1207068110.

Walker, D. A., Auerbach, N. A., Bockheim, J. G., *et al.* (1998), Energy and trace-gas fluxes across a soil pH boundary in the Arctic, *Nature*, **394** 469–472.

Walker, D. A., Raynolds, M. K., Daniëls, F. J., *et al.* (2005), The Circumpolar Arctic vegetation map, *Journal of Vegetation Science*, **16** 267–282.

Wang, J., Zeng, N., and Wang, M. R. (2016), Interannual variability of the atmospheric CO_2 growth rate: relative contribution from precipitation and temperature, *Biogeosciences*, **13**(8) 2339–2352, doi:10.5194/bg-13-2339-2016.

Welker, J. M., Fahnestock, J. T., Henry, G. H. R., O'Dea, K. W., and Chimner, R. A. (2004), CO2 exchange in three Canadian High Arctic ecosystems: response to long-term experimental warming, *Global Change Biology*, **10**(12) 1981–1995, doi:10.1111/j.1365-2486.2004.00857.x.

Wheeler, T. and von Braun, J. (2013), Climate Change Impacts on Global Food Security, *Science*, **341**(6145) 508–513, doi:10.1126/science.1239402.

White, K., Pontius, J., and Schaberg, P. (2014), Remote sensing of spring phenology in northeastern forests: A comparison of methods, field metrics and sources of uncertainty, *Remote Sensing of Environment*, **148** 97 – 107, doi:http://dx.doi.org/10.1016/j.rse.2014.03.017.

White, M. A., De Beurs, K. M., Didan, K., *et al.* (2009), Intercomparison, interpretation, and assessment of spring phenology in North America estimated from remote sensing for 1982-2006, *Global Change Biology*, **15**(10) 2335–2359, doi:10.1111/j.1365-2486.2009.01910.x.

Wielicki, B. A., Barkstrom, B. R., Harrison, E. F., Lee III, R. B., Smith, G. L., and Cooper, J. E. (1996), Clouds and the Earth's Radiant Energy System (CERES): An Earth Observing System Experiment, *Bulletin of the American Meteorological Society*, **77**(5) 853–868, doi:10.1175/1520-0477(1996)077⟨0853:CATERE⟩2.0.CO;2.

Wieneke, S., Ahrends, H., Damm, A., Pinto, F., Stadler, A., Rossini, M., and Rascher, U. (2016), Airborne based spectroscopy of red and far-red sun-induced chlorophyll fluorescence: Implications for improved estimates of gross primary productivity, *Remote Sensing of Environment*, doi:http://dx.doi.org/10.1016/j.rse.2016.07.025.

Williams, M. and Rastetter, E. (1999), Vegetation characteristics and primary productivity along an arctic transect: implications for scaling-up, *Journal of Ecology*, **87**(5) 885–898, doi:10.1046/j.1365-2745.1999.00404.x.

Wilson, K. B., Baldocchi, D. D., and Hanson, P. J. (2000), Spatial and seasonal variability of photosynthetic parameters and their relationship to leaf nitrogen in a deciduous forest, *Tree Physiology*, **20**(9) 565–578, doi:10.1093/treephys/20.9.565.

Wilson, K. B., Baldocchi, D. D., and Hanson, P. J. (2001), Leaf age affects the seasonal pattern of photosynthetic capacityand net ecosystem exchange of carbon in a deciduous forest, *Plant, Cell & Environment*, **24**(6) 571–583, doi:10.1046/j.0016-8025.2001.00706.x.

Wolf, S., Keenan, T. F., Fisher, J. B., *et al.* (2016), Warm spring reduced carbon cycle impact of the 2012 US summer drought, *Proceedings of the National Academy of Sciences of the United States of America PNAS*, 1–6, doi:10.1073/pnas.1519620113.

Wong, C. Y. S. and Gamon, J. A. (2014), Three sources of variation in the photochemical reflectance index (PRI) in evergreen conifers, *New Phytologist*, **206**(1) 187–195, doi:10.1111/nph.13159.

Wong, C. Y. S. and Gamon, J. A. (2015), The photochemical reflectance index provides an optical indicator of spring photosynthetic activation in evergreen conifers, *New Phytologist*, **206**(1) 196–208, doi:10.1111/nph.13251.

Wood, W. H. J., MacGregor-Chatwin, C., Barnett, S. F. H., Mayneord, G. E., Huang, X., Hobbs, J. K., Hunter, C. N., and Johnson, M. P. (2018), Dynamic thylakoid stacking regulates the balance between linear and cyclic photosynthetic electron transfer, *Nature Plants*, **4** 116–127, doi:10.1038/s41477-017-0092-7.

Wu, C., Chen, J. M., and Huang, N. (2011), Predicting gross primary production from the enhanced vegetation index and photosynthetically active radiation: Evaluation and calibration, *Remote Sensing of Environment*, **115**(12) 3424–3435, doi:https://doi.org/10.1016/j.rse.2011.08.006.

Wu, J., Kobayashi, H., Stark, S. C., *et al.* (2018), Biological processes dominate seasonality of remotely sensed canopy greenness in an Amazon evergreen forest, *New Phytologist*, **217**(4) 1507–1520, doi:10.1111/nph.14939.

Wu, J., van der Linden, L., Lasslop, G., Carvalhais, N., Pilegaard, K., Beier, C., and Ibrom, A. (2012), Effects of climate variability and functional changes on the interannual variation of the carbon balance in a temperate deciduous forest, *Biogeosciences*, **9**(1) 13–28, doi:10.5194/bg-9-13-2012.

Xiao, X., Zhang, Q., Braswell, B., Urbanski, S., Boles, S., Wofsy, S., Moore III, B., and Ojima, D. (2004), Modeling gross primary production of temperate deciduous broadleaf forest using satellite images and climate data, *Remote Sensing of Environment*, **91**(2) 256–270, doi:http://dx.doi.org/10.1016/j.rse.2004.03.010.

Yang, H., Yang, X., Zhang, Y., Heskel, M. A., Lu, X., Munger, J. W., Sun, S., and Tang, J. (2017), Chlorophyll fluorescence tracks seasonal variations of photosynthesis from leaf to canopy in a temperate forest, *Global Change Biology*, **23**(7) 2874–2886, doi:10.1111/gcb.13590.

Yang, X., Tang, J., and Mustard, J. F. (2014), Beyond leaf color: Comparing camera-based phenological metrics with leaf biochemical, biophysical, and spectral properties throughout the growing season of a temperate deciduous forest, *Journal of Geophysical Research: Biogeosciences*, **119**(3) 181–191, doi:10.1002/2013JG002460, 2013JG002460.

Yang, X., Tang, J., Mustard, J. F., *et al.* (2015), Solar-induced chlorophyll fluorescence that correlates with canopy photosynthesis on diurnal and seasonal scales in a temperate deciduous forest, *Geophysical Research Letters*, **42**(8) 2977–2987, doi:10.1002/2015GL063201, 2015GL063201.

Yi, Y., Kimball, J. S., and Reichle, R. H. (2014), Spring hydrology determines summer net carbon uptake in northern ecosystems, *Environmental Research Letters*, **9**(6) 064003.

Yoshida, Y., Joiner, J., Tucker, C., *et al.* (2015), The 2010 Russian drought impact on satellite measurements of solar-induced chlorophyll fluorescence: Insights from modeling and comparisons with parameters derived from satellite reflectances, *Remote Sensing of Environment*, **166**(0) 163–177, doi:http://dx.doi.org/10.1016/j.rse.2015.06.008.

Yuan, W., Liu, S., Dong, W., *et al.* (2014), Differentiating moss from higher plants is critical in studying the carbon cycle of the boreal biome, *Nature communications*, **5**(4270), doi:10.1038/ncomms5270.

Zarco-Tejada, P. J., Morales, A., Testi, L., and Villalobos, F. J. (2013), Spatio-temporal patterns of chlorophyll fluorescence and physiological and structural indices acquired from hyperspectral imagery as compared with carbon fluxes measured with eddy covariance, *Remote Sensing of Environment*, **133** 102 – 115, doi:http://dx.doi.org/10.1016/j.rse.2013.02.003.

Zhang, K., Kimball, J. S., Hogg, E. H., Zhao, M., Oechel, W. C., Cassano, J. J., and Running, S. W. (2008), Satellite-based model detection of recent climate-driven changes in northern high-latitude vegetation productivity, *Journal of Geophysical Research: Biogeosciences*, **113**(G3), doi:10.1029/2007JG000621.

Zhang, X., Friedl, M. A., and Schaaf, C. B. (2006), Global vegetation phenology from Moderate Resolution Imaging Spectroradiometer (MODIS): Evaluation of global patterns and comparison with in-situ measurements, *Journal of Geophysical Research: Biogeosciences*, **111**(G4), doi:10.1029/2006JG000217, g04017.

Zhang, X., Friedl, M. A., Schaaf, C. B., and Strahler, A. H. (2004), Climate controls on vegetation phenological patterns in northern mid- and high latitudes inferred from MODIS data, *Global Change Biology*, **10**(7) 1133–1145, doi:10.1111/j.1529-8817.2003.00784.x.

Zhang, Y., Guanter, L., Berry, J. A., van der Tol, C., Yang, X., Tang, J., and Zhang, F. (2016a), Model-based analysis of the relationship between sun-induced chlorophyll fluorescence and gross primary production for remote sensing applications, *Remote Sensing of Environment*, **187** 145–155, doi:https://doi.org/10.1016/j.rse.2016.10.016.

Zhang, Y., Guanter, L., Berry, J. A., *et al.* (2014), Estimation of vegetation photosynthetic capacity from space-based measurements of chlorophyll fluorescence for terrestrial biosphere models, *Global Change Biology*, **20**(12) 3727–3742, doi:10.1111/gcb.12664.

Zhang, Y., Song, C., Band, L. E., Sun, G., and Li, J. (2017), Reanalysis of global terrestrial vegetation trends from MODIS products: Browning or greening?, *Remote Sensing of Environment*, **191** 145–155, doi:https://doi.org/10.1016/j.rse.2016.12.018.

Zhang, Y., Voigt, M., and Liu, H. (2015), Contrasting responses of terrestrial ecosystem production to hot temperature extreme regimes between grassland and forest, *Biogeosciences*, **12**(2) 549–556, doi:10.5194/bg-12-549-2015.

Zhang, Y., Xiao, X., Jin, C., *et al.* (2016b), Consistency between sun-induced chlorophyll fluorescence and gross primary production of vegetation in North America, *Remote Sensing of Environment*, **183** 154–169, doi:http://dx.doi.org/10.1016/j.rse.2016.05.015.

Zhang, Y., Xiao, X., Zhang, Y., *et al.* (2018), On the relationship between sub-daily instantaneous and daily total gross primary production: Implications for interpreting satellite-based SIF retrievals, *Remote Sensing of Environment*, **205** 276–289, doi:https://doi.org/10.1016/j.rse.2017.12.009.

Zhang, Y., Xiao, X., Zhou, S., Ciais, P., McCarthy, H., and Luo, Y. (2016c), Canopy and physiological control of GPP during drought and heatwave, *Geophysical Research Letters*, doi:10.1002/2016GL068501, 2016GL068501.

Zhang, Y., Zhu, Z., Liu, Z., Zeng, Z., Ciais, P., Huang, M., Liu, Y., and Piao, S. (2016d), Seasonal and interannual changes in vegetation activity of tropical forests in Southeast Asia, *Agricultural and Forest Meteorology*, **224** 1 – 10, doi:http://dx.doi.org/10.1016/j.agrformet.2016.04.009.

Zhao, M. and Running, S. (2010), Drought-Induced Reduction in Global Terrestrial Net Primary Production from 2000 Through 2009, *Science*, **329**(5994) 940–943, doi:10.1126/science.1192666.

Zhou, L., Tucker, C. J., Kaufmann, R. K., Slayback, D., Shabanov, N. V., and Myneni, R. B. (2001), Variations in northern vegetation activity inferred from satellite data of vegetation index during 1981 to 1999, *Journal of Geophysical Research: Atmospheres*, **106**(D17) 20069–20083, doi:10.1029/2000JD000115.

Zhou, S., Zhang, Y., Caylor, K. K., Luo, Y., Xiao, X., Ciais, P., Huang, Y., and Wang, G. (2016), Explaining inter-annual variability of gross primary productivity from plant phenology and physiology, *Agricultural and Forest Meteorology*, **226–227** 246–256, doi:http://dx.doi.org/10.1016/j.agrformet.2016.06.010.

Zhu, Z., Piao, S., Myneni, R. B., *et al.* (2016), Greening of the Earth and its drivers, *Nature Climate Change*, **6**(791) 791–795, doi:10.1038/nclimate3004.

Zona, D., Oechel, W. C., Richards, J. H., Hastings, S., Kopetz, I., Ikawa, H., and Oberbauer, S. (2011), Light-stress avoidance mechanisms in a Sphagnum-dominated wet coastal Arctic tundra ecosystem in Alaska, *Ecology*, **92**(3) 633–644, doi:10.1890/10-0822.1.

Zscheischler, J., Mahecha, M. D., Harmeling, S., and Reichstein, M. (2013), Detection and attribution of large spatiotemporal extreme events in Earth observation data, *Ecological Informatics*, **15** 66–73, doi:http://dx.do.org/10.1016/j.ecoinf.2013.03.004.

Zscheischler, J., Orth, R., and Seneviratne, S. I. (2015), A submonthly database for detecting changes in vegetation-atmosphere coupling, *Geophysical Research Letters*, **42**(22) 9816–9824, doi:10.1002/2015GL066563, 2015GL066563.

Zscheischler, J., Reichstein, M., Harmeling, S., Rammig, A., Tomelleri, E., and Mahecha, M. D. (2014), Extreme events in gross primary production: a characterization across continents, *Biogeosciences*, **11**(11) 2909–2924, doi:10.5194/bg-11-2909-2014.

ACRONYMS

APAR absorbed photosynthetically active radiation, approximated as the product of PAR and fPAR

ATP Adenosine triphosphate, an energetic compound needed in photosynthesis, created by proton movement from the lumen to the stroma across the thylakoid membrane through ATP-synthase

CET Cyclic Electron Transport: Movement of electrons around PSI by passing from the RC of PSI back to redox systems in the chain between PSII and PSI and back 'downstream' to the RC of PSI creating additional ATP

EC Eddy-covariance: simultaneous measurements of turbulent fluctuations of the vertical wind component and of gas concentrations in parcels of air with instruments mounted on towers or masts inform about the turbulent fluxes of trace gases between the land surface and the atmosphere at selected sites

ENSO El Niño Southern Oscillation, coupled oscillation of sea level pressure and sea surface temperatures in the equatorial Pacific ocean that affects much larger regions due to teleconnections

fPAR fraction of incident photosynthetically active radiation that is absorbed, for photosynthesis the fPAR that is absorbed by photoynthesising material is important (in contrast to non-photosynthesising material)

GPP gross flux of carbon taken up by the plants via photosynthesis in gC per time and area

LET Linear Electron Transport: during the light reactions of photosynthesis electrons move from the oxygen-evolving complex, via the RC of PSII, several redox systems and RC of PSI, further redox systems to $NADP^+$ creating the energetic compounds of NADPH and ATP

LUE Light-use-efficiency or yield: differentiated are LUE_p, the photosynthetic LUE describing the ratio of absorbed energy that is quenched photochemically to the total absorbed energy, and LUE_f, relating to the amount of absorbed energy being quenched as chlorophyll fluorescence

NADPH The reduced form of Nicotinamide adenine dinucleotide phosphate, $NADP^+$; an energetic compound needed in photosynthesis

NEE Net ecosystem exchange: net flux of carbon between the land surface and the atmosphere, represents the difference between GPP and plant and soil respiration, measured *in-situ* by EC

NIR near-infrared

NPQ Non-photochemical quenching: physiological mechanism of quenching excess absorbed energy as heat

PAR photosynthetically active radiation, roughly 400-700 nm

PS Photosystem, a compound of a light-harvesting complex (pigment-protein complex) and a RC in a chloroplast, two types of PS are differentiated, PSI and PSII, named in the order of their discovery, that have different wavelengths of maximal absorption

RC Reaction centre, a complex of pigments and proteins with a special pair of chlorophyll-a in the chloroplasts, site of primary charge separation during the photosynthetic light reactions

RuBP ribulose 1,5-bisphosphat, a five-carbon molecule that is the reaction partner of CO_2

rubisco ribulose 1,5 bishosphat-carboxylase/oxygenase, enzyme that catalizes the reaction between RuBP and CO_2 in the dark reactions, and also the oxygenation of RuBP

SAA South Atlantic Anomaly, a weak anomaly in the magnetic field of the Earth which allows cosmic particles to affect the at-sensor-radiances when the satellite passes through the SAA area in the southern Atlantic off the South American Coast

SIF sun-induced chlorophyll fluorescence, tiny part of APAR that is re-emitted by chlorophyll-a in photosynthesizing plants

S0 Ground electrical state of molecules

S1 First electrical excited state of a molecule, can be attained by absorption of red light or by decay from higher electrical states, comparativey long-lived, decays via photochemical quenching, non-photochemical quenching or fluorescence

S2 Second electrical excited state of a molecule, can be attained by absorption of blue light and will decay to S1 fast

VOD Vegetation optical depth, parameter derived from microwave measurements as an indicator of biomass

LIST OF FIGURES

LIST OF TABLES

ACKNOWLEDGEMENTS

That's it - four years of work in about 150 pages. Imagining the moment when I could finally write the acknowledgements of my thesis has always been a source of motivation and strength on the long way, especially during the last intense six months. I am proud and happy to have completed the 'project doctorate' and at this point take the chance to thank the many people who have supported me in this.
Doktorpapa Luis, mi agradecimiento mas importante a tì por la asistencia y tu apoyo siempre y en todos los aspectos. Gracias for making me curious about this strange fluorescence thing and for always patiently explaining and discussing. I appreciate your quick, honest and critical feedback and most importantly - I cannot rate your supportive and motivating nature high enough. Thank you for always being there, for giving me all the time that I needed and so much freedom. And for making the time in Ispra possible.
Greg, Alessandro - if there is a plural of this word, I sincerely feel that you are my other Doktorpapas. I learned so much from you and the time I spent with you was incredibly enriching, both professionally and personally! Grazie di cuore a tutti voi! Anche agli altri colleghi e nuovi amici (Guido, Yeray, Elias, Thomas)! Guido, mi sento molto fortunata di averti incontrato e ti ringrazio di cuore per la tua amicizia e le tante esperienze uniche in montagna e al lago. E Giorgio, per fortuna ci si incontra sempre due volte nella vita, no?
Philipp, Max, Ola, I enjoyed it so much to share office with you, share experiences in every day work and on conferences and discuss on- and off-topic. Max, I'll never forget all your help and support, especially in the beginning.
Next to all co-authors of the papers I owe my PhD buddies Giorgio, Ola, Philipp and Greg for giving me valuable and critical comments on the thesis itself.
Lunch girls, thanks for making me looking forward to each and every lunch break and the evenings out together. Especially you, Shuping! The evenings spent with my yogis to come back down to Earth after work are wonderful moments to think of.
Schliesslich haben mir meine Lieben ausserhalb der Wissenschaftswelt sehr geholfen, und zwar mit offenen Ohren in enthusiastischen, spannenden und auch frustrierten Momenten und auch mit harter Arbeit, wenn sie mir helfen wollten, auch in relativen (absoluten?) Motivationsminima bei Laune und Disziplin zu bleiben. Kai, du bist mein Gegenpol, der mich im Gleichgewicht hält. Eine Umarmung von dir und die Welt sieht schon ganz anders aus. Danke für dein Verständnis für all die Wochenenden vor dem Laptop. Mama, Papa, Toni, Oma, Opa, danke, dass ihr mich machen lasst und stolz auf mich seid. Und für die Begleitung auf/nach Konferenzen :)